

## Redox behaviour and fining of molten glass

**Citation for published version (APA):**

de Best, A. W. M. (1994). *Redox behaviour and fining of molten glass*. [Phd Thesis 2 (Research NOT TU/e / Graduation TU/e), Chemical Engineering and Chemistry]. Technische Universiteit Eindhoven.  
<https://doi.org/10.6100/IR426291>

**DOI:**

[10.6100/IR426291](https://doi.org/10.6100/IR426291)

**Document status and date:**

Published: 01/01/1994

**Document Version:**

Publisher's PDF, also known as Version of Record (includes final page, issue and volume numbers)

**Please check the document version of this publication:**

- A submitted manuscript is the version of the article upon submission and before peer-review. There can be important differences between the submitted version and the official published version of record. People interested in the research are advised to contact the author for the final version of the publication, or visit the DOI to the publisher's website.
- The final author version and the galley proof are versions of the publication after peer review.
- The final published version features the final layout of the paper including the volume, issue and page numbers.

[Link to publication](#)

**General rights**

Copyright and moral rights for the publications made accessible in the public portal are retained by the authors and/or other copyright owners and it is a condition of accessing publications that users recognise and abide by the legal requirements associated with these rights.

- Users may download and print one copy of any publication from the public portal for the purpose of private study or research.
- You may not further distribute the material or use it for any profit-making activity or commercial gain
- You may freely distribute the URL identifying the publication in the public portal.

If the publication is distributed under the terms of Article 25fa of the Dutch Copyright Act, indicated by the "Taverne" license above, please follow below link for the End User Agreement:

[www.tue.nl/taverne](http://www.tue.nl/taverne)

**Take down policy**

If you believe that this document breaches copyright please contact us at:

[openaccess@tue.nl](mailto:openaccess@tue.nl)

providing details and we will investigate your claim.

# **Redox behaviour and fining of molten glass**

**Annemieke Wondergem-de Best**



# **Redox behaviour and fining of molten glass**

PROEFSCHRIFT

ter verkrijging van de graad van doctor aan de Technische Universiteit Eindhoven, op gezag van de Rector Magnificus, prof.dr. J.H. van Lint, voor een commissie aangewezen door het College van Decanen in het openbaar te verdedigen op donderdag 1 december 1994 om 14.00 uur

door

**Anna Wilhelmina Maria Wondergem-de Best**

Geboren te Berchem (België)

**Dit proefschrift is goedgekeurd  
door de promotoren  
prof.dr.ir. H. de Waal  
prof.dr.rer.nat. H.A. Schaeffer  
en de copromotor  
dr.ir. R.G.C. Beerkens**

## ABSTRACT

In the glass manufacturing process gases are released during the melting of the batch materials, resulting in an enormous amount of bubbles in the glass melt. These bubbles diminish the strength and the optical quality of the final glass product. Therefore they have to be removed from the melt. This process is called the fining of the glass melt.

In industrial glass melting tanks chemical agents are used to enhance the fining process. All common chemical fining agents are harmful. Two alternative physical fining methods, "temperature-gradient-induced migration of bubbles" and "ultrasonic fining", appeared after thorough examination of the theoretical backgrounds to be unsuitable for the use in industrial glass melting tanks. Chemical fining agents will also in the future remain necessary. The use of these chemicals should be reduced as much as possible by an optimization of the fining process. This requires more knowledge on the fining reactions.

The chemical fining agents consist of oxides of polyvalent ions, which are present in the most oxidized form in the batch. At an increase of the temperature, the fining agents are reduced while oxygen gas is released. This fining gas diffuses into existing bubbles, causing them to grow. The so enlarged bubbles have a higher rising velocity and are able to leave the melt in shorter time.

Examples of such fining agents are antimony and cerium oxide. When sulphate is used as a fining agent, sulphur dioxide is released as a fining gas as well. Redox reactions also occur when the glass melt contains other polyvalent elements, such as iron or chromium. The valency state of these ions determine the colour of the melt (and with that the heat distribution in the glass melting tank) and the colour of the final product. The temperature dependent equilibrium constants of the various redox reactions are of major importance for the desired optimization of the fining process.

The redox reaction equilibrium constants can be determined by various methods. After discussion of the advantages and disadvantages of all methods, two methods are selected, by which the equilibrium state of the reactions in the molten glass can be measured as a function of temperature. The theoretical backgrounds and elaborations of these methods, square wave voltammetry and

## Abstract

---

oxygen equilibrium pressure measurements, are discussed in detail. The results of the measurements of the redox reaction equilibrium of iron, antimony, cerium, chromium and sulphur in three commercially available glasses (soda-lime-silica, TV-screen and E-glass) are given as well.

The equilibrium state of the redox reaction depends not only on the temperature, but also on the composition of the glass melt. A prediction of the equilibrium constant of a redox reaction in a glass melt with a certain composition on the basis of measurements in glass with a different composition appears to be impossible. Therefore, the redox reaction equilibrium constant have to be determined for each glass composition separately.

The equilibrium states of the redox reactions of iron and antimony are measured using both techniques. The results agree very well, and are also similar to the data from the literature.

The equilibrium state of cerium in TV-screen glass could not be determined using square wave voltammetry. Square wave voltammetry measurements in sulphur-containing glass melts produced results which can not be explained (yet). Therefore the equilibrium constants of the redox reactions of cerium and sulphur have been derived from oxygen equilibrium pressure measurements in combination with wet-chemical analyses.

The equilibrium constants of the two reduction steps of chromium in a soda-lime-silica melt have been determined using square wave voltammetry.

From measurements in glass melts containing iron, antimony or cerium, it is clear that the total concentration of the polyvalent element has a strong effect on the equilibrium state. In TV-screen glass the most oxidized form of the polyvalent element is promoted at low concentrations. The opposite applies for iron in soda-lime-silica glass melts. This illustrates the strong effect of the exact glass composition on the equilibrium state.

The equilibrium states of the various redox reactions can also be determined in glass melts containing more than one polyvalent element using oxygen equilibrium pressure measurements or square wave voltammetry. The equilibrium constants appear not to be effected by the presence of the other ions. However, since oxygen is a participant in all redox reactions, the oxygen equilibrium pressure is strongly influenced. Therefore the redox ratio (the ratio of reduced

## Abstract

---

to oxidized species) in a melt containing several polyvalent elements differs from the redox ratio in a melt containing only one polyvalent element.

During cooling of the glass melt, the stronger reductor will consume so much oxygen that the weaker reductor is reduced. Therefore the redox ratios may change considerably during cooling of the melt. Such a shift in the redox ratios is demonstrated in a TV-screen glass containing both iron and cerium.

It appears to be possible to determine the physical solubility of oxygen in glass melts by combining the results from square wave voltammetry measurements and oxygen equilibrium pressure measurements. The physical solubility of oxygen in TV-screen glass at temperatures between 1000 and 1400°C is about  $1 \text{ mole}\cdot\text{m}^{-3}\cdot\text{bar}^{-1}$ .

The data on the temperature dependent equilibrium constants are introduced in a 3-D glass tank simulation model, which has been developed at the TNO Institute of Applied Physics (the Netherlands). With the aid of this computer model, the flow pattern, temperature distribution and gas concentration profiles in an industrial glass melting tank are calculated for a given set of processing conditions. Then the calculations are repeated for a different set of processing conditions. By thorough examination of the results, the fining process in the industrial glass melting tank can be optimized. As an example, the results of calculations for a TV-screen glass melt with two different concentrations of the fining agent antimony oxide are given.

### **SAMENVATTING**

Bij de glasfabricage komen tijdens het insmelten van het gemeng gassen vrij waardoor veel belletjes ontstaan. Belletjes verminderen de sterkte en optische kwaliteit van het eindprodukt en moeten daarom uit de smelt verwijderd worden. Dit proces wordt het louteren van de glassmelt genoemd.

In industriële glasovens worden chemicaliën gebruikt om het louteren te bevorderen. Alle gebruikelijke chemische loutermiddelen zijn in zekere mate schadelijk voor het milieu. Twee alternatieve fysische loutermethoden, "temperature-gradient-induced migration" en "ultrasoon louteren", blijken na bestudering van de achterliggende theorieën niet praktisch toepasbaar te zijn in industriële glasovens. Chemische loutermiddelen blijven daarom nodig. Het gebruik ervan dient zoveel mogelijk te worden beperkt door een optimalisatie van het louterproces. Hiervoor is meer kennis over de louterreacties nodig.

De chemische loutermiddelen bestaan uit oxides van polyvalente ionen, die in het gemeng in de meest geoxideerde toestand aanwezig zijn. Bij verhoging van de temperatuur worden de loutermiddelen gereduceerd, waarbij zuurstof als loutergas vrijkomt. Het loutergas diffundeert naar bestaande bellen en blaast ze op. De grotere gasbellen hebben een hogere stijgsnelheid en zullen de smelt sneller verlaten.

Voorbeelden van deze loutermiddelen zijn antimoon- en ceriumoxide. Bij het gebruik van het loutermiddel sulfaat komt er naast zuurstof ook zwaveldioxide vrij als loutergas. Redoxreacties vinden ook plaats als andere polyvalente ionen zoals ijzer of chroom in de smelt aanwezig zijn. De valentie-toestand van deze ionen bepaalt de kleur van de smelt (en daarmee de warmte-huishouding in de oven) en de kleur van het eindprodukt. De temperatuur-afhankelijke evenwichtsliggingen van de diverse redoxreacties zijn van groot belang voor de gewenste optimalisatie van het louterproces.

De reactie-evenwichtsliggingen kunnen op diverse manieren bepaald worden. Na bespreking van de voor- en nadelen van alle methoden wordt in dit proefschrift gekozen voor twee methoden waarbij metingen in de glassmelt kunnen worden gedaan, te weten square wave voltammetry en zuurstofevenwichtsdrukmetingen. De theoretische achtergronden en de uitwerking van de resultaten van deze methoden komen uitvoerig aan de orde. Tevens zijn de



## Samenvatting

---

evenwichtsconstanten van de redoxreacties van ijzer, antimoon, cerium, chroom en zwavel in verschillende commerciële glassoorten (natron-kalk, TV-scherm en E-glas) als functie van de temperatuur bepaald.

De ligging van de reactie-evenwichten hangt, behalve van de temperatuur, ook af van de samenstelling van de glassmelt. Het blijkt niet mogelijk te zijn de evenwichtsligging als functie van de temperatuur in één glassmelt te voorspellen op grond van metingen in een smelt met een andere samenstelling. Daarom moeten de reactie-evenwichtsliggingen voor alle samenstellingen apart worden bepaald.

De evenwichtsliggingen van de redoxreacties van ijzer en antimoon zijn met beide technieken gemeten. De resultaten komen goed met elkaar en met gegevens uit de literatuur overeen.

Het bleek niet mogelijk te zijn de reactie-evenwichtsligging van cerium in TV-schermglas te bepalen met square wave voltammetry. Square wave voltammetry metingen in een zwavelhoudende glassmelt leverden resultaten op die (nog) niet verklaard kunnen worden. Daarom zijn de reactie-evenwichtsconstanten van de redoxreacties van cerium en zwavel bepaald met behulp van zuurstofevenwichtsdrummetingen in combinatie met nat-chemische analyses.

De reactie-evenwichtsconstanten van de twee redoxreacties van chroom in natronkalkglas zijn bepaald met behulp van square wave voltammetry.

Uit de metingen in ijzer-, antimoon- en ceriumhoudende smelten blijkt dat de totale concentratie van het polyvalente ion een grote invloed heeft op de evenwichtsligging van de redoxreactie. In TV-schermglas blijkt de meest geoxideerde vorm bij lagere concentraties bevorderd te worden voor zowel ijzer, antimoon als cerium. Voor natronkalkglas met ijzer geldt het tegenovergestelde. Dit illustreert duidelijk dat de evenwichtsliggingen sterk afhangen van de exacte samenstelling van het glas en daarom voor ieder glas apart bepaald moeten worden.

De evenwichtsliggingen van de verschillende redoxreacties kunnen ook worden bepaald met behulp van zuurstofevenwichtsdrummetingen of square wave voltammetry als de glassmelt meerdere polyvalente ionen bevat. De evenwichtsconstanten van de afzonderlijke redoxreacties blijken hierdoor niet te veranderen. Aangezien zuurstof aan alle redoxreacties deelneemt, wordt de

## Samenvatting

---

zuurstofevenwichtsdruck wel sterk beïnvloed. Daardoor is de redox ratio (verhouding gereduceerde/geoxideerde ionen) in een smelt met meerdere polyvalente ionen anders dan in een smelt met maar één ion.

Bij afkoelen van de glassmelt zal de sterkste reductor zoveel zuurstof opnemen dat de zwakkere reductor gereduceerd wordt. Hierdoor kunnen de redox ratio's sterk verschuiven tijdens afkoelen van een glassmelt met meerdere polyvalente ionen. Dit is aangetoond met metingen aan TV-schermglas met ijzer en cerium.

Het blijkt mogelijk te zijn de fysische oplosbaarheid van zuurstof in de glassmelt te bepalen door de resultaten van square wave voltammetry en zuurstofevenwichtsdruckmetingen te combineren. Bij een temperatuur tussen 1000 en 1400°C is de fysische oplosbaarheid van zuurstof in TV-schermglas ongeveer  $1 \text{ mol}\cdot\text{m}^{-3}\cdot\text{bar}^{-1}$ .

De gegevens over de temperatuur-afhankelijke evenwichtsliggingen worden ingevoerd in een door TNO ontwikkeld glasovensimulatiemodel. Met dit model worden vervolgens het stromingspatroon, de temperatuurverdeling en de locale glassamenstelling (inclusief gassen) in een industriële glasoven berekend. Op basis van deze gegevens kan worden voorspeld of een glasoven onder bepaalde procescondities (bijvoorbeeld concentratie van het loutermiddel of de belading van de oven) bellenvrij glas kan produceren. Vervolgens kunnen dezelfde berekeningen worden doorgevoerd voor andere procescondities. Op deze manier kan het louterproces in een industriële glasoven geoptimaliseerd worden. Als voorbeeld worden de resultaten van de berekeningen voor een TV-scherm oven met antimoonoxide als loutermiddel in twee verschillende concentraties gepresenteerd.

## Contents

---

### CONTENTS

1	THE GLASS MELTING PROCESS	
1.1	An introduction to the glass melting process	1
1.2	The fining of glass melts/ a guide to this thesis	2
2	THE FINING OF GLASS MELTS	
2.1	Introduction	5
2.2	Gases in glass	6
2.2.1	The glass structure	6
2.2.2	The occurrence of gases in glass	8
2.2.3	Gases in bubbles	9
2.2.4	Physically dissolved gases	9
2.2.5	Chemically dissolved gases	10
2.2.6	Relationships	12
2.2.7	The fining process	14
2.3	The behaviour of bubbles in the glass melt	15
2.3.1	Buoyancy rate of bubbles	15
2.3.2	Ascension of clouds of bubbles	17
2.3.3	Coalescence and breaking up of bubbles	19
2.3.4	Dissolution	19
2.3.5	Formation of new bubbles	20
2.4	Fining methods	21
2.5	Some physical fining methods	22
2.5.1	Thermal-gradient-induced migration of bubbles	22
2.5.2	Ultrasonic fining	22
2.6	Chemical fining agents	30
2.7	Published data on chemical fining agents	32
2.8	Objective of this study	35
	Literature chapter 2	36
3	REDOX REACTIONS IN MOLTEN GLASS DEPENDING ON THE GLASS COMPOSITION	
3.1	Introduction	43
3.2	Redox reactions in glass	44
3.2.1	Redox reaction equilibria	44
3.2.2	The redox reaction equilibrium constant as a function of enthalpy and entropy	46
3.2.3	The redox reaction equilibrium for one polyvalent element during cooling to room temperature	47
3.2.4	Interaction of different polyvalent elements	48
3.2.5	Interaction of polyvalent elements during cooling to room temperature	48
3.3	Consequences of the redox reaction equilibrium states for the glass	49
3.3.1	Colour of the melt and the final product	49
3.3.2	The fining of glass melts	51
3.4	The effect of the glass composition on the redox reaction equilibria	53
3.4.1	The relation between the glass composition and the oxygen ion activity	53
3.4.2	Oxygen in glass	54
3.4.3	Basicity number concepts	54
3.4.4	The influence of the basicity on the redox reaction equilibria	58
3.5	Explanations for the influence of the basicity on the redox reaction equilibria	58
3.5.1	Standard free energies	59
3.5.2	Complex formation	59
3.5.3	The formation of peroxide ions	60
3.5.4	The interaction of bridging, non-bridging and free oxygen ions	60
3.5.5	A thermodynamic approach, based on activity coefficients	62
3.6	Predictions of the redox reaction equilibrium constant, based on the glass composition	64
	Literature chapter 3	67

## Contents

---

4	DETERMINATION OF THE EQUILIBRIUM CONSTANTS OF REDOX REACTIONS IN MOLTEN GLASS -AN OVERVIEW-	
4.1	The redox reaction equilibrium	71
4.2	Measurements of the redox reaction equilibrium state after cooling	73
4.2.1	Spectral techniques to investigate the valency state of polyvalent elements	74
4.2.2	Other techniques to determine the concentration of polyvalent elements in glass samples	74
4.2.3	Wet-chemical analysis of the valency state of polyvalent elements in glass samples	75
4.2.4	Other analysing methods for the determination of the valency state of polyvalent elements in acid solutions	75
4.2.5	Advantages and disadvantages of redox ratio measurements after cooling	76
4.3	Direct measurements of the redox reaction equilibrium in the molten glass	78
4.3.1	Emission spectroscopy	78
4.3.2	Electrochemical techniques	79
4.4	The techniques used for the present study	85
	Literature chapter 4	86
5	ELECTROCHEMICAL METHODS: OXYGEN EQUILIBRIUM PRESSURE MEASUREMENTS AND SQUARE WAVE VOLTAMMETRY	
5.1	Introduction	89
5.2	Electrochemistry/ some basic concepts	89
5.2.1	The electrochemical potential of a species $i$	89
5.2.2	The interface between two phases	90
5.2.3	Charge and charge transfer within one phase	91
5.2.4	Charge transfer through the interface electrode/electrolyte	91
5.2.5	The electrochemical cell	92
5.2.6	The three-electrode system	93
5.2.7	Response of the system to a change in potential	95
5.2.8	Standard, formal and half-wave potential	98
5.2.9	Sign of potential and current	98
5.3	Electrochemistry in molten glass	99
5.3.1	The glass melt	99
5.3.2	The potentiostat	100
5.3.3	The electrodes	100
5.3.4	The experimental set-up	102
5.3.5	Positioning of the electrodes	102
5.3.6	IR-compensation	104
5.4	Oxygen equilibrium pressure measurements	107
5.4.1	Oxygen equilibrium pressure	107
5.4.2	The oxygen sensor	107
5.4.3	Electrochemical description of the oxygen sensor	108
5.4.4	Calculation of the oxygen equilibrium pressure in the melt	111
5.4.5	Properties of the reference and platinum electrode	111
5.4.6	Oxygen equilibrium pressure measurements	111
5.4.7	Calculation of the redox reaction equilibrium constants, enthalpy and entropy	112
5.4.8	Restrictions of the described method	114
5.4.9	Advantages of the described method	118
5.5	Square wave voltammetry measurements	118
5.5.1	The experimental set-up	119
5.5.2	The applied potential	119
5.5.3	The voltammogram	121
5.5.4	The $i_p$ , $i_r$ and $\delta i$ curves: a general description	122
5.5.5	The $i_p$ , $i_r$ and $\delta i$ curves: a mathematical description	125
5.5.6	Real voltammograms	127
5.5.7	Data derived from square wave voltammograms	133
5.5.8	Calculation of the redox reaction equilibrium constant $K^{**}(T)$	136
5.5.9	Calculation of the redox ratio	138

## Contents

---

5.5.10	Calculation of the redox reaction enthalpy and entropy changes	138
5.5.11	Limitations of the application of square wave voltammetry in molten glass	139
	Literature chapter 5	142
6	<b>RESULTS</b>	
6.1	Introduction	144
6.2	Iron	
6.2.1	Iron in glass	148
6.2.2	Oxygen equilibrium pressure measurements	148
6.2.3	Square wave voltammetry measurements	154
6.2.4	Comparison of the results of oxygen equilibrium pressure measurements and square wave voltammetry measurements	177
6.2.5	Comparison of the results with data from the literature	178
6.2.6	Conclusions	183
6.3	Antimony	
6.3.1	Antimony in glass	184
6.3.2	Oxygen equilibrium pressure measurements	185
6.3.3	Square wave voltammetry measurements	188
6.3.4	Comparison of the results from oxygen equilibrium pressure measurements and square wave voltammetry measurements	208
6.3.5	Comparison of the results with data from the literature	209
6.3.6	Conclusions	212
6.4	Cerium	
6.4.1	Cerium in glass	213
6.4.2	Oxygen equilibrium pressure measurements	213
6.4.3	Square wave voltammetry measurements	217
6.4.4	Wet-chemical analysis	217
6.4.5	Comparison of the results with data from the literature	221
6.4.6	Conclusions	224
6.5	Chromium	
6.5.1	Chromium in glass	224
6.5.2	Square wave voltammetry measurements	225
6.5.3	Comparison of the results with data from the literature	235
6.5.4	Conclusions	237
6.6	Sulphur	
6.6.1	Sulphur in glass	238
6.6.2	Oxygen equilibrium pressure measurements	240
6.6.3	Square wave voltammetry measurements	248
6.6.4	Comparison of the results with data from the literature	255
6.7	Combinations of two polyvalent elements	
6.7.1	Purpose of this section	256
6.7.2	Effect of iron impurities on the redox reaction equilibrium constant of antimony	256
6.7.3	Interaction of iron and cerium	257
6.7.4	Conclusions	264
6.8	Physical solubility of O <sub>2</sub>	
6.8.1	Measurements of the physical solubility of O <sub>2</sub>	265
6.8.2	Effect of the value chosen for the physical solubility of oxygen on the calculated enthalpy and entropy	267
6.8.3	Conclusions	268
	Literature chapter 6	269
7	<b>THE APPLICATION OF THE MEASURED DATA IN COMPUTER MODELS</b>	
7.1	Introduction	272
7.2	Mathematical models	272
7.3	The "bubble behaviour model"	274
7.4	The "3-D glass tank model"	275
7.5	Examples of calculations with the "3-D glass tank model"	276
	Literature chapter 7	289

# Chapter 1

## The glass melting process

### 1.1 AN INTRODUCTION TO THE GLASS MELTING PROCESS

Nowadays, most glass products like container glass, flat glass, TV-screen glass and reinforcement fibers are made in a continuous process. The raw material components for these products are generally silica sand, soda ash, limestone, alumina components, cullet and some other components. The raw materials have to be well mixed and the batch is continuously charged to the glass tank. Furnace temperatures normally range from 1300 to 1600°C, depending on the glass composition, the required quality and the production rate.

In most industrial glass tanks the batch is heated by gas or oil fired flames. The burners are placed above the surface of the glass melt in burner ports. The flames fan out horizontally over the glass melt and so the glass is heated from above. Figure 1.1 shows a schematic presentation of a cross-section of a cross-fired glass tank.

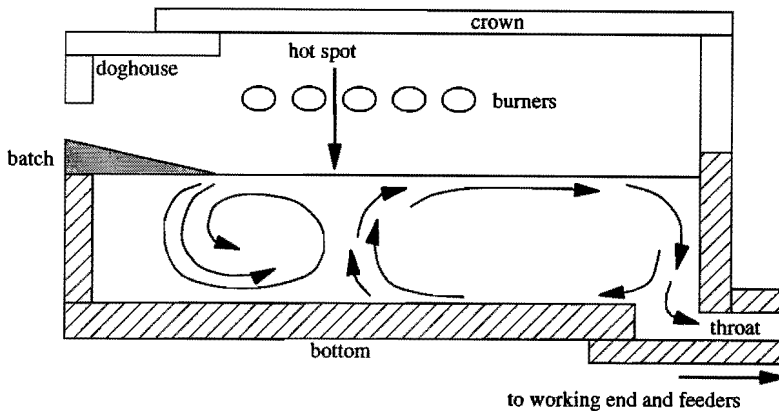


Figure 1.1  
Schematic presentation of a cross-fired industrial glass tank

In the doghouse, the raw material batch mixture is charged to the tank. The produced molten glass flows to the working end and the feeders, where the glass melt is prepared for the forming process. The temperature of the melt in the working end and feeders is some hundred degrees centigrade lower than in

the hot spot of the melter. From the working end or feeders, the glass is transported to the sections where the forming of the final product takes place.

The flow pattern in the tank is determined by the pull rate, geometrical factors (dimension of the tank, presence or absence of a throat), free convection caused by temperature differences and forced convection (caused by forced bubbling or the presence of a hot spot).

In the tank, melting, fining and homogenisation of the melt has to take place. During the melting process, the batch particles react and dissolve in the already formed liquid phase. Especially the dissolution of the quartz particles takes some time. A strong convective flow, high temperatures and uniform sand grain sizes enhance the dissolution of the sand grains in the silicate rich melt.

Gas bubbles and gases dissolved in the melt are formed during the melting process, resulting from:

- a. reactions of the batch materials;
- b. air inclusions;
- c. interaction of the glass melt and refractory materials.

The gases and gas bubbles have to be removed from the melt. This is called the fining of the glass melt. Generally bubble ascension in the viscous glass melt is relatively slow. The melt should be free of bubbles before it enters the feeders because there the viscosity of the melt is too high to permit enough bubble ascension.

Finally, homogenisation of the melt is necessary in order to avoid the occurrence of cords. In practice melting, fining and homogenisation can take place at the same time.

## **1.2 THE FINING PROCESS/ A GUIDE TO THIS THESIS**

The subject of this thesis is to provide a better insight in the fining process, both in qualitative and quantitative way.

Bubbles can be removed from the melt in two ways:

- by ascension to the surface of the melt;
- by complete dissolution in the melt.

Both mechanisms can be promoted with different fining methods. The most common method is the enhancement of the fining process by addition of

chemical fining agents. But for environmental reasons, the use of the (generally air-polluting) volatile chemical agents should be reduced. The fining process has to be optimized in order to avoid unnecessary losses of the chemicals. However, basic knowledge on the fining actions of the chemical agents is missing. Therefore this thesis is concerned with the chemical action of fining agents, both on a fundamental and on a practical basis.

Chapter 2 deals with the behaviour of gases and gas bubbles in the molten glass. The techniques to enhance the fining of the melt will be reviewed, and some of them will be discussed in detail. It will follow that a fundamental knowledge of the fining actions (qualitative and especially quantitative) of these methods is often missing. For the practical situation, the enhancement of the fining process with the aid of chemical fining agents is the most important. Therefore, this method is selected for further investigations.

The most commonly used chemical fining agents are NaCl, Na<sub>2</sub>SO<sub>4</sub>, As<sub>2</sub>O<sub>5</sub> and Sb<sub>2</sub>O<sub>5</sub>. The last three fining agents undergo a redox reaction in the molten glass. The polyvalent elements shift from the highest valency state to a lower valency state. This is accompanied by a release of gases (O<sub>2</sub> or SO<sub>2</sub>/O<sub>2</sub>) in the melt. These gases diffuse in the melt to existing bubbles, which will grow. The growing bubbles may also take up other gases from the melt and thus provide for the degassing of the glass melt. The so obtained larger bubbles ascend more easily to the surface of the melt. The composition of the melt appears to have a major influence on the action of the chemical fining agents. In the glass melts, the fining agents are surrounded by oxide ions. The effect of the composition is often estimated by the calculation of the "basicity" of the melt, a measure of the activity of the free oxide ions in the molten glass. Chapter 3 gives an outline of the knowledge on the influence of the basicity (or glass composition) on the redox reaction equilibria.

In chapter 4, some methods to analyse the redox reaction equilibria of the chemical fining agents Na<sub>2</sub>SO<sub>4</sub>, As<sub>2</sub>O<sub>5</sub> and Sb<sub>2</sub>O<sub>5</sub> are described. The knowledge of the temperature dependent equilibria will provide a better (quantitative) insight in the fining action of these agents. The analysing methods are also suitable for the examination of other important redox active elements in the molten glass, like iron and chromium. The valency state of these polyvalent elements determine the colour of the glass melt and the final product, and the heat transmission through the melt.



Two of the electrochemical techniques for the analysis of the redox reaction equilibria, the oxygen equilibrium pressure measurements and the square wave voltammetry measurements, are used to evaluate the behaviour of the redox couples  $\text{Fe}^{3+}/\text{Fe}^{2+}$ ,  $\text{Sb}^{5+}/\text{Sb}^{3+}/\text{Sb}^0$ ,  $\text{Ce}^{4+}/\text{Ce}^{3+}$ ,  $\text{Cr}^{6+}/\text{Cr}^{3+}/\text{Cr}^{2+}$  and  $\text{S}^{6+}/\text{S}^{4+}/\text{S}^0/\text{S}^{2-}$  in different glass melts. Chapter 5 describes the use of the oxygen equilibrium pressure measurements for the determination of the reaction enthalpy and entropy of the redox reactions. In addition to this, the applications of the square wave voltammetry measurements are discussed in chapter 5. The results of the measurements and the calculations are given in chapter 6.

Chapter 7 concerns with the practical applications of these investigations. The behaviour of a single bubble in the molten glass in industrial furnaces can be described with the aid of a computer model in which the values for redox reaction enthalpy and entropy, and the physical solubility of oxygen have to be inserted. With the aid of this program, the optimum process conditions for the fining of the melt to obtain a glass without gaseous inclusions can be predicted.

## Chapter 2

### The fining of glass melts

#### 2.1 INTRODUCTION

The objective of the fining process is the removal of bubbles and dissolved gases from the melt before the molten glass enters the working end of the furnace. Some physical and chemical methods to aid the removal of gases from the melt are known. In order to understand the fining mechanisms, some concepts that are related to the behaviour of bubbles in molten glass will be discussed in this chapter. Subsequently the fining methods will be treated in detail.

The behaviour of a bubble in molten glass can be characterized by its size, composition and position in the melt as a function of temperature. These parameters are influenced by:

- (selective) transport of gases to and from the bubble;
- the ascension of the bubbles due to the gravitation;
- forces, other than the gravitational force, that act upon the bubble.

Figure 2.1 shows a schematic presentation of a bubble ascending in a glass melt. Some parameters that influence its behaviour are displayed. They will be discussed in sequence in this chapter.

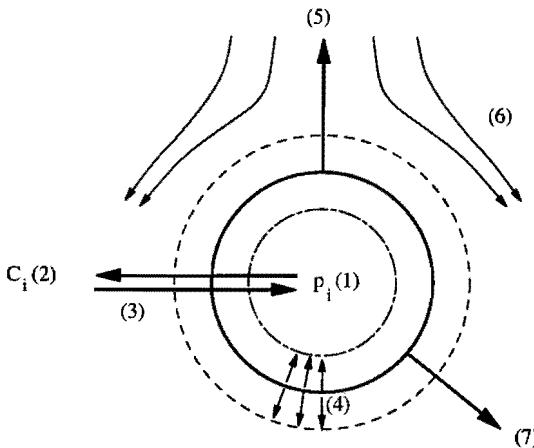


Figure 2.1  
A schematic presentation of the interactions of a bubble with the surrounding melt

- (1) The composition of the bubble is defined by the partial pressures of the gases (2.2.3).
- (2) The distribution of the gases between bubble and melt in equilibrium is governed by the solubility of the gases in the melt (both physical: section 2.2.4 and chemical: section 2.2.5).
- (3) Transport of the gases can take place if the gases in melt and bubble are not in equilibrium (2.2.6); the rate of transport is determined by the concentration gradient in the melt surrounding the bubble and the diffusivity values of the gases.
- (4) The transport of gases can result in the growth or shrinkage of the bubble (2.2.7). Changes in the bubble size can also be caused by coalescence or breaking up of bubbles (2.3.3).
- (5) Due to the gravitational force, the bubble ascends to the surface of the melt (2.3.1).
- (6) The melt exercises an opposing force to the movement of the bubble. The flow pattern of the melt around the bubble is determined by the movement of the bubble relative to the melt and the presence or absence of other bubbles or obstacles (2.3.2).
- (7) Forces, other than the gravitational force, can be generated in the melt. This can influence the motion of the bubble. Some physical fining methods like thermal-gradient induced fining and acoustical fining are based on this principle (2.5).

## **2.2 GASES IN GLASS**

The solubility of gases in molten glass is strongly influenced by the glass structure. Therefore, the glass structure and its relation to the glass composition is dealt with before the behaviour of the gases in the glass is discussed.

### **2.2.1 The glass structure**

The term "glass" is generally used for all inorganic, amorphous materials [1,2]. Although other definitions of "glass" are known, the glasses mentioned in this thesis meet this description. These glasses are produced by cooling the molten material to a rigid condition without crystallisation of the product. Their main constituent is  $\text{SiO}_2$ , to which various oxides of alkali and earth alkali ions are added.

The glass structure is built up by ions that are arranged more or less randomly. The difference between crystalline quartz and vitreous silica is represented in figures 2.2a and 2.2b.

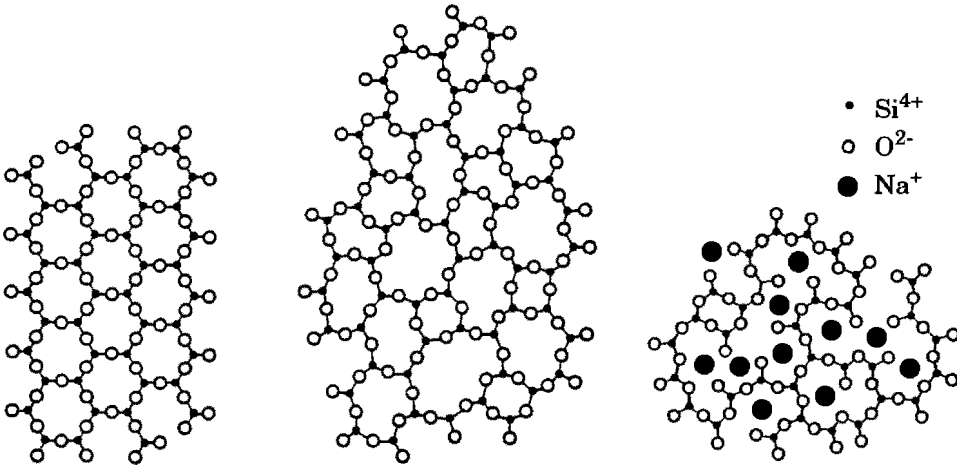


Figure 2.2a  
A two-dimensional  
presentation of  
crystalline quartz

Figure 2.2b  
A two-dimensional  
presentation of  
amorphous silica

Figure 2.3  
A two-dimensional  
presentation of a  
soda-lime glass

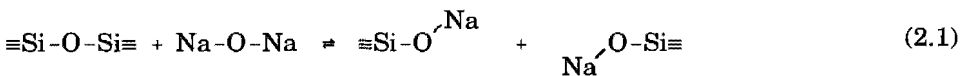
Glasses consist of network formers, network modifiers and intermediates [1,2].

### Network formers

Network formers are cations with a coordination number of 4 or 3, like Si and B. They form with anions, normally oxygen, a 3-dimensional network. The oxygen ions in this network are called "bridging oxygen ions". The binding of the network formers and the anions is covalent.

### Network modifiers

Alkali and earth alkali ions like Li, Na, K, Ca and Mg are network modifiers. The binding between the network modifiers and the anions is strongly ionogenic. The network modifiers can break up the covalent bonds between the network formers and the anions. An example is given in figure 2.3: addition of  $\text{Na}_2\text{O}$  to a pure  $\text{SiO}_2$ -glass leads to a change in the glass structure [2]:



This mechanism is important for the dissolution of gases in the melt, especially for the chemical solubility.

Some oxygen ions are attached to only one network former. These oxygen ions are called "non-bridging oxygen ions". Because the very stable covalent oxygen bridges are broken by the network modifiers, the viscosity of the glass melt will be reduced. Network modifiers also influence other properties of the glass melts and final products. For instance the chemical resistance decreases and the electrical conductivity of the final product generally increases.

### **Intermediates**

Certain elements like aluminium and lead may act as modifiers or as network formers. They are called intermediates. The binding of intermediates and the anions is slightly covalent. The coordination tendency of these ions is insufficient to establish a 3-dimensional network. However, the addition of intermediates to a silica glass does not lead to the complete breaking up of the polyeder network because the intermediates can establish a bond with two or three oxygen ions. The presence of the intermediates generally suppresses the tendency of the glass melt to form crystals during cooling.

Depending on the applications of the glass product, network modifiers and intermediates are introduced in the glass composition. The base composition of some glasses is given in appendix I [1]. The glass structure and the chemical composition have an enormous effect on many properties. The viscosity of the melt and the tendency to form crystals during cooling have already been mentioned. But also the solubility and mobility of gases in the melt, the basicity of the glass and the valency state of polyvalent elements depend strongly on the glass structure. The importance of these properties on the fining of molten glass will be explained in chapter 3.

#### **2.2.2 The occurrence of gases in glass**

During the melting process, chemical reactions between the batch materials take place, often resulting in the formation of gaseous components. Generally network modifiers like Na, Ca and Mg are added to the batch in the form of carbonates. Thus carbon dioxide enters the melt as the dissociation product of carbonates. Furthermore sulphur dioxide results from dissociation reactions of sulphates, and water vapour from hydrated batch materials. In addition, gases may be released by reactions of glass melt components with refractory material. Gases can also be introduced in the melt by air inclusions in the batch or absorption of components from the furnace atmosphere.

In the melt, gases can be present in different forms [1]:

- in bubbles;
- physically dissolved;
- chemically dissolved.

The solubility of the gases strongly depends on the glass structure.

### 2.2.3 Gases in bubbles

Bubbles in the glass melt can consist of one or more species. The most important are  $N_2$ ,  $O_2$ ,  $SO_2$ ,  $CO$ ,  $CO_2$ ,  $H_2O$  and Ar. The internal pressure of the bubble,  $P_{\text{bubble}}$ , is the sum of the partial pressures  $p_i$  of all gases present.

$P_{\text{bubble}}$  also depends on the atmospheric pressure  $P^0$ , the hydrostatic pressure and the surface tension [1]:

$$P_{\text{bubble}} = \sum_i p_i = P^0 + \rho \cdot g \cdot h + \frac{2\sigma}{R} \quad (2.2)$$

with $\rho$	= density of the melt	[kg·m <sup>-3</sup> ]
$g$	= gravitational constant	[9.8 m·s <sup>-2</sup> ]
$h$	= depth of the bubble in the melt	[m]
$\sigma$	= surface tension	[N·m <sup>-1</sup> ]
$R$	= radius of the bubble	[m]

### 2.2.4 Physically dissolved gases

Solid glasses are not perfectly tight against some gases. An explanation can be found in the open structure of the glasses. The holes with diameters of about 3 Å correspond to that of the sizes of many gas molecules or atoms. Therefore, it is possible for small particles to migrate through the glass [3].

Solid glasses can be seen as frozen-in melts as their structure is similar to that of the melts at the "solidification temperature", usually referred to as the transformation temperature. Therefore one must assume that gas atoms or molecules can be interstitially present in molten glass as well. Between the gases and the constituents of the glasses the bond strengths are small and the solubility discussed is called 'physical'. Examples of gases that dissolve mainly physically are noble gases and nitrogen under oxidizing conditions [3].

The solubilities of He, Ne and  $N_2$  in a soda-lime-silica melt under oxidizing conditions have been determined by Mulfinger [4,5,6]. The physical solubilities increase with increasing temperature. The enlarged specific volume of the glass melt probably might result in a higher physical solubility of these gases.

Solubilities calculated on the basis of the size of the gas particles and the distribution of the free sites in the melt are approximately one order of magnitude too high. To give agreement, the particle radii would have to be increased, and the discrepancy may thus be due to the greater space requirements of the particles due to their thermal vibrations [3].

With increasing particle size, the solubility diminishes. Apparently, the solubility is determined only by the number of free holes which are large enough to contain the gas molecules or atoms [3].

The composition of the melt has a significant influence on the physical solubility of He and Ne. With increasing alkali content, the solubility decreases [4]. According to Scholze, the alkali ions fill up the free volumes in the glass matrix (see figure 2.3) [3]. However, the decrease of solubility is less than the rate of filling. Probably the structure of the glass is expanded due to an increasing alkali content, thus creating additional cavities, which may partly compensate the first mentioned effect. At the moment, no theoretical estimation of the solubility of a gas is possible.

Generally the physical solubility in molten glass is low [3]. An increase of the gas concentration in the atmosphere provides for a proportional increase in the concentration of the gas in the glass. Consequently Henry's Law is valid. Only at very high gas pressures, the solubility can reach considerable values and then divergencies from Henry's Law occur [7] (see also chapter 2.2.6).

### 2.2.5 Chemically dissolved gases

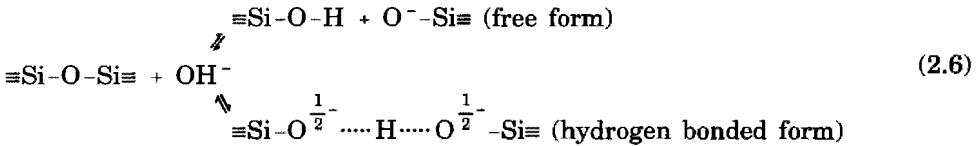
Degassing experiments at high temperatures yield large quantities of gases like H<sub>2</sub>O, CO<sub>2</sub> and SO<sub>2</sub>, and sometimes smaller amounts of N<sub>2</sub> and O<sub>2</sub>. These amounts are often much too large to be explained from their physical solubility. Some gases react with components of the glass melt [3] and are thus dissolved chemically.

The following reaction schemes have been proposed for the chemical solubility of water, carbon dioxide and sulphur dioxide, interacting with non-bridging oxygen ions [3]:



These reaction schemes suggest that the chemical solubility of  $\text{CO}_2$ ,  $\text{H}_2\text{O}$  and  $\text{SO}_3$  will increase with increasing concentration of free oxide ion,  $\text{O}^{2-}$ , or more strictly the ion activity, which is a measure of the basicity of the melt. The basicity of a glass melt increases at an increasing alkali content, and indeed the predicted dependency has been measured by Scholze and Franz [8]. The agreement however appeared to be only qualitative.

Budd suggested that hydroxylation of the silica network might take place by reaction with the  $\text{OH}^-$  ion [9]:



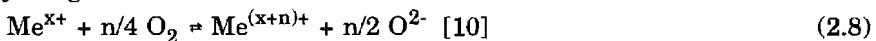
and the hydroxyl group will recombine to form  $\text{H}_2\text{O}$ :



Just as in the reaction scheme proposed by Scholze, the water content in the glass is proportional to the square root of the equilibrium water pressure [3,9].

At high temperatures, stable hydroxides connected to polyvalent cations exist and therefore the chemical solubility of water increases slightly with temperature [3]. Similar phenomena are not known for  $\text{CO}_2$  and  $\text{SO}_3$ . Their measured solubilities decrease with increasing temperatures for soda-lime glass compositions [3].

Oxygen,  $\text{O}_2$ , oxidizes polyvalent elements in the melt, such as iron and antimony. In general:

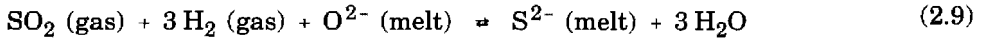


The chemical solubility depends on the concentration of the polyvalent elements, and thus on the content of impurities, colouring ions (iron, chromium) or fining agents (antimony, arsenic, sulphate/sulphide). The reaction scheme for the individual polyvalent elements will be given in chapter 3. The dependency of the solubility on the basicity of the melt is not correctly predicted by equation 2.8, as will be shown in chapter 3.

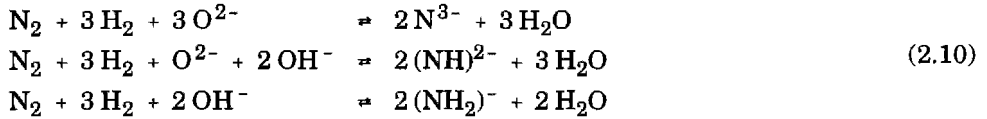
Oxidizing or reducing conditions in the atmosphere can influence the solubility of some gases [3]. The solubility of  $\text{SO}_3$  has already been mentioned. It is proportional to the  $\text{SO}_3$  partial pressure, but the latter is determined by the



SO<sub>2</sub> and O<sub>2</sub> partial pressures in the atmosphere. With SO<sub>2</sub> in the atmosphere, a change to reducing conditions causes the sulphur to enter in the glass as sulphide. If H<sub>2</sub> is used as a reducing agent the reaction may be written



Nitrogen can be present in the melt under reducing conditions both as =NH and -NH<sub>2</sub>:



In general, the chemical solubility of the gases is one or two orders of magnitude larger than their physical solubility [3]. Except for H<sub>2</sub>O, the chemical solubilities generally decrease at increasing temperatures.

## 2.2.6 Relationships

### 2.2.6.1 Physically dissolved gases-partial gas pressures

The amount of gas that can be taken up physically in the melt depends on the partial pressure of this gas in the surrounding atmosphere or in bubbles. An increase in the He, Ar, N<sub>2</sub> or O<sub>2</sub> concentration in the gaseous phase involves a proportional increase in the concentration of the gas in the molten glass under equilibrium conditions [7,11,12]. Only at very high gas pressures (for example 2 kbar in B<sub>2</sub>O<sub>3</sub>-glass, >10 kbar in K<sub>2</sub>O·4SiO<sub>2</sub> at 950°C), this statement no longer holds.

This deviation is probably due to the compressibility of the gases.

At equilibrium, the concentration of physically dissolved gas can be described by Henry's Law [13]:

$$C_i^* = L_i \cdot p_i \quad (2.11)$$

with  $C_i^*$  = concentration of gas i in the melt in equilibrium with the gas phase [mole·m<sup>-3</sup>]

$L_i$  = physical solubility of gas i in the melt [mole·m<sup>-3</sup>·bar<sup>-1</sup>]

$p_i$  = partial pressure of gas i in the gas phase [bar]

The diffusion coefficients of the gases depend on the temperature and the glass composition. According to Scholze [3], the order of magnitude of the diffusivity of small atoms like He at temperatures between 1000 and 1400°C is 10<sup>-8</sup> m<sup>2</sup>·s<sup>-1</sup>.

For the larger  $N_2$  molecules, the diffusion coefficient is about  $10^{-11} \text{ m}^2\cdot\text{s}^{-1}$  [3] and for  $O_2$  molecules, the measured diffusion coefficient in various glass melts is about  $10^{-10} \text{ m}^2\cdot\text{s}^{-1}$  [3,14,15]. Oxygen pressure measurements in glass melts indicate, that equilibration of the melt with the atmosphere takes several hours, even for very small glass samples [16,17]. In continuous operating glass melting tanks, the residence time of the melt is too short to establish equilibrium between melt and furnace atmosphere. Only in the top layer and at gas bubble interfaces equilibrium according to equation 2.11 can exist between the physically dissolved gas and the partial pressures of the different gas species.

#### 2.2.6.2 Physically and chemically dissolved gas

The chemically and physically dissolved gases can be correlated by the reaction equilibrium constant. Electron transfer reactions (redox reactions) are assumed to be fast at high temperatures. This is supported, but not proven, by the results of Rüssel [18]. He examined the ratio of reduced to oxidized iron as a function of (increasing) temperature in a glass containing only iron, both iron and arsenic or iron and manganese. At temperatures above  $400^\circ\text{C}$ , the ratio of reduced to oxidized iron in the three glasses started to diverge. If arsenic was present in the melt the redox ratio  $[\text{Fe}^{2+}]/[\text{Fe}^{3+}]$  increased relative to the redox ratio in the glass sample containing only iron. The ratio decreased if manganese was present. This shift in the redox state must have been caused by a (fast) redox reaction between the two polyvalent elements [18].

From theoretical considerations based on the experimental diffusion coefficients of iron, Rüssel predicted that the redox reaction between two polyvalent elements would always be in equilibrium at temperatures above  $625^\circ\text{C}$ , even if the temperature of the glass is changed with  $10^3 \text{ K}\cdot\text{s}^{-1}$ . At lower temperatures, it takes some time before the equilibrium is established [18].

If the electron transfer reactions are indeed fast, local equilibrium between physically and chemically dissolved gases exist. At longer distances, the diffusivities of the reacting species may play an important role.

#### 2.2.6.3 Dissolved gases and bubbles

Supersaturation occurs, when the total equilibrium gas pressure of the dissolved gases,  $\Sigma p_i$ , exceeds 1 bar. The formation of bubbles in a glass melt requires supersaturation. Gases can be released in the melt by chemical reactions. This can occur at a change of temperature, or a change of compo-

sition if the solubility of the gas is strongly dependent on temperature and composition. As discussed above the chemical solubility of gases depends upon composition. Bubbles can arise in the neighbourhood of a dissolving quartz grain, because the solubility of most gases is lower in silicate rich melts.

Supersaturation can also occur when the mechanism of solubility changes from chemical to physical. Here the polyvalent elements are of primary importance, e.g.



and



The considerations apply not only to oxygen but also to nitrogen, which can only be dissolved chemically under reducing conditions. When the atmosphere becomes oxidizing and oxygen diffuses relatively easily into the glass, according to the equations 2.10 bubbles containing nitrogen will develop [3] on the condition that nucleation sites are available (see section 2.3.5).

### 2.2.7 The fining process

Bubbles in the final product are undesirable, because they diminish the optical quality and decrease the strength of the glass product. Therefore, the bubbles must be removed from the melt. This is done during the so-called fining process. However, even in a melt which previously seemed plain, bubbles can appear. This is called reboil. The origin of reboil bubbles lies in inhomogeneities in the melt or a sudden increases in temperature [19]. In order to prevent reboil, not only the bubbles should be removed during the fining process, but also as much of the physically and chemically dissolved gases as is possible. This will lower the chance of supersaturation.

The fining process can be divided into two stages:

- the first stage, or primary fining, occurs at high temperatures. Because the chemical solubility of most gases decreases, gases are released in the melt. Especially if chemical fining agents are added to the batch, large amounts of fining gas will be generated. The melt becomes supersaturated with these gases. The gases diffuse to existing bubbles or form new ones. During this stage, small bubbles grow by taking up fining gases from the melt. Other gases, initially present in the bubble, will be diluted. This enhances the driving force for transport of these gases into the bubbles. This

effect is even more significant because the surface area of the bubbles increases during bubble growth [20]. The increased bubble ascension rate provides for a fast replacement of the melt at the surface of the bubble.

As a matter of fact, chemical fining agents aid the degassing of the glass melt at high temperatures because of the low melt viscosity and high gas diffusivities.

- the second stage, or "refining", takes place at lower temperatures, at the end of the glass tank (also called "refiner"). The remaining bubbles predominantly contain fining gases. Since the chemical solubility of these gases increase at decreasing temperature, the fining agents react with the fining gases from the bubbles. The partial pressures of the other gases in the bubbles increase. The melt contains hardly any gases at this point of the fining process, and may be able to take up the gases. The bubbles shrink and may even disappear completely [20].

So, at low temperatures, the chemical fining agents enhance the resorption of small bubbles.

### **2.3 THE BEHAVIOUR OF BUBBLES IN THE GLASS MELT**

Clouds of bubbles of various diameters exist immediately after the formation of a liquid phase. The number and composition of bubbles in the melt can change by:

- removal by buoyancy driven ascension to the surface of the melt;
- shrinkage which may lead to complete dissolution;
- selective dissolution into the melt;
- coalescention;
- breaking up of bubbles;
- formation of new bubbles (reboil).

#### **2.3.1 Buoyancy rate of bubbles [21]**

The gravity causes bubbles to rise to the surface of the melt.

The viscosity of a glass melt,  $\mu$ , at melting temperatures is in the order of 10 to 100 Pa·s. The density  $\rho$  of soda-lime glass melts is about 2300 kg/m<sup>3</sup>. The Reynolds number,  $Re = \rho \cdot v \cdot d / \mu$ , will therefore be much less than unity for small bubbles. There will be laminar flow around the bubble, and the bubble will maintain its spherical shape. The dependency of the Reynolds number on the viscosity of the melt and the bubble diameter is represented in figure 2.4.

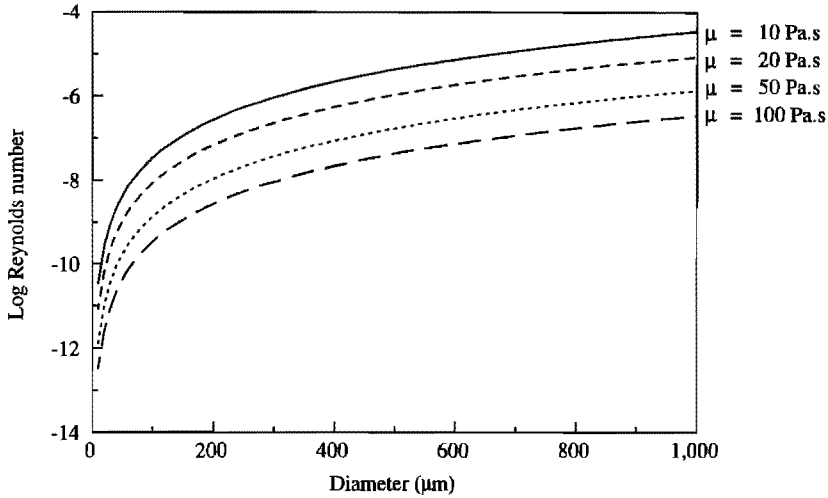


Figure 2.4.

The Reynolds number,  $Re=4 \cdot \rho^2 \cdot g \cdot R^3 / 9\mu^2$  of a bubble ascending in a melt (density= $2300 \text{ kg}\cdot\text{m}^{-3}$ ) as a function of viscosity and bubble diameter, according to Stokes' expression (2.16)

Hadamard and Rybczynski independently determined the rising velocity of a spherical gas bubble in an infinite fluid medium. The velocity strongly depends on the ratio of the dynamic viscosities of bubble and medium,  $\kappa$ .

$\kappa = \mu_{\text{bubble}} / \mu_{\text{medium}}$ . The magnitude of the terminal velocity  $v$  of a bubble with radius  $R$  is:

$$v = \frac{2R^2}{3\mu} \cdot \left( \frac{1 + \kappa}{2 + 3\kappa} \right) \cdot (\rho_{\text{medium}} - \rho_{\text{bubble}}) \cdot g \quad (2.14)$$

with  $g$  is the gravitational acceleration. The relation is valid for pure isothermal fluids for which the surface tension is uniform [derivation in 21]. For gas bubbles in a viscous glass melt, the ratio of the viscosities  $\kappa$  is approximately zero. Internal flow of the gas in the bubble can occur, and the gas molecules will adapt velocities equal to the velocity of the surrounding melt. The ascension rate of the bubble then equals:

$$v_{\text{Hadamard}} = \frac{\rho_{\text{melt}} \cdot g \cdot R^2}{3 \cdot \mu} \quad (2.15)$$

Surfactants present in the fluid may be adsorbed at the surface of the bubble and this will alternate the degree of internal circulation. The bubble can then be seen as a rigid sphere, and the effective viscosity of the bubble is approximated by  $\infty$ -value. The rising velocity can now be derived by substituting  $\kappa$  by  $\infty$ :

$$v_{\text{Stokes}} = \frac{2 \cdot \rho_{\text{melt}} \cdot g \cdot R^2}{9 \cdot \mu} \quad (2.16)$$

It is often referred to as Stokes' expression.

Traces of impurities in the liquid or melt can act as surfactants. Since small bubbles are more strongly affected by the surfactants, sufficiently small gas bubbles undergo a gradual transition as the bubble volume is increased from a noncirculating regime in which Stokes' law is applicable to a freely circulating regime in which Hadamard-Rybczynski's law is valid.

Gailhbaud and Zortea carried out bubble ascension experiments in a liquid with a temperature dependent viscosity [22]. They found a dependency of the rising velocity on the viscosity of the liquid. At high viscosities (>60 Pa·s) the ascension rate of the bubbles was even faster than  $v_{\text{Hadamard}}$ , and at a viscosity of 30 Pa·s or less, Stokes' law was applicable. Krämer [23] applied these results to a soda-lime-silica glass melt and predicted for temperatures up to 1200°C bubble ascension velocities described by equation 2.15, and for temperatures exceeding 1250°C according to Stokes' law (equation 2.16).

Publications on measurements of rising velocities of bubbles in molten glass have been only a few. Hornyak and Weinberg [24] measured the rise of a single bubble in a soda-lime-silica glass at 1200°C. They concluded that at these conditions the bubbles rise according to the equation derived by Hadamard. Němec [25] also carried out experiments in soda-lime-silica glass. He made photographs of groups of bubbles at 1400°C, and observed a behaviour according to Stokes' Law. This difference might arise from a difference in viscosity as predicted by Krämer. However, this dependency of the ascension rate on the viscosity is not found by Jucha [26], although he covered a wide viscosity range in his investigations of the rising velocity of single bubbles in borate glass melts. Even at low viscosity, the bubble motion corresponded with the Hadamard approach.

### 2.3.2 Ascension of clouds of bubbles

Two bubbles,  $B_1$  and  $B_2$ , influence each others velocity and also the rising path, depending on the distance between the bubbles and the radii. Both bubbles will go faster than for the case of single bubbles [27,28,29], large bubbles having a stronger influence on smaller ones than vice versa. The resulting velocity of bubble  $B_1$  can be estimated by assuming that the melt at the position of bubble

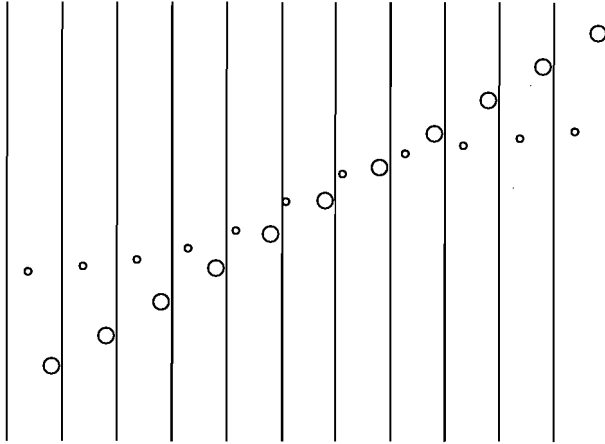


Figure 2.5  
The effect of a large bubble on a small ascending bubble in a viscous liquid

$B_2$  has a buoyance velocity identical to the rising velocity of the single bubble  $B_2$ . This motion in the melt diminishes the resistance of the melt to the ascension of bubble  $B_1$  [28] (see figure 2.5).

During the upward movement of a bubble, the same volume of fluid must move downward. For a large size of the vessel relative to the bubble diameter, this downward movement can be neglected. However, in a melt of finite dimension, this downward motion of the fluid can slow down the ascension of a bubble to some extent. This effect can be noticeable if the diameter of the bubble exceeds  $0.06 \cdot$ the diameter of the vessel [26].

For bubbles ascending in groups, the melt can not be regarded as an infinite medium. Bubbles in a cloud, especially at higher volume concentrations, have a very low rising speed relative to the velocity of a single bubble [29].

This phenomenon is identical to the settling down of slurries.

When a group of solid spheres moves through a limited space, the continuous phase will develop a velocity in the direction opposing the movement of the solid spheres.

With  $\varepsilon$  = the volume fraction of the fluid medium

$v$  = the settling velocity of the solid spheres

and  $u$  = the opposing velocity of the fluid

the relation between the velocities is given by [29]:

$$v \cdot (1 - \varepsilon) = u \cdot \varepsilon \quad (2.17)$$

The resulting stationary settling velocity of the solid spheres  $v_{\text{stationary}}$  can be obtained if Stokes' Law still holds [29]:

$$v_{\text{stationary}} = \frac{\varepsilon \cdot d_{\text{particle}}^2 \cdot g \cdot \Delta \rho}{18 \cdot \mu} \quad (2.18)$$

In very concentrated slurries, the flow pattern around the solid spheres does not resemble the flow around a single sphere. The resistance of the fluid medium increases, because the fluid has to move zigzag between the solid spheres. The solid sphere settling velocity can then be approached by the Ergun equation. It can be expressed as [29]:

$$v_{\text{stationary}} = \frac{\varepsilon^3 \cdot d_{\text{particle}}^2 \cdot g \cdot \Delta \rho}{150 \cdot (1 - \varepsilon) \cdot \mu} \quad (2.19)$$

This formula holds if the continuous phase  $\varepsilon$  is 60 volume-% or less. Other models to describe the settling down of slurries exist [29], for instance if the size distribution of the solid spheres is known. The larger solid spheres settle down more easily than smaller ones, thus causing a concentration gradient, which opposes the settling-down even more.

The equations for the 'hindered settling' are also applicable for ascending groups of bubbles on the condition that they behave like solid spheres.

### 2.3.3 Coalescention and breaking up of bubbles

Little is known about coalescence or the breaking up of gas bubbles in molten glass. Němec assumes that coalescention is the principal mechanism for bubble growth in the first part of the fining process [25]. When after some time the density of the bubbles diminishes, coalescention no longer plays a significant role [23].

### 2.3.4 Dissolution

Bubbles can shrink by the diffusion of gases from the bubble into the glass melt if the melt is undersaturated. The surface tension becomes more and more important as the bubble diameter decreases (see equation 2.2). At a certain critical diameter, the bubble becomes unstable. Finally, it will implode due to the large internal pressure ( $2\sigma/R$ ).



The surface tension of a soda-lime-silica melt at 1400°C is about 0.31 N·m<sup>-1</sup>. Greene observed a shrinking bubble (initially containing oxygen) in a soda-lime-silica melt. Just before the tiny bubble disappeared, its diameter was 76 μm [30]. Janssen examined the gas content of bubbles in glass products at room temperature [31]. The smallest bubble found was 35 μm.

### 2.3.5 Formation of new bubbles

Homogeneous nucleation of bubbles is unfavourable due to the last term in equation 2.2. The supersaturation of the gases must be enormous before the surface tension can be surmounted and formation of new bubbles takes place.

The investigations of Wilt concerning the formation of bubbles in beverages containing CO<sub>2</sub> demonstrate, that homogeneous nucleation is highly unlikely [32]. Supersaturation ratios (actual concentration of gas in the liquid, divided by the equilibrium concentration of this gas) of 1100 to 1700 would be required for homogeneous nucleation near room temperatures. Since this ratio is near 5 for opened carbonated beverages, this will not occur. The bubble formation results from heterogeneous nucleation at irregularly formed pores in the container walls. Supersaturation ratios of this order of magnitude in molten glass, as required for homogeneous nucleation, are equally unlikely.

Budd decreased the pressure  $P^0$  above plain glass melts and found that reboil bubbles occurred at pressures of 2700 to 19000 Pa at 1200°C, depending on the glass composition and particularly the water content in the melt [9].

Faile and Roy [11] also demonstrated, that spontaneous bubble formation can take place in glass melts that are supersaturated with physically dissolved gases. This can be explained by taking into account the ever present inhomogeneities in glass melts (cords, concentration variations), which make heterogeneous nucleation processes possible.

Bubbles can grow when the total gas pressure in the melt exceeds the pressure in the bubble that is formed:

$$p_{\text{melt}} = \sum p_i > P^0 + \rho \cdot g \cdot h + \frac{2 \cdot \sigma}{R} \quad (2.20)$$

but the growth of the bubbles also depends on the solubilities and diffusivities of the gases in the melt [33]. A mathematical model describing the growth of gas bubbles in glass melts is given in [33].

## 2.4 FINING METHODS

Bubbles are undesirable in the final product. They must be removed from the melt, before it reaches the low-temperature zone of the glass tank. Furthermore, most of the dissolved gases must be removed from the melt too, in order to lower the chance of reboil. Large bubbles can disappear by ascension due to the buoyancy forces to the surface of the melt, very small bubbles will implode. The elimination of bubbles of intermediate diameter (50  $\mu\text{m}$ -1 mm) is a difficult and slow process. Increasing of the temperature level of the tank leads to a decrease of the viscosity and this speeds up the buoyance rise of the bubbles. However, this method is costly and reduces furnace lifetimes. Therefore, investigations are done on other methods to increase the ascension rate or fasten up the resorption of the small bubbles. A speeding up of the degassing process can be achieved by transfer of impuls, energy or mass. Examples are:

- 1.- controlling of the flow of the melt in the glass tank. Each volume element in the molten glass should come close to the surface of the melt before entering the working end. Then the bubbles can cover the distance to the surface within a short time. Generally the flow is determined by:
  - furnace construction;
  - forced bubbling [34];
  - electric boosting;
  - local hot spots;
  - stirring.
- 2.- thermal-gradient-induced migration of bubbles;
- 3.- ultrasonic fining;
- 4.- imposing of pressure or vacuum above the melt [35];
- 5.- addition of chemical fining agents. The fining agents release gases during an increase of the temperature, and these gases will diffuse into bubbles which will grow.

Both thermal-gradient-induced migration of bubbles and ultrasonic fining can be used for the fining of molten glass made under zero-g conditions [36]. Upon close consideration of the literature on these two physical fining methods (section 2.5), it will be decided that these methods are unsuitable for practical application in industrial glass melting tanks.

## 2.5 SOME PHYSICAL FINING METHODS

### 2.5.1 Thermal-gradient-induced migration of bubbles

The surface tension of a bubble in molten glass,  $\sigma$ , depends on the temperature. For most glass compositions, the surface tension slightly decreases at an increasing temperature. Temperature differences can therefore produce a displacive force on bubbles. The contribution of thermal migration to the velocity is given by [37]:

$$v_{\text{thermal gradient}} = \frac{R \left( \frac{d\sigma}{dT} \right) \left( \frac{dT}{dx} \right)}{2 \mu} \quad (2.21)$$

with  $R$  = radius of the bubble [m]  
 $d\sigma/dT$  = surface-tension gradient [ $\text{N}\cdot\text{m}^{-1}\cdot\text{K}^{-1}$ ]  
 $dT/dx$  = temperature gradient [ $\text{K}\cdot\text{m}^{-1}$ ]  
 $\mu$  = viscosity of the melt [ $\text{Pa}\cdot\text{s}$ ]

Mattox et al [37] investigated the influence of thermal-gradient-induced migration of bubbles in four different glasses. One of them was borax. Borax glass (69.2  $\text{B}_2\text{O}_3$ -30.8  $\text{Na}_2\text{O}$ ) has a surface tension gradient  $d\sigma/dT$  of  $-7.6\cdot 10^{-5} \text{ N}\cdot\text{m}^{-1}\cdot\text{C}^{-1}$ . Its viscosity at  $800^\circ\text{C}$  is about  $1.5 \text{ Pa}\cdot\text{s}$ . A bubble with a radius of  $150 \mu\text{m}$  would reach a velocity of  $114 \mu\text{m}\cdot\text{s}^{-1}$  in a temperature gradient of  $300^\circ\text{C}/\text{cm}$ . In continu tanks, temperature gradients never reach such values, and their influence on bubble motion is negligible. However, thermal-gradient induced migration may be the principal mechanism of bubble elimination in sealing and enameling operations, and in the production of glass in a low-gravity environment [37].

### 2.5.2 Ultrasonic fining

According to Klein [38], sonic and especially ultrasonic waves, generated in the melt, have a degassing effect. Krüger [39] indeed succeeded in obtaining a bubble-free glass melt using a sound field with a frequency of  $16 \text{ kHz}$  at  $1350^\circ\text{C}$ . An identical melt, that was not treated with ultrasonics, still contained a lot of bubbles after the same period.

Eden [40] optimized the device of Krüger by supplying a strong, stationary magnetic field to the sound field. In this way, a powerful magnetic vibration is obtained in the melt. At  $1100^\circ\text{C}$ , a melt initially containing a large number of bubbles was made bubble-free in half an hour. And some other authors [41] also have demonstrated that sonic energy can indeed be applied to aid the fining of molten glass.

The effect of sonic and ultrasonic waves on bubbles in a liquid is plentyfold and very complicated. Therefore the theory of wave movement will be explained here in some detail, and subsequently the mechanisms that can play a part in the degassing of glass melts will be discussed.

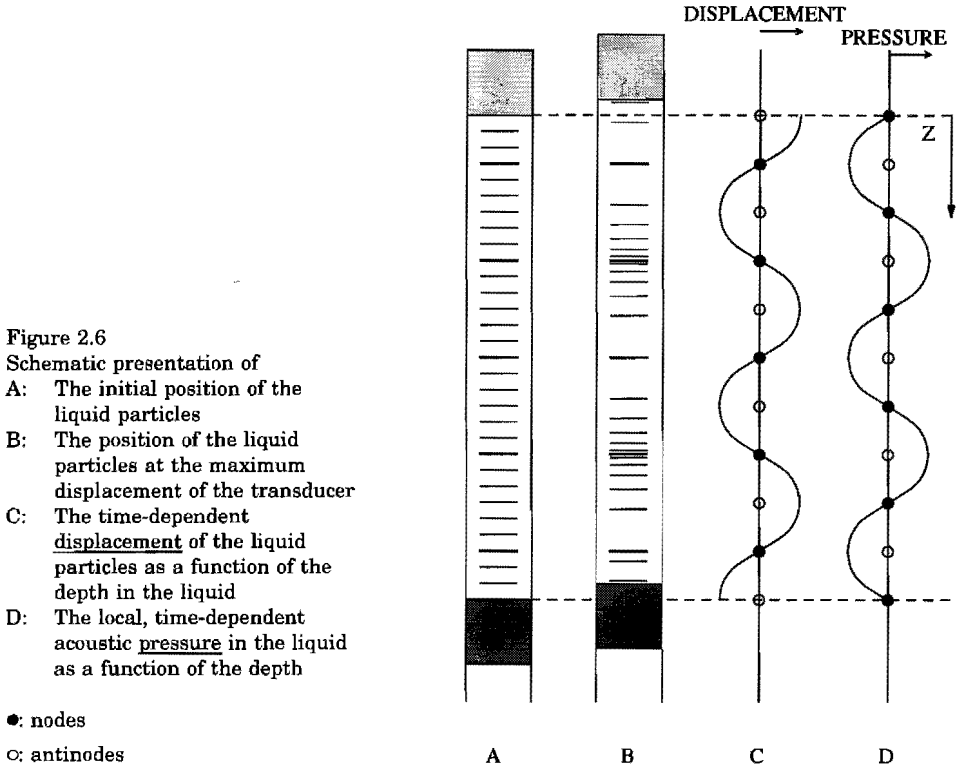
### 2.5.2.1 The acoustic field

A travelling sound wave can be introduced in a liquid with the aid of a transducer. The transversal wave should have a frequency of 10 till 20 kHz. The molecules in the liquid are forced to follow the movements of the sound wave. This alternately provides for a compression and dilatation of the liquid particles (see figure 2.6A and B).

The sound wave travels through the liquid until it reaches the surface. Here, the wave is reflected. Because the reflection appears at a free surface, no difference in phase occurs (see fig 2.6). If the sound wave reaches a wall, the reflected wave will lag  $\frac{1}{4}\lambda$  in phase with the original wave.

The opposing waves interfere with one another. The displacement of the liquid particles is amplified. The amplitude of the final wave can be estimated by summation of the amplitudes of the individual waves. The result is a standing wave with an amplitude, that is only limited by the attenuation of the waves in the liquid.

The local time-dependent displacement is represented in figure 2.6C as a function of the position in the liquid. The displacement of the liquid particles at the free surface will reach some maximum value. This maximum displacement also occurs at other locations in the melt, at inter distances of  $\frac{1}{2}\lambda$ . These positions are represented by  $\circ$  in figure 2.6C. At the intermediate positions, represented by a  $\bullet$  in figure 2.6C, the liquid particles remain at the same place: the displacement there is always zero. At these positions, the changes in the pressure vary from a maximum to a minimum value. Here the so-called pressure antinodes are located (a  $\circ$  in figure 2.6D). At the positions where the displacement of the liquid can reach maximum values, the pressure in the liquid remains constant. The so-called pressure nodes (a  $\bullet$  in figure 2.6D) are located at a distance of  $n \cdot \frac{1}{2}\lambda$  of the free surface (with  $\lambda$ =length of the sound wave, and  $n=0,1,2,\dots$ ). As can be seen from figures 2.6C and 2.6D, a lag of  $\frac{1}{4}\lambda$  between the displacement of the liquid particles and the local pressure occurs.



At a solid wall, the displacement of liquid particles is inhibited. Here, a pressure antinode is located. Due to the alternating pressures, the mass transfer which determines the corrosion rates of the refractory wall material is enhanced [42]. This is a serious drawback for the practical application of this method.

Note:

The location of pressure nodes and antinodes is well-defined if the length of the vessel is equal to  $n \cdot \lambda$ , and its diameter small in comparison to the length of the sound wave. In vessels of other geometry, pressure nodes and antinodes can appear too, but the exact locations are less distinct.

### 2.5.2.2 The effect of a standing acoustic wave on bubble behaviour

In a standing wave, dissolved gases will form new bubbles, and small bubbles can combine to larger ones [38]. Various explanations for these phenomena have been proposed in literature.

### The translation of bubbles due to acoustic migration

- Bubbles in a standing acoustic wave not only experience a time-dependent pressure, but also an (alternating) pressure gradient along the z-axis (see figure 2.7). This causes a translational force in the (temporary) direction of the lowest pressure. The magnitude of this force  $F_a$  is proportional to the bubble volume [43]:

$$F_a = -V(t) \cdot \nabla p_a(z,t) \quad (2.22)$$

$$\text{and } p_a(z,t) = P_a \cdot \sin\left(\frac{2\pi z}{\lambda_z}\right) \cdot \sin(\omega t) \quad (2.23)$$

with $V$	= time-dependent bubble volume	[m <sup>3</sup> ]
$F_a$	= acoustic force	[Pa·m <sup>2</sup> ]
$p_a$	= local, time-dependent pressure in the liquid	[Pa]
$P_a$	= applied acoustic pressure	[Pa]
$z$	= distance to the surface of the melt (see figure 2.7)	[m]
$\lambda_z$	= length of the sound wave in the z-direction	[m]
$\omega$	= applied frequency of the acoustic field	[Hz]

The bubble volume is not constant, because the bubble radius oscillates about its equilibrium value in the acoustic field. Therefore, the average translational force is only zero at a pressure node. The direction of the average force depends on bubble radius and frequency of the acoustic wave. The resonance frequency of a bubble,  $\omega_0$ , is given by [43]:

$$\omega_0^2 = \frac{3 P^0}{\rho \cdot R_n^2} \quad (2.24)$$

with $P^0$	= hydrostatic pressure (depends on the vertical position in the melt)	[Pa]
$\rho$	= density of the liquid	[kg·m <sup>-3</sup> ]
$R_n$	= equilibrium bubble radius	[m]

The volume of bubbles with a resonance frequency that is larger than the applied frequency, oscillate with the applied frequency. When the pressure is at its maximum value, the bubble volume is small. It is then forced to the nearest pressure node, but the exercised force is small. The bubble grows when the pressure decreases, and when the pressure reaches its minimum value, the bubble volume is at its maximum. The bubble is driven with greater force to the nearest pressure minimum, and this is located at the pressure antinode.

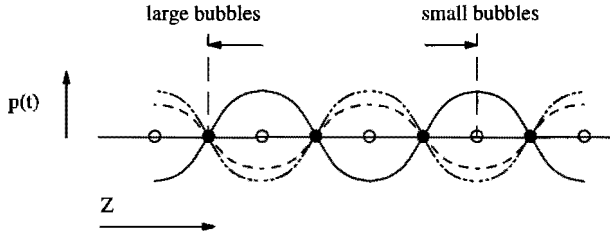


Figure 2.7  
The movement of 'large' and 'small' bubbles under the influence of the acoustic force

Therefore, sufficiently small bubbles travel to the pressure antinodes.

If the resonance frequency of the bubble is less than the applied frequency of the acoustic field, the bubble is not able to keep up with the applied frequency. The larger bubbles are forced towards a pressure node, where the bubbles do not experience the influence of the alternating pressure.

The time averaged acoustic force  $\bar{F}_a$  in the  $z$  direction is given by [43]:

$$\bar{F}_a = \frac{2 \pi^2 R_n^2 P_A^2}{3 P_0 \lambda_z \left( 1 - \frac{\omega^2}{\omega_0^2} \right)} \sin \left( \frac{4 \pi z}{\lambda_z} \right) \quad (2.25)$$

with  $P_A$  = acoustic pressure amplitude [Pa]  
 $\lambda_z$  = wavelength in the  $z$  direction [m]

In molten glass, the resonance frequency of the bubbles is generally larger than 10 kHz if the bubble size is less than 1 mm. Therefore, the small bubbles in a standing wave tend to travel to the antinode (see figure 2.7). At the pressure antinodes (and nodes), the different sized bubbles are concentrated and can easily coalescent [39,40,41,44].

### The translation of the bubbles due to Bjerknes forces

- Oscillating bubbles in a sound field exercise a force on one another. The velocity of fluid particles between the bubbles, caused by the motion of the bubbles, is larger than on the other sides of the bubbles. Therefore, the pressure in the fluid between the bubbles is lower, and the bubbles exercise an attractive force, a so called Bjerknes force. Analysis of the Bjerknes

force indicates, that when two spheres pulsate with the same frequency, but with different velocities  $v_1$  and  $v_2$ , an average force  $\bar{F}$  sets in [44]:

$$\bar{F} = 4 \pi \rho R_1^2 R_2^2 \left( \frac{v_1 v_2}{l^2} \right) \cos \varphi \quad (2.26)$$

with  $R_{1,2}$  = radii of bubbles 1 and 2 [m]

$l$  = distance between the centra of the bubbles [m]

$v_{1,2}$  = grow rate of the bubble [m·s<sup>-1</sup>]

$\varphi$  = phase difference [°]

According to Shutilov [45], experiments have indicated that agglomeration of bubbles during ultrasonic degassing of liquids is mainly caused by Bjerknes forces.

### Growth of bubbles due to rectified diffusion

- In a standing wave, a bubble alternately contracts and expands. During contraction, the pressure of the gases in the bubble increases, and the gases tend to diffuse out of the bubble. Similarly, when the bubble expands, the pressure decreases and gases could diffuse from the melt to the bubble. However, the surface area of the bubble is larger during the expanded period. As a result of this, more gas will enter the bubble during the expansion period than leave during the contracted period of the bubble, resulting in a net time averaged flux of gas into the bubble. This phenomenon is called 'rectified diffusion' [46].

Rectified diffusion only comes into action if the pressure in the liquid exceeds a threshold value. Depending on the equations used, the calculated threshold value for a soda-lime-silica melt at 1400°C varies from 0.3 [47] to 0.9 bar [46]. The growth rate of an air bubble of 100 μm diameter in saturated water would account to 2·10<sup>-8</sup> m·s<sup>-1</sup> in an 11 kHz sound field. The growth rate of air bubbles in glass melts due to rectified diffusion is, according to the equations, a factor 3 less [46], about 24 μm·hour<sup>-1</sup>. Therefore it can be concluded that rectified diffusion will not play an important role in the acoustic fining of glass melts.

### Bubble growth owing to the "shell effect" [46]

- When a bubble contracts, the thickness of a spherical shell of liquid of constant volume surrounding the bubble increases. The gas concentration gradient between bubble and bulk of the liquid, which is thought to be



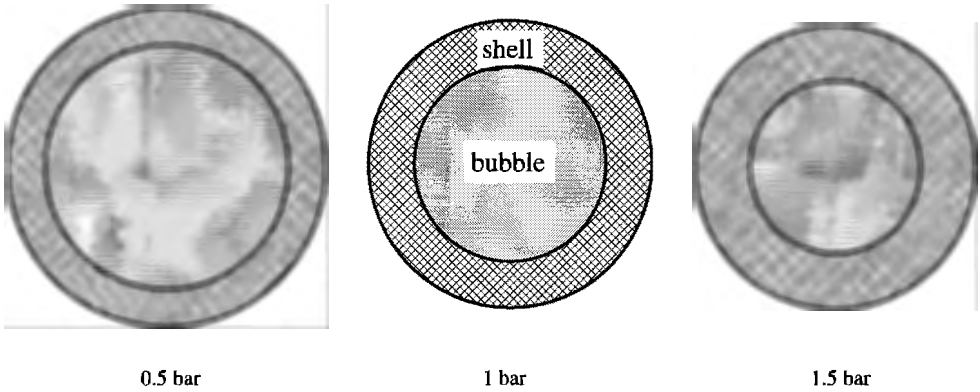


Figure 2.8

The change in thickness of a spherical shell of liquid surrounding the bubble under the influence of the acoustic field. The concentration gradient of gas between bubble and bulk of the liquid is thought to be entirely located in this spherical shell

entirely located in this shell, is thereby reduced, and the rate of diffusion of gas away from the bubble wall decreases. When the bubble expands, the thickness of the spherical shell surrounding the bubble decreases, the concentration gradient increases and so the rate of diffusion of gas towards the bubble increases. The net effect leads to an extra increase of the rectified diffusion process, apart from the increase due to the expanded bubble surface [46].

By formulating two time-dependent boundary layers (one during expansion and one during contraction), Skinner was able to derive a set of mathematical equations for this process [48]. But even if this effect is taken into account, the theory of the rectified diffusion effects does not account for the rapid transport of gas towards the bubble that has been observed during experiments in water [49]. Therefore it is assumed that another phenomenon, called "acoustic streaming", plays a mayor role.

### **Growth of bubbles due to acoustic streaming**

- When a bubble is pulsating in a sound field, crispations can occur on the surface, even if the radius of the bubble is smaller than the resonant size for volume oscillations. Due to the crispations, the surface of the bubbles are continuously renewed.

Gould demonstrated, that the acoustic streaming accompanying the surface activity can intensify the growth rate of the bubble up to twentyfold [50]. He also gave a mathematical approach to acoustic streaming. Mironov combined acoustic streaming with rectified diffusion in a mathematical approach [52].

The extent of the phenomena, mentioned in this section, on the behaviour of gas bubbles in a glass melt is unknown at the moment.

### 2.5.2.3 Application of sound waves in molten glass

A standing wave results when an infinite number of travelling waves meet. The amplitudes of the waves can simply be added. However, due to attenuation, the amplitude of the wave decreases.

Attenuation of the sound signal arises due to geometrical dispersal, reflection and absorption in the fluid. The absorption depends on viscosity, heat transfer capacity and molecular relaxation. Attenuation in molten glass will be very high because of the high viscosity values. Therefore, it is difficult to obtain standing waves with large amplitudes in a glass melt.

Eden introduced the standing sound waves in a small platinum crucible [40]. Some losses due to reflection occurred, but the experiment with a 100 kHz field resulted in bubble-free glass, while a reference melt still contained an enormous number of bubbles. Spinosa and Ensminger generated a travelling wave and predicted, that travelling waves can also achieve the desired effect [41]. However, they could not find their assumption with theoretical equations or practical results.

In practice, installation of ultrasonic devices in the fining area of an industrial tank will be very difficult [52]. Besides, extra corrosion of the refractory material is to be expected due to the local vibration in the melt. Therefore ultrasonic fining has mainly been used for experimental studies, for example under zero-g conditions [36].

## 2.6 CHEMICAL FINING AGENTS

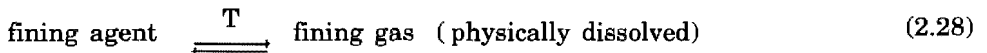
Transfer of a single gas  $i$  from the melt to a bubble can be described by

$$J_i = k_i \cdot (C_{i,\text{melt}} - C_{i,\text{bubble}}) \quad (2.27)$$

where $J_i$	= flux of gas $i$	[mole·m <sup>-2</sup> ·s <sup>-1</sup> ]
$k_i$	= mass transfer coefficient	[m·s <sup>-1</sup> ]
$C_{i,\text{melt}}$	= concentration of physically dissolved gas $i$ in the melt far away from the bubble	[mole·m <sup>-3</sup> ]
$C_{i,\text{bubble}}$	= concentration of physically dissolved gas $i$ at interface melt/bubble, where equilibrium with the pressure of gas $i$ in the bubble according to Henry's law is established	[mole·m <sup>-3</sup> ]

The change of bubble composition depends on the ratio's of the  $J_i$ -values for the different diffusing gases, the change in bubble size depends on  $\Sigma J_i$ .

The transport of gases can be enhanced by an increase (or decrease in case of shrinking bubbles) of the gas concentration in the melt. Since the chemical solubility is much larger than the physical solubility, a way to achieve supersaturation of a gas in the melt is the release of chemically bounded gas. Fining agents are able to release large amounts of gases at a (small) increase of temperature:



This chemical fining process is most effective if the gases are released when the viscosity of the melt is low, this is at high melting temperatures.

Generally a chemical reaction can be described by:



The reaction equilibrium can be described by the reaction equilibrium constant  $K(T)$ :

$$K(T) = \Pi_i (a_i)^{v_i} \quad (2.30)$$

with  $a_i$  = activity of component  $i$

$i$  = reacting species (ions or molecules)

$v_i$  = change in moles of component  $i$  on reaction

$v_i$  is negative for reactants and positive for products

$\Pi_i$  = product of factors  $i$

The dependency of K on the temperature is given by

$$K(T) = \exp \left( \frac{-\Delta H}{R_g \cdot T} + \frac{\Delta S}{R_g} \right) \quad (2.31)$$

with  $\Delta H$  = enthalpy of the reaction [J·mole<sup>-1</sup>]

$\Delta S$  = entropy of the reaction [J·mole<sup>-1</sup>·K<sup>-1</sup>]

$R_g$  = molar gas constant = 8.314 J·mole<sup>-1</sup>·K<sup>-1</sup>

$\Delta H$  and  $\Delta S$  are assumed to be temperature independent in the relevant temperature range.

For an efficient fining agent,  $\Delta H$  should be large. The temperature range at which the equilibrium constant changes from a very small value to a large value depends on the nature of the fining agent. The melting temperature differs for various glass compositions and glass furnaces. The most efficient fining agent therefore depends mainly on the type of glass. Some examples of fining agents are [1]:

- NaCl. NaCl does not react, but it evaporizes into bubbles as NaCl-vapour at high temperatures. It is used in glasses with a very high melting temperature, like some borosilicate glasses.

- oxides of polyvalent elements like arsenic and antimony. Arsenic is introduced in the glass melt as arsenate or as  $As_2O_3$ . The last component has to be oxidized to  $As_2O_5$  to be active as fining agent. This can be promoted by the addition of nitrate to the batch. The pentavalent arsenic then reacts at 1400-1500°C into the trivalent form, and thereby releases  $O_2$ . It is still used in lead glass and lead cristal glass.

Antimony is also used in the trivalent form,  $Sb_2O_3$ , in combination with an oxidant.  $Sb_2O_5$  generally dissociates at a lower temperature than  $As_2O_5$ , and therefore it is used in glasses in tanks with temperature levels mainly below 1450°C, like TV-screen glass melts.

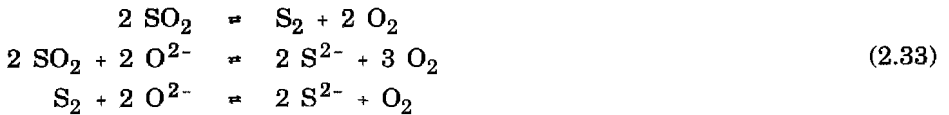
- sulphates like  $Na_2SO_4$ . The oxygen pressure has probably a great effect on the reaction mechanism of sulphate [53]. Under oxidizing conditions, sulphate will dissociate at temperatures above 1350°C to form both  $SO_2$  and  $O_2$  gas:



$SO_2$  and  $O_2$  are present as physically dissolved gases in the glass melt and act as fining gases. The other components are dissolved in the melt.

More reducing conditions, for instance when the oxygen equilibrium pressure is less than  $10^{-5}$  atm, may occur when reducing agents such as

carbon are added to the batch. Under these conditions sulphate,  $\text{SO}_4^{2-}$ , starts to dissociate at lower temperatures, when viscosities might still be high. Under very reducing conditions, sulphur dioxide will probably react to gaseous  $\text{S}_2$  and  $\text{S}^{2-}$ , while the reducing agent takes up the oxygen. Schreiber has proposed the following reaction scheme [53]:



$\text{S}_2$  is probably released as a gas and diffuses as a fining gas to existing bubbles,  $\text{S}^{2-}$  easily dissolves in the melt.

**NOTE :**

Sulphate/sulphide is used as fining agent in green container glass, float glass, E-glass and some technical glasses. Strangely enough, hardly anything is known about the exact fining mechanism and the equilibrium constants of the reactions 2.32 and 2.33.

The reactions of the chemical fining agents will be discussed in more detail in chapter 3.

## 2.7 PUBLISHED RESEARCH DATA ON CHEMICAL FINING AGENTS

Although chemical fining agents are generally applied, the knowledge on the fining mechanism is insufficient for optimizing the fining process or predicting the effect of changes in the process conditions.

The experimental investigations and quantifications on the fining action of chemical agents can be divided into three groups:

- a. experimental investigations on the amount and/or composition of gas bubbles in quenched glass samples after different melting procedures;
- b. determination of the equilibrium of the (proposed) reversible fining reaction of the chemical agent or the amount of the produced fining gases;
- c. mathematical calculations of the effect of chemical fining agents on the behaviour of bubbles in the glass melt.

**Ad a.**

In these investigations, raw batch materials are mixed using a certain concentration of the required fining agent. The batch is melted at a fixed temperature during a fixed period. Then the melt is cooled rapidly, and the amount of the

remaining bubbles, their size distribution and/or their composition is determined. This method is used to distinguish between the fining qualities of different chemical agents at different concentrations or redox levels, or to optimize the temperature and duration of the fining process. Little information is obtained on the actual mechanism of the fining process. The results are therefore hardly applicable for glass melts with different compositions. Furthermore, these experiments can generally not be used to predict the efficiency of the chemical agents in industrial continuous operating glass tanks, because no account has been given on the influence of other process parameters like furnace atmosphere and temperature distribution in the tank.

In the early days Gehlhoff [54] compared the amount of bubbles remaining in glasses melted from batches with sodium sulphate, carbon, potassium nitrate, arsenic, ammonium salts, alkali chlorides and combinations of these chemical agents. Mulfinger [55] analysed the bubbles remaining in an arsenic-containing glass and concluded that the bubbles take up oxygen from the dissociation of arsenic (V) oxide. The effects of the addition of  $\text{CeO}_2$ ,  $\text{MnO}_2$ ,  $\text{Fe}_2\text{O}_3$  or  $\text{Cr}_2\text{O}_3$  to the batch on the remaining number of bubbles after a certain melting procedure was investigated by Apak and Cable [56] and van Erk reported the influence of fluorides on antimony fining [57].

Often, the results of the experimental investigations are contradictory, probably because not all conditions of the experiments have been taken into account. For example, the fining action of arsenic oxide is sometimes attributed to the enhanced (chemical) solubility of oxygen [58], or the increase of the  $\text{CO}_2$  solubility in the melt [59] or the decomposition of  $\text{As}_2\text{O}_5$  to  $\text{As}_2\text{O}_3$  at high temperatures, together with the formation of  $\text{O}_2$ , that diffuses into existing bubbles [60].

#### **Ad b.**

The fining reactions of the chemical agents are all redox reactions (see chapter 3).

Investigations of the temperature dependent equilibrium constants of most of the redox reactions can be performed indirectly, by measuring the oxygen pressure in the melt as a function of temperature [61,62,63,17]. The amount of free  $\text{O}_2$  in the melt increases as the temperature increases, due to the shift of reaction 2.8 to the left. The oxygen molecules can be transported to existing bubbles. Then the bubbles will grow and leave the melt by ascension. This

method can be used to make a comparison between the oxygen release from different chemical fining agents during the heating of the melt. The results can not be used to predict the oxygen liberation in other glass melt compositions.

Another method to determine the equilibrium of a proposed redox reaction is to equilibrate a melt with a certain concentration of a fining agent at a fixed temperature with a well defined atmosphere. The melt is then cooled rapidly, and the valency state of the fining agent is examined. Assumptions are made on the oxygen and/or sulphur dioxide pressures, and the reaction equilibrium constant  $K(T)$  is calculated from equation 2.30. This method is applicable if the melt contains only one polyvalent element and if the content of physically dissolved oxygen is low (see chapter 4.2). By this method, the behaviour of  $\text{As}^{5+}/\text{As}^{3+}$  [64],  $\text{Sb}^{5+}/\text{Sb}^{3+}$  [65,66,67],  $\text{Ce}^{4+}/\text{Ce}^{3+}$  [65,68],  $\text{Fe}^{3+}/\text{Fe}^{2+}$  [69,70], and various other polyvalent elements [65] have been studied, mostly in model soda-lime-silica glasses. Furthermore, some investigations have been carried out on the reaction equilibria of  $\text{SO}_4^{2-}/\text{SO}_2$  and  $\text{Fe}^{3+}/\text{Fe}^{2+}$  in glasses containing both sulphur and iron [71,72,73].

A requirement of this method is, that the reaction scheme is known in order to calculate the reaction equilibrium constant according to equation 2.30.

### **Ad c.**

Mathematical models have been drawn up to predict the behaviour of single bubbles in a glass melt under different conditions without taken into account the chemical fining reactions [74-82]. Other authors have included the chemical reactions in their models [83,84,85,20]. In this way, no expensive and time-consuming experiments have to be performed to estimate the effect of a change in concentration of the fining agent, temperature of the melt etc. Because the models are based on the mass transfer of the gases between the bubble and the surrounding melt, the following factors have to be known:

- the concentrations of all dissolved gases in the melt;
- the temperature dependent solubilities of the gases;
- the temperature dependent diffusivities of the gases.

The concentrations of the released fining gases can be calculated from the reaction equilibrium constants of the fining reactions. Therefore, it is important that these data are available for all possible industrial glass compositions.

## 2.8 OBJECTIVE OF THIS STUDY

A lot of questions on the mechanisms of different fining methods remain. However, the practical application of the physical fining methods described in this chapter, thermal-gradient-induced fining and acoustic fining, seems unlikely. Chemical agents will also in the future be necessary for the fining of molten glass. The fining process could be optimized if the reaction mechanisms and the reaction equilibria are known as a function of glass composition, melting temperature etc.

Therefore the main objective of this thesis is to investigate the behaviour of polyvalent elements in molten glass, and to determine the influence of these elements on the amounts of gases released in the melt. This can be achieved by redox equilibria measurements (by electrochemical methods or wet-chemical analysis) or oxygen pressure measurements in order to obtain redox (fining) reaction equilibria constants. Then these results are used in a computer model which describes the fining gas concentrations in the glass melt as a function of the position in an industrial furnace. The results are used, in combination with the calculated flow pattern in the glass tank, to predict whether small bubbles in the melt are able to grow and ascend or dissolve completely (see chapter 7). In this way, the fining action of chemical fining agents in an industrial tank can be studied quantitatively in detail.



## Literature

- [1] Simonis, F. (editor)  
"NCNG-Glascursus"  
TPD-TNO in samenwerking met de gezamenlijke Nederlandse Glasindustrieën (1990)
- [2] Scholze, H.  
Glas. Natur, Struktur und Eigenschaften  
Springer-Verlag Berlin Heidelberg New York (1977)
- [3] Scholze, H.  
Gases in glass  
*Proceedings of the 8<sup>th</sup> Int. Congress on Glass* (1968) p.69-83  
Society of Glass Technology Sheffield
- [4] Mulfingher, H.O.; Scholze, H.  
Löslichkeit und Diffusion von Helium in Glasschmelzen  
*Glastechnische Berichte* **35** (1962) no.12 p.495-500
- [5] Mulfingher, H.O.  
Physical and chemical solubility of nitrogen in glass melts  
*Journal of the American Ceramic Society* **49** (1966) no.9 p.462-467
- [6] Scholze, H.; Mulfingher, H.O.; Franz, H.  
Bestimmung der physikalischen und chemischen Löslichkeit von Gasen in Glasschmelzen  
*Tech. Papers Intern. Congr. Glass, 6th* (1962) p.230-248  
Washington D.C.
- [7] Faile, S.P.; Roy, D.M.  
Solubilities of Ar, N<sub>2</sub>, CO<sub>2</sub>, and He in glasses at pressures to 10 Kbars  
*Journal of the American Ceramic Society* **49** (1966) no.12 p.638-643
- [8] Franz, H.; Scholze, H.  
Die Löslichkeit von H<sub>2</sub>O-Dampf in Glasschmelzen verschiedener Basizität  
*Glastechnische Berichte* **36** (1963) p.347-356
- [9] Budd, S.M.; Exelby, V.H.; Kirwan, J.J.  
The formation of gas bubbles in glass  
*Glass Technology* **3** (1962) p.124-129
- [10] Johnston, W.D.  
Oxidation-reduction equilibria in molten Na<sub>2</sub>O-2SiO<sub>2</sub> glass  
*Journal of the American Ceramic Society* **48** (1965) no.4 p.184-190
- [11] Faile, S.P.; Roy, D.M.  
Gas solubility in relation to the structures of glasses and liquids  
*Journal of the American Ceramic Society* **56** (1973) p.12-16
- [12] Nair, K.M.; White, W.B.; Roy, R.  
Solubility of oxygen in glasses  
*Journal of the American Ceramic Society* **48** (1965) p.52
- [13] Jebesen-Marwedel, H.; Brückner, R.  
"Glastechnische Fabrikationsfehler", Chapter 4.3.1  
Springer-Verlag Berlin Heidelberg (1980)

- [14] Schreiber, H.D. et.al.  
Redox kinetics and oxygen diffusion in a borosilicate melt  
*Physics and Chemistry of Glasses* **27** (1986) no.4 p.152-177
- [15] Dunn, T.  
Oxygen diffusion in three silicate melts along the join diopside-anorthite  
*Geochimica et Cosmochimica Acta* **46** (1982) p.2293-2299
- [16] Lenhart, A.; Schaeffer, H.A.  
Elektrochemische Messung der Sauerstoffaktivität in Glasschmelzen  
*Glastechnische Berichte* **58** (1985) no.6 p.139-147
- [17] Lafroukhi, O.; Hertz, J.; Hilger, J.P.  
Electrochemical measurement of oxygen activity in lead glass by means of a stabilized  $ZrO_2$  sensor. Part 2. Determination of the equilibrium constants in the redox systems arsenic and antimony  
*Glastechnische Berichte* **64** (1991) no.10 p.253-260
- [18] Rüssel, C.  
Polyvalent ions in glass melts  
*Glastechnische Berichte* **63K** (1990) p.197-211
- [19] Cowan, J.H.; Buehl, W.M.; Hutchins, J.R.III  
An electrochemical theory for oxygen reboil  
*Journal of the American Ceramic Society* **49** (1966) no.10 p.559-562
- [20] Beerkens, R.G.C.  
Chemical equilibrium reactions as driving forces for growth of gas bubbles during refining  
*Glastechnische Berichte* **63K** (1990) p.222-242
- [21] Sangani, A.S.  
Creeping flow around bubbles, in  
"Encyclopedia Fluid Mechanics": 3 Gas-liquid flows p.89-109  
editor: N.P. Chermisinoff  
Gulf Publishing Company Houston-London-Paris-Tokyo (1986)
- [22] Gailhbaud, J.; Zortea, M.  
Recherches sur la coalescence des bulles dans un liquide visqueux  
*Rev. Gen. Therm.* **8** (1969) p.433-453
- [23] Jebsen-Marwedel, H.; Brückner, R. (editors)  
"Glastechnische Fabrikationsfehler", Chapter 4.4.1  
Springer-Verlag Berlin Heidelberg (1980)
- [24] Hornyak, E.J.; Weinberg, M.C.  
Velocity of a freely rising gas bubble in a soda-lime-silica glass melt  
*Communications of the American Ceramic Society* (1984) p.244-246
- [25] Némec, L.  
A contribution to the study of glass melting and refining  
Proceedings of the XI International Congress on Glass Prague (1977) **4** p.155-165
- [26] Jucha, R.B. et.al.  
Bubble rise in glass melts  
*Journal of the American Ceramic Society* **65** (1982) no.6 p.289-292

- [27] Auerbach, F.  
Mehrere Körper in einer Flüssigkeit, in "Handbuch der Physik" p.1038  
Editor: A. Winkelmann Barth Leipzig (1909)
- [28] Berker, R.  
Mouvement d'un fluide visqueux incompressible: translation rectiligne et uniforme de deux sphères  
Handbuch der Physik (1963) **Band VIII/2** Strömungsmechanik II p.247-252
- [29] Soo, S.L.  
"Fluid dynamics of multiphase systems" Chapter 5: Transport properties of a cloud of particles  
Blaisdell Publishing Company Waltham Massachusetts Toronto London (1967)
- [29] Bauer, H.  
Grundlagen der Einphasen- und Mehrphasenströmungen  
Sauerländer (1971)
- [30] Greene, C.H.; Gaffney, R.F.  
Apparatus for measuring the rate of absorption of a bubble in glass  
*Journal of the American Ceramic Society* **42** (1959) no.6 p.271-276
- [31] Janssen, R.K.; Krol, D.M.  
Micro-Raman spectroscopy: a technique for analyzing bubbles in glass  
*Applied Optics* **24** (1985) no.2 p.275-279
- [32] Wilt, P.M.  
Nucleation rates and bubble stability in water-carbon dioxide solutions  
*Journal of Colloid and Interface Science* **112** (1986) no.2 p.530-538
- [33] Némec, L.; Muhlbauer, M.  
Verhalten von Gasblasen in der Glasschmelze bei konstanter Temperatur  
*Glastechnische Berichte* **54** (1981) no.4 p.99-108
- [34] Högerl, K.; Frischat, G.H.  
Homogenization of glass melts by bubbling  
*Proceedings of the XVI International Congress on Glass Madrid* (1992) **vol. 6** p.179-184
- [35] Takeshita, S. et.al.  
Refining of glasses under sub-atmospheric pressures III.  
*Proceedings of the XVI International Congress on Glass Madrid* (1992) **vol. 6** p.173-178
- [36] Weinberg, M.C.  
Fining of glasses: Present problems and speculations of things to come  
*Journal of Non-Crystalline Solids* **87** (1986) no.3 p.376-386
- [37] Mattox, D.M.; Smith, H.D.; Wilcox, W.R.; Subramanian, R.S.  
Thermal-gradient-induced migration of bubbles in molten glass  
*Journal of the American Ceramic Society* **65** (1982) no.9 p.437-442
- [38] Klein, V.  
Die Entgasung von Glasschmelzen durch Schallwellen  
*Glastechnische Berichte* **16** (1938) no.7 p.232-233

- 
- [39] Krüger, F.  
Ueber die Entgasung von Glasschmelzen durch Schallwellen  
*Glastechnische Berichte* **16** (1938) no.7 p.233-236
- [40] Eden, C.  
Ultraschall-Entgasung von Glasschmelzen im Hochfrequenzinduktionsofen  
*Glastechnische Berichte* **25** (1952) no.3 p.83-86
- [41] Spinosa, E.D.; Ensminger, D.E.  
Sonic energy as a means to reduce energy consumption during glass melting  
*Ceram. Engng. Sci. Proc.* **7** (1986) no.3-4 p.410-425
- [42] Dunkl, M.; Brückner, R.  
Bestimmung der Korrosionsrate feuerfester Baustoffe durch Glasschmelzen bei freier laminarer Dichte- und Grenzflächen Konvektion unter besonderer Berücksichtigung von Gefügeeinflüssen  
*Glastechnische Berichte* **58** (1985) no.10 p.273-281
- [43] Eller, A.  
Force on a bubble in a standing acoustic wave  
*Journal of the Acoustical Society of America* **43** (1968) no.1 p.170-171
- [44] Blake, F.G.jr.  
Bjerknes forces in stationary sound fields  
*Journal of the Acoustical Society of America* **21** (1949) no.5 p.551
- [45] Shutilov, V.A.  
"Fundamental physics of ultrasound"  
Chapter 5.3: Steady forces acting on suspended particles in an ultrasonic field p.139-140  
Gordon and Breach Science Publishers London (1988)
- [46] Eller, A.; Flynn, H.G.  
Rectified diffusion during nonlinear pulsations of cavitation bubbles  
*Journal of the Acoustical Society of America* **37** (1965) no.3 p.493-503
- [47] Strasberg, M.  
Rectified diffusion: Comments on a paper of Hsieh and Plesset  
*Journal of the Acoustical Society of America* **33** (1961) p.359
- [48] Skinner, L.A.  
Acoustically induced gas bubble growth  
*Journal of the Acoustical Society of America* **51** (1972) no.1 p.378-382
- [49] Eller, A.  
Bubble growth by diffusion in an 11-kHz sound field  
*Journal of the Acoustical Society of America* **52** (1972) no.5 p.1447-1449
- [50] Gould, R.K.  
Rectified diffusion in the presence of, and absence of, acoustic streaming  
*Journal of the Acoustical Society of America* **56** (1974) no.6 p.1740-1746
- [51] Mironov, M.A.  
Influence of microstreaming on the growth of gas bubbles due to rectified diffusion  
*Sov. Phys. Acoust.* **23** (1977) no.5 p.476-478

- [52] Gaar, H.  
Glasläuterung durch Ultraschall  
Vortrag im Fachausschuß III der DGG am 13. Oktober 1987 in Würzburg
- [53] Schreiber, H.D.; Kozak, S.J.; Leonhard, P.G.; McManus, K.K.  
Sulfur chemistry in a borosilicate melt, Part 1: Redox equilibria and solubility  
*Glastechnische Berichte* **60** (1987) no.12 p.389-398
- [54] Gehlhoff, G.; Kalsing, H.; Thomas, M.  
Ueber die Läuterung des Glases  
*Glastechnische Berichte* **8** (1930) no.1 p.1-24
- [55] Mulfinger, H.O.  
Gasanalytische Verfolgung des Läutervorganges im Tiegel und in der Schmelzwanne  
*Glastechnische Berichte* **49** (1976) no.10 p.232-245
- [56] Apak, C.; Cable, M.  
Effect of transition metal-oxides on the refining behaviour of soda-lime-silica glasses  
*Proceedings of the 11<sup>th</sup> International Congress on Glass Prague* (1977) **vol.4** p.167-176
- [57] Erk, K. van; Papanikolau, E.; Pelt, W. van  
The effect of fluorides on antimony refining  
*Proceedings of the 11<sup>th</sup> International Congress on Glass Prague* (1977) **vol.4** p.137-146
- [58] Greene, C.H.; Haynes, A.L.jr.  
Effect of  $As_2O_3$  and  $NaNO_3$  on the solution of  $O_2$  in soda-lime glass  
*Journal of the American Ceramic Society* **48** (1965) no.10 p.528-533
- [59] Cable, M.; Haroon, M.A.  
The action of arsenic as a refining agent  
*Glass Technology* **11** (1970) no.2 p.48-53
- [60] Němec, L.  
Refining in the glass melting  
*Journal of the American Ceramic Society* **60** (1977) p.436-440
- [61] Kohl, R.; Schaeffer, H.A.  
Oxidation states of glass melts  
*Diffusion and defect Data* **53-54** (1987) p.325-334
- [62] Lenhart, A.; Schaeffer, H.A.  
Redox behaviour of glass melts  
*Diffusion and defect Data* **53-54** (1987) p.335-344
- [63] Müller-Simon, H.; Mergler, K.W.  
Electrochemical measurements of oxygen activity of glass melts in glass melting furnaces  
*Glastechnische Berichte* **61** (1988) no.10 293-299
- [64] Paul, A.; Lahiri, D.  
A note on the study of the  $As_2O_3$ - $As_2O_5$  equilibrium in glass  
*Transactions of the Indian Ceramic Society* **22** (1963) no.4 p.146-150
- [65] Johnston, W.D.  
Oxidation-reduction equilibria in molten  $Na_2O \cdot 2SiO_2$  glass  
*Journal of the American Ceramic Society* **48** (1965) no.4 p.184-191

- [66] Krol, D.M.; Rommers, P.J.  
Oxidation-reduction behaviour of antimony in silicate glasses prepared from raw material and cullet  
*Glass Technology* **25** (1984) no.2 p. 115-118
- [67] Stahlberg, B.; Mosel, B.D.; Müller-Warmuth, W.; Baucke, F.G.K.  
Combined electrochemical and Mössbauer studies of the  $\text{Sb}^{3+}/\text{Sb}^{5+}$  equilibrium in a silicate glassforming melt  
*Glastechnische Berichte* **61** (1988) p.335-340
- [68] Paul, A.; Douglas, R.W.  
Cerous-ceric equilibrium in binary alkali borate and alkali silicate glasses  
*Physics and Chemistry of Glasses* **6** (1965) no.6 p.212-215
- [69] Johnston, W.D.  
Oxidation-reduction equilibria in iron-containing glass  
*Journal of the American Ceramic Society* **47** (1964) no.4 p.198-201
- [70] Paul, A.; Douglas, R.W.  
Ferrous-ferric equilibrium in binary alkali silicate glasses  
*Physics and Chemistry of Glasses* **6** (1965) no.6 p.207-211
- [71] Chopinet, M.H.; Massol, J.J.; Barton, J.L.  
Factors determining the residual sulphate content of glass  
*Glastechnische Berichte* **56K**(1983) no.1 p.596-601
- [72] Chopinet, M.H.; Barton, J.L.  
The effect of the melting temperature on the residual sulphate content of glass  
*Proceedings of the XIV International Congress on Glass New Delhi* (1986) **vol.3** p.9-15
- [73] Wermter, F.  
Sauerstoffpartialdruck und Redoxzustand in einer industriellen Glasschmelze  
Vortrag im Fachausschuß III der DGG am 20. April 1988 in Würzburg
- [74] Krämer, F.  
Mathematisches Modell der Veränderung von Gasblasen in Glasschmelzen  
*Glastechnische Berichte* **52** (1979) no.2 p.43-50
- [75] Némec, L.  
The behaviour of bubbles in glass melts. Part 1. Bubble size controlled by diffusion  
*Glass Technology* **21** (1980) no.3 p.134-138
- [76] Weinberg, M.C.; Onorato, P.I.K.; Uhlmann, D.R.  
Behavior of bubbles in glass melts. I. Dissolution of a stationary bubble containing a single gas  
*Journal of the American Ceramic Society* **63** (1980) no.3-4 p.175-180
- [77] Weinberg, M.C.; Onorato, P.I.K.; Uhlmann, D.R.  
Behavior of bubbles in glass melts. II. Dissolution of a stationary bubble containing a diffusing and a nondiffusing gas  
*Journal of the American Ceramic Society* **63** (1980) no.7-8 p.435-438
- [78] Onorato, P.I.K.; Weinberg, M.C.; Uhlmann, D.R.  
Behavior of bubbles in glass melts. III. Dissolution and growth of a rising bubble containing a single gas  
*Journal of the American Ceramic Society* **64** (1981) no.11 p.676-682

- [79] Weinberg, M.C.; Subramanian, R.S.  
Dissolution of multicomponent bubbles  
*Journal of the American Ceramic Society* **63** (1980) no.9-10 p.527-531
- [80] Ramos, J.I.  
Behavior of multicomponent gas bubbles in glass melts  
*Journal of the American Ceramic Society* **69** (1986) no.2 p.49-54
- [81] Cable, M.; Frade, J.R.  
The diffusion-controlled dissolution of spheres  
*Journal of Material Science* **22** (1987) p.1894-1900
- [82] Cable, M.; Frade, J.R.  
Theoretical analysis of the dissolution of multi-component gas bubbles  
*Glastechnische Berichte* **60** (1987) no.11 p.355-362
- [83] Němec, L.  
The behaviour of bubbles in glass melts. Part 2. Bubble size controlled by diffusion and chemical reaction  
*Glass Technology* **21** (1980) no.3 p.134-138
- [84] Weinberg, M.C.  
Dissolution of a stationary bubble in a glass melt with a reversible chemical reaction: rapid forward reaction rate constant  
*Journal of the American Ceramic Society* **65** (1982) no.10 p.479-485
- [85] Hübenthal, H.; Frischat, G.H.  
Formation and behaviour of nitrogen bubbles in glass melts  
*Glastechnische Berichte* **60** (1987) no.1 p.1-10

## Chapter 3

### Redox reactions in molten glass depending on the glass composition

#### 3.1 INTRODUCTION

In the molten glass electron transfer from one species to another can take place. These processes are called redox reactions. In many cases, oxygen is one of the reactants. The equilibrium state of these reactions dominate many properties of the melt and the final product. Some examples are the colour of the melt and the final product [1], the viscosity of the melt [2] and crystallisation [2] and the visco-elastic behaviour of the glass during the forming of the product [3]. Apparently, the rejection percentage of the glass products is related to the redox state [4]. Furthermore, the fining of glass melts using fining agents like antimony oxide or sulphate is governed by redox reactions. For these reasons, it is important to understand and to quantify the redox reactions in commercial glasses.

The equilibrium state of the redox reactions strongly depends on the glass composition [5,6,7]. The activity of the free oxide ion  $O^{2-}$  in the structure is probably responsible for this effect. The oxide ion activity is usually indicated by the "basicity" of the melt. Some methods have been proposed to estimate the basicity of the melt on the basis of the batch compositions. Other methods for the determination of the basicity are based on measurable properties of the final glass product.

With the aid of the calculated or measured basicity, one should be able to predict some properties of melt and product and the equilibrium state of the redox reactions for any glass composition, if these redox reaction equilibria have been determined for one glass composition.

In this chapter, the commonly used definitions for the redox reaction equilibrium constants will be described. The redox reaction equilibria are influenced by the oxygen content of the melt (the concentration of physically dissolved  $O_2$ ). The effect of the presence of other redox active species will be discussed in detail. Then the importance of the redox reactions on the glass colour and the fining process will be explained. Next, the influence of the glass composition on the reaction equilibria is examined. The reaction scheme that is generally used



to describe the redox reactions in the melt is not in agreement with the results. Some explanations for this discrepancy are given at the end of this chapter. However, at the moment it is hardly possible to predict accurately the redox reaction equilibria on the basis of the composition of the melt.

## 3.2 REDOX REACTIONS IN GLASS

### 3.2.1 Redox reaction equilibria

Polyvalent ions are able to convert from one valency state into another:



$n$  is the number of electrons that is transferred when the polyvalent ion is converted from one valency state to another.

The electrons can be provided or taken up by oxygen:



The overall reaction scheme is then described by [8]:



and the reaction equilibrium constant  $K(T)$  can be defined by:

$$K(T) = \frac{a_{M^{x+}} \cdot a_{O_2}^{n/4}}{a_{M^{(x+n)+}} \cdot a_{O^{2-}}^{n/2}} \quad (3.4)$$

$a_i$  is the activity of component  $i$ .

The oxide ions in the melt can be bridging, non-bridging (see chapter 2.2.1) and free oxide ions. Generally, the free oxide ion ( $O^{2-}$ ) activity in molten glass, which appears in equation 3.4, is not known, but the total oxide ion concentration in the melt is large. The concentration of the polyvalent element is assumed to be relatively small in comparison to the free oxide ion concentration. Therefore it is generally accepted that for a given glass composition, the  $O^{2-}$  activity remains constant during the redox reaction [8,9,10] (see also chapter 3.4.2). The free oxide ion activity can be included in the adjusted reaction equilibrium constant  $K^*(T)$ :

$$K^*(T) = \frac{a_{M^{x+}} \cdot a_{O_2}^{n/4}}{a_{M^{(x+n)+}}} \quad (3.5)$$

**Note:** this reaction equilibrium constant  $K^*(T)$  strongly depends on the glass composition, while the activity of the free oxide ion will be dominated by the surrounding ions in the melt. Some authors however assume that the oxide ion

activity is equal to unity [11], and in this case  $K^*(T)$  is equal to  $K(T)$ , and  $K^*(T)$  is valid for all glass compositions.

The adapted equilibrium constant  $K^*(T)$  can also be written as:

$$K^*(T) = \frac{\gamma_{M^{x+}} \cdot [M^{x+}] \cdot f_{O_2}^{n/4}}{\gamma_{M^{(x+n)+}} \cdot [M^{(x+n)+}]} \quad (3.6)$$

with  $\gamma_i$  = the activity coefficient of component  $i$  in the glass melt  
 $[M_i]$  = concentration of component  $i$  in the glass melt [mole·m<sup>-3</sup>]  
 $f_i$  = fugacity of gas  $i$

Since the concentration of the polyvalent ions in the glass melt is usually low, the ratio of the activities of the polyvalent elements is generally approximated by the ratio of their concentrations [5,11]:

$$\frac{a_{M^{x+}}}{a_{M^{(x+n)+}}} \approx \frac{[M^{x+}]}{[M^{(x+n)+}]} \quad (3.7)$$

This actually implies, that the activity coefficients of  $M^{x+}$  and  $M^{(x+n)+}$  are assumed to be independent of concentration, and that their ratio is constant for any temperature:

$$\frac{\gamma_{M^{x+}}(T)}{\gamma_{M^{(x+n)+}}(T)} \approx \text{constant (for any temperature (T) and concentration)} \quad (3.8)$$

This enables a further simplification of the redox reaction equilibrium constant. The constant of equation 3.8 is incorporated in the equilibrium constant  $K^{**}(T)$ , and the fugacity of the gaseous oxygen,  $O_2$ , is replaced by its partial equilibrium pressure  $p_{O_2}$  in the glass melt:

$$K^{**}(T) = \frac{[M^{x+}] \cdot p_{O_2}^{n/4}}{[M^{(x+n)+}]} \quad (3.9)$$

In this equation, the ratio reduced to oxidized species,  $[M^{x+}]/[M^{(x+n)+}]$ , depends for a given temperature linearly on the oxygen pressure to the power  $n/4$ :  $p_{O_2}^{n/4}$ .

According to Johnston, this equation is qualitatively valid for titanium, iron, cerium, manganese, cobalt, nickel, antimony, tin and vanadium in soda-silica melts [8], and Schreiber [12,13] indicates, that the equation is equally valid for

the redox reactions of chromium ( $\text{Cr}^{6+}/\text{Cr}^{3+}$  or  $\text{CrO}_4^{2-}/\text{Cr}^{3+}$  and  $\text{Cr}^{3+}/\text{Cr}^{2+}$ ). The equilibrium state of reaction 3.3 shifts to the right side at an increase of temperature. Only in melts containing more than one polyvalent element the equilibrium of one redox reaction may shift to the oxidized side (left side) because of the strong oxidizing effect of the other polyvalent species.

Because all the quantities in equation 3.9 ( $p_{\text{O}_2}$ ,  $[\text{M}^{x+}]$  and  $[\text{M}^{(x+n)+}]$ ) are accessible for measurements (see chapter 4), this definition of the redox reaction equilibrium constant is commonly used [5,6,9,11,12,13,14,15,16,17]

### 3.2.2 The redox reaction equilibrium constant as a function of enthalpy and entropy

The equilibrium state of equation 3.3 depends on the temperature. A change in the temperature is accompanied by a change in the Gibbs free energy  $\Delta G$  of the reaction, with

$$-\Delta G = R_g \cdot T \cdot \ln K \quad (3.10)$$

with  $R_g$  = gas constant [8.314 J·mole<sup>-1</sup>·K<sup>-1</sup>]

$T$  = absolute temperature [K]

The redox reaction equilibrium constant has been defined in equation 3.4.

Two other thermodynamic quantities, the change in enthalpy  $\Delta H$  and the change in entropy  $\Delta S$ , can be derived from the temperature dependent Gibbs free energy:

$$\Delta S = - \left( \frac{\delta \Delta G}{\delta T} \right)_p \quad (3.11)$$

$$\Delta H = \Delta G + T \Delta S \quad (3.12)$$

The subscript p refers to a constant pressure.

Now the redox reaction equilibrium constant can be written as a function of the changes in enthalpy and entropy:

$$K(T) = \exp \left( \frac{-\Delta G}{R_g \cdot T} \right) = \exp \left( \frac{-\Delta H}{R_g \cdot T} + \frac{\Delta S}{R_g} \right) \quad (3.13)$$

$K(T)$  is the ratio of the activities of products and reactants. The activities of the polyvalent ions and the free oxide ion in molten glass are generally unknown

and can not be measured directly. Because the polyvalent ion concentrations and oxygen gas pressure can be measured, the reaction equilibrium constant  $K^{**}(T)$  is based on these quantities. It has been defined in equation 3.9. The effect of the temperature on  $K^{**}(T)$  can be expressed in the "enthalpy and entropy changes" of the redox reaction,  $\Delta H^{**}$  and  $\Delta S^{**}$ :

$$K^{**}(T) = \exp \left( \frac{-\Delta H^{**}}{R_g \cdot T} + \frac{\Delta S^{**}}{R_g} \right) \quad (3.14)$$

Note:  $\Delta H^{**}$  and  $\Delta S^{**}$  are only equal to  $\Delta H$  and  $\Delta S$  if the free oxide ion activity  $a_{O_2}$  equals unity and if equation 3.7 is valid for all temperatures. Then  $K(T)$ ,  $K^*(T)$  and  $K^{**}(T)$  are identical. Since it is hardly likely that all conditions will be satisfied, the values of  $\Delta H^{**}$  and  $\Delta S^{**}$  are exclusively valid for the glass composition and the concentrations of polyvalent elements, for which they have been determined.

### 3.2.3 Redox reaction equilibrium for one polyvalent element during cooling to room temperature

The redox reaction equilibrium constant  $K^{**}(T)$  strongly depends on temperature. Electron transfer is usually very fast at elevated temperatures. The redox reaction is assumed to be in local equilibrium at temperatures above 600°C independent on the cooling rate (see chapter 2.2.4 and [18]), and equation 3.9 is continuously valid. At lower temperatures, the kinetics of the reaction may play an important role.

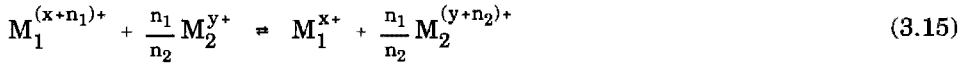
During cooling of the glass melt to room temperature, a polyvalent element can be converted to a higher valency state, if sufficiently gaseous oxygen  $O_2$  is present. Usually, the concentration of physically dissolved  $O_2$  in the melt is assumed to be far less than the concentration of the polyvalent ion [19,20,21]. The diffusivity of oxygen from the atmosphere into the melt is low compared to the normal quenching rates [22]. Therefore the deficiency of oxygen can not be supplied by diffusion from the atmosphere if the cooling rate is relatively fast (see chapter 2.2.4). In this case only a few reduced polyvalent ions can donate electrons to oxygen and thus become oxidized. The ratio reduced to oxidized species  $[M^{x+}]/[M^{(x+n)+}]$  remains roughly the same during cooling, and the equilibrium at the initial temperature is 'frozen in'. By measuring the redox ratio at room temperature, the redox ratio at the melting temperature can be determined.

### 3.2.4 Interaction of different polyvalent elements

Not only oxygen, but also other polyvalent elements can act as electron donors or acceptors in the multi-component glass melt. On the condition that no complex formation between the polyvalent elements takes place, the redox reaction equilibria constants of both elements will satisfy equation 3.9 [20,23]. The resulting oxygen equilibrium pressure in the melt  $p_{O_2}$  will be effected by both reactions.

A glass melt which is equilibrated with a certain atmosphere will obtain a certain oxygen equilibrium pressure. The redox ratios of all polyvalent elements present are theoretically established independently according to equation 3.9. And indeed, voltammetric studies at 1000°C in sodium borate glasses containing  $CeO_2$ ,  $Fe_2O_3$  or both  $CeO_2$  and  $Fe_2O_3$  indicate, that the polyvalent element can adjust its redox ratio to the existing oxygen equilibrium pressure independent of the second polyvalent element (see [20] and chapter 6.7).

At a decrease of temperature, all elements prefer the oxidized state. In the melt, only a small amount of physically dissolved oxygen is present. Therefore, one of the polyvalent elements will generally act as an electron acceptor [18]:



and the resulting reaction equilibrium constant is

$$K_{\text{interaction}} = \frac{[M_1^{x+}] \cdot [M_2^{(y+n_2)+}]^{n_1/n_2}}{[M_1^{(x+n_1)+}] \cdot [M_2^{y+}]^{n_1/n_2}} = \frac{K_1^{**}(T)}{K_2^{**}(T)} \quad (3.16)$$

### 3.2.5 Interaction of polyvalent elements during cooling to room temperature

Since electron transfer reactions are very fast at high temperatures, the redox ratio can be assumed to be controlled by diffusion and thermodynamics, and not by reaction kinetics [18]. Equation 3.16 is presumably valid at sufficiently high temperatures. If the temperature becomes very low, diffusion of the polyvalent elements can not occur and the (at that time existing) redox ratios will be frozen in.

However the redox ratio of a polyvalent species can change during cooling from the melting temperature to room temperature according to reaction scheme 3.15, if more than one polyvalent ion is present in the melt. A shift in the redox ratio at room temperature in glasses containing two polyvalent elements, in respect to the ratio in glasses containing only one element, has indeed been found by some authors [20,24,25,this thesis chapter 6.7]. For example, after quenching of soda-lime-silica glasses containing  $\text{CeO}_2$ ,  $\text{Fe}_2\text{O}_3$  or both  $\text{CeO}_2$  and  $\text{Fe}_2\text{O}_3$ , the measured ratio  $[\text{Fe}^{3+}]/[\text{Fe}^{2+}]$  was higher in the glass containing both  $\text{CeO}_2$  and  $\text{Fe}_2\text{O}_3$  than in the glass containing only  $\text{Fe}_2\text{O}_3$ . Apparently cerium is able to oxidize  $\text{Fe}^{2+}$  to  $\text{Fe}^{3+}$  during the cooling of the melt [20, this thesis chapter 6.7].

Some authors assume that the resulting redox ratios depend on the cooling rate [18,22]. Close and Tillman [25] actually found that the cooling rate determines the final redox ratios for glasses containing both  $\text{Fe}_2\text{O}_3$  and  $\text{Cr}_2\text{O}_3$ . Therefore the redox ratios at room temperature can not be used in equation 3.9 to calculate the redox reaction equilibrium constant at elevated temperatures if the glass contains more than one polyvalent element.

### 3.3 CONSEQUENCES OF THE REDOX REACTION EQUILIBRIUM STATES FOR THE GLASS

#### 3.3.1 Colour of the melt and the final product

Colours originate from the interactions of electromagnetic waves with the glass melt or the final product. Radiation with a frequency in the visible range can be absorbed by electrons of some polyvalent elements. The colour of the absorbed light depends on the valency state of the polyvalent elements and on their coordination [1]. The coordination is strongly influenced by the activity of the free oxide ions, and therefore by the glass composition.

The total concentration of the polyvalent ion  $M$  and its redox ratio,  $[\text{M}^{x+}]/[\text{M}^{(x+n)+}]$ , determine the colour of the glass. This ratio is given by equation 3.9. Again it should be noted, that the equilibrium constant  $K^{**}(T)$  may differ for various glass compositions.

Combinations of ions can also produce a colour, like the  $\text{Fe}^{3+}/\text{S}^{2-}$ -complex in amber glass [1].

### Colour of the molten glass

Colourizing elements also absorb heat radiation, depending on their redox state. The colouring of molten glass is predominantly determined by the presence of iron and chromium ions [1,26,27].  $\text{Fe}^{2+}$  absorbs heat (infrared) radiation.  $\text{Fe}^{3+}$  has little effect on the heat transfer while it absorbs in the ultraviolet region [Combination of 17 and 26,27]. The redox reaction of iron in molten glass is generally represented as [5,17]:



Three valency states of chromium in the glass melt are known [18]. The heat absorption capacity of the  $\text{Cr}^{3+}$  ions is much larger than that of  $\text{Cr}^{6+}$  or  $\text{Cr}^{2+}$  [Combination of 18 and 26,27].

The ratios  $\text{Fe}^{2+}/\text{Fe}^{3+}$  and  $\text{Cr}^{3+}/\text{Cr}^{6+}$  or  $\text{Cr}^{2+}/\text{Cr}^{3+}$  determine the heat penetration from the flame by radiation in the glass melting tank.

In continuous melting tanks, the glass melt is generally heated from above with the aid of gas or oil burners. The temperature of the melt at bottom positions can be strongly influenced by the oxidation state of the glass melt.

### Colour of the final glass product

The colour of the final glass product is determined by the valency state of some polyvalent elements at room temperature.

In table I, the colours which are obtained by various polyvalent elements in soda-lime-silica melts at room temperature are listed. The colours may differ somewhat in glass melts of deviating compositions due to a difference in coordination [1].

Table I.  
The colours of various polyvalent elements in soda-lime-silica melts [1,28]

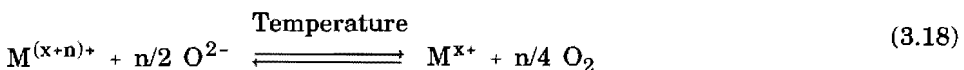
Ion	valency	coordination state	colour
Fe	3+	tetraedric	yellow
	2+	octaedric	green-blue
Ni	2+		brown
Co	2+	tetraedric	blue
Cr	6+	tetraedric	yellow
	4+		blue
	3+	octaedric	green
	2+		blue-violet
Cu	2+		blue(turquoise)
	1+		-
Mn	3+	octaedric	purple
	2+	octaedric	-
Ce	4+		-
	3+		-
Fe/S	Fe <sup>3+</sup> /S <sup>2-</sup>	tetraedric	amber brown

### 3.3.2 The fining of glass melts

The fining of molten glass can be influenced by the addition of chemical fining agents like oxides of polyvalent elements. The fining actions of these chemicals are based on redox reactions in the melt.

Usually the oxidized form of the polyvalent elements are added to the batch. If reducing agents are present in the batch or the reduced form is added (as is sometimes the case with arsenic or antimony aided fining), the multivalent element has to be oxidized before the melting of the batch takes place. This is achieved by adding an oxidizing agent like nitrate to the batch.

At a (further) increase of the temperature, the polyvalent element will be reduced:



Hereby gaseous oxygen is released in the melt. The physically dissolved O<sub>2</sub>



molecules diffuse to existing bubbles, causing them to grow [29]. The fining process is governed by the redox reaction equilibrium constant, because this determines the amount of oxygen that is released and is available for bubble growth. Especially at oxygen pressures exceeding 1 bar fining is strongly enhanced by fast bubble growth.

According to Johnston [8], Krol [9] and Stahlberg [11], the fining action of antimony for a given glass composition is adequately described by



For a given glass composition and temperature, the redox ratio  $[\text{Sb}^{3+}]/[\text{Sb}^{5+}]$  is, after equilibration with a certain atmosphere, proportional to the square of the oxygen pressure in the atmosphere [8]. The redox reaction equilibrium constant for the change in valency state of antimony is given by

$$K_{\text{Sb}}^{**}(\text{T}) = \frac{[\text{Sb}^{3+}] \cdot p_{\text{O}_2}^{1/2}}{[\text{Sb}^{5+}]} \quad (3.20)$$

A similar reaction scheme has been proposed for the redox reaction of arsenic and tin, because for these elements a reduction of one mole of the oxidized species involves the transfer of two moles of electrons.

Some changes in valency states require only one electron. The ratio of reduced to oxidized species, or redox ratio, is then expected to be proportional to the fourth root of the oxygen pressure in the atmosphere [8] for a given glass composition and temperature. This is the case for iron (see equation 3.17) and cerium:

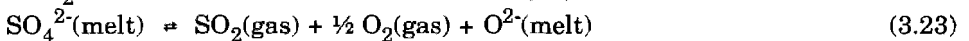


The reaction equilibrium constant for this reaction is described as [6,8]:

$$K_{\text{Ce}}^{**}(\text{T}) = \frac{[\text{Ce}^{3+}] \cdot p_{\text{O}_2}^{1/4}}{[\text{Ce}^{4+}]} \quad (3.22)$$

for a given glass composition.

Sulphates too can undergo a change in valency state, as discussed in chapter 2.6. Under oxidizing conditions, the sulphate is at relatively low temperatures present as  $\text{SO}_4^{2-}$  [12,14]. At an increase of temperature, it is converted to  $\text{SO}_2$  and  $\text{O}_2$ . The reaction can be described as [13,15,16]:



For this reaction, a reaction equilibrium constant  $K^{**}$  can be defined:

$$K_{\text{sulphate}}^{**} = \frac{p\text{SO}_2 \cdot p\text{O}_2^{1/2}}{[\text{SO}_4^{2-}]} \quad (3.24)$$

It is not known if the proposed reaction actually takes place in the melt. However, the reaction constant given in equation 3.24 is used by some authors [15,16] to describe the fining action of sulphates.

The fining action of sulphates under reducing atmospheres has not been described quantitatively in terms of reaction equilibrium constants yet [12,14]. The basic knowledge on the reaction mechanism and quantitative information are still missing (see chapter 2.6).

### 3.4 THE EFFECT OF THE GLASS COMPOSITION ON THE REDOX REACTION EQUILIBRIA

#### 3.4.1 The relation between the glass composition and the oxygen ion activity

In a melt with a large oxide ion activity, electron donation from  $\text{O}^{2-}$  to the oxidized form of a polyvalent ion can take place in accordance with equation 3.3. The composition of the glass governs the total oxide ion content in the glass.

The free oxide ion activity is assumed to be dependent on the nature of the neighbouring cations. If the attracting forces of these cations on the oxygen ions are strong, the oxygen ion activity will be small. Just as the acidity of a solution is a measure for the  $\text{H}^+$  activity, the "basicity" of the glass is a measure for the  $\text{O}^{2-}$  activity in the melt [30]. Because the basicity can not be measured directly in the molten glass, some methods have been proposed to estimate the basicity, starting from the batch composition. Other methods are based on the properties of the melt or the final product (for instance the  $[\text{Fe}^{2+}]/[\text{Fe}^{3+}]$ -ratio).

From this simple scheme it is to be expected that the ratio  $[\text{M}^{x+}]/[\text{M}^{(x+n)+}]$  increases as the activity of free oxide ions, or in other words the basicity, of a melt is increased under otherwise equal conditions.

In order to understand the influence of the glass composition on the redox

reaction equilibria in the melt, the behaviour of oxygen (as ions and molecules) in the molten glass will be discussed. Then various methods to estimate the basicity of a glass are given. Finally, an attempt has been made to verify the effect of the basicity on the redox reaction equilibria.

### 3.4.2 Oxygen in glass

Oxygen may be present in the glass melt phase in different forms:

- as molecular  $O_2$ , it occupies interstitial holes within the glass matrix. It is physically dissolved. This can be concluded from the fact that solid glasses are permeable for  $O_2$  [31]. Nair et.al. have made it plausible that the same mechanism of solubility occurs in molten glass [32].
- polyvalent elements are able to take up physically dissolved  $O_2$  by a redox reaction in the form of  $O^{2-}$ . The oxygen is then dissolved chemically [8,31].
- And of course oxygen ions are present in the glass matrix of oxidic glass melts as bridging oxygen ions or non-bridging ions.

According to Toop [33] free oxide ions  $O^{2-}$  are in equilibrium with bridging  $O^0$  and (singly bonded) nonbridging oxygen  $O^-$ :



The nonbridging oxygen ion concentration in glass is high if the amount of network modifiers is high (see chapter 2.2.1). Then the removal of free oxide ions from the melt due to a shift of reaction 3.3 to the right at an increase of temperature will be followed by the production of free oxide ions, because the equilibrium of reaction 3.25 tends to shift to the right. Due to this replenishment, the free oxide ion activity for a given glass composition is often considered to remain roughly invariable with temperature [6,8].

### 3.4.3 Basicity number concepts

Free "oxide ions" are produced within the melt by the addition of network modifiers, such as  $Na_2O$  and  $CaO$ , into a system of network formers, such as  $SiO_2$  and  $B_2O_3$  (see chapter 2.2.1). Increasing the amount of network modifiers results in an increase of the concentration of non-bridging oxygen ions, and probably also free oxygen ions, in the glass, and thus to an increase of the basicity.

The basicity of a glass is often estimated on the basis of the composition of the glass. The "basicity" is the sum of the contributions of the various oxides, proportional to their weight percentage [30].

In addition to the "oxide ion activity", some other expressions are used to characterize the chemical activity of the molten glass. The concepts "redox" and "oxidation state" refer to the ratio of reduced to oxidized species in the melt, but sometimes they are used as synonyms for the oxygen gas pressure at a certain temperature. No unambiguous definition of the redox or oxidation state is available.

#### 3.4.3.1 The basicity number

##### **Cation field strength**

The  $O^{2-}$ -ion is attracted by the neighbouring cations. The oxide ion activity will be smaller as the attraction force is stronger. Besides the charge of the cation ( $z$ ), the distance between cation and oxide ion ( $a$ ) plays an important role. Therefore Dietzel [34] classifies the behaviour of the cations on their field strength  $F_{\text{Field}}$ , with  $F_{\text{Field}}=z/a^2$ . For example if sodium ( $F_{\text{Field}}=0.18$ ) is replaced by potassium ( $F_{\text{Field}}=0.13$ ), the field strength is decreased and therefore the basicity is increased.

The calculation of the basicity number is based on the final glass composition, assuming the cations to be present as oxides. No distinction is made between sodium ions that are added as carbonates or as oxides.

##### **Cation-oxygen bond strength**

In the theory of Dietzel, the real charge distribution of the ion neighbourhood and geometric factors have not been taken into account. Sun [35] estimated the bond strength from the dissociation energy of the oxides in the melt. The basicity of a melt of a certain composition can then be calculated from the contributions of all ions. Per definition the basicity value of  $B_2O_3$  is set to zero, the basicities of other melts are relative to this. For instance the basicity of  $20Na_2O-80SiO_2$  (in mole%) is 30.2, and  $20K_2O-80SiO_2$  has a basicity of 31.6.

#### 3.4.3.2 Characterization of the redox behaviour

##### **Carbon number/ redox number of the batch**

In the glass industry, some methods to estimate the oxidizing or reducing effects of additives in the batch mixture have been developed. Both the carbon number [36] and the redox number concept [37] give an indication of the effect of batch additives to the oxidation state of the melt. The numbers are based on experience. The "redox" of the melt can be adjusted by adding certain amounts of oxidizing or reducing agents to the batch.

Sometimes however it is very difficult to predict the efficiency of the reducing agent carbon [38,39]. Furthermore, the carbon number and redox number concepts do not take into account the type of furnace, firing conditions, bubbling, residence time, maximum temperature and furnace atmosphere, although they can have a marked influence on the oxidation state during melting and of the glass product [40].

### **Chemical oxygen demand of the batch**

A relatively simple method has been developed to determine the oxidizing action of raw materials [40]. The raw materials are grinded and subsequently soluted in 50% sulfuric acid in an inert atmosphere. This solution is then refluxed for several hours with a 0.25 N potassium dichromate solution. Afterwards, the solution is titrated with ferrous ammonium to determine the amount of remaining dichromate. The amount of dichromate, necessary to oxidize batch components, is a measure for the Chemical Oxygen Demand (COD) [40]. The very important oxidizing actions of nitrates and sulphates, however, only start at elevated temperatures, and can not be determined by this method.

Recycling cullet contains many different organic components. Therefore it is very difficult to estimate the carbon number, redox number or Chemical Oxygen Demand of the batch if recycling cullet is added to the batch mixture.

### **Fe<sup>2+</sup>/Fe<sup>3+</sup> ratio in the final glass product**

The ratio reduced to oxidized iron, Fe<sup>2+</sup>/Fe<sup>3+</sup>, in the melt is directly related to the partial oxygen vapour pressure and the redox state of the glass melt. Johnston [17] investigated the behaviour of iron in a sodium disilicate glass which was equilibrated with a certain atmosphere and showed that [Fe<sup>2+</sup>]/[Fe<sup>3+</sup>] is directly proportional to the fourth root of the partial oxygen pressure in the atmosphere. The ratio [Fe<sup>2+</sup>]/[Fe<sup>3+</sup>] is often used to classify the oxidation state, for instance in sulphate-containing glass products [7,14,15,16].

The ratio reduced to oxidized iron is measured at room temperature. Because the equilibrium can shift during cooling in the case that there is more than one polyvalent element present in the melt, or by diffusion of oxygen from the atmosphere at slow cooling rates, this method is insignificant. The final redox ratio [Fe<sup>2+</sup>]/[Fe<sup>3+</sup>] may then not be representative for the redox conditions at the elevated temperature (see chapter 3.2.5).

The composition of the melt has a great effect on the ratio  $\text{Fe}^{2+}/\text{Fe}^{3+}$ , when iron is the only polyvalent element present [5]. However, it is only roughly possible to predict the effect of a change in batch composition on the redox ratio without taking the process parameters into account.

### **Oxygen equilibrium pressure**

The oxygen equilibrium pressure can be measured in situ in the melt with the aid of an oxygen sensor [28,41]. At the moment, it is not entirely clear in which way the sensor can be used for the on-line controlling of the redox state of the molten material.

According to Wermter [4], no direct relation between the Chemical Oxygen Demand of the batch and the oxygen pressure of the melt could be demonstrated. There was however a relation between the COD and the sulphur content (measured as %  $\text{SO}_3$  in the final product), and between the COD and the redox ratio  $[\text{Fe}^{2+}]/[\text{Fe}^{3+}]$  in the final product. The rejection percentage (caused by the presence of bubbles and seeds) could be correlated to the oxygen pressure in the melt.

### **Basicity moderating power**

A change in the chemical activity of the free oxide ion  $\text{O}^{2-}$  is caused by a change in the (mean) electron density on the  $\text{O}^{2-}$  ion. If a glass contains a suitable Lewis acid for probing electron density, like  $\text{Pb}^{2+}$ , the basicity of this glass can be estimated by comparing its spectral data to those of other glasses [42].

Some ions like  $\text{Pb}^{2+}$  act as electron acceptor (Lewis acid), and a coordination bond can be formed between these ions and the  $\text{O}^{2-}$  ion which acts as an electron donor (Lewis base). The effect of the electron donation is to expand the outer orbitals (and decrease the orbital energies) of the Lewis acid. The orbital energies of  $\text{Pb}^{2+}$  can be measured with optical spectroscopy. A shift of the absorption peak to lower frequencies occur if the  $\text{Pb}^{2+}$  ion is surrounded by oxidic media. Baucke measured the optical basicity factors for several glass components [42]. The reference oxide is  $\text{CaO}$ , because it exhibits a very strong electron donation. Optical basicity measurements have been done for glasses at ambient temperature. According to Baucke, there is very strong evidence from measurements in molten silicate melts that the resulting basicity factors are useful for the molten state as well. The exact basicity values may shift during

the cooling of the melts, but the ranking of the different compositions will likely remain the same.

#### 3.4.4 The influence of the basicity on the redox reaction equilibrium

Although the various methods to describe the basicity of a glass or the concepts to characterize its redox behaviour or oxidation state lead to different values, the qualitative results are almost identical. The effect of a change in the glass composition is in all cases similar.

If equation 3.3 gives a correct description of the reactions that take place in the glass melt, it is to be expected, that the ratio  $[M^{x+}]/[M^{(x+n)+}]$  increases as the activity of the free oxide ions (the basicity of the melt) is increased under otherwise equal conditions. One must assume that, for instance, the ratio  $[Fe^{2+}]/[Fe^{3+}]$  is larger in a 30K<sub>2</sub>O-70SiO<sub>2</sub> melt than in a 30Na<sub>2</sub>O-70SiO<sub>2</sub> melt at the same temperature and oxygen pressure.

Experiments have shown that this assumption is not true in most cases. On the contrary: for most polyvalent elements M, the redox ratio  $[M^{x+}]/[M^{(x+n)+}]$  decreases at increasing basicity [5,6,43,44].

At this moment, it is still not possible to predict the reaction equilibrium constant for a certain element in a certain glass with known basicity on the basis of experimental data in a melt with a different composition, irrespective of the definition for the basicity.

### 3.5 EXPLANATIONS FOR THE INFLUENCE OF THE BASICITY ON THE REDOX REACTION EQUILIBRIA

The apparent deviation between the theoretical effect of the basicity of the melt on the redox reaction equilibrium and the experimental results has been the subject of some recent papers. Explanations have been found in:

- standard free energies of the reacting species;
- complex formation;
- the formation of peroxide ions;
- the interaction of bridging, non-bridging and free oxygen ions in the melt;
- a thermodynamic approach, based on activity coefficients of the ions or molecules, involved in the redox reaction.

### 3.5.1 Standard free energies

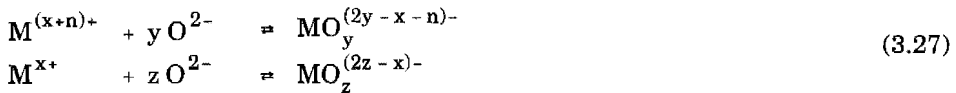
According to Baucke and Duffy [42] the standard free energy of each species involved changes as the glass composition changes. The simplification

$$\frac{a_{\text{Fe}^{2+}}}{a_{\text{Fe}^{3+}}} \approx \frac{[\text{Fe}^{2+}]}{[\text{Fe}^{3+}]} \quad (3.26)$$

for instance, is NOT valid. Instead of equation 3.9, equation 3.4 should therefore be used to calculate the reaction equilibrium constant. The oxide ion activity can not be estimated directly from the composition of the batch materials. However, the free oxide ion activity of various glass melts can be ranked when the electron density of the free oxygen ions in the melt is known. There should be an empirical relation between the redox ratio of a melt and its ranking number, or "optical basicity". The redox ratios can therefore be predicted semi-quantitatively by measuring the optical basicity of a glass and comparing this to a gauge curve.

### 3.5.2 Complex formation

Equation 3.3 can be preceded or followed by a complex-forming reaction in the melt [45]:



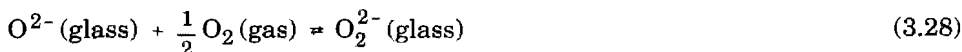
The coordination numbers of the polyvalent ions in the glass product, determined by spectroscopic methods such as optical absorption, ESR or Mössbauer, indicates that these reactions can indeed occur [references in 45]. The coordination of  $\text{M}^{x+}$  and  $\text{M}^{(x+n)+}$  can be concluded from measurements in glasses with different basicity. Then the overall reaction scheme can be given, and the influence of  $\text{O}^{2-}$  is given correctly.

Application of this method for example in the case of iron leads to five possible overall reaction schemes [45] for different temperatures and iron concentrations. To confirm the effect of complex formation on the redox equilibria, more quantitative data of oxygen activities in glass melts as a function of temperature, composition and basicity will be needed, in combination with other measurements (Mössbauer, ESR, square wave voltammetry).

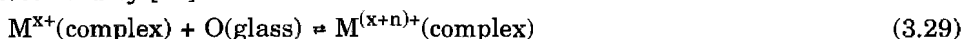


### 3.5.3 The formation of peroxide ions

Electropositive elements such as Li, Na and K are known to form peroxide ions in molten oxides [44]. It was therefore suggested that the formation of peroxide ions in glasses could occur, due to a reaction of the oxide ion and molecular oxygen:



Not the  $\text{O}^{2-}$  ions oxidize the polyvalent elements, but the much stronger oxidizing agent  $\text{O}_2^{2-}$ . The reaction is then (incompletely and confusingly) described by [44]:



Whether this reaction implies the existence of free oxygen atoms in the melt or not is not discussed by Pyare. But according to Pyare [44], the activity of this oxygen  $\text{O}(\text{glass})$  is proportional to the peroxide activity in the melt.

$$a_{\text{O}}(\text{glass}) \propto a_{\text{O}_2^{2-}}(\text{glass}) = K_{\text{peroxide}} \cdot \left( a_{\text{O}^{2-}}(\text{glass}) \cdot p_{\text{O}_2}^{1/2} \right) \quad (3.30)$$

with  $K_{\text{peroxide}}$  is the equilibrium constant for equation 3.28. The redox reaction equilibrium according to Pyare, "K", is approximated by [44]:

$$\text{"K"} = \frac{[\text{M}^{x+}] \cdot [\text{O}(\text{glass})]^{n/2}}{[\text{M}^{(x+n)+}]} = \frac{[\text{M}^{x+}] \cdot K_{\text{peroxide}}^{n/2} \cdot [\text{O}^{2-}(\text{glass})]^{n/2} \cdot p_{\text{O}_2}^{n/4}}{[\text{M}^{(x+n)+}]} \quad (3.31)$$

and the concentration of the free oxide ion  $\text{O}^{2-}$  appears in the numerator. The values of  $[\text{O}^{2-}]$  and  $K_{\text{peroxide}}$  cannot be determined directly, and therefore it is not possible to predict the exact influence of the glass composition on the redox reaction equilibrium. Only a qualitative relation can be obtained by this method. For example if the logarithm of  $[\text{As}^{5+}]/[\text{As}^{3+}] \cdot (p_{\text{O}_2})^{1/2}$  is plotted against the percentage of  $\text{R}_2\text{O}$  in  $\text{R}_2\text{O}-\text{SiO}_2$  glasses, straight lines are obtained (but different lines for Na, K and Li).

### 3.5.4 The interaction of bridging, non-bridging and free oxygen ions

Douglas et al. [46] pointed out, that the total concentration of oxygen (as  $\text{O}^0$ ,  $\text{O}^-$  and  $\text{O}^{2-}$ ) diminishes as the basicity of the melt increases. For the estimation of the oxide ion activity the presence of bridging and non-bridging oxygens in the melt should be taken into account. The following reaction scheme has been suggested:



and the concentration of the free oxygen ion  $\text{O}^{2-}$  is assumed to depend on the

ratio P, with  $P = [\text{bridging oxygen}]^{1/2} / [\text{non-bridging oxygen}]$ :

$$[\text{O}^{2-}] = \text{constant} \cdot \frac{[\equiv\text{Si}-\text{O}^-]^2}{[\equiv\text{Si}-\text{O}-\text{Si}\equiv]} = \text{constant} \cdot P^{-2} \quad (3.33)$$

P can be derived directly from the glass composition.

To support this theory, glass melts with various P-factors containing only one polyvalent element (iron, cerium or chromium) have been equilibrated with air at a given temperature. Then the melts were quenched to room temperature and the ratios oxidized to reduced species were determined. The ratio  $[\text{M}^{x+}] / [\text{M}^{(x+n)+}]$  is expected to be proportional to  $[\text{O}^{2-}]^{n/2}$  or to  $P^{-n}$ . If the logarithm of this redox ratio is plotted against  $\log P$ , straight lines are obtained, but the slopes differ from the expected value  $-n$ . Therefore the effect of the glass composition on the redox ratio can be estimated qualitatively but not quantitatively.

Papadopoulos [47] uses reaction 3.32 to predict the solubility of  $\text{SO}_3$  in soda-lime-silica melts. He therefore couples the equilibrium constant  $K_A$  of this reaction:

$$K_A = \frac{a_{\text{O}^-}^2}{a_{\text{O}^{2-}} \cdot a_{\text{O}^0}} \quad (3.34)$$

with the equilibrium constant  $K_B$  for the dissociation reaction for sodium sulphate (according to Papadopoulos the most stable sulphate in molten glass):



$$K_B = \frac{a_{\text{Na}_2\text{SO}_4}}{P_{\text{SO}_3} \cdot a_{\text{Na}_2\text{O}}} \quad (3.36)$$

Subsequently, the activity of  $\text{Na}_2\text{O}$  is written as [47]:

$$a_{\text{Na}_2\text{O}} = a_{\text{Na}^+}^2 \cdot a_{\text{O}^{2-}} \quad (3.37)$$

Rearrangement of equations 3.34, 3.36 and 3.37 leads to:

$$a_{\text{Na}_2\text{SO}_4} = P_{\text{SO}_3} \cdot \frac{K_B}{K_A} \cdot \frac{a_{\text{Na}^+}^2 \cdot a_{\text{O}^{2-}}^2}{a_{\text{O}^0}} \quad (3.38)$$

and written in concentrations:

$$[\text{SO}_3] \approx [\text{Na}_2\text{SO}_4] = p_{\text{SO}_3} \cdot \frac{K_B}{K_A} \cdot \frac{\gamma_{\text{Na}^+}^2 \cdot \gamma_{\text{O}^-}^2}{\gamma_{\text{O}^0} \cdot \gamma_{\text{Na}_2\text{SO}_4}} \cdot \frac{[\text{Na}^+]^2 \cdot [\text{O}^-]^2}{[\text{O}^0]} \quad (3.39)$$

with  $\gamma_i$  = the activity coefficient of component i.

The parameter  $[\text{Na}^+]^2 \cdot [\text{O}^-]^2 / [\text{O}^0]$  can be calculated for any glass melt on the basis of the theoretical composition. Papadopoulos plotted the  $\text{SO}_3$ -content (calculated for a standard  $\text{SO}_3$  pressure of 0.010 atm) in various soda-lime-silica glasses against this parameter, and obtained a straight line. The  $\text{SO}_3$  solubility can be predicted for any soda-silica glass composition by calculating the parameter  $[\text{Na}^+]^2 \cdot [\text{O}^-]^2 / [\text{O}^0]$  and reading off the  $\text{SO}_3$  content from the gauge curve.

The solubility of  $\text{SO}_3$  in glass melts containing little or no soda can not be predicted by this method.

### 3.5.5 A thermodynamic approach, based on activity coefficients

According to Buhler [48], the difficulty in describing the experimental facts with the existing theory (equation 3.3) can be overcome by starting from reaction schemes based on molecules instead of ions. In general, the redox reaction scheme should be given by



The redox reaction of iron in molten glass can then be described by:

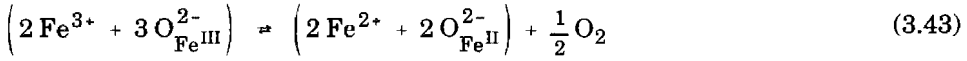


and the reaction equilibrium constant  $K(T)$  by:

$$K(T) = \frac{a_{\text{FeO}}^2 \cdot a_{\text{O}_2}^{1/2}}{a_{\text{Fe}_2\text{O}_3}} = \frac{\gamma_{\text{FeO}}^2 \cdot \gamma_{\text{O}_2}^{1/2}}{\gamma_{\text{Fe}_2\text{O}_3}} \cdot \frac{[\text{FeO}]^2}{[\text{Fe}_2\text{O}_3]} \quad (3.42)$$

This reaction equilibrium constant does not contain the activity of the free oxide ion. It is applicable for all glass compositions, with the restriction that the activity coefficients of FeO and  $\text{Fe}_2\text{O}_3$  depend on the glass structure, the temperature and the FeO and  $\text{Fe}_2\text{O}_3$  concentrations. The measurements of the redox reaction equilibria can be used to calculate these activity coefficients. According to Buhler [48], the ratio of the activity coefficients,  $\gamma$  ( $\gamma = \gamma_{\text{Ox}}^y / \gamma_{\text{Red}}^x$ ), for iron ( $\text{FeO}-\text{Fe}_2\text{O}_3$ ) ranges from 0.8 to 30 at 1200°C in different glasses. For chromium ( $\text{CrO}_3-\text{Cr}_2\text{O}_3$ ) the ratio of the activity coefficients in  $\text{Na}_2\text{O} \cdot 2\text{SiO}_2$  at 1400°C is  $10^{-9}$  [48].

The redox reaction of iron can also be described as:



If all  $\text{O}^{2-}$ -ions exhibit the same behaviour, independent of the nature of their neighbouring cations, the reaction scheme proposed by Johnston is valid. The condition can be formulated as:

$$\text{O}_{\text{FeIII}}^{2-} \equiv \text{O}_{\text{FeII}}^{2-} \equiv \text{O}^{2-} \quad (3.44)$$

and the redox reaction scheme then becomes:



The redox reaction equilibrium constant of this reaction is:

$$K_{\text{Fe,ionic}}^{**}(\text{T}) = \frac{[\text{Fe}^{2+}] \cdot p_{\text{O}_2}^{1/4}}{[\text{Fe}^{3+}]} \quad (3.46)$$

For a given glass composition, temperature and oxygen equilibrium pressure, the percentage of reduced iron (%  $\text{Fe}^{2+}$ ) is according to equation 3.46 independent of the total iron concentration:

$$\% \text{Fe}^{2+} = \frac{100\% \cdot [\text{Fe}^{2+}]}{[\text{Fe}]_{\text{total}}} = \frac{100\% \cdot K_{\text{Fe,ionic}}^{**}(\text{T})}{K_{\text{Fe,ionic}}^{**}(\text{T}) + p_{\text{O}_2}^{1/4}} \quad (3.47)$$

The results of Paul [5] indicate, that the percentage of reduced iron does depend on the total iron concentration. Therefore reaction 3.45 appears to be incorrect. If the reaction scheme based on molecules is taken as starting-point, the percentage of reduced iron does depend on the total iron concentration.

The reaction equilibrium constant of reaction 3.41 is given by:

$$K_{\text{Fe,molecular}}(\text{T}) = \frac{a_{\text{FeO}}^2 \cdot \sqrt{p_{\text{O}_2}}}{a_{\text{Fe}_2\text{O}_3}} = \frac{\gamma_{\text{FeO}}^2}{\gamma_{\text{Fe}_2\text{O}_3}} \cdot \frac{\beta^2}{\alpha} \cdot \frac{[\text{Fe}^{2+}]^2 \cdot p_{\text{O}_2}^{1/2}}{[\text{Fe}^{3+}]} \quad (3.48)$$

with  $a_i = \gamma_i \cdot [i]$

$$\begin{aligned} [\text{Fe}_2\text{O}_3] &= \alpha \cdot [\text{Fe}^{3+}] \\ [\text{FeO}] &= \beta \cdot [\text{Fe}^{2+}] \end{aligned} \quad (3.49)$$

and under certain conditions [48,49], the percentage of reduced iron is according to Buhler:

$$\% \text{Fe}^{2+} = \frac{100\%}{1 + \sqrt{g \cdot [\text{Fe}]_{\text{total}}}} \quad (3.50)$$

and  $g$  is defined in [48]. With the aid of this approximation, the qualitative effect of the total iron concentration on the percentage reduced iron can be predicted. The quantitative effect cannot be predicted, because the factor  $g$  includes the activity coefficients of  $\text{FeO}$  and  $\text{Fe}_2\text{O}_3$ , and they depend on their concentrations.

### 3.6 PREDICTIONS OF THE REDOX REACTION EQUILIBRIUM CONSTANT, BASED ON THE GLASS COMPOSITION

The various methods to predict the redox reaction equilibrium constant based on the glass composition all have their disadvantages. The method proposed by Pyare (chapter 3.5.3), based on the hypothetical presence of peroxides in the molten glass, provides for additional questions. The reaction schemes are incomplete and the nature of the reacting oxygen  $\text{O}(\text{glass})$  is not discussed. Moreover, the free oxygen ion activity  $a_{\text{O}_2^-}$  and the new parameter  $K_{\text{peroxide}}$  are unknown. Therefore this method is both from a theoretical and a practical point of view useless and senseless.

The disadvantages of the method proposed by Hirashima (complex formation of the metal ions, chapter 3.5.2) are:

- the activity of the free oxygen ion,  $a_{\text{O}_2^-}$ , remains present as an unknown parameter in the equation for the redox reaction equilibrium constant;
- more data on the redox reaction equilibrium constants of all polyvalent elements as a function of glass composition and temperature are needed to obtain usable reaction schemes;
- in many cases (iron, vanadium, tin) more than one reaction scheme is needed to account for the behaviour of the polyvalent elements in high and low temperature regions;
- the data concerning the coordination states of the transition metals have generally been derived for glasses at room temperature. These data may not be representative for the "tendency to form complexes" in the molten glass.

It is unlikely that in the near future the redox reaction equilibria of polyvalent elements in molten glass can be predicted from simple reaction schemes for the complex formation.

The presence of metaloxide molecules in the molten glass, as suggested by Buhler (chapter 3.5.5), is highly unlikely. In the glass melt, the metal ions will be surrounded by oxide ions. It is impossible to identify discrete molecular units [42].

Moreover, the theory has no practical application because the activity coefficients of the metaloxides in molten glass are unknown. The ratio of the activity coefficients can be obtained by measuring the redox ratios of the metal ions in the selected glass melt with the exact metal concentration and comparing the redox ratios with the theoretical data for pure solid metaloxide systems. But then, the measured redox ratios might as well be used directly in the redox reaction equilibrium equation 3.9.

Furthermore, the reaction equilibrium 3.48 implies that the following relation between oxygen equilibrium pressure and the valency state of iron holds:

$$\frac{[\text{Fe}^{2+}]^2}{[\text{Fe}^{3+}]} \sim \sqrt{p_{\text{O}_2}} \quad (3.51)$$

while the data of Johnston [17] indicate that for the redox ratio the equation:

$$\frac{[\text{Fe}^{2+}]}{[\text{Fe}^{3+}]} \sim p_{\text{O}_2}^{1/4} \quad (3.52)$$

is approximately valid. By applying an assumption with relation to the activity coefficients of  $\text{Fe}_2\text{O}_3$  and  $\text{FeO}$  and  $\alpha$  and  $\beta$  (as defined in equations 3.48 and 3.49), Buhler was able to arrive at the same equation. This assumption however is not verifiable, because  $\alpha$  and  $\beta$  are unknown.

The main advantage of the theory proposed by Buhler is that it provides for an explanation for the dependency of the redox ratio of iron on the total iron concentration. This concentration dependency was found by several workers [5] in quenched glass samples containing 0.04-1 weight-% Fe. However this phenomenon can also be explained by assuming the activity coefficients of the  $\text{Fe}^{2+}$  and  $\text{Fe}^{3+}$  ions to be dependent of the concentration. Then equation 3.7 is not valid. The redox reaction equilibrium constant  $K^{**}(\text{T})$  should then be established again for any concentration of M. Therefore the theory proposed by Buhler can be regarded as unlikely and insignificant.

Two of the methods described in chapter 3.5 have practical significance. Baucke determined the optical basicity of glass samples with spectral measurements. The redox ratios of some polyvalent ions in the sample could be predicted with the aid of a gauge curve, in which the redox ratio of one polyvalent element is plotted against the optical basicity of glass samples. The composition of the glass samples however may not differ too much. According to Baucke, the measurements at room temperature are also representative for the redox ratios at elevated temperatures, even if the glass sample contains two polyvalent elements [22]. This method therefore offers the possibility to predict redox

ratios on the basis of the glass composition, but does not provide for a theoretical background.

The method proposed by Douglas et.al. and Papadopoulos (chapter 3.5.4) accounts for the amount of bridging, non-bridging and free oxide ions in the melt. If a gauge curve of the redox ratio of the polyvalent element of interest has been made for glass samples of (slightly) varying composition, the redox ratio of this polyvalent element can be predicted for a glass with an intermediate composition. This method is even valid for sulphur-containing glasses.

At the moment, it is not possible to predict the redox reaction equilibrium constant  $K^{**}$  of a polyvalent ion for any glass composition. Only if the redox reaction equilibria have been determined in various glass samples with a slightly different composition, a reliable prediction can be made. But for deviating glasses, or for glasses containing lower or higher concentrations of the polyvalent element, the reaction equilibrium constant  $K^{**}(T)$  has to be determined independently.

In this thesis, the reaction equilibrium constants of iron, antimony, cerium, chromium and sulphur in soda-lime-silica glass, TV-glass and E-glass will be treated. The constants could not be predicted on the basis of the glass composition, because adequate gauge curves are not available. For the three glass compositions, separate measurements have been made. It was not possible to prove or disprove the presented theories for the dependency of the redox ratios on the glass composition on the basis of these measurements.

## Literature

- [1] Bamford, C.R.  
"Colour generation and control in glass (Glass science and technology 2)"  
Elsevier Scientific Publishing Company Amsterdam-Oxford-New York (1977)
- [2] Rüssel, C.  
Polyvalente Elemente in oxidischen Glasschmelzen  
Thesis, Universität Erlangen (1991)
- [3] Hessenkemper, H.; Brückner, R.  
Influence of redox conditions on the isothermal workability of glass melts  
*Glastechnische Berichte* **63** (1990) p.244-254
- [4] Wermter, F.  
Sauerstoffpartialdruck und Redoxzustand in einer industriellen Glasschmelze  
Vortrag im Fachausschuß III der DGG am 20. April 1988
- [5] Paul, A.; Douglas, R.W.  
Ferrous-ferric equilibrium in binary alkali silicate glasses  
*Physics and Chemistry of Glasses* **6** (1965) no.6 pp.207-211
- [6] Paul, A.; Douglas, R.W.  
Cerous-ceric equilibrium in binary alkali borate and alkali silicate glasses  
*Physics and Chemistry of Glasses* **6** (1965) no.6 pp.212-215
- [7] Harding, F.L.  
Effect of base glass composition on amber colour  
*Glass Technology* **13** (1972) no.2 pp.43-49
- [8] Johnston, W.D.  
Oxidation-reduction equilibria in molten  $\text{Na}_2\text{O}\cdot 2\text{SiO}_2$  glass  
*Journal of the American Ceramic Society* **48** (1965) no.4 pp.184-190
- [9] Krol, D.M.; Rommers, P.J.  
Oxidation-reduction behaviour of antimony in silicate glasses prepared from raw material and cullet  
*Glass Technology* **25** (1984) no.2 pp. 115-118
- [10] Freude, E.  
Voltammetrische Untersuchung des Redoxverhaltens polyvalenter Ionen in Glasschmelzen, insbesondere von Technetium  
Thesis, Universität Erlangen (1989)
- [11] Stahlberg, B.; Mosel, B.D.; Müller-Warmuth, W.; Baucke, F.G.K.  
Combined electrochemical and Mössbauer studies of the  $\text{Sb}^{3+}/\text{Sb}^{5+}$  equilibrium in a silicate glassforming melt  
*Glastechnische Berichte* **61** (1988) pp.335-340
- [12] Schreiber, H.D.; Kozak, S.J.; Leonhard, P.G.; McManus, K.K.  
Sulfur chemistry in a borosilicate melt, Part 1: Redox equilibria and solubility  
*Glastechnische Berichte* **60** (1987) no.12 pp.389-398
- [13] Schreiber, H.D.; Fowler, R.W.; Ward, C.C.  
Sulphate as a selective redox buffer for borosilicate melts  
*Physics and Chemistry of Glasses* **34** (1993) no.2 p.66-70



- [14] Goldman, D.S.  
Redox and sulfur solubility in glass melts  
"Gas bubbles in glass", published by the International Commission on Glass Robert Louis  
Brussels (1985) pp.74-91
- [15] Chopinet, M.H.; Massol, J.J.; Barton, J.L.  
Factors determining the residual sulfate content of glass  
*Glastechnische Berichte Sonderband Kongreßvorträge* (1983) band 1 Hamburg pp.596-601
- [16] Chopinet, M.H.; Barton, J.L.  
The effect of melting temperature on the residual sulfate content of glass  
Collected papers of the XIV International Congress on Glass New Delhi (1986) 3 pp.9-15
- [17] Johnston, W.D.  
Oxidation-reduction equilibria in iron-containing glass  
*Journal of the American Ceramic Society* 47 (1964) no.4 pp.198-201
- [18] Rüssel, C.  
Polyvalent ions in glass melts  
*Glastechnische Berichte* 63K (1990) pp.197-211
- [19] Lenhart, A.; Schaeffer, H.A.  
Elektrochemische Messung der Sauerstoffaktivität in Glasschmelzen  
*Glastechnische Berichte* 58 (1985) no.6 pp.139-147
- [20] Lenhart, A.; Schaeffer, H.A.  
Redox behaviour of glass melts  
*Diffusion and defect Data* 53-54 (1987) pp.335-344
- [21] Rüssel, C.; Kohl, R.; Schaeffer, H.A.  
Interaction between oxygen activity of  $\text{Fe}_2\text{O}_3$  doped soda-lime-silica glass melts and  
physically dissolved oxygen  
*Glastechnische Berichte* 61 (1988) no.8 p.209-213
- [22] Baucke, F.G.K.; Duffy, J.A.  
Redox reactions between cations of different polyvalent elements in glass melts: an optical  
basicity study  
*Physics and Chemistry of Glasses* 34 (1993) no.4 p.158-163
- [23] Rüssel, C.; Freude, E.  
Voltammetric studies in a soda-lime-silica glass melt containing two different polyvalent  
ions  
*Glastechnische Berichte* 63 (1990) no.6 p.149-153
- [24] Müller-Simon, H.; Ernas, T.  
The influence of chromium on the oxidation state of an industrially melted amber glass  
Proceedings of the XVI International Congress on Glass Madrid (1992) 6 p.197-202
- [25] Close, W.P.; Tillman, J.F.  
Chemical analysis of some elements in oxidation-reduction equilibria in silicate glasses  
*Glass Technology* 10 (1969) no.5 p.134-146
- [26] Grove, F.J.  
Spectral transmission of glass at high temperatures and its application to heat-transfer  
problems  
*Journal of the American Ceramic Society* 44 (1961) p.317-320

- 
- [27] Kruszewski, S.  
Total heat-transmission coefficients of amber and green glasses in temperatures of melting range  
*Journal of the American Ceramic Society* **44** (1961) p.333-339
- [28] Müller-Simon, H.  
Die elektrochemische Sauerstoffaktivitätsmessung in industriellen Glasschmelzanlagen  
Thesis Fachbereich Werkstoffwissenschaften der Technischen Universität Berlin (1992)
- [29] Beerkens, R.G.C.  
Chemical equilibrium reactions as driving forces for growth of gas bubbles during refining  
*Glastechnische Berichte* **63K** (1990) pp.222-242
- [30] Krämer, F.W.  
A basicity number concept to estimate the chemical gas solubility of oxygen in technical antimony refined glass melts  
*Glastechnische Berichte* **63K** (1990) pp.243-252
- [31] Scholze, H.  
Gases in glass  
*Proceedings of the 8<sup>th</sup> Int. Congress on Glass* (1968) pp.69-83  
Society of Glass Technology Sheffield
- [32] Nair, K.M.; White, W.B.; Roy, R.  
Solubility of oxygen in glasses  
*Journal of the American Ceramic Society* **48** (1965) pp.52
- [33] Toop, G.W.; Samis, C.S.  
Some new ionic concepts of silicate slags  
*Can. Met. Quart.* **1** (1962) pp.129-152
- [34] Dietzel, A.  
Die Kationenfeldstärken und ihre Beziehungen zu Entglasungsvorgängen, zur Verbindungsbildung und zu den Schmelzpunkten von Silicaten  
*Z. Elektrochem.* **48** (1942) pp.9-23
- [35] Sun, K.H.  
A scale of acidity and basicity in glass  
*The Glass Industry* **73-74** (1948) pp. 98
- [36] Manring, W.H.; Hopkins, R.W.  
Use of sulfates in glass  
*The Glass Industry* **39** (1958) pp.139-142,170
- [37] Simpson, W.; Myers, D.D.  
The redox number concept and its use by the glass technologist  
*Glass Technology* **19** (1978) no.4 pp.82-85
- [38] Barton, J.L.; Chopinet, M.-H.  
The problem of predicting the redox state of a glass  
*Proceedings of the First International Conference on Advances in the Fusion of Glass, The American Ceramic Society New York* (1988) pp.30.1-30.8
- [39] Dubois, B.; Chopinet, M.-H.; Barton, J.  
A study of the efficiency of reducing agents in glass melting  
*Proceedings of the XV International Congress on Glass Leningrad* (1989) **3b** pp.82-85

- 
- [40] Manring, W.H.; Davis, R.E.  
Controlling redox conditions in glass melting  
*The Glass Industry* **59** (1978) pp.13-16,23-24,30
- [41] Kohl, R.; Schaeffer, H.A.  
Oxidation states of glass melts  
*Diffusion and Defect Data* **53-54** (1987) pp.325-343
- [42] Baucke, F.G.K.; Duffy, J.A.  
The effect of basicity on redox equilibria in molten glasses  
*Physics and Chemistry of Glasses* **32** (1991) no.5 pp.211-218
- [43] Paul, A.; Lahiri, D.  
A note on the study of the  $\text{As}_2\text{O}_3$ - $\text{As}_2\text{O}_5$  equilibrium in glass  
*Transactions of the Indian Ceramic Society* **22** (1963) no.4 pp.146-150
- [44] Pyare, R.; Singh, S.P.; Singh, A.; Nath, P.  
The  $\text{As}^{3+}$ - $\text{As}^{5+}$  equilibrium in borate and silicate glasses  
*Physics and Chemistry of Glasses* **23** (1982) no.5 pp.158-168
- [45] Hirashima, H.; Yoshida, T.  
Redox equilibria and constitution of polyvalent ions in oxide melts and glasses  
*Glastechnische Berichte* **61** (1988) no.10 pp.283-292
- [46] Douglas, R.W.; Nath, P.; Paul, A.  
Oxygen ion activity and its influence on the redox equilibrium in glasses  
*Physics and Chemistry of Glasses* **6** (1965) no.6 pp.216-223
- [47] Papadopoulos, K.  
The solubility of  $\text{SO}_3$  in soda-lime-silica melts  
*Physics and Chemistry of Glasses* **14** (1973) no.3 pp.60-65
- [48] Buhler, P.; Weißmann, R.  
Thermodynamics of the  $\text{Fe}^{2+}$ - $\text{Fe}^{3+}$  equilibrium in glass melts  
Proceedings of the XVI International Congress on Glass Madrid (1992) **6** p.203-207
- [49] Buhler, P.; Weißmann, R.  
Thermodynamik der Wechselwirkung: oxide polyvalenter Elemente in der Glasschmelze-Sauerstoff  
To be published (in russian)

Chapter 4  
 Determination of the equilibrium constants  
 of redox reactions in molten glass  
 - An overview -

**4.1 THE REDOX REACTION EQUILIBRIUM**

As we have seen in chapter 3, polyvalent elements like iron, antimony and sulphur in molten glass can convert from one valency state into another. The electron donator or acceptor for this conversion in silica-based glasses is usually oxygen. The overall-reaction is generally presented by:



The importance of the equilibrium state of these redox reactions has been discussed in chapter 3. The redox reaction equilibrium constant  $K^{**}(T)$  has been defined as

$$K^{**}(T) = \frac{[M^{x+}] \cdot p_{O_2}^{n/4}}{[M^{(x+n)+}]} \quad (4.2)$$

The equilibrium state of this reaction depends strongly on the temperature. The redox reaction equilibrium constant can be written as a function of the enthalpy  $\Delta H^{**}$  and entropy  $\Delta S^{**}$  (assuming the enthalpy and entropy are no functions of the temperature):

$$K^{**}(T) = \exp \left\{ \frac{-\Delta H^{**}}{R_g \cdot T} + \frac{\Delta S^{**}}{R_g} \right\} \quad (4.3)$$

with  $R_g$  = gas constant 8.314 J·mole<sup>-1</sup>·K<sup>-1</sup>  
 $T$  = absolute temperature [K]

Note: the reaction equilibrium constant  $K^{**}(T)$  is based on ion concentrations and the oxygen equilibrium gas pressure, because these quantities can be measured. The equilibrium constant  $K^{**}$  strongly depends on the glass composition and may also depend on the concentration of the polyvalent element. The effect of the glass composition on the equilibrium  $K^{**}(T)$  is not clear. Therefore, measurements of the equilibrium state as a function of temperature in one glass composition can not be used to predict the equilibrium state in another glass (see chapter 3).

The colour of the glass melt and the final product depend on the equilibrium state of some polyvalent elements like iron, chromium and sulphur. The fining action of fining agents like antimony and cerium is dependent on their equilibrium state (see chapter 3). A qualitative and quantitative insight in the redox reaction equilibrium of the elements iron, antimony, cerium, chromium and sulphur in some commercial glasses is the main objective of this thesis. Therefore, the equilibrium constants  $K^{**}$  have been measured as a function of temperature.

The equilibrium constants of the redox reactions can be determined by different methods. The methods can be divided into two categories:

1. A glass melt is equilibrated with a certain atmosphere at a fixed temperature, and then the melt is cooled down rapidly to room temperature. Subsequently the valency state of the polyvalent elements is determined with spectrophotometric or wet chemical analysis (redox titration).
2. With the aid of electrochemical or spectral methods the equilibrium of the redox reaction is measured in situ in the molten glass.

Various techniques from both categories have been applied by several researchers to determine the redox reaction equilibrium constants in glasses. The results are not always in agreement, and this might arise from the differences in the analysing methods or conditions. Therefore, the main lines of the different methods will be discussed in this chapter: the analysis of glass samples after the cooling of molten glass in section 4.2 and the in situ measurements in section 4.3. The advantages and disadvantages of all methods will be outlined briefly.

For the determination of the equilibrium constants for iron, antimony, cerium, chromium and sulphur in some commercial glasses in this thesis, different analysing methods have been used. The emphasis however lies on two electrochemical methods. These are:

- the on-line measurements of the oxygen equilibrium pressure in the molten glass with the aid of an oxygen sensor;
- square wave voltammetry measurements.

In section 4.4, the choice for these methods is motivated.

Some processing of the results of these measurements is necessary to obtain information on the redox reaction equilibria. This is rather complicated and requires a thorough knowledge of the theoretical backgrounds of the techniques. Therefore, the basic principles of the electrochemistry will be elucidated in chapter 5.2. Subsequently, the applications and processing of the oxygen equilibrium pressure measurements will be explained in section 5.4 and the square wave voltammetry measurements are discussed in section 5.5.

#### **4.2 MEASUREMENTS OF THE REDOX REACTION EQUILIBRIUM STATE AFTER COOLING**

A glass with a well-known composition containing one polyvalent element is heated in a certain atmosphere at a fixed temperature. After some time, the gases in the molten glass are assumed to be in equilibrium with the atmosphere. The melt should then be free of bubbles. Generally the oxygen pressure  $p_{O_2}$  of equation 4.2 is assumed to be equal to the partial oxygen pressure in the atmosphere. Then the melt is cooled down rapidly by quenching it in water or by pouring it out on a cool surface.

If the melt contains only one polyvalent element, and if the concentration of this element is much larger than the concentration of oxygen which can be physically dissolved, the redox ratio does not shift if the temperature decreases fast enough (see chapter 3.2.3). The oxygen pressure of equation 4.2 is then known, and the valency state of the polyvalent element can be measured with spectral techniques or chemical analysis.

Note: if the glass contains more than one polyvalent element, or if the oxygen concentration lies in the same order of magnitude as the concentration of the polyvalent element (or larger), the redox reaction equilibrium may change during cooling (see chapter 3, sections 2.3 and 2.5).

Furthermore, the equilibrium state may shift if the cooling of the melt takes a long time, because then oxygen from the surrounding atmosphere diffuses into the melt.

## **4.2.1 Spectral techniques to investigate the valency state of polyvalent elements**

### 4.2.1.1 Spectrophotometry

The absorption of infrared, visible and ultraviolet radiation in a glass sample can depend on the amount and valency state of the polyvalent ions, for instance iron, chromium, nickel and copper. By comparing the transmission spectra of the glass sample with the spectra of standards, the concentration of these polyvalent elements in the different valency states can be determined [1,2,3,4]. The wavelength region that should be scanned depends on the polyvalent element to be investigated. Often, only the concentration of one of the valency states of the polyvalent ion is measured. The concentration of the other valency state is then calculated from the difference between the total concentration of the polyvalent element and the measured concentration of the first mentioned valency state.

Spectrophotometric measurements are often used to determine the amount of  $\text{Fe}^{2+}$  and  $\text{Fe}^{3+}$  in glass samples.  $\text{Fe}^{2+}$  gives a broad absorption peak at 1000 nm and  $\text{Fe}^{3+}$  gives small peaks at about 300 nm [1].

### 4.2.1.2 Other spectral methods

Depending on the nature of the polyvalent element, some other spectral methods can be used to measure the concentration of the different valency states. For instance, the concentration of pentavalent and trivalent antimony,  $[\text{Sb}^{5+}]$  and  $[\text{Sb}^{3+}]$ , can be determined using Mössbauer spectroscopy [5]. The concentrations of the pentavalent and of the trivalent state of arsenic,  $[\text{As}^{+3}]$  and  $[\text{As}^{5+}]$ , in glass samples have been determined with the aid of Raman-scattering [6,7].

## **4.2.2 Other techniques to determine the concentration of polyvalent elements in glass samples**

The total concentration of the different elements can be measured with X-ray fluorescence. The sulphide and total sulphur concentrations in flat glass samples can be determined with optical and electron paramagnetic resonance investigations [8].

### 4.2.3 Wet-chemical analysis of the valency state of polyvalent elements in glass samples

After equilibration and cooling of the molten glass, the glass samples are grinded. Subsequently, they are dissolved in a strong acid (HF or a combination of HF and another acid). It is assumed that during this procedure, the valency state of the polyvalent element does not change. Sometimes the decomposition of the glass samples have to be performed under an atmosphere without oxygen (Ar [9] or CO<sub>2</sub> [10]) in order to avoid oxidation of the reduced form of the polyvalent element.

The concentration of (one of) the valency states can then be determined by titration with the proper oxidator or reductor. The methods are called after the determination of the endpoint: potentiometry, polarography or colorimetry. The procedures of the chemical analyses of the following polyvalent elements are described in detail in:

Fe <sup>2+</sup>	[10]
Fe <sup>2+</sup> /Fe <sub>total</sub>	[8,11]
Fe <sup>2+</sup> /Fe <sup>3+</sup> /Fe <sub>total</sub>	[12]
Sb <sup>3+</sup>	[9,10,13]
As <sup>5+</sup> /As <sub>total</sub>	[14]
As <sup>3+</sup> /As <sup>5+</sup> /As <sub>total</sub>	[10]
Ce <sup>4+</sup> /Ce <sub>total</sub>	[9,15,16]
Cr <sup>6+</sup>	[15]
S <sup>2-</sup> /S <sub>total</sub>	[8,15,17]

The presence of other polyvalent elements may inhibit an accurate determination of the valency state of the element of interest.

### 4.2.4 Other analysing methods for the determination of the valency state of polyvalent elements in acid solutions

After dissolution of the grinded glass samples in strong phosphoric acid, the sulphide and total sulphate concentrations can be determined with ion chromatography [17]. The amounts of SO<sub>4</sub><sup>2-</sup> and SO<sub>3</sub><sup>2-</sup> in a strong HF/HCl solution can be measured spectrophotometrically, at wavelenghts of 530 nm and 520 nm respectively [18].

Glass samples containing antimony can be dissolved in a mixture of HClO<sub>4</sub>, HF and HNO<sub>3</sub>. The total concentration of antimony in this solution can be deter-



mined by inductively coupled plasma emission spectrometry, using the Sb emission at a wavelength of 231.15 nm [13].

In these cases, it is assumed that during the dissolution procedure, the valency state of the polyvalent element does not change.

#### **4.2.5 Advantages and disadvantages of redox ratio measurements after cooling**

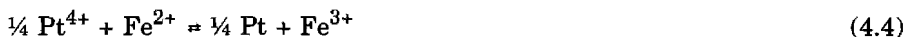
Advantages of analysis of the valency state of polyvalent elements at room temperature are:

- the analyses can be performed with a relatively simple laboratory set-up and chemicals. In principle standard equipment can be used.

Disadvantages:

- The molten glass has to come in equilibrium with the surrounding atmosphere. This will take some time, because the diffusion of oxygen into or out of the glass melt is slow (see chapter 2.2.6). The time, necessary to equilibrate the glass, must be determined experimentally. Many glass samples should be exposed to a certain atmosphere for different times, and then cooled rapidly to room temperature. Subsequently, the redox ratios in all glass samples must be determined. Only if the redox ratios are the same in samples molten during different periods, the molten glass will probably have been equilibrated [11,16]. The final redox ratio should not depend on the initial valency state of the polyvalent element. For instance if ferrous oxalate is added to the batch instead of  $\text{Fe}_2\text{O}_3$ , the final redox ratio  $[\text{Fe}^{2+}]/[\text{Fe}^{3+}]$  should obtain the same value [11].
- Paul [11,15] demonstrated, that the equilibration time for small glass samples (about 10 grams) is extremely long (60 hours). The equilibration can be speeded up somewhat by stirring of the glass. The long waiting time can lead to other problems:
  - \* evaporation of glass components like Na or B. This will change the glass composition;
  - \* corrosion of the crucible material. An increase in the  $\text{Al}_2\text{O}_3$  content of the glass, due to corrosive attack of the  $\text{Al}_2\text{O}_3$ -crucible by the molten glass (8-10%) altered the ferrous-ferric equilibrium to a considerable extent [11].  $\text{SiO}_2$ -crucibles are corroded by the molten glass as well, but have little influence on the redox ratio [11];

\* a shift of the redox ratio due to interactions with the crucible material. Platinum may have an oxidizing influence on the ferrous-ferric equilibrium in glasses containing less than about 30 mole% alkali oxide [11]. As an explanation for this phenomenon, Paul [11] assumed that platinum dissolves in the melt as  $\text{Pt}^{4+}$  and then reacts with iron:



This theory is supported by the fact that on the surface of the glass melt metallic platinum has been found.

- The redox reaction equilibrium can change during the cooling of the melt. Close and Tillman have demonstrated that the cooling rate has an influence on the final redox ratio of glasses containing both iron and chromium [15]. The redox ratio should, according to the theory (chapter 3) not shift during cooling if the melt contains only one polyvalent element and if the concentration of  $\text{O}_2$  in the melt is small in comparison to the concentration of the polyvalent ion. The physically dissolved  $\text{O}_2$  equilibrium concentration is thought to be linearly dependent on the oxygen partial pressure in the surrounding atmosphere (chapter 2):

$$[\text{O}_2] = L_{\text{O}_2} \cdot p_{\text{O}_2} \quad (4.5)$$

The physical solubility of oxygen  $L_{\text{O}_2}$  is not known for most glasses, and therefore the concentration of  $\text{O}_2$  in the molten glass can not be estimated. However it is generally assumed to be less than  $10 \text{ mole} \cdot \text{m}^{-3}$  at 1 bar  $\text{O}_2$  pressure (see chapter 5.4). Many reseachers therefore assume that the concentration of the polyvalent element exceeds that of the physically dissolved oxygen by some orders of magnitude [5,19].

- In order to avoid shifts in the redox ratio during cooling, the melt should contain only one polyvalent element. Therefore the batch ingredients should be chosen with care.
- In case of wet-chemical analysis, the redox ratio may change while the glass is grinded and dissolved in the acid solution. In order to avoid oxidation of the reduced form of the polyvalent element, the dissolution is sometimes performed under an argon [9] or  $\text{CO}_2$  [10] atmosphere. It is uncertain if these precautions are sufficient to prevent conversion of the valency state of polyvalent elements.
- The concentrations of the polyvalent elements in the glass samples is usually low, in the order of 0.5 weight-%. The accuracy of the analysis might be insufficient, especially if the concentration of only one valency state is determined, while the total concentration of the polyvalent element is

derived from the prepared glass composition.

- Reliable standards are necessary to calibrate the analysing methods, for instance in the case of spectrometric measurements.

### 4.3 DIRECT MEASUREMENTS OF THE REDOX REACTION EQUILIBRIUM IN THE MOLTEN GLASS

In order to avoid shifts in the redox reaction equilibrium during cooling, the equilibrium can best be measured in situ. Up to now, two kinds of analysing methods which are applicable for molten glass have been developed:

- emission spectroscopy;
- electrochemical methods.

#### 4.3.1 Emission spectroscopy

##### 4.3.1.1 Emission spectroscopic measurements of molten glass [2,20]

The radiation emitted from the glass and its surroundings at high temperatures can be measured using a Fourier transform infrared spectrophotometer. The signal can be converted into the absorption coefficient of  $\text{Fe}^{2+}$ , and this quantity is directly related to the volume average  $\text{Fe}^{2+}$  content of the glass melt.

##### 4.3.1.2 Procedure [2]

A Pt75-Rh25-crucible containing the melt is placed in a small, electrically heated furnace. The radiation emitted from the glass and the crucible leaves the furnace through an aperture in the top, and is collimated into a Fourier transform infrared spectrophotometer. The emissivity of the platinum crucible can be mathematically subtracted from the emissivity of the glass melt. The resulting emissivity is converted into the absorption coefficient of  $\text{Fe}^{2+}$ . Goldman and Berg [21] demonstrated that room- and high- temperature absorptions due to  $\text{Fe}^{2+}$  are identical at 1.67  $\mu\text{m}$ . They also showed that  $\text{Fe}^{2+}$  absorption in the melt is related to the  $\text{Fe}^{2+}$  concentration. Based on these conclusions, a volume average  $\text{Fe}^{2+}$  content can be obtained directly, and  $\text{Fe}^{3+}$  can be calculated from the difference in total iron content and  $\text{Fe}^{2+}$  content. After some time the ratio  $[\text{Fe}^{3+}]/[\text{Fe}^{2+}]$  remained constant. The melt was assumed to be in equilibrium with air, and the oxygen equilibrium pressure  $p_{\text{O}_2}$  in the glass is taken to be 0.21 bar. Since the concentrations of  $\text{Fe}^{2+}$  and  $\text{Fe}^{3+}$  are known, the redox reaction equilibrium constant  $K^{**}(\text{T})$  can be calculated.

### 4.3.1.3 Advantages and disadvantages of emission spectroscopy

Advantages of this method are:

- the measurements can be made in situ;
- the method is fast, and therefore oxidation processes that take place in the melt can be followed;
- the analysing method has no influence on the oxidation state of the molten glass;
- the results can be related directly to the transmission coefficient in the molten glass, which is the deciding parameter for the heat penetration in the industrial glass melting tank [20].

Disadvantages:

- the measurements require a rather complicated experimental set-up;
- the measured data (the emissivity of both glass and crucible) has to be converted to the concentration of  $\text{Fe}^{2+}$  by way of comprehensive mathematical Fourier transformations;
- at the moment, the method is only applicable for iron-containing glasses;
- the influence of other polyvalent elements on the measurement of ferrous iron is not clear.

## **4.3.2 Electrochemical techniques**

### 4.3.2.1 Electrochemical techniques in molten glass

Molten glass is, just like an aqueous solution, an electrolyte. The electrical conduction through molten glass takes place by migration of the mobile alkali ions  $\text{Li}^+$ ,  $\text{Na}^+$  and  $\text{K}^+$  [22]. Barton proved, that migration of sodium ions in molten glass indeed occurs [23]. Therefore all electrochemical techniques that are used to measure the ion concentrations or the redox reaction equilibria in aqueous solutions can be applied in the glass melts on the condition that suitable electrodes (especially reference electrodes and selective electrodes) can be found.

### 4.3.2.2 Quantities that can be measured with electrochemical methods

The electrochemical methods can be divided into the categories:

- potentiometric experiments, in which the current is zero. In this type of measurements, a deviation from the equilibrium state, usually a concentration difference, between two electrodes is measured as the potential difference between these electrodes;

- voltammetric techniques: the potential of one electrode, the working electrode, is forced to adhere to a known program. The resulting current is measured as a function of the applied potential. So in this type of measurements, the existing equilibrium state is disturbed by applying a potential difference, and the reaction of the system to this disturbance, a current, is measured;
- other techniques (not discussed in this thesis).

### Potentiometric experiments

In potentiometric experiments, the difference in electrochemical potential between two electrodes is measured. This potential difference can under certain conditions be converted into a difference in concentration of a certain ion at the two electrodes.

With potentiometric experiments, the oxygen equilibrium pressure in the molten glass can be measured. To do this, two platinum electrodes are used. One of them is dipped in the glass melt, the other is flushed with a reference gas with a known partial oxygen pressure  $p_{O_2}$ (reference gas). This reference electrode and gas are separated from the melt by an  $O^{2-}$ -conducting material. If the oxygen equilibrium pressure in the molten glass,  $p_{O_2}$ (glass melt), differs from the partial oxygen pressure in the reference gas, a potential difference between the electrodes arises.

If the electrodes were short-circuited, redox reactions would take place at the electrodes in order to neutralize the difference. At the electrode, at which the oxygen pressure is higher, the following reaction would take place:



The  $O^{2-}$ -ions travel through the  $O^{2-}$ -conducting material to the electrode at which the oxygen pressure is lower. There it reacts to  $O_2$ :



The electrons that are liberated during this reaction are transported to the other electrode. This process continues until the oxygen pressure is the same at both electrodes.

During the potentiometric experiments, the electrodes are not short-circuited, but are connected with a high impedance voltmeter. Now a negligible small current flows through the system. The driving force of the redox reactions is measured as the potential difference  $E_m$  between the two electrodes:

$$E_m = \frac{R_g \cdot T}{4 \cdot F} \ln \frac{p_{O_2}(\text{glass melt})}{p_{O_2}(\text{reference gas})} \quad (4.8)$$

The oxygen equilibrium pressure in the glass melt,  $p_{O_2}(\text{glass melt})$ , is now given by:

$$p_{O_2}(\text{glass melt}) = p_{O_2}(\text{reference gas}) \cdot \exp \left\{ \frac{4 \cdot F \cdot E_m}{R_g \cdot T} \right\} \quad (4.9)$$

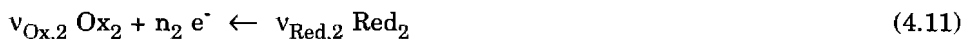
Since the oxygen equilibrium pressure dominates the redox state of the glass, this quantity is of great interest for glass technologists. If the dependency of the oxygen equilibrium pressure on the temperature is known, the redox reaction equilibrium constant  $K^{**}(T)$  and the enthalpy  $\Delta H^{**}$  and entropy  $\Delta S^{**}$  can be obtained by mathematical operation of the experimental data (see chapter 5.4).

### Voltammetric techniques [24]

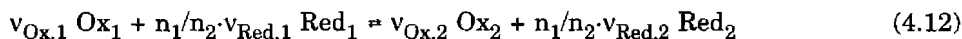
Three electrodes are dipped in the molten glass: the working, counter and reference electrode. By applying a potential difference between the working electrode and the reference electrode in a glass melt containing electro-active species, the redox reaction equilibrium of these components in the surroundings of the working electrode can be forced in one direction. For instance, if the potential of the working electrode is sufficiently negative with respect to its equilibrium value, the reaction



occurs at the working electrode, and the equilibrium of this reaction is forced to the right. The electrons that are needed for this reaction are released by a redox reaction at the counter electrode. This reaction can be written as:



and the equilibrium of this reaction is shifted to the left. The overall reaction scheme is:



The electrons are not transferred through the glass melt, but flow from the counter to the working electrode. The current can be measured as a function of the applied potential between working and reference electrode. Since no current passes through the reference electrode, the potential of this electrode can be regarded as constant (see chapter 5.2.6).

Notice that in the voltammetric techniques, the redox reaction equilibrium state is deliberately disturbed by changing the activation energy of the reaction. The extent of the shift of the equilibrium state at a certain potential is measured as the current that flows between the electrodes.

The applied potential-time curve might be very complicated. In a *voltammogram*, the measured current is plotted against the applied potential. The shape of this curve depends on many factors. The height of the current in a convection-free system is governed by:

- the total concentration of the reacting species (1),  $C_{\text{reactant}}$ , which is in most voltammetric experiments equal to the total concentration of the redox-active species (1),  $C_{\text{total}}$ ;
- the diffusion coefficient of the reacting species (1),  $D_{\text{reactant}}$  (the reactants have to be transported to the surface of the electrodes before they can react);
- the surface area of the working electrode  $A$ ;
- the amount of electrodes transferred  $n_1$ .

One of these factors can be derived from the voltammogram if the others are known.

The shape of the voltammogram depends on the applied potential-time curve. For instance a Square Wave Voltammogram shows an almost symmetrical peak at  $E^0$  (or more exactly: the formal potential  $E^{0'}$ , see chapter 5.5) for a reversible redox reaction. At the standard potential, the following statement is valid [24]:

$$\frac{a_{\text{Ox}_1}^{v_{\text{Ox},1}}}{a_{\text{Red}_1}^{v_{\text{Red},1}}} = 1 \quad (4.13)$$

in which  $a_{\text{Ox}}$  is the activity of the oxidant. The equilibrium state of the redox reaction at any potential  $E$  can be calculated by [24]:

$$\frac{R_g \cdot T}{n_1 \cdot F} \ln \frac{a_{\text{Ox}_1}^{v_{\text{Ox},1}}}{a_{\text{Red}_1}^{v_{\text{Red},1}}} = E - E^0 \quad (4.14)$$

Note: the measured potential is the potential *difference* between working and reference electrode. Only if the reference electrode is the standard hydrogen electrode (at which the potential is always zero), the standard potential  $E^0$  reflects the potential of the half cell

$v_{\text{Ox},1} \text{Ox}_1 + n_1 e^- \rightleftharpoons v_{\text{Red},1} \text{Red}_1$  at the working electrode.

In molten silicate glass, the electroactive species are the polyvalent elements and oxygen. If the working electrode is negative with regard to its equilibrium value, the following reaction may occur at the working electrode:



and at the counter electrode,  $O^{2-}$  from the melt can be oxidized:



The overall reaction scheme is:



The measured potential  $E^0$  now reflects the potential difference between working and reference electrode, and at the standard potential of this reaction the following statement applies:

$$\frac{a_{M^{x+}}(\text{melt}) \cdot p_{O_2}^{n/4}(\text{reference gas})}{a_{M^{(x+n)+}}(\text{melt}) \cdot a_{O^{2-}}^{n/2}(\text{reference electrode})} = 1 \quad (4.18)$$

At any other potential  $E$ , the reaction equilibrium constant can be determined:

$$\frac{R_g \cdot T}{n \cdot F} \ln \frac{a_{M^{x+}}(\text{melt}) \cdot p_{O_2}^{n/4}(\text{reference gas})}{a_{M^{(x+n)+}}(\text{melt}) \cdot a_{O^{2-}}^{n/2}(\text{reference electrode})} = E - E^0 \quad (4.19)$$

Before the beginning of the experiment, the potential difference between working and reference electrode is  $E_{\text{melt}}$ . This potential difference is caused by the difference in oxygen equilibrium pressure in the melt at the surface of the working electrode,  $p_{O_2}(\text{melt})$ , and the partial oxygen pressure in the reference electrode,  $p_{O_2}(\text{reference gas})$ . Similar to equation 4.8, the potential difference  $E_{\text{melt}}$  is given by:

$$E_{\text{melt}} = \frac{R_g \cdot T}{4 \cdot F} \ln \frac{p_{O_2}(\text{melt})}{p_{O_2}(\text{reference gas})} \quad (4.20)$$

The equilibrium state of the redox reaction in the molten glass, before the beginning of the experiment, can be found by combining 4.19 and 4.20:

$$\frac{a_{M^{x+}}(\text{melt}) \cdot p_{O_2}^{n/4}(\text{melt})}{a_{M^{(x+n)+}}(\text{melt}) \cdot a_{O^{2-}}^{n/2}(\text{reference electrode})} = \exp \left( \frac{n \cdot F \cdot E^0}{R_g \cdot T} \right) \quad (4.21)$$

The activity of  $O^{2-}$  both in the molten glass and at the reference electrode is usually assumed to be at unity (see chapter 5.5).

Strictly speaking, the peak in the square wave voltammograms is not located at the standard potential of the redox reaction, but at the "formal potential  $E^{0'}$ "



(see chapter 5.5). Then the activities in equation 4.21 have to be replaced by concentrations:

$$\frac{[M^{x+}](\text{melt}) \cdot p_{O_2}^{n/4}(\text{melt})}{[M^{(x+n)+}](\text{melt})} = \exp\left(\frac{n \cdot F \cdot E^{0'}}{R_g \cdot T}\right) \quad (4.22)$$

So from the position of the peak in the square wave voltammogram, the equilibrium state of reaction 4.1 can be derived directly. Furthermore, since the oxygen equilibrium pressure at the working electrode can be calculated from  $E_{\text{melt}}$  with the aid of equation 4.9, the redox ratio  $[M^{x+}]/[M^{(x+n)+}]$  at the working electrode can be calculated.

The formal potential  $E^{0'}$  depends on the temperature. The temperature dependency can be expressed in terms of the enthalpy  $\Delta H^{**}$  and entropy  $\Delta S^{**}$  as defined in equation 3.14:

$$\Delta S^{**} = n \cdot F \cdot \left( \frac{\delta E^{0'}}{\delta T} \right)_p \quad (4.23)$$

$$\Delta H^{**} = n \cdot F \cdot \left[ T \left( \frac{\delta E^{0'}}{\delta T} \right)_p - E^{0'} \right] \quad (4.24)$$

The subscript p refers on a constant pressure, and this condition is usually satisfied in voltammetric experiments.

In case the redox reaction at the working electrode is not reversible, the shape of the curve can give information on the kinetics of the reaction. And if the reversible electron transfer is preceded or succeeded by a chemical reaction, as in the case of complex formation, the shape of the voltammogram is altered. With the aid of voltammetric measurements, the mechanism of the redox reaction can be established.

#### 4.3.2.3 Advantages and disadvantages of the electrochemical determination of the redox reaction equilibrium in molten glass

The electrochemical techniques have their own advantages and disadvantages. Some general advantages are:

- electrochemical techniques can be applied to the molten state;
- some electrochemical techniques are very fast and can therefore be applied to study the equilibration time of the glass melt with the surrounding

atmosphere;

- a lot of information can be obtained with the electrochemical methods. The following parameter can be found:
  - \* total concentration of the reactant;
  - \* the oxygen equilibrium pressure in the melt  $p_{O_2}$ ;
  - \* the redox ratio  $[M^{x+}]/[M^{(x+n)+}]$ ;
  - \* the equilibrium state of the redox reaction 4.1 as defined in equation 4.2;
  - \* the diffusion coefficient of the reacting species (in both oxidized state  $D_{Ox}$  and reduced state  $D_{Red}$ , see chapter 5.5);
  - \* the amount of electrons transferred.

Besides, the reaction mechanism can be unraveled.

- measurements can be performed in glasses containing a polyvalent element that has more than three valency states, like chromium [25];
- measurements can be performed in glasses containing more than one polyvalent element [26].

Disadvantages for the voltammetric measurements are:

- the potential region in which measurements can take place is limited: at positive potentials, oxygen gas is formed at the platinum working electrode. At potentials, less than -0.8 V, the glass matrix is reduced [25]. This restricts the applicability of the method to polyvalent elements that react in the potential region between 0 and -0.8 V at the temperatures of interest;
- expensive equipment is required (potentiostat).

#### 4.4 THE TECHNIQUES USED FOR THE PRESENT STUDY

The in-situ techniques are clearly the most suitable for the determination of the redox reaction equilibrium constants as a function of temperature. Emission spectroscopy is at the moment only applicable for iron, while the electrochemical methods are suitable for most polyvalent elements. For these reasons, the electrochemical methods have been chosen for the determination of the redox behaviour of iron, cerium, antimony, chromium and sulphur in some commercial glasses. One of the voltammetric techniques, the square wave voltammetry, provides for accurate measurements of the standard potential of redox reactions, even at high temperatures. From this standard potential, the redox reaction equilibrium constant and the reaction enthalpy and entropy can be calculated. The square wave voltammetry has been used to study the redox reactions of iron, antimony, chromium and sulphur in molten glass. Due to the

limitations in the potential region that can be scanned, square wave voltammetry is not suitable for the determination of the redox reaction equilibrium constant of cerium in glass melts.

The oxygen equilibrium pressure measurements have been used to study the evolution of O<sub>2</sub> in glass batches and molten glass containing iron, antimony, cerium and sulphate. The measurements have also been used to calculate the enthalpy and entropy of the redox reactions or to verify the results from the square wave voltammetry experiments.

Unfortunately, the measurements of the two electrochemical techniques offer in some cases (particularly for glasses containing cerium or sulphate) insufficient information to obtain a complete picture of the redox reactions in the melts. Therefore, the measurements have in these cases been combined with wet-chemical measurements at room temperature. Before cooling the glass samples quickly to room temperature, the oxygen equilibrium pressure in the molten glass has been measured. This offers the following advantages:

- p<sub>O<sub>2</sub></sub> from equation 4.2 is known exactly;
- the glass melt doesn't have to be in equilibrium with the surrounding atmosphere. Therefore no long equilibration times are needed and evaporation of glass components and corrosive attack of the crucible material will largely be avoided.

The theoretical backgrounds, experimental procedures and mathematical processing of the results of square wave voltammetry and oxygen equilibrium pressure measurements will be given in chapter 5.

#### Literature

- [1] Bamford, C.R.  
"Colour generation and control in glass (Glass science and technology 2)"  
Elsevier Scientific Publishing Company Amsterdam-Oxford-New York (1977)
- [2] Goldman, D.S.; Gupta, P.K.  
Diffusion-controlled redox kinetics in a glassmelt  
*Journal of the American Ceramic Society* **66** (1983) no.3 p.188-190

- [3] Maxwell, C.J.; Brungs, M.D.  
Simple and rapid spectrophotometric methods for the determination of the ferrous-ferric ratio in glass and geological materials  
*Glass Technology* **25** (1984) no.5 p.244-246
- [4] Nofz, M.; Stösser, R.; Herrmann, W.  
Indication and characterization of Fe(II) and Fe(III) species in silicate and aluminosilicate glasses  
Proceedings of the XVI International Congress on Glass Madrid (1992) **6** p.209-214
- [5] Stahlberg, B.; Mosel, B.D.; Müller-Warmuth, W.; Baucke, F.G.K.  
Combined electrochemical and Mössbauer studies of the  $\text{Sb}^{3+}/\text{Sb}^{5+}$  equilibrium in a silicate glassforming melt  
*Glastechnische Berichte* **61** (1988) pp.335-340
- [6] Konijnendijk, W.L.; Busture, J.H.J.M.  
Raman-scattering measurements of arsenic-containing oxide glasses  
*Journal of Non-Crystalline Solids* **17** (1975) p.293-297
- [7] Verweij, H.  
Raman study of the reactions in a glassforming mixture with molar composition:  $30\text{K}_2\text{CO}_3\text{-}70\text{SiO}_2\text{-}1\text{As}_2\text{O}_3$   
*Journal of the American Ceramic Society* **62** (1979) no.9-10 p.450-455
- [8] Mestdagh, M.M.; Dauby, C.; Van Cangh, L.; Dupont, C.  
Optical and electron paramagnetic resonance investigations of colour instabilities in amber glass as a function of melting temperature and batch redox conditions  
*Glass Technology* **24** (1983) no.4 p.184-191
- [9] Johnston, W.D.  
Oxidation-reduction equilibria in molten  $\text{Na}_2\text{O}\cdot 2\text{SiO}_2$  glass  
*Journal of the American Ceramic Society* **48** (1965) no.4 pp.184-190
- [10] Close, P.; Shepherd, H.M.; Drummond, C.H.  
Determination of several valences of iron, arsenic and antimony, and selenium in glass  
*Journal of the American Ceramic Society* **41** (1958) no.11 pp.455-460
- [11] Paul, A.; Douglas, R.W.  
Ferrous-ferric equilibrium in binary alkali silicate glasses  
*Physics and Chemistry of Glasses* **6** (1965) no.6 pp.207-211
- [12] Johnston, W.D.  
Oxidation-reduction equilibria in iron-containing glass  
*Journal of the American Ceramic Society* **47** (1964) no.4 pp.198-201
- [13] Krol, D.M.; Rommers, P.J.  
Oxidation-reduction behaviour of antimony in silicate glasses prepared from raw material and cullet  
*Glass Technology* **25** (1984) no.2 pp. 115-118
- [14] Paul, A.; Lahiri, D.  
A note on the study of the  $\text{As}_2\text{O}_3\text{-As}_2\text{O}_5$  equilibrium in glass  
*Transactions of the Indian Ceramic Society* **22** (1963) no.4 pp.146-150

- [15] Close, W.P.; Tillman, J.F.  
Chemical analysis of some elements in oxidation-reduction equilibria in silicate glasses  
*Glass Technology* **10** (1969) no.5 p.134-146
- [16] Paul, A.; Douglas, R.W.  
Cerous-ceric equilibrium in binary alkali borate and alkali silicate glasses  
*Physics and Chemistry of Glasses* **6** (1965) no.6 pp.212-215
- [17] Shi, X.Y.; Nasev, K.S.; Brungs, M.P.; Young, D.J.  
Determination of total and sulphide sulphur in float glass by ion chromatography  
*Glass Technology* **33** (1992) no.5 p.173-175
- [18] Pyare, R.; Nath, P.  
A simple and rapid spectrophotometric method for determination of sulphite and sulphate in binary sodium silicate glasses  
*Glass Technology* **27** (1986) no.1 p.21-23
- [19] Rüssel, C.; Kohl, R.; Schaeffer, H.A.  
Interaction between oxygen activity of  $\text{Fe}_2\text{O}_3$  doped soda-lime-silica glass melts and physically dissolved oxygen  
*Glastechnische Berichte* **61** (1988) no.8 p.209-213
- [20] Banner, D.  
Propriétés radiatives des verres et des fontes de silicates. Modélisation des transferts de chaleur.  
Thesis, Ecole Centrale de Paris (1990)
- [21] Goldman, D.S.; Berg, J.I.  
Spectral study of ferrous iron in Ca-Al-Borosilicate glass at room and melt temperatures  
*Journal of Non-Crystalline Solids* **38-39** (1980) p.183-188
- [22] Simonis, F. (editor)  
"NCNG-Glascursus"  
TPD-TNO in samenwerking met de gezamenlijke Nederlandse Glasindustrieën (1990)
- [23] Barton, J.L.; Banner, D.; Caurant, D.; Pincemin, F.  
The oxidation of ferrous iron in glass at high temperatures  
Proceedings of the XVI International Congress on Glass Madrid (1992) **6** p.215-220
- [24] Bard, A.J.; Faulkner, L.R.  
Electrochemical methods: fundamentals and applications  
John Wiley & Sons, Inc. New York Chichester Brisbane Toronto (1980)
- [25] Rüssel, C.; Freude, E.  
Voltammetric studies of the redox behaviour of various multivalent ions in soda-lime-silica glass melts  
*Physics and Chemistry of Glasses* **30** (1989) no.2 p.62-68
- [26] Rüssel, C.; Freude, E.  
Voltammetric studies in a soda-lime-silica glass melt containing two different polyvalent ions  
*Glastechnische Berichte* **63** (1990) no.6 p.149-153

# Chapter 5

## Electrochemical methods: Oxygen equilibrium pressure measurements and square wave voltammetry

### 5.1 INTRODUCTION

In the previous chapter the methods for the determination of the redox reaction equilibria in molten glass have been discussed. Two of these methods have been applied for the present investigation on the behaviour of iron, antimony, cerium, chromium and sulphur in soda-lime-silica glass, TV-screen glass and E-glass. These methods are:

- oxygen equilibrium pressure measurements;
- square wave voltammetry measurements.

The data from square wave voltammetry measurements can be related directly to the equilibrium constants of the redox reactions. In combination with oxygen pressure measurements the ratio of reduced to oxidized species in the glass melt can be derived. From the temperature dependency of the redox reaction equilibrium constants the redox reaction enthalpy and entropy can be calculated.

The oxygen equilibrium pressure measurements can also be used by themselves to estimate  $\Delta H^{**}$  and  $\Delta S^{**}$  values. For this purpose a computer program has been developed.

The theoretical backgrounds, practical application and the mathematical elaborating of the results from these applied techniques will be given in this chapter (5.4 and 5.5). Some basic knowledge on electrochemistry is necessary to elucidate some of the aspects that will be discussed. Therefore the next two sections of this chapter are dedicated to electrochemical concepts (5.2) and the application of electrochemistry in molten glass (5.3).

### 5.2 ELECTROCHEMISTRY/ SOME BASIC CONCEPTS [1,2]

#### 5.2.1 The electrochemical potential of a species i

The electrochemical potential of a species i depends on:

- the chemical potential;
- the electrical properties of the environment.

The chemical potential manifests itself through short-range forces which are almost electrical in nature. The chemical potential  $\mu_i$  in a phase  $\alpha$  is given by:

$$\mu_i^\alpha = \left( \frac{\delta G}{\delta n_i} \right)_{T,P,n_{j \neq i}} \quad (5.1)$$

with  $\mu_i^\alpha$  = chemical potential of species  $i$  in phase  $\alpha$  [J·mole<sup>-1</sup>]  
 $G$  = Gibbs-free energy [J·mole<sup>-1</sup>]  
 $n_i$  = number of moles of  $i$  in phase  $\alpha$

The subscripts  $T,P,n_{j \neq i}$  refer to a constant temperature, pressure and number of moles of all the other species  $j$  in this system. This chemical potential can also be expressed using the activity of species  $i$  in phase  $\alpha$ ,  $a_i^\alpha$ :

$$\mu_i^\alpha = \mu_i^{0\alpha} + R_g \cdot T \cdot \ln a_i^\alpha \quad (5.2)$$

with  $\mu_i^{0\alpha}$  = chemical potential of species  $i$  in the pure phase at unit activity [J·mole<sup>-1</sup>]  
 $R_g$  = gas constant 8.314 J·mole<sup>-1</sup>·K<sup>-1</sup>  
 $T$  = absolute temperature [K]  
 $a_i^\alpha$  = activity of component  $i$  in phase  $\alpha$

The electrical properties of the environment are governed by its potential. The potential at any particular point  $\phi(x,y,z)$  is defined as the work required to bring a unit positive charge, without material interactions, from an infinite distance to point  $(x,y,z)$ .

The electrochemical potential  $\bar{\mu}_i^\alpha$  for species  $i$  with charge  $z_i$  in phase  $\alpha$  is then given by:

$$\bar{\mu}_i^\alpha = \mu_i^\alpha + z_i \cdot F \cdot \phi^\alpha \quad (5.3)$$

and  $z_i$  = charge of species  $i$   
 $F$  = Faraday constant (charge of one mole of electrons) 96495 C·mole<sup>-1</sup>  
 $\phi^\alpha$  = potential of phase  $\alpha$  [V]

### 5.2.2 The interface between two phases

A system may consist of two different phases  $\alpha$  and  $\beta$  separated by a phase boundary. If the system is in equilibrium, the chemical potentials of all species  $i$  present are equal in both phases:

$$\bar{\mu}_i^\alpha = \bar{\mu}_i^\beta \quad \text{for all species } i \quad (5.4)$$

chemical investigations, because it can give qualitative and quantitative insight in the electrochemical behaviour of a chemical system.

### 5.2.3 Charge and charge transfer within one phase

The phases in electrochemical measurements should be conducting phases. If the charge is carried through the phase by the movement of ions, the phase is called an electrolyte. If the movement of electrons provides for the transport of charge, the phase is called an electrode.

If no current flows through a conductive phase, the potential  $\phi$  is constant everywhere within this phase. Otherwise, the mobile charge carriers would move in response to the difference in potential in order to eliminate this difference. An excess charge on a conducting phase in equilibrium is therefore always located on the surface.

In metals, the thickness of the layer in which the excess of charge is located is negligibly thick. In electrolytes the excess charge is present as an excess of ions. The thickness of the layer that holds this excess of ions can range from a few angstroms to several thousands of angstroms [1].

Sometimes a real electrolyte features different behaviour at different locations. Then the electrolyte can be thought of as two solutions, separated by an interface. At this point mass transport processes attempt to mix the solutions until the two electrolytes are identical. The potential difference between the "two solutions"  $\gamma$  and  $\delta$  is called the junction potential  $E_{\text{junction}}$ . Its magnitude is given by [1]:

$$E_{\text{junction}} = (\phi^{\delta} - \phi^{\gamma}) = \frac{-R_g \cdot T}{F} \int_{\gamma}^{\delta} \frac{t_i}{z_i} d \ln a_i \quad (5.5)$$

with  $t_i$  = transport number of component  $i$

### 5.2.4 Charge transfer through the interface electrode/electrolyte

#### 5.2.4.1 Current-determining processes at the surface of the electrode

A system consisting of an electrode and an electrolyte which are not in equilibrium may try to (re)establish equilibrium by transport of charge through the interface. In the electrode the charge is carried by electrons, in the electrolyte by the migration of ions. At the interface between the two phases, the electrons must be donated to or extracted from the ions. The rate of this electron transfer, the current, is governed by the rate of processes such as:



- mass transfer (of the reacting species from the bulk of the electrolyte to the electrode surface, and of the products from the electrode surface to the bulk of the electrolyte);
- electron transfer at the electrode surface by redox reactions;
- chemical reactions preceding or following the electron transfer;
- other surface reactions, such as adsorption, desorption or electro-deposition.

#### 5.2.4.2 Potential of the electrode, relative to the potential of the electrolyte

When a current  $i$  flows through the system each of these processes opposes the current, resulting in a certain resistance or, to be more precise, an impedance. The processes therefore cause potential differences or overpotentials [2]. The sum of these overpotentials is represented by the symbol  $\eta$ . The potential of the electrode with regard to the potential of the electrolyte,  $E$ , is then equal to the sum of the overpotential terms associated with the different reaction steps and the potential difference at which no charge transfer takes place ( $E_{\text{eq}}$ ). In electrochemical experiments, the overpotentials are usually not constant, but a function of the current. Therefore the potential of the electrode changes upon passage of current.

#### 5.2.4.3 The relation between potential, applied potential and current

By applying an external voltage on the system with the aid of a power supply, a current  $i$  can be forced through the system. The potential of the electrode (relative to the potential of the electrolyte) shifts to a new value  $E$ . This potential is not equal to the applied potential because the transport of charge through the electrolyte experiences a resistance  $R_s$  by the electrolyte. This causes a voltage drop equal to  $i \cdot R_s$ .

If the desired potential between the two phases is  $E$ , the magnitude of the required potential  $E_{\text{appl}}$  is given by:

$$E_{\text{appl}} = E + i \cdot R_s = E_{\text{eq}} + \eta + i \cdot R_s \quad (5.6)$$

- with  $R_s$  = solution resistance [Ω]  
 $E_{\text{eq}}$  = potential at which no net charge transfer takes place [V]  
 $\eta$  = sum of the overpotentials [V]

### **5.2.5 The electrochemical cell**

A real electrochemical system through which a current can be forced with the aid of a power supply always consists of at least three phases: two electrodes and the electrolyte of interest. The electrodes are both connected to the external power supply. The circuit is closed when the electrodes are dipped in the electrolyte.

We can never examine the phenomena which appear at the surface of one of the electrodes directly: the results of electrochemical measurements are always dependent on phenomena which take place on all the interfaces of the circuit. This means that measured potential-current diagrams reflect the behaviour of electro-active species at both electrodes.

Most of the time only reactions that occur at one electrode are of analytical interest. If the potential of one of the electrodes does not change upon passage of current (ideal non-polarizable electrode,  $\eta$  at this electrode is zero), the potential of this electrode is fixed. If in addition the potential drop caused by the resistivity of the electrolyte,  $i \cdot R_s$  (see chapter 5.2.4) is low, the measured potential-current diagram reflects the electrochemical phenomena at the other electrode. However, in practise ideal non-polarizable behaviour does not occur and  $i \cdot R_s$  may be high. Therefore the experimental set-up of electrochemical measurements is designed to minimize the effects of the reactions on all but one interface. In case a current flows through the system this can be achieved by using a three-electrode system.

### 5.2.6 The three-electrode system

In the electrolyte (like molten glass) polyvalent ions may be present. These ions can donate or accept electrons at the electrode surface and therefore apply for electron transfer across the interfaces. In this thesis, the behaviour of the polyvalent ions is the subject of electrochemical studies.

The response of the system electrode-electrolyte after an abrupt change in one of the cell variables ( $T, E, i$ ) can give information on the redox reactions of the polyvalent ions. For example if the applied potential is changed, a current between the electrodes can be measured. The current is related to the amount of electrons transferred, and therefore also to the redox ratio (ratio of reduced to oxidized polyvalent ions) in the electrolyte. However, the current can only be related to a redox ratio if the current is due to reactions at just one electrode surface. Therefore in most electrochemical measurements the three-electrode system is used.

The desired potential  $E$  is then applied between two of the electrodes (the working and the reference electrode), while the current that is accompanied by this potential flows through one of these electrodes (the working electrode) and the third electrode (the counter electrode). The resistance between working and

reference electrode is very high. Because negligible current flows through the reference electrode no current-dependable potential drop will occur at its interface, and therefore its potential can be regarded as constant.

#### 5.2.6.1 Working electrode

The reactions of interest take place at the surface of the working electrode. Therefore the material of which this electrode is made and the dimensions of the electrode should be chosen with care.

The surface area of the working electrode should be large enough to permit surface redox reactions and electron transfer to occur at a high rate. In some cases, also adsorption and desorption of electro-active species will occur. However, the dimensions of the working electrode should be much smaller than those of the electrolyte, because otherwise the current will be restricted by lack of reactants, and not by electrochemical properties of the polyvalent ions [3]. The depletion of the reactant at the surface area must be compensated by diffusion of the reactant from the bulk of the electrolyte to the surface of the electrode.

#### 5.2.6.2 Counter electrode

The current flows through working and counter electrode. At the surface of the counter electrode, redox reactions occur to allow for electron transfer. These reactions should not determine the current rate. Therefore the reactions must be fast and the reactants of these reactions should be present in excess. Furthermore the surface area of the counter electrode should be much larger than that of the working electrode. The reaction products should not interfere with reactions at the working electrode. Then the current reflects only electrochemical or electrical phenomena at the working electrode.

#### 5.2.6.3 Reference electrode

Because a current flows through the counter electrode, the processes mentioned in section 5.2.4 may occur at its interface. Therefore the potential of this electrode may not be constant upon passage of current. If we want to control the potential difference between working electrode and electrolyte exactly to a certain value, we need a second counter electrode, or reference electrode, with a constant potential. This reference electrode should be placed close to the surface of the working electrode in order to minimize the effects of the resistance of the electrolyte ( $i \cdot R_s$ ). But since the current path between working and counter electrode ought not to be

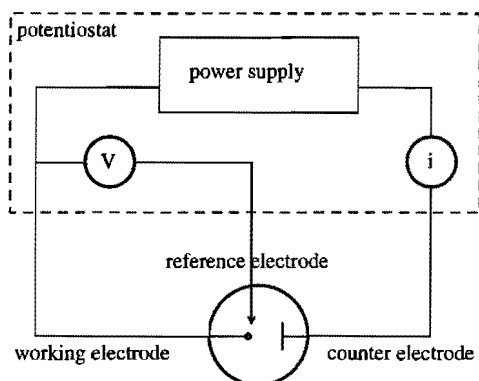


Figure 5.1  
A schematic presentation of a three-electrode cell

blocked by the reference electrode, it can not be placed exactly at the surface of the working electrode. Therefore some fraction of  $i \cdot R_s$  (called  $i \cdot R_u$ , where  $R_u$  is the uncompensated solution resistance) will remain.

Between the working electrode and this reference electrode, an accurate potential can be applied or monitored by a special device (potentiostat). This device has a high input impedance so that a negligible current is drawn through the reference electrode. Therefore the potential drop at this electrode is practically zero, and its potential can be seen as constant.

A schematic presentation of a three electrode cell is given in figure 5.1.

### 5.2.7 Response of the system to a change in potential

If a potential difference is applied between working and reference electrode, a current can flow between working and counter electrode. This current can be due to redox reactions in the electrolyte if the applied potential difference is sufficient to allow for electron donation or acceptance. This kind of current is called faradaic current.

#### 5.2.7.1 The charging current

But even if the potential difference is too low for redox reactions to occur, a current may flow due to capacitive effects. The potential difference may cause ions to migrate to or from the electrode surface, depending on their charge.

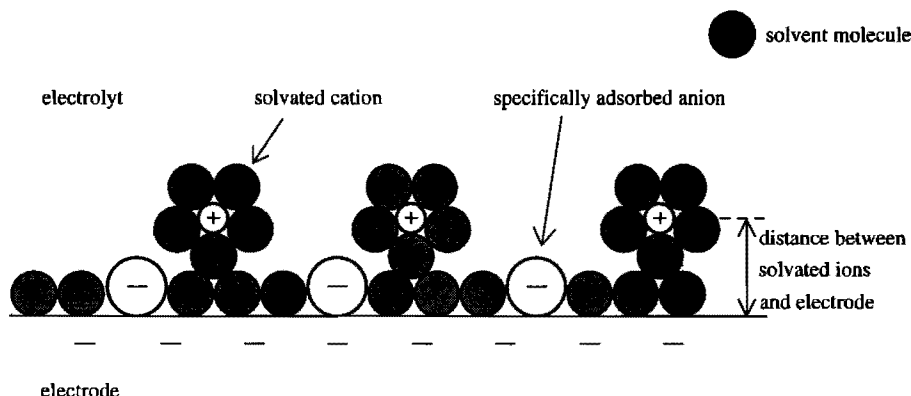


Figure 5.2  
A schematic presentation of the electrochemical double layer

The ions of opposite charge will try to approach the surface, but may be hindered by specifically adsorbed ions and electrolyte molecules (see figure 5.2). An electrochemical double layer is formed and the opposing charges are separated by some distance ( up to several thousand angstroms, see chapter 5.2.3).

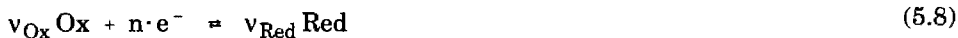
The double layer acts as a capacitor (with capacity =  $C_d$ ) and at a change in potential the double layer is gradually charged or discharged. This is accompanied by a charging current  $i_c$  which decreases exponentially as a function of time  $t$ :

$$i_c = \frac{E}{R_s} \cdot e^{-\frac{t}{R_s \cdot C_d}} \quad (5.7)$$

with  $i_c$  = charging current [A]  
 $C_d$  = double layer capacity [F]

#### 5.2.7.2 The faradaic current

If the applied potential difference between working electrode and electrolyte is sufficiently high, the polyvalent ions in the electrolyte are able to accept or donate electrons:



$v_{Ox}$  is the amount of molecules or ions of Ox in the stoichiometrical reaction equation.  $n$  is the amount of electrons that is necessary to reduce  $v_{Ox}$  molecules or ions of Ox to its reduced form Red. At the electrode surface, both oxidized and reduced polyvalent ions can be present. The ratio of oxidized to reduced ions at

equilibrium depends on the applied potential and is given by the Nernst equation:

$$\frac{R_g \cdot T}{n \cdot F} \ln \frac{a_{Ox}^{v_{Ox}}}{a_{Red}^{v_{Red}}} = E - E^0 \quad \text{at equilibrium} \quad (5.9)$$

$E^0$  is the standard potential, this is the potential of the half cell Ox/Red if all activities are at unity. By definition the equilibrium for reversible redox reactions is reached fast. The faradaic current is determined by the reaction rate of reaction 5.8, and therefore by the applied potential.

As the applied potential difference changes from a potential where the polyvalent element is predominantly present in the oxidized state to a potential where it is mainly present in the reduced state, the resulting faradaic current is (initially) at its maximum. For instance if the potential of the working electrode is made sufficiently negative the polyvalent element will be transferred to the reduced state at the highest rate possible. But the concentration of the oxidized form at the electrode surface soon becomes almost zero. The reaction rate, and therefore also the faradaic current, decreases. The depletion at the surface causes the diffusion of oxidized ions from the bulk of the electrolyte to the surface of the electrode according to Fick's Law:

$$\left( \frac{\delta C_{Ox}(x,t)}{\delta t} \right) = D_{Ox} \left( \frac{\delta^2 C_{Ox}(x,t)}{\delta x^2} \right) \quad (5.10)$$

with  $D_{Ox}$  = diffusion coefficient of the oxidized ions  $[m^2 \cdot s^{-1}]$   
 $C_{Ox}(x,t)$  = concentration of the oxidized ions at a distance  $x$   
                     from the surface of the working electrode at time  $t$   $[mole \cdot m^{-3}]$   
 $x$  = distance from the surface of the working electrode  $[m]$   
 $t$  = time  $[s]$

The solution of this diffusion equation with certain boundary conditions is known as the Cottrell equation [1]:

$$i_f = \frac{n \cdot F \cdot A \cdot D_{Ox}^{1/2} \cdot C_{Ox}^{bulk}}{\pi^{1/2} \cdot t^{1/2}} \quad (5.11)$$

with  $i_f$  = faradaic current  $[A]$   
 $F$  = Faraday constant  $96495 \text{ C} \cdot \text{mole}^{-1}$   
 $A$  = surface area of the working electrode  $[m^2]$   
 $C_{Ox}^{bulk}$  = concentration of the oxidized ions in the  
                     bulk of the electrolyte  $[mole \cdot m^{-3}]$

Note that the faradaic current  $i_f$  depends on the negative square root of the time  $t$  elapsed since the change in potential.

### 5.2.8 Standard, formal and half-wave potential

The standard potential  $E^0$  of a half cell is the potential at which the activities of the reacting species are at unity (see section 5.2.7). Usually the activities of the species are unknown. Therefore the formal potential  $E^{0'}$  has been defined as the potential at which the ratio of the concentrations of reactants and products is at unity:

$$\text{At } E^{0'}: \frac{[\text{Ox}]^{v_{\text{Ox}}}}{[\text{Red}]^{v_{\text{Red}}}} \equiv 1 \quad (5.12)$$

The potential of a half-cell is now given as:

$$E = E^{0'} + \frac{R_g \cdot T}{n \cdot F} \ln \frac{[\text{Ox}]^{v_{\text{Ox}}}}{[\text{Red}]^{v_{\text{Red}}}} \quad (5.13)$$

Since equation 5.9 can also be written as:

$$E = E^0 + \frac{R_g \cdot T}{n \cdot F} \ln \frac{(\gamma_{\text{Ox}} \cdot [\text{Ox}])^{v_{\text{Ox}}}}{(\gamma_{\text{Red}} \cdot [\text{Red}])^{v_{\text{Red}}}} \quad (5.14)$$

it follows that:

$$E^{0'} = E^0 + \frac{R_g \cdot T}{n \cdot F} \ln \frac{(\gamma_{\text{Ox}})^{v_{\text{Ox}}}}{(\gamma_{\text{Red}})^{v_{\text{Red}}}} \quad (5.15)$$

Note that  $E^{0'}$  will vary from medium to medium, and may depend on the concentration of the reacting species.

In voltammetric measurements the so-called half-wave potential  $E_{1/2}$  is an important quantity. It is defined as:

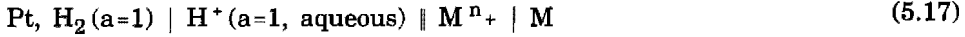
$$E_{1/2} = E^{0'} + \frac{R_g \cdot T}{n \cdot F} \ln \frac{D_{\text{Red}}^{1/2}}{D_{\text{Ox}}^{1/2}} \quad (5.16)$$

### 5.2.9 Sign of potential and current

#### 5.2.9.1 Sign of the potential

In order to be able to rank the standard potentials of different half cells Ox/Red a reference half cell has been formulated: per definition the potential of the Normal Hydrogen Electrode is zero at all temperatures. The NHE consists of a

platinum electrode submerged in a solution of  $H^+$  ions with unity activity. The solution is bubbled with  $H_2$  gas with a pressure of exactly 1 bar. The potential of any half cell  $M^{n+}/M$  can be determined by linking this half cell to the NHE. This can be schematically represented by



The potential of this cell is:

$$E_{\text{cell}} = E_{\text{right}} - E_{\text{left}} = E_{\text{right}} - 0 = E_{\text{half cell}} \quad (5.18)$$

If the NHE is turned positive after connection of the two half cells by donating electrons to  $H^+$  in order to form  $H_2$ , the potential of the half cell  $M^{n+}/M$  is negative. If on the other hand hydrogen molecules are ionized to  $H^+$ , the half cell is positive. If the electrochemical cell does not contain the NHE, the electrode that is the most negative in relation to the NHE is the negative electrode in the cell. In schematic presentations it is written at the left side.

### 5.2.9.2 Sign of the current

In this thesis the European Convention is used to define the sign of the current. If the electrons are transferred from electrode to electrolyte, the current is cathodic. Because reactants in the electrolyte are being reduced, this current is also called reducing current. In the European Convention, this current is defined as a positive current [1].

## 5.3 ELECTROCHEMISTRY IN MOLTEN GLASS

In our experiments the electrochemical cell consists of:

- the molten glass;
- the potentiostat;
- two platinum electrodes;
- one  $ZrO_2/Pt$ /air electrode.

### 5.3.1 The glass melt

In molten glass, charge transport can take place by migration of ions. Monovalent cations such as  $Li^+$ ,  $Na^+$  and  $K^+$  are only loosely bonded in the glass structure (chapter 2.2.1). Because they are more mobile than the other ions, the transport of charge will be dominated by the migration of these cations (see also chapter 4.3.2.1). The resistivity for charge transport therefore depends on the amount of  $Li^+$ ,  $Na^+$  and  $K^+$  in the melt. The resistivity in molten soda-lime-silica glass at melting temperatures for instance is relatively low and amounts up to about 5 to 50  $\Omega \cdot \text{cm}^{-1}$  [4]. E-glass (which is used for glass fibres) contains only very little



amounts of the conductive cations  $\text{Li}^+$ ,  $\text{Na}^+$  and  $\text{K}^+$ . Its resistivity at  $1300^\circ\text{C}$  is more than 10 times higher than in soda-lime-silica glass [4].

### **5.3.2 The potentiostat**

The potentiostat model 273 from EG&G is used as the external power supply and also as a potential and current measuring instrument. This potentiostat is able to apply an accurate potential to the working and reference electrode, and changes in the potential can be made very fast (within  $\mu\text{s}$ ). Furthermore the resulting current between working and counter electrode can be measured each  $10 \mu\text{s}$ . For controlling the potentiostat and filing and processing of the data a computer is necessary. Therefore the potentiostat is linked in this case to a 286 pc with expanded memory.

### **5.3.3 The three electrodes**

#### **5.3.3.1 The working electrode**

In this study, platinum electrodes are used in the molten glass. Platinum is an excellent electron conductor, it is solid up to more than  $1500^\circ\text{C}$  (maximum temperature of the molten glass) and is hardly corroded by the glass melts. However, if the potential of a platinum electrode is set to a positive value with respect to the potential of the counter electrode, the electrode will dissolve [5]. This restricts the potential range that can be scanned during the square wave voltammetry measurements. Other electrode materials have been tested to overcome this restriction, but with negative results (see chapter 5.5.11).

In this study, the working electrode is a platinum wire with a diameter of 1 mm. Its depth in the melt is 10 mm at most. The surface area in contact with the molten glass is therefore  $32 \text{ mm}^2$  at maximum. The volume of the  $\text{Al}_2\text{O}_3$ -crucible that contains the glass melt is 270 ml. The crucible usually contains 300 gram glass (about 130 ml). So the working electrode is small in comparison to the glass melt volume (see section 5.2.6.1).

#### **5.3.3.2 The counter electrode**

The counter electrode is a platinum plate of about  $200 \text{ mm}^2$  that is suspended from a platinum wire (diameter 1 mm). The area of the counter electrode exceeds that of the working electrode by one order of magnitude. The platinum plate is placed under the surface of the molten glass in order to diminish the three phase contact (glass melt-platinum-air) as much as possible, for reasons that will be discussed in chapter 5.4.5.

### 5.3.3.3 The reference electrode

The required qualities of the reference electrode are:

- it should maintain a constant potential throughout the experiments;
- it should not be corroded by the molten glass;
- it should be stable at temperatures between 800 and 1500°C.

A simple platinum electrode does not meet the requirement of a constant potential. At this electrode the following reaction might occur if the potential of the working electrode is set to a negative value [6]:



The potential of the platinum electrode then becomes:

$$E_{\text{half cell}} = E_{\text{O}_2/\text{O}^{2-}}^0 + \frac{R_g \cdot T}{4 \cdot F} \ln \frac{p_{\text{O}_2}}{a_{\text{O}^{2-}}^2} \quad (5.20)$$

with  $p_{\text{O}_2}$  = oxygen equilibrium pressure in the melt [bar]

Generally the molten glass is not in equilibrium with the surrounding atmosphere, so the oxygen equilibrium pressure in the melt is not the same as in the atmosphere [7]. Furthermore the oxygen pressure within the molten glass,  $p_{\text{O}_2}$ , is not constant but varies with temperature and distance from the surface of the melt (as will be seen in chapter 5.4). Under some conditions, oxygen bubbles can be formed. The potential of a platinum wire dipped in the melt is not reversible and constant.

Therefore a reference electrode is constructed in which the platinum wire is separated from the molten glass by a  $\text{O}^{2-}$ -conducting material (solid electrolyte). The platinum wire is fixed in the cylindrical solid electrolyte like a spring in order to provide for a good contact (see figure 5.3, electrode 2). The solid electrolyte is glued to a gas-tight  $\text{Al}_2\text{O}_3$ -tube with a ceramic bounding. The platinum wire is flushed with a gas with a known oxygen pressure (usually air,  $p_{\text{O}_2}=0.21$  bar). The oxygen pressure within the glass melt does not influence the potential of the reference electrode [8]. Electrical contact between the melt and the reference electrode is established by migration of  $\text{O}^{2-}$ -ions through the solid electrolyte.

Zirconia with a cubic structure is known as an oxygen ion conducting material [9]. It is stabilized with 8 wt%  $\text{Y}_2\text{O}_3$ , because unstabilized zirconia will obtain a monoclinic structure at about 1000°C. This monoclinic structure provides for a high electronic conductivity and therefore the zirconia will no longer act as a ionic conductor at temperatures above 1000°C [9]. The  $\text{Y}_2\text{O}_3$ -stabilized  $\text{ZrO}_2/\text{Pt}:\text{O}_2$

electrode was found to behave ideally as a reference electrode at temperatures up to 1350°C [7,9,10]. Although the zirconia is dissolved in the molten glass at a slow rate, this does not influence the electrical properties [9]. To prevent unnecessary attack of the zirconia, the reference electrode only touches the glass melt.

#### **5.3.4 The experimental set-up**

An Al<sub>2</sub>O<sub>3</sub>-crucible containing the glass of interest is placed in the hot-zone of an electrically heated furnace. The hot-zone is about 30 cm long. The height of the crucible is 10 cm. The temperature gradient in the hot-zone is less than 0.5°C/cm. Therefore the temperature of the hot-zone is assumed to be homogeneous. It is measured with a Pt/Pt-10%Rh thermocouple just outside the crucible. The three electrodes are dipped in the glass. A schematic presentation of the experimental set-up is given in figure 5.3.

#### **5.3.5 Positioning of the electrodes**

The electrodes are placed above the surface of the glass while the glass is at room temperature. Then the glass and the electrodes are heated up slowly in order to prevent damage which may occur due to thermo-shock. At a temperature of 1400°C, the electrode positions are lowered with a speed of some mm per minute with the aid of an electromotor. The resistance between the platinum working electrode (1) and counter electrode (3) is measured. If the electrodes are above the surface of the glass melt the resistance is high, in the order of 10 kΩ. As soon as electrodes (1) and (3) have reached the molten glass the resistance drops to a much lower value (in the order of 0.1 kΩ for soda-lime-silica and TV-screen glass, and about 1 kΩ for E-glass). Then the three electrodes are lowered for another few mm until the reference electrode (2) just touches the glass melt.

The effective surface area of the working electrode can not be calculated accurately from the dip-in length, because the molten glass will adhere to the electrode as sketched in figure 5.4. For long dip-in lengths this effect becomes less important.

As the temperature of the molten glass changes, the dip-in length of the electrodes may vary due to expansion or contraction of the melt. This effect further complicates the determination of the effective surface area of the working electrode.

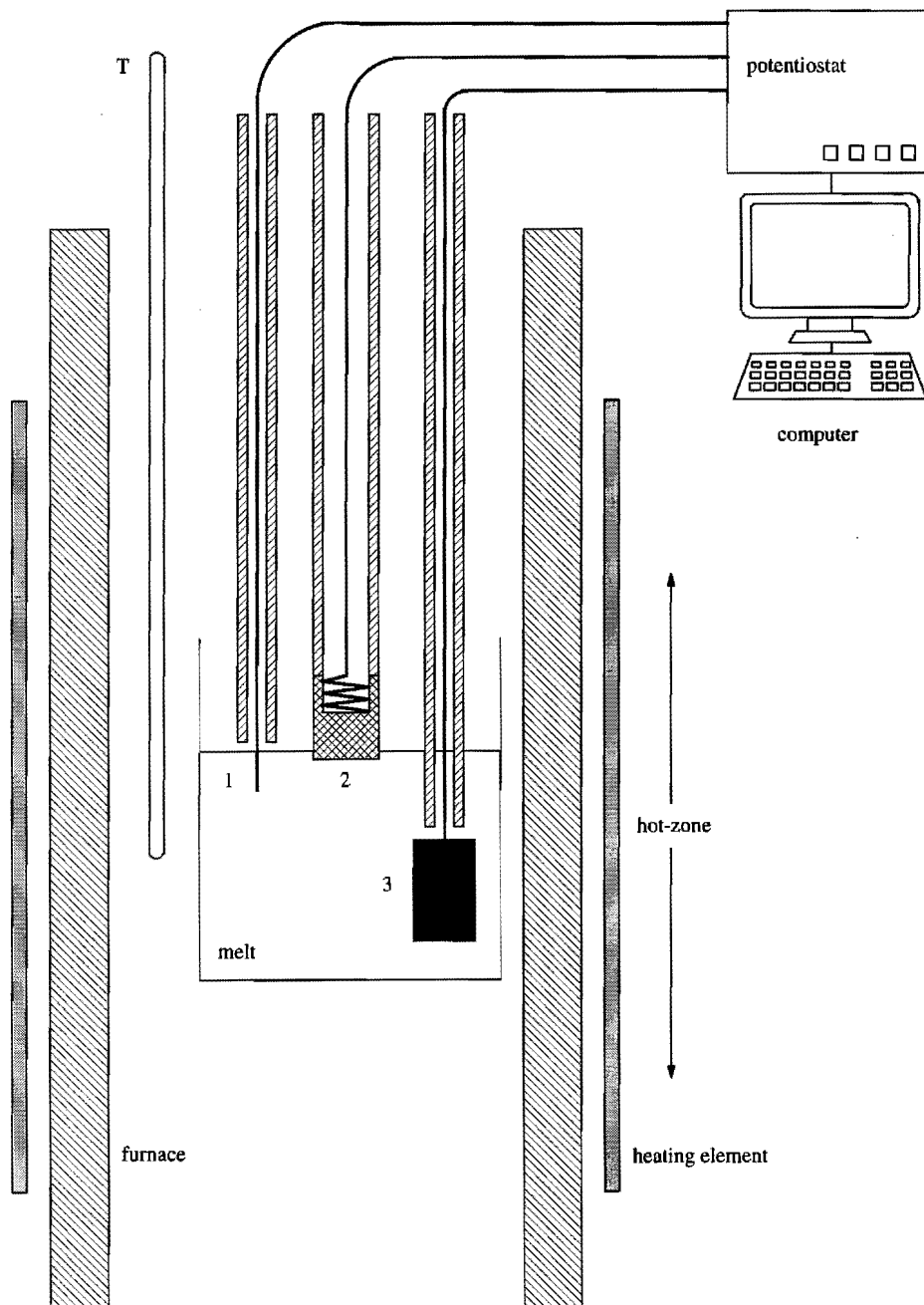


Figure 5.3

A schematic presentation of the experimental set-up

- 1 = working electrode
- 2 = reference electrode
- 3 = counter electrode

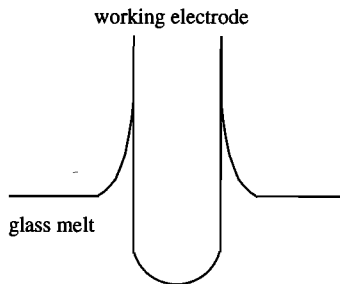


Figure 5.4  
The adhesion of molten glass to the working electrode

### 5.3.6 I.R.-compensation

#### 5.3.6.1 Measurement of the uncompensated resistance

The resistivity of the glass melt causes a potential drop  $i \cdot R_u$  between the working and the reference electrode (see chapter 5.2.6.3). The actual potential difference at the working electrode  $E$  will therefore be smaller than the applied potential  $E_{\text{apply}}$  (see equation 5.6). With the aid of positive feedback circuits the model 273 potentiostat is able to compensate for this potential drop  $i \cdot R_u$  if  $R_u$  is known. Therefore  $i \cdot R_u$  compensation measurements are performed before running voltammetric experiments.

At the beginning of the  $i \cdot R_u$  compensation measurement, the potential of the working electrode is held at a value where no oxidation or reduction occurs (usually 0 V). Then the potential is brought to a small negative value (usually -0.01 V, without  $i \cdot R_u$  compensation) during a time interval of 0.5 ms. The pulse height should not be large enough to cause a reduction. After 0.5 ms the potential is brought to its original value. The current is sampled every 0.05 ms seconds for 5 ms. The uncompensated resistance  $R_u$  is calculated from equation 5.7.

Compensation of the potential with exactly  $i \cdot R_u$  may lead to oscillation. Therefore the procedure outlined above is repeated, but now the applied potential is compensated for 5% of  $i \cdot R_u$ . Again the current is sampled. This step is repeated until the desired compensation level is reached or oscillation of the measured current exceeds an acceptable level. In the second case the best value for  $i \cdot R_u$  compensation for the voltammetric experiments is the compensation level of the preceding measurement. An example of an  $i \cdot R_u$  compensation measurement for a soda-lime-silica glass without polyvalent elements at 1200°C is shown in figure 5.5.

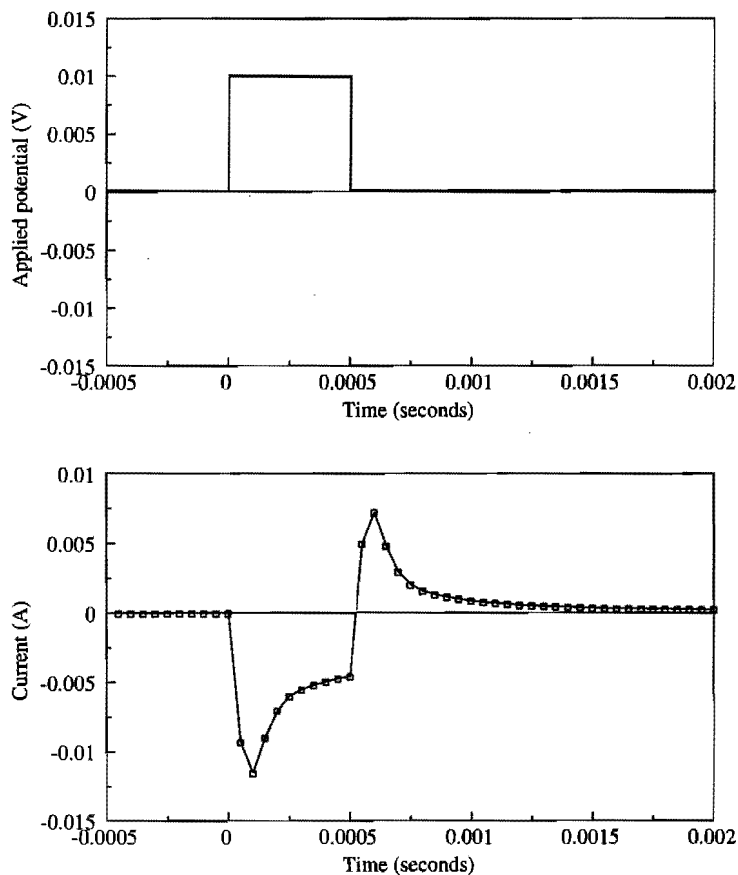


Figure 5.5

Applied potential-time diagram and current-time plot of an  $i-R_u$  measurement in soda-lime-silica glass without polyvalent elements at 1200°C

Note:

The  $i-R_u$  measurements have to be performed before each voltammetric measurement because the resistance strongly depends on:

- dip-in length of the working electrode;
- distance between the working and reference electrode;
- temperature;
- nature of the molten glass.

### 5.3.6.2 Calculation of the resistivity of the glass melt

The uncompensated resistance depends on the distance of the working and reference electrodes and the effective surface area of the working electrode. Since it is difficult to calculate the surface area (see section 5.3.5), the resistivity of the glass melts can not be calculated accurately. However, from rough calculations it follows that the resistivity ranges from 5 to 250  $\Omega \cdot \text{cm}^{-1}$  (uncompensated resistance  $\times$  distance / surface area) at temperatures varying between 800 and 1300°C. This is in agreement with the data from [4].

The current is usually in the order of 1 mA. This means that if the uncompensated resistance is 500  $\Omega$ , the potential drop due to the resistivity of the molten glass is 0.5 V! In order to obtain meaningful results, voltammetric experiments have only been performed when the uncompensated resistance was less than 100  $\Omega$ .

### 5.3.6.3 Calculation of the capacity of the electrochemical double layer

From the  $i \cdot R_u$  measurements, also the capacity of the double layer at the interface of the working electrode can be calculated with the use of equation 5.7. In soda-lime-silica glass without polyvalent elements it ranges from 100 to 500  $\mu\text{F} \cdot \text{cm}^{-2}$  at 1000-1400°C. It is somewhat lower in TV-glass: about 100 to 350  $\mu\text{F} \cdot \text{cm}^{-2}$  in TV-screen glass without polyvalent elements at 700-1400°C and  $\pm 100 \mu\text{F} \cdot \text{cm}^{-2}$  in glass with iron. The capacity of the electrochemical double layer in E-glass with iron or chromium is still less and ranges from 30 to about 120  $\mu\text{F} \cdot \text{cm}^{-2}$  at 1000-1400°C. These values are only rough estimates since the effective surface area of the working electrode is not exactly known.

The double layer capacities in molten oxides, and especially in soda-lime-silica glass, are larger than the double layer capacitance of aqueous solutions (10 to 40  $\mu\text{F} \cdot \text{cm}^{-2}$  [1]). This is in good agreement with the observations of Moortgat-Hasthorpe et.al. [3]. According to these authors the capacity of a sodium disilicate melt at 1100°C is about 300  $\mu\text{F} \cdot \text{cm}^{-2}$  at a potential of 0 V. It decreases non-linearly if the potential becomes more negative to a value of 50  $\mu\text{F} \cdot \text{cm}^{-2}$  at -0.6 V. It is suggested that the electrochemical double layer results from the chemisorption of oxygen (at potentials above the point of zero charge) and sodium (at potentials below the PZC). This is schematically represented in figure 5.6.

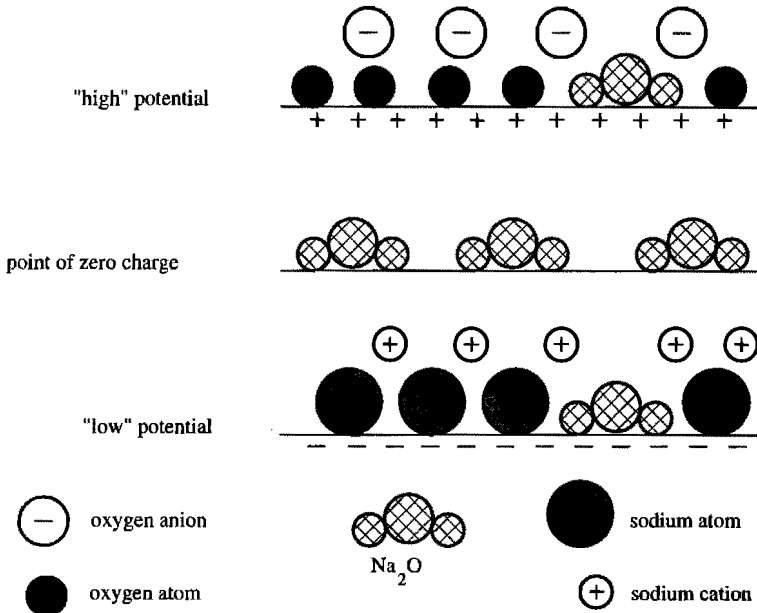


Figure 5.6

A schematical presentation of the electrochemical double layer in a sodium disilicate melt [3]

## 5.4 OXYGEN EQUILIBRIUM PRESSURE MEASUREMENTS

### 5.4.1 Oxygen equilibrium pressure

As we have seen in chapter 3, the oxidation state of the molten glass dominates many properties of the melt and the final product. The local oxidation state determines the local ratios of reduced to oxidized polyvalent elements in the melt. This parameter is directly related to the activity of the molecular oxygen  $O_2$  in the melt through redox reaction:



The oxygen activity in the melt can be represented by the partial oxygen pressure in the atmosphere with which the glass melt would be in equilibrium. This is often referred to as "the oxygen equilibrium pressure" in the melt.

### 5.4.2 The oxygen sensor

In practice, glass melts are usually not in equilibrium with the surrounding atmosphere [7,11,12]. The oxygen equilibrium pressure in the melt depends on the amount of reducing or oxidizing components in the batch, the type of furnace (oil

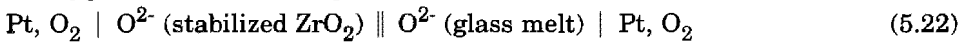


or gas fired), the melting history etc. (see chapter 3). Oxygen sensors for the in-situ measurement of the oxygen activity in the molten glass have been developed to study the effect of oxidation states at high temperatures [7,8,9,11].

The oxygen sensor consists of two platinum electrodes. One of them is dipped in the glass melt, the other (reference electrode) is flushed with a gas with a known partial oxygen pressure. The melt is separated from the gas by  $Y_2O_3$ -stabilized zirconia. The properties of this material have been described in section 5.3.3.3. A difference in oxygen activity between melt and gas will lead to a potential difference between the two electrodes [10]. The potential difference is measured with the aid of a high-impedance voltmeter. From this potential difference the oxygen equilibrium pressure in the melt can be calculated.

### 5.4.3 Electrochemical description of the oxygen sensor

The oxygen sensor can be represented schematically by:



In figure 5.7 the phases and interfaces are defined.

The measured potential difference  $\Delta E$  is the sum of the potential differences across each interphase and within each phase (see sections 5.2.3 and 4):

$$\begin{aligned} \Delta E = & (\phi_{\text{voltmeter (I)}} - \phi_{\text{Pt (I)}}) + (\phi_{\text{Pt (I)}} - \phi_{\text{Pt (II)}}) + \\ & (\phi_{\text{Pt (II)}} - \phi_{\text{melt (II)}}) + (\phi_{\text{melt (II)}} - \phi_{\text{melt (III)}}) + \\ & (\phi_{\text{melt (III)}} - \phi_{ZrO_2 \text{ (III)}}) + (\phi_{ZrO_2 \text{ (III)}} - \phi_{ZrO_2 \text{ (IV)}}) + \\ & (\phi_{ZrO_2 \text{ (IV)}} - \phi_{\text{Pt (IV)}}) + (\phi_{\text{Pt (IV)}} - \phi_{\text{Pt (V)}}) + \\ & (\phi_{\text{Pt (V)}} - \phi_{\text{voltmeter (V)}}) \end{aligned} \quad (5.23)$$

The interfaces between the voltmeter and the platinum electrodes, I and V, are both at room temperature. Therefore:

$$(\phi_{\text{voltmeter (I)}} - \phi_{\text{Pt (I)}}) = - (\phi_{\text{Pt (V)}} - \phi_{\text{voltmeter (V)}}) \quad (5.24)$$

Within the platinum wires a potential difference arises due to the temperature gradient from room to melt temperature or vice versa. Since the interfaces II and IV are located in the hot zone of the furnace, where the temperature is assumed to be homogeneous, the potential differences cancel out:

$$(\phi_{\text{Pt (I)}} - \phi_{\text{Pt (II)}}) = - (\phi_{\text{Pt (IV)}} - \phi_{\text{Pt (V)}}) \quad (5.25)$$

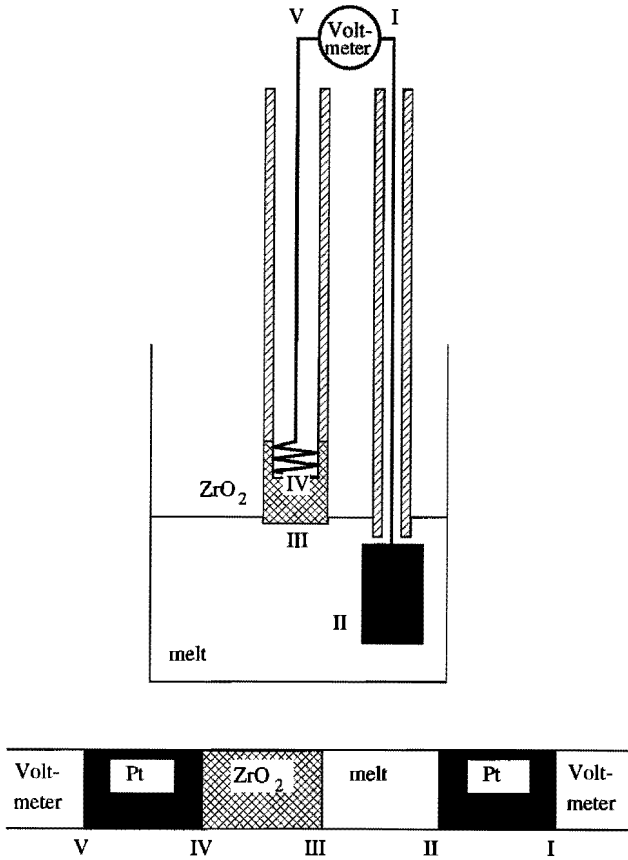
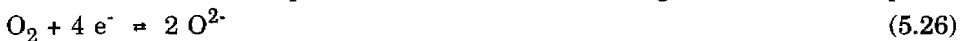


Figure 5.7  
A schematical presentation of the oxygen sensor

At the interface between platinum and melt the following reaction can take place:



The potential difference at this interface can be described by [1,7]:

$$(\phi_{\text{Pt(II)}} - \phi_{\text{melt(II)}}) = E_{\text{O}_2/\text{O}^{2-}}^0 + \frac{R_g \cdot T_{\text{melt}}}{4 \cdot F} \ln \frac{p_{\text{O}_2(\text{II})}}{(a_{\text{O}^{2-}(\text{II})})^2} \quad (5.27)$$

In the molten glass a potential difference will arise if a temperature gradient exists between the surface of the platinum counter electrode (II) and the zirconia (III). Then the potential difference is governed by transport of ions in the melt as represented by equation 5.5. In soda-lime-silica glass melts,  $\text{Na}^+$  is the mobile ion

that provides charge transport. The migration of  $\text{Na}^+$  determines the junction potential within the melt (see equation 5.5). According to Baucke [8] the transport number of the  $\text{Na}^+$  ions in soda-lime-silica glass melts is 1. However, the temperature in the glass melt is assumed to be homogeneous. The phase is in equilibrium and no potential difference occurs in the melt. The activity of the oxide ions near the surface of the zirconia is equal to the activity at the counter electrode:

$$a_{\text{O}^{2-}}(\text{melt (II)}) = a_{\text{O}^{2-}}(\text{melt (III)}) \quad (5.28)$$

At the interface III oxide ions  $\text{O}^{2-}$  are exchanged between the melt and the zirconia. At equilibrium the activities of  $\text{O}^{2-}$  in both phases are equal (see equation 5.4 and [8]):

$$a_{\text{O}^{2-}}(\text{melt (III)}) = a_{\text{O}^{2-}}(\text{ZrO}_2 \text{ (III)}) \quad (5.29)$$

Within the stabilized zirconia a potential difference arises due to migration of ions, because the electrochemical potential of these ions in the gas phase differ from those in the glass phase (see chapter 5.2.2):

$$\left( \phi_{\text{ZrO}_2 \text{ (III)}} - \phi_{\text{ZrO}_2 \text{ (IV)}} \right) = \frac{R_g \cdot T_{\text{melt}}}{F} \int_{\text{III}}^{\text{IV}} \frac{t_i}{z_i} d \ln a_i \quad (5.30)$$

In stabilized zirconia the transport number  $t_i$  of  $\text{O}^{2-}$  is 1, while the transport number of all other ions is zero [9]. Electronic conduction is negligible [9]. Therefore the potential difference in the zirconia can be written as:

$$\left( \phi_{\text{ZrO}_2 \text{ (III)}} - \phi_{\text{ZrO}_2 \text{ (IV)}} \right) = \frac{R_g \cdot T_{\text{melt}}}{-2 \cdot F} \ln \frac{a_{\text{O}^{2-}}(\text{ZrO}_2 \text{ (IV)})}{a_{\text{O}^{2-}}(\text{ZrO}_2 \text{ (III)})} \quad (5.31)$$

At the platinum reference electrode the reaction 5.26 takes place.

The potential difference is given by:

$$\left( \phi_{\text{ZrO}_2 \text{ (IV)}} - \phi_{\text{Pt (IV)}} \right) = - \left( \phi_{\text{Pt (IV)}} - \phi_{\text{ZrO}_2 \text{ (IV)}} \right) = - E_{\text{O}_2/\text{O}^{2-}}^0 - \frac{R_g \cdot T_{\text{melt}}}{4 \cdot F} \ln \frac{p_{\text{O}_2} \text{ (IV)}}{\left( a_{\text{O}^{2-}} \text{ (IV)} \right)^2} \quad (5.32)$$

The overall potential difference is then given by:

$$\Delta E = \frac{R_g \cdot T_{\text{melt}}}{4 \cdot F} \ln \frac{a_{\text{O}_2} \text{ (II)}}{a_{\text{O}_2} \text{ (IV)}} = \frac{R_g \cdot T_{\text{melt}}}{4 \cdot F} \ln \frac{p_{\text{O}_2} \text{ (melt)}}{p_{\text{O}_2} \text{ (reference gas)}} \quad (5.33)$$

#### 5.4.4 Calculation of the oxygen equilibrium pressure in the melt

The oxygen equilibrium pressure in the melt can be calculated for a known partial oxygen pressure in the reference gas by:

$$p_{\text{O}_2}(\text{melt}) = p_{\text{O}_2}(\text{reference gas}) \cdot \exp\left(\frac{4 \cdot F \cdot \Delta E}{R_g \cdot T_{\text{melt}}}\right) \quad (5.34)$$

#### 5.4.5 Properties of the reference and platinum electrode

##### 5.4.5.1 The reference electrode

The reference electrode as described in chapter 5.3.3.3 has been tested by various investigators [7,9,10]. The reference electrode proved to behave ideally at temperatures up to 1350°C. After a change in the partial oxygen pressure of the reference gas, a new equilibrium is reached very fast. The new potential difference is in accordance with Nernst Law. The results were shown to be reproducible within 2 mV.

##### 5.4.5.2 The platinum electrode

The design of the platinum electrode has a large effect on the oxygen equilibrium pressure measurements [13,14]. According to Lenhart [13] oxygen diffusion along the interface platinum/glass is faster than oxygen diffusion in the bulk of the melt. If the partial oxygen pressure in the atmosphere exceeds the oxygen equilibrium pressure in the melt, diffusion of O<sub>2</sub> from atmosphere to the melt takes place particularly along the platinum electrode. In that case the oxygen equilibrium pressure increases faster in the neighbourhood of the platinum electrode than in the bulk of the melt. The measured potential difference does not represent the oxygen equilibrium pressure in the bulk of the molten glass, but the pressure at the platinum electrode (interface II in figure 5.7).

To avoid enhanced oxygen diffusion from the atmosphere to the melt, the three-phase contact area should be as small as possible, and the surface area of the platinum electrode in the molten glass itself should be large. Therefore the platinum electrode used for the oxygen equilibrium pressure measurements mentioned in this thesis consists of a platinum wire of 1 mm diameter to which a platinum plate with a surface area of about 200 mm<sup>2</sup> is attached (electrode 3 in figure 5.3). This platinum plate is entirely immersed in the glass melt.

#### 5.4.6 Oxygen equilibrium pressure measurements

The experimental set-up for the oxygen equilibrium pressure measurements is

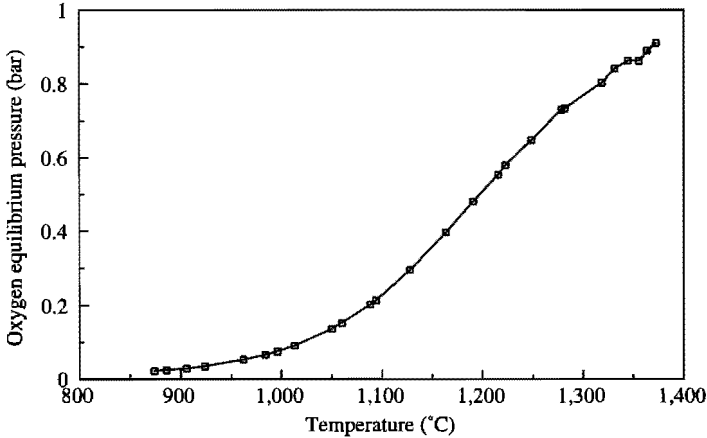


Figure 5.8

The oxygen equilibrium pressure as a function of temperature in TV-screen glass containing 0.4 weight-%  $\text{Fe}_2\text{O}_3$

drawn in figure 5.3. Electrode 2 is the reference electrode, electrode 3 the measuring electrode. The oxygen equilibrium pressure was measured as a function of temperature in glass melts containing one or two polyvalent elements. As an example the oxygen equilibrium pressure in TV-screen glass containing 0.4 weight-%  $\text{Fe}_2\text{O}_3$  is plotted in figure 5.8.

If the oxygen equilibrium pressure in the melt exceeds 1 bar, accelerated bubble formation will occur [10,14]. The bubbles can rise to the surface of the melt, removing oxygen from the molten glass. The oxygen equilibrium pressure does not exceed the 1 bar level (unless the temperature of the melt is increased very fast and the melt contains elements that supply large amounts of oxygen gas).

#### 5.4.7 Calculation of the redox reaction equilibrium constants, enthalpy and entropy

The equilibrium constant of the redox reaction



is given by the redox reaction equilibrium constant  $K^{**}(T)$  as defined in equation 3.9 and 3.14:

$$K^{**}(T) = \frac{[\text{M}^{x+}] \cdot p_{\text{O}_2}^{n/4}}{[\text{M}^{(x+n)+}]} = \exp \left( \frac{-\Delta H^{**}}{R_g \cdot T} + \frac{\Delta S^{**}}{R_g} \right) \quad (5.36)$$

The oxygen equilibrium pressure measurements can be used in combination with chemical analysis of the concentrations of  $M^{(x+n)+}$  and  $M^{x+}$  to calculate the redox reaction equilibrium constant as a function of temperature (see chapter 4.2). From these data the values for the enthalpy and entropy of the redox reaction,  $\Delta H^{**}$  and  $\Delta S^{**}$ , can be calculated.

The reaction enthalpy and entropy can also be derived directly from oxygen measurements. For this purpose, the oxygen equilibrium pressure in a molten glass containing  $C_M$  mole·m<sup>-3</sup> polyvalent species M is measured as a function of temperature. The temperature is changed fast (by some degrees per minute) in order to avoid transfer of oxygen between atmosphere and melt during the experiment. The oxygen equilibrium pressure should remain below 1 bar throughout the experiment to avoid the formation of bubbles. If no oxygen transfer between melt and atmosphere takes place, a change in oxygen equilibrium pressure can only result from a shift in the equilibrium state of reaction 5.35.

At a decrease of temperature the polyvalent element will generally be transferred to the oxidized state if no other polyvalent elements are present (chapter 3.2.2. and 3.2.4). The equilibrium of reaction 5.35 will shift to the left. If one mole of the reduced polyvalent element is oxidized during a temperature decrease from  $T_1$  to  $T_2$ ,  $n/4$  moles of  $O_2$  are consumed:

$$[M^{x+}]_{T_1} - [M^{x+}]_{T_2} = \frac{n}{4} \left\{ [O_2]_{T_1} - [O_2]_{T_2} \right\} \quad (5.37)$$

The oxygen concentration  $[O_2]$  (physically dissolved) is directly related to the oxygen equilibrium pressure according to Henry's Law (see chapter 2.2.6):

$$[O_2] = L_{O_2} \cdot p_{O_2} \quad (5.38)$$

The physical solubility of oxygen,  $L_{O_2}$ , is given in mole·m<sup>-3</sup>·bar<sup>-1</sup>.

Equation 5.37 can therefore be written as:

$$L_{O_2}(T_1) \cdot p_{O_2}(T_1) - L_{O_2}(T_2) \cdot p_{O_2}(T_2) = \frac{4}{n} \left\{ [M^{x+}]_{T_1} - [M^{x+}]_{T_2} \right\} \quad (5.39)$$

The concentration of the polyvalent element  $C_M$  is assumed to remain constant during the experiment. The concentration of the reduced polyvalent element at any temperature T is given by:

$$[M^{x+}]_T = C_M - [M^{(x+n)+}]_T \quad (5.40)$$

Rearrangement of equation 5.36 leads to:

$$[M^{x+}]_T = \frac{K^{**}(T) \cdot [M^{(x+n)+}]_T}{(p_{O_2}(T))^{n/4}} \quad (5.41)$$

Combining of equations 5.40 and 5.41 leads to:

$$[M^{x+}]_T = \frac{K^{**}(T) \cdot C_M}{K^{**}(T) + (p_{O_2}(T))^{n/4}} \quad (5.42)$$

And the combination of equations 5.39 and 5.42 results in:

$$L_{O_2}(T_1) \cdot p_{O_2}(T_1) - L_{O_2}(T_2) \cdot p_{O_2}(T_2) = \frac{n}{4} \cdot C_M \cdot \left\{ \frac{K^{**}(T_1)}{K^{**}(T_1) + p_{O_2}^{n/4}(T_1)} - \frac{K^{**}(T_2)}{K^{**}(T_2) + p_{O_2}^{n/4}(T_2)} \right\} \quad (5.43)$$

The redox reaction equilibrium constant depends on the redox reaction enthalpy and entropy  $\Delta H^{**}$  and  $\Delta S^{**}$  as defined in equation 5.36. The non-linear equation 5.43 can be solved with the aid of a computer program for various values of  $\Delta H^{**}$  and  $\Delta S^{**}$ . By comparing the measured oxygen equilibrium pressures with those calculated by the computer program the values of  $\Delta H^{**}$  and  $\Delta S^{**}$  can be found using fitting procedures.

No other investigator has used the oxygen equilibrium pressure measurements to calculate both  $\Delta H^{**}$  and  $\Delta S^{**}$ . However, comparison of the results obtained with this technique with those obtained by other techniques show that the results are very close and reliable, as will be seen in chapter 6.

#### 5.4.8 Restrictions of the described method

The computer program for the calculation of  $\Delta H^{**}$  and  $\Delta S^{**}$  values from oxygen equilibrium pressure measurements can only be used if:

- no exchange of oxygen between glass melt and atmosphere takes place during the measurement (closed system);
- the glass melt contains only one polyvalent element, or the glass melt contains more polyvalent elements but the  $\Delta H^{**}$ 's and  $\Delta S^{**}$ 's of all but one redox reaction are known;
- the concentration of the polyvalent element  $C_M$  remains constant during the

oxygen equilibrium pressure measurements (no volatilization);

d. the physical solubility of oxygen is known as a function of temperature.

Ad a.

The equilibration of a glass melt with the surrounding atmosphere takes a long time (see chapter 4.2) because the diffusivity of oxygen in molten glass is small (about  $10^{-10} \text{ m}^2 \cdot \text{s}^{-1}$ , chapter 2.2.6). Even for small samples of 30 gram the equilibration time is according to Paul [12] at least 70 hours for a motionless glass melt.

The samples that are used for the oxygen equilibrium pressure measurements weigh about 300 grams, the volumes are about  $130000 \text{ mm}^3$ . The temperature varies from  $1400^\circ\text{C}$  to  $800^\circ\text{C}$  and back again with a rate of  $3^\circ\text{C} \cdot \text{min}^{-1}$ . A complete experiment is done within 7 hours. It is unlikely that oxygen transport from atmosphere to melt influences the oxygen equilibrium pressure in the glass melt within this time.

If the oxygen equilibrium pressure exceeds 1 bar, bubbles will be formed in the melt. These bubbles will ascend to the surface of the melt. Oxygen can be transferred to the surrounding atmosphere at a fast rate. Therefore equation 5.43 is only valid if the oxygen equilibrium pressure remains below this value. Calculations of  $\Delta H^{**}$  and  $\Delta S^{**}$  have only been performed for melts with oxygen equilibrium pressures of less than 0.5 bar.

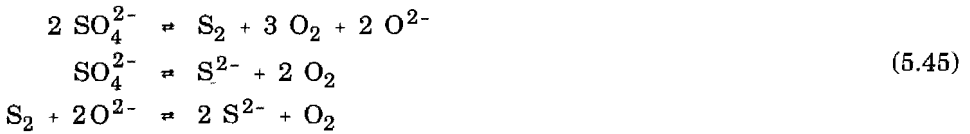
In glass melts containing sulphate, both  $\text{O}_2$  and  $\text{SO}_2$  are released as fining gases (see chapter 2.4.3). The total gas pressure can exceed 1 bar while the oxygen equilibrium pressure is still very low. The condition of a closed system is then not satisfied. If the sulphate-containing glass is melted under oxidizing conditions the following reaction is assumed to take place at an increase of temperature:



and if the physical solubilities of  $\text{SO}_2$  and  $\text{O}_2$  are in the same order of magnitude, the oxygen equilibrium pressure at high temperatures will be about half of the  $\text{SO}_2$  equilibrium pressure in the melt. Calculations of  $\Delta H^{**}$  and  $\Delta S^{**}$  for sulphate-containing glasses have only been performed for melts with oxygen equilibrium pressures of less than 0.2 bar.

Under reducing conditions, the following reactions may take place in sulphate-containing glasses:





The total gas pressure depends on the equilibrium constants of all reactions 5.44 and 5.45. We can therefore not be sure that the total gas pressure is less than 1 bar while the oxygen equilibrium pressure remains below 1 bar. For this reason, in this study no oxygen equilibrium pressure measurements have been used to derive a sulphate/redox equilibrium constant in sulphate-containing glass melts under reducing conditions.

Ad b.

In the case the melt contains more than one polyvalent element, the oxygen equilibrium pressure depends on the equilibria of all redox reactions. In case no complexes are formed between the polyvalent elements  $M_a$ ,  $M_b$  etc. the change in oxygen concentration is given by:

$$\begin{aligned}
 L_{\text{O}_2}(\text{T}_1) \cdot p_{\text{O}_2}(\text{T}_1) - L_{\text{O}_2}(\text{T}_2) \cdot p_{\text{O}_2}(\text{T}_2) = \\
 \frac{4}{n_a} \left\{ \left[ M_a^{x_a+} \right]_{\text{T}_1} - \left[ M_a^{x_a+} \right]_{\text{T}_2} \right\} + \frac{4}{n_b} \left\{ \left[ M_b^{x_b+} \right]_{\text{T}_1} - \left[ M_b^{x_b+} \right]_{\text{T}_2} \right\} + \dots
 \end{aligned}
 \tag{5.46}$$

The enthalpy and entropy of the redox reaction of element  $M_a$  can be estimated from the measured oxygen pressure as a function of temperature if  $\Delta H^{**}$  and  $\Delta S^{**}$  of all the other redox reactions are exactly known.

It is also possible to predict the oxygen equilibrium pressure as a function of temperature for glass melts containing two or more polyvalent elements on the basis of measurements in glasses containing only one of these elements. For example the values of  $\Delta H^{**}$  and  $\Delta S^{**}$  of the redox reactions of iron and of cerium in TV-screen glass have been calculated from oxygen equilibrium pressure measurements (chapter 6.2 and 6.4). Subsequently the oxygen pressure for a glass containing both iron and cerium has been calculated from equation 5.46 and compared with measured data (chapter 6.7). The excellent agreement between measured data and theory supports the validity of equation 5.46.

Ad c.

The concentration of the polyvalent element should be known and remain constant during the experiments. For most polyvalent elements these conditions will be

satisfied, but some polyvalent elements like  $\text{Sb}_2\text{O}_3$  are volatile. Special care should be taken to prevent loss of these elements during the melting process. Antimony for instance can be added to the batch as  $\text{Sb}_2\text{O}_5$  which is far less volatile. Evaporation of this antimony from the molten glass during the experiments is unlikely and the total concentration of Sb species will remain constant.

The conditions will not be satisfied if sulphate is added to the batch. At an increase of temperature the sulphate is reduced to  $\text{SO}_2$  and  $\text{O}_2$ . If the total gas pressure in the melt exceeds 1 bar bubbles containing  $\text{SO}_2$  and  $\text{O}_2$  will be formed. Sulphur species then leave the melt in the form of  $\text{SO}_2$ . This phenomenon may even take place at low temperatures.

The gas pressure is determined by the physical solubility of the gas in the melt:

$$P_i = \frac{C_i}{L_i(T)} \quad (5.47)$$

In some glasses the solubility of sulphur oxides is assumed to be very low. The total gas pressure can then easily exceed 1 bar and sulphur species are driven out of the melt at a high rate. The oxygen equilibrium pressure measurements in glass melts containing sulphur have to be performed during cooling of the melt, because then the loss of  $\text{SO}_2$  is less likely. After the experiments the sulphur concentration has to be measured in order to be able to apply equation 5.43 to the results.

Ad d.

In the literature, hardly any data on the physical solubility of oxygen in molten soda-lime, TV-screen and E-glass has been published. Sasabe [15] derived the physical solubility of oxygen for various  $\text{PbO-SiO}_2$  melts from permeability and diffusivity measurements. He obtained a value between 20 and 200  $\text{mole}\cdot\text{m}^{-3}\cdot\text{bar}^{-1}$ . Schreiber [16] estimated the chemical solubility in soda-lime-silica glass melts to be 20  $\text{mole}\cdot\text{m}^{-3}\cdot\text{bar}^{-1}$ . The physical solubility will probably be much less (see chapter 2.2.6). Beerkens [17] estimated the physical oxygen solubility from the solubility of  $\text{N}_2$ . He obtained a value of about 0.1  $\text{mole}\cdot\text{m}^{-3}\cdot\text{bar}^{-1}$ . Recent measurements using the helium-extraction technique indicate, that the physical solubility of oxygen in soda-lime-silica and TV-screen glass melts at temperatures ranging from 1200 to 1450°C lies in the order of 0.1 to 1  $\text{mole}\cdot\text{m}^{-3}\cdot\text{bar}^{-1}$  [18].

The physical solubility of oxygen can be calculated from oxygen equilibrium pressure measurements using equation 5.43 when the enthalpy and entropy of a redox reaction are already known (for instance from square wave voltammetry

measurements). The nature of the polyvalent element and its concentration should have no influence on the result. Experiments in TV-screen glass containing 0.4 weight-%  $\text{Fe}_2\text{O}_3$  indicate, that the oxygen solubility at temperatures between 900 and 1400°C is in the order of  $1 \text{ mole}\cdot\text{m}^{-3}\cdot\text{bar}^{-1}$  (see chapter 6.8). However, these results could not be reproduced in TV-screen glass containing antimony (see chapter 6.8). Up to now, no data on the physical solubility of oxygen in soda-lime-silica and E-glass have been produced by this method.

For the calculation of the enthalpies and entropies of the redox reactions of iron, antimony, cerium and sulphate in soda-lime-silica, TV-screen and E-glass melts, the physical solubility of oxygen is set to a value of  $1 \text{ mole}\cdot\text{m}^{-3}\cdot\text{bar}^{-1}$ . In chapter 6.8, the effect of the value chosen for the oxygen solubility on the calculated  $\Delta H^{**}$  and  $\Delta S^{**}$  will be discussed.

#### 5.4.9 Advantages of the described method

Oxygen equilibrium pressure measurements can be performed in any glass melt containing any polyvalent element. The reaction enthalpy and entropy changes can therefore be calculated for any redox active species as long as the conditions mentioned in section 5.4.8 are fulfilled.

### 5.5 SQUARE WAVE VOLTAMMETRY MEASUREMENTS

Square wave voltammetry is a pulse voltammetric technique which enables us to measure the formal potential of a redox reaction that occurs at the working electrode with regard to the potential of the reference electrode. From this formal potential the enthalpy and entropy of the redox reaction can be calculated. In combination with oxygen equilibrium pressure measurements the redox ratio (the ratio of reduced to oxidized species) in the glass melt without externally applied voltage can be found.

From square wave voltammograms some other properties like the diffusion coefficient of the reacting species or its concentration can be determined. In addition to this, the voltammograms may give information on the reaction mechanism. The amount of electrons that is transferred during reduction of one mole of reactant can be determined, and the shape of the curve in the voltammogram may indicate irreversibility or the occurrence of reactions preceding or following the redox reaction of interest.

### 5.5.1 The experimental set-up

For the square wave voltammetry measurements mentioned in this thesis, the three-electrode system as sketched in figure 5.3 has been used. The reference electrode was flushed with clean, dry air. Before each measurement the temperature in the furnace was held constant for at least 15 minutes. The temperature within the molten glass is then assumed to be homogeneous and equal to the temperature measured outside the crucible with the thermocouple.

### 5.5.2 The applied potential

#### 5.5.2.1 The potential program

Before each square wave voltammetry experiment the uncompensated resistance  $R_u$  in the melt is measured following the procedure described in section 5.3.6. Then a rapidly changing potential is applied between the working and the reference electrode with the aid of a potentiostat. The applied potential is corrected for  $i \cdot R_u$  with the aid of positive feedback circuits.

The applied potential is composed of a staircase base potential  $E_b$  with step height  $\Delta E_b$  and a blocklike potential pulse with pulse height  $\Delta E_p$  (see figure 5.9). The base potential is changed with a frequency  $f$  of 5 to 500 Hz. The pulse time  $t_p$  is defined as the time during which the base potential remains constant:  $t_p = 1/f$ . During the pulse time  $t_p$  the resulting potential changes two times. A potential pulse  $E_p$  in the scan direction is called a 'forward pulse'. A potential pulse in the reverse direction is called a 'reverse pulse' (see figure 5.9).

The current is measured at the end of each potential pulse.

#### 5.5.2.2 The value of the potential

Before the measurement the potential is held at a value  $E_i$  (usually 0 V with regard to the potential of the reference electrode). At the end of a measurement the base potential is  $E_{end}$ . A scan of the entire potential range is completed in:

$$\text{scan time} = \frac{(E_{end} - E_i + \Delta E_b) \cdot t_p}{\Delta E_b} = \frac{(E_{end} - E_i + \Delta E_b)}{\Delta E_b \cdot f} \quad (5.48)$$

During this time, the potential changes  $m$  times, with

$$m = \frac{\text{scan time}}{t_p} \cdot 2 \quad (5.49)$$

The potential during the  $m^{\text{th}}$  potential pulse is given by:

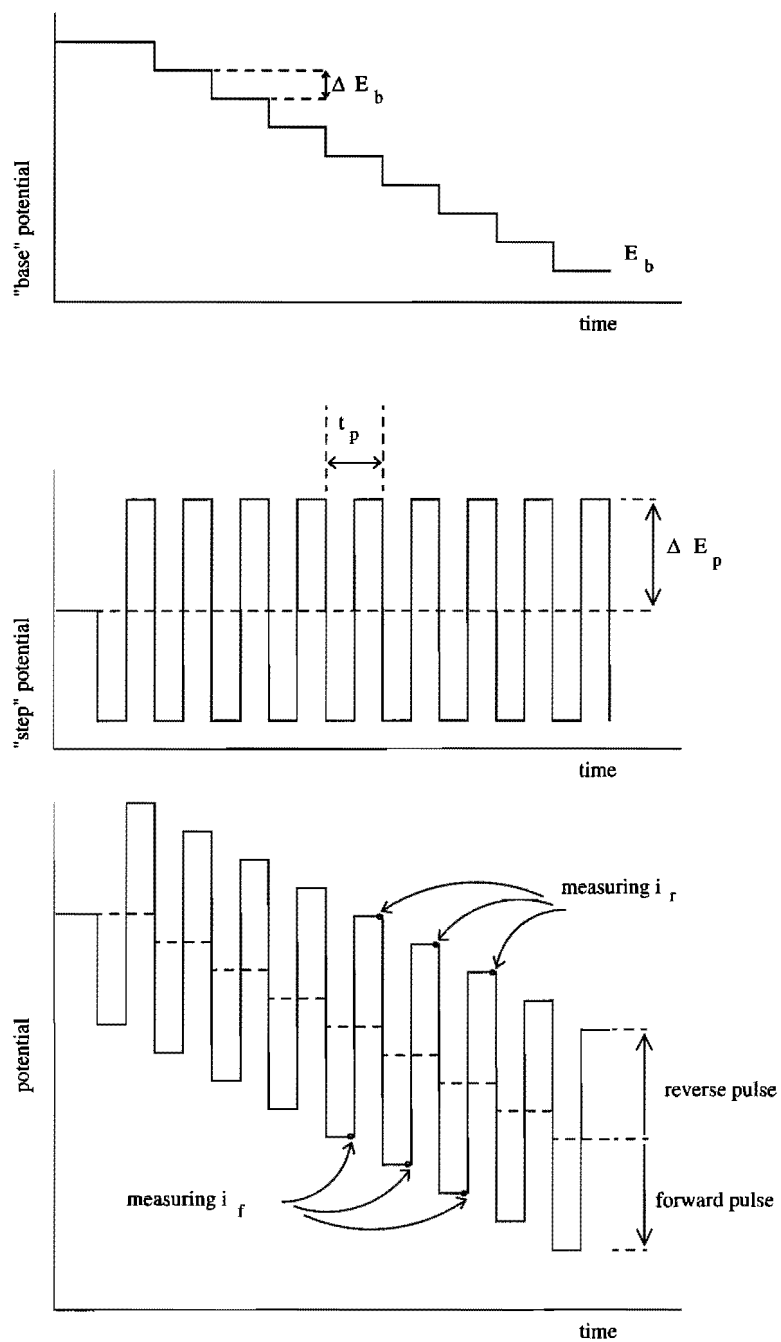


Figure 5.9  
Potential program in a square wave voltammetry experiment

$$E_m = E_i + \text{TRUNC} \left( \frac{m-1}{2} \right) \cdot \Delta E_b - (-1)^m \cdot \Delta E_p \quad (5.50)$$

and  $m$  is 1,2,3,...

### 5.5.3 The voltammogram

The currents that flow during forward pulses ( $m$  is odd) are referred to as 'forward current',  $i_f$ . Likewise, currents measured during a reverse pulse ( $m$  is even) are called 'reverse currents',  $i_r$  (see figure 5.9). In the voltammogram the forward and reverse currents are plotted against the base potential. Then the current measured at the reverse pulse is subtracted from the current measured at the preceding forward pulse. The resulting current  $\delta i$  ( $\delta i = i_f - i_r$ ) is also plotted against the base potential. The voltammogram shows a peak in the  $\delta i$ -curve at the half-wave potential  $E_{1/2}$  of a redox reaction.

In figure 5.10a, an arbitrary voltammogram is illustrated for a redox reaction with a half-wave potential of  $-0.4$  V with regard to the reference electrode. The temperature of the melt is  $1200^\circ\text{C}$ . During the reaction, 2 electrons are transferred while one ion of Ox is reduced.

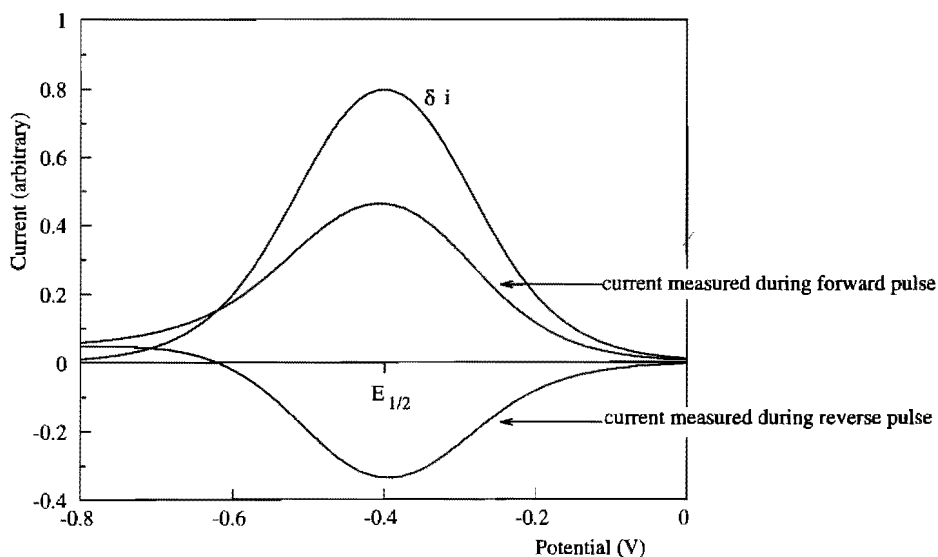


Figure 5.10a

An arbitrary voltammogram for a redox reaction with a half-wave potential of  $-0.4$  V with regard to the reference electrode. The temperature is  $1200^\circ\text{C}$ . During the reaction, 2 electrons are transferred while one ion of Ox is reduced.

The redox active species is assumed to be completely in the oxidized form at the initial potential, 0 V, and entirely in the reduced form at the final potential, -0.8 V (with regard to the reference electrode).

#### 5.5.4 The $i_p$ , $i_r$ and $\delta i$ curves: a general description

In the curves of  $i_p$ ,  $i_r$  and  $\delta i$  a peak occurs. In this section a descriptive explanation for the occurrence of the peaks will be given with the help of figure 5.10b.

##### 5.5.4.1 The measured current, consisting of faradaic and charging currents

During a potential pulse a current, consisting of a faradaic and a charging current, may arise. The faradaic current originates from a redox reaction, while the charging current results from the charging of the electrochemical double layer (chapter 5.2.7). The current is measured at the end of each potential pulse at time  $\frac{1}{2} \cdot t_p$  from the change in potential. Both the faradaic and the charging current have dropped in time  $t$ , elapsed since the potential was changed: the faradaic current decreases with  $t^{-1/2}$  (under the assumption that the reaction rate is diffusion-controlled, see section 5.2.7) and the charging current decreases exponentially with  $t$ . The contribution of the charging current to the resulting current therefore becomes less if the time during which the potential is held constant,  $\frac{1}{2} \cdot t_p$ , is fixed at a higher value.

For the descriptive explanation of  $i_p$ ,  $i_r$  and  $\delta i$  the contribution of the charging current in the value of the measured current will be neglected.

##### 5.5.4.2 The faradaic currents during "forward" and "reverse" pulses as a function of the applied potential

A "forward" pulse is a pulse in the direction of the scan. In most measurements the potential is changed from 0 to -0.8 V. A pulse in the forward direction is then a pulse in the negative direction (see figure 5.9). A pulse in the "reverse" direction opposes the scan-direction.

#### **Potential region a in figure 5.10b**

Before the beginning of the experiment, at a potential of 0 V relative to the potential of the reference electrode, the polyvalent element is practically completely in its oxidized state, Ox.

At the beginning of the experiment a potential pulse in the forward direction (the negative direction) results in a potential that is not sufficient for a measurable

reduction of the redox active species. The equilibrium of the reaction at the working electrode:



is still on the left side. Since hardly any electron transfer takes place,  $i_f$  is practically zero.

Because hardly any reduced ions are present yet, a pulse in the reverse (positive) direction does not bring about a current either.  $i_r \approx 0$ .

### Potential region b in figure 5.10b

At a certain point, the base potential becomes low enough and the equilibrium of reaction 5.51 is shifted somewhat to the right side, according to Nernst Law. A small part of the oxidized polyvalent element close to the working electrode is reduced in order to satisfy equation 5.9. During forward potential pulses, electrons flow from electrode to electrolyte causing a positive current.  $i_f > 0$ . This current will be higher if the applied potential is more negative. Because enough reactant is available, diffusion of the oxidized polyvalent element from the bulk of the melt to the surface of the working electrode does not play a significant part at this stage of the measurement.

During the reverse potential pulse, most of the reduced species, formed during the preceding forward potential pulse, will be transferred to the oxidized state again. This causes a negative current nearly equal in value to the positive current that flew during the preceding forward pulse.  $i_r < 0$ ,  $i_r \approx -i_f$ .

### Potential region c in figure 5.10b

If the value of the base potential is close to the half-wave potential (with regard to the potential of the reference electrode), both oxidized and reduced species will be present at the surface of the working electrode. This is the case at about -0.4 V for this arbitrary illustrative voltammogram. A pulse in the forward direction yields a potential of  $E_{1/2} - \Delta E_p$ . At this potential the reduced form is favoured. This causes the reduction of the oxidized form. The equilibrium of reaction 5.51 shifts to the right according to the Nernst Law. Electrons flow from electrode to electrolyte, causing a large positive current.  $i_f > 0$ .

During the following pulse in the reverse direction, the potential of the working electrode is increased to a value where the oxidized form of the reacting species is favoured ( $E_{1/2} + \Delta E_p$ ). The equilibrium of equation 5.51 shifts to the left. The



electrons flow from electrolyte to electrode, resulting in a large negative current.

### Potential region d in figure 5.10b

A little later in the experiment, the base potential is slightly more negative than the half-wave potential. But still there are both oxidized and reduced ions present at the surface of the working electrode after a pulse in the reverse direction. During the pulse in the forward direction the oxidized ions are now nearly all reduced, and the concentration of oxidized ions during the forward pulse becomes almost zero. The current  $i_f$  is then dominated by the transport of oxidized ions from the bulk of the electrolyte (see section 5.2.7). At first, this transport occurs at a high rate because the concentration gradient is very high: only at the surface of the working electrode the redox active species is reduced completely.  $i_f$  reaches its maximum value.  $i_f = i_{f,max}$ .

### Potential region e in figure 5.10b

But gradually the concentration gradient of the oxidized species at the surface of the working electrode decreases because of depletion of the electrolyte near the working electrode (see equation 5.10). Therefore the currents during succeeding "forward" pulses decrease more and more.  $i_f > 0, < i_{f,max}$ .

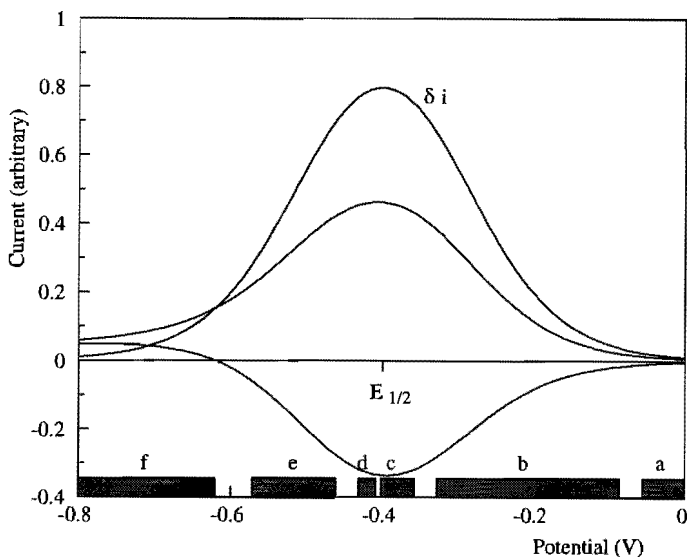


Figure 5.10b

An arbitrary illustrative voltammogram for a redox reaction with a half-wave potential of -0.4 V with regard to the reference electrode. The temperature is 1200°C. During the reaction, 2 electrons are transferred while one ion of Ox is reduced.

**Potential region f in figure 5.10b**

During pulses in the reverse direction the potential is much more negative than the half-wave potential. At these potential levels only the reduced form of the redox active species is stable, and the equilibrium of equation 5.51 is on the right side. No oxidized species are formed during the reverse pulses, but instead the oxidized form of the polyvalent element is reduced at the working electrode, resulting in a small positive current. But the concentration of the oxidized form of the polyvalent element at the working electrode is almost zero, and the current during reverse pulses is also governed by the supply of oxidized ions from the bulk of the melt. Therefore the current during reverse pulses is positive, and depends on the diffusion coefficient of the oxidized form of the polyvalent element.  $i_r$  approaches  $i_f$  until both have the same positive value.

The peaks in  $i_f$  and  $i_r$  are not located exactly at the half-wave potential  $E_{1/2}$  of the reaction. The drop in the  $i_f$  curve is not caused by thermodynamics but by a depletion of the electrolyte. The diffusion of the oxidized form of the polyvalent element only starts to become important as the concentration of Ox at the surface of the working electrode is practically zero. The magnitude of the potential pulse  $\Delta E_p$  determines at which base potential this condition is satisfied. Therefore the position of the peaks of the  $i_f$  and  $i_r$  depend on this quantity: if  $\Delta E_p$  is small, the peak in  $i_f$  is located at a more negative, and the peak in  $i_r$  at a more positive potential than the half-wave potential  $E_{1/2}$ .

The curve of  $i_r$  is subtracted from the curve of  $i_f$ , resulting in  $\delta i$ . In this curve a sharp peak appears at the formal potential  $E^0$  of the redox reaction if the diffusion coefficients of the oxidized and reduced species are equal. Otherwise the peak occurs at the half-wave potential  $E_{1/2}$ .

**5.5.5 The  $i_f$ ,  $i_r$  and  $\delta i$  curves: a mathematical description**

The equilibrium concentrations of the oxidized and reduced species close to the working electrode depend on the applied potential according to Nernst Law (equation 5.9). The currents depend on the concentrations, but also on the concentration gradient and therefore on the concentrations at the working electrode obtained during the preceding potential pulse and the diffusion rate of these ions. The currents that flow during the forward and reverse potential pulses can be calculated by the application of the so-called superposition theorem using some assumptions. Solutions to this problem are given in [6,19,20].

The assumptions are:

- the working electrode is a planar plate with surface area  $A \text{ m}^2$ ;
- the diffusion of oxidized and reduced species is semi-infinite and linear;
- the redox reaction is strictly reversible;
- at the initial potential the redox active species is only present in the oxidized state; its concentration is  $C_{\text{Ox}}$ ;
- no charging current flows;
- $\Delta E_p$  is smaller than  $R_g \cdot T/n \cdot F$ .

The current that flows during the  $m^{\text{th}}$  potential pulse  $i_m$  is given by [6]:

$$i_m = n \cdot F \cdot A \cdot C_{\text{Ox}} \sqrt{\frac{D_{\text{Ox}}}{\pi \cdot \frac{1}{2} t_p}} \sum_{j=1}^m \frac{Q_{m-1} - Q_m}{\sqrt{m - j + 1}} \quad (5.52)$$

$$\text{with } Q_m = \frac{\epsilon_m}{1 + \epsilon_m} \quad (5.53)$$

$$\text{and } \epsilon_m = \exp \left\{ \frac{n \cdot F \cdot (E_m - E_{1/2})}{R_g \cdot T} \right\} \quad (5.54)$$

$E_m$  is given in equation 5.50.  $\delta i$  can be calculated by subtracting  $i_{m=\text{odd}}$  from the preceding  $i_{m-1}$ . In the  $\delta i$ -curve a peak appears at  $E_{1/2}$ ; the height of this current peak is given by [6]:

$$\delta i_{\text{max}} = \frac{0.3 \cdot n^2 \cdot F^2 \cdot A \cdot C_{\text{Ox}} \cdot \Delta E_p}{R_g \cdot T} \sqrt{\frac{D_{\text{Ox}}}{\pi \cdot \frac{1}{2} t_p}} \quad (5.55)$$

A computer program has been written to solve equation 5.52. By comparing the recorded voltammograms with the theoretical curves a more exact value for  $E_{1/2}$  can be found, and also some other valuable data can be derived from it.

For reactions that are quasi-reversible, or reactions that are preceded or followed by relatively slow chemical processes (e.g. adsorption/desorption), the theoretical currents can also be calculated [21]. The equations describing the currents for quasi-reversible reactions are very complicated and will not be discussed in this thesis. A commercially available computer program (COOL from EG&G) has also been used in this study to compare recorded voltammograms with theoretical voltammograms for reactions that are not strictly reversible.

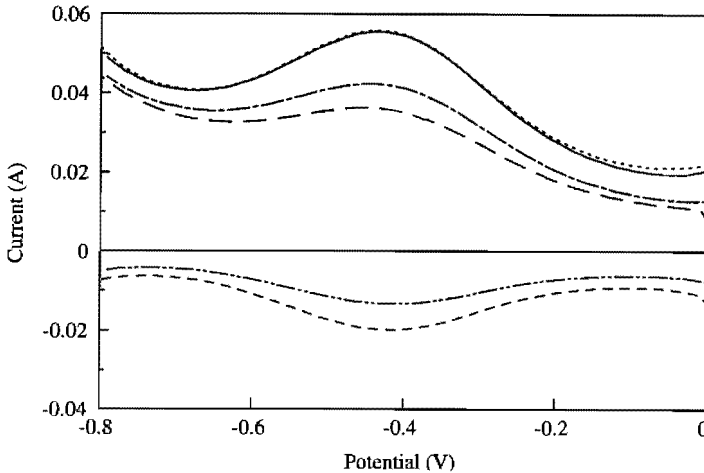


Figure 5.11 The  $i_f$ ,  $i_r$  and  $\delta i$  curves of a square wave voltammogram recorded in a TV-screen glass containing 0.4 weight-%  $Fe_2O_3$  at  $1400^\circ C$ , compared to a theoretically derived voltammogram

Recorded voltammogram		Theoretically derived voltammogram	
$i_f$	— — — — —	$i_f$	— — — — —
$i_r$	— — — — —	$i_r$	— — — — —
$\delta i$	— — — — —	$\delta i$	— — — — —
$E_i$	= 0 V	$E_i$	= 0 V
$E_{end}$	= -0.8 V	$E_{end}$	= -0.8 V
$\Delta E_b$	= 0.002 V	$\Delta E_b$	= 0.002 V
$\Delta E_p$	= 0.1 V	$\Delta E_p$	= 0.1 V
$f$	= 100 Hz	$n$	= 2
$R_u$	= 0 V	$E_{1/2}$	= -0.440 V
		$nFAc_{Ox}\sqrt{D_{Ox}}/(\pi^{1/2}t_p)^{1/2}$	= 0.675

**5.5.6 Real voltammograms**

**5.5.6.1 The influence of electrode geometry on  $i_f$ ,  $i_r$  and  $\delta i$**

The working electrode that has been used in the square wave voltammetry measurements mentioned in this thesis is not a planar plate. Therefore the shapes of  $i_f$  and  $i_r$  may differ slightly from the theoretical curves. However the influence of the shape of the working electrode on  $\delta i$  is much smaller [22]. Therefore mainly the  $\delta i$ 's of the recorded voltammograms are used for comparison with theoretical curves.

Figure 5.11 shows a recorded and a theoretical square wave voltammogram.

**5.5.6.2 Charging currents**

In real square wave voltammetric measurements a charging current flows. If the potential program is the same, the charging currents are probably the same for a glass containing a polyvalent element and for the same glass without polyvalent elements. The voltammogram of the latter glass (blank) can be subtracted from

the voltammogram recorded in the glass with the polyvalent element in order to minimize the contribution of the charging current to the voltammogram.

If no blank voltammogram is available, the charging current is assumed to be a linear function of the applied potential. A straight line is subtracted from the recorded voltammogram in such a way, that the resulting voltammogram gives the best fit with the theoretical curve. This simplification of the contribution of the charging current is strictly speaking incorrect, since the charging current is not exactly a linear function of the applied potential [3].

### 5.5.6.3 Background currents

The potential range that can be scanned using square wave voltammetry has an anodic and a cathodic limit. At positive potentials with regard to the reference electrode a large current flows. According to Rüssel [5] this current is caused by the dissolution of the platinum working electrode. Claes [23] assumes that the current arises due to the evolution of oxygen by oxidation of silicate ions. For reasons that will be discussed later on in section 5.5.11, the second explanation appears to be more probable. At potentials less than -0.8 V, the current increases due to a reduction of the silicon ions to elementary silicium [5], the formation of a silicon-platinum alloy [5,23] or the formation of a sodium-platinum alloy [24].

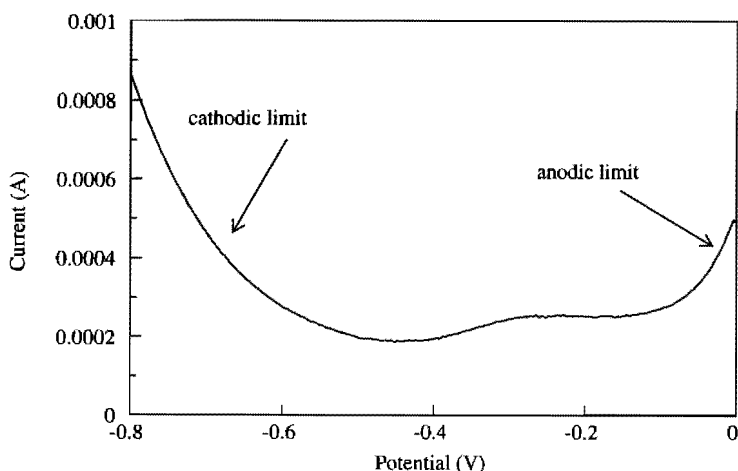


Figure 5.12

A square wave voltammogram recorded in a soda-lime-silica glass without polyvalent elements at 1000°C

$$\begin{array}{llll}
 E_i = 0 \text{ V} & \Delta E_b = 0.002 \text{ V} & f = 100 \text{ Hz} & R_u = 10.70 \text{ } \Omega \\
 E_{\text{end}} = -0.8 \text{ V} & \Delta E_p = 0.1 \text{ V} & & 
 \end{array}$$

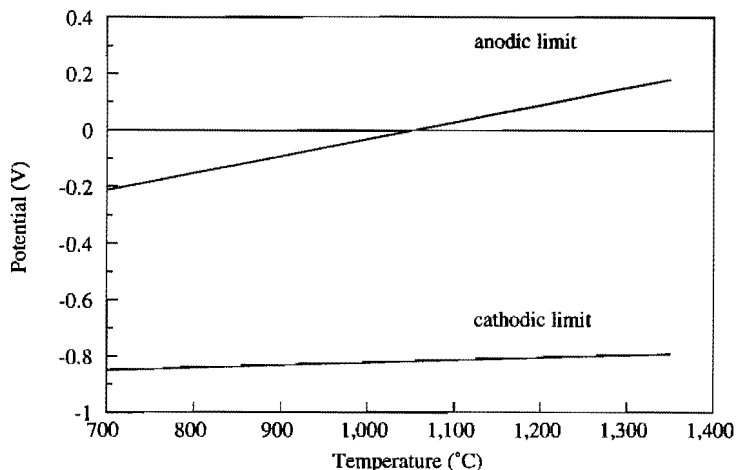


Figure 5.13

The potential limits for square wave voltammetry measurements in soda-lime-silica glass

Figure 5.12 shows the voltammogram recorded in a soda-lime-silica melt without polyvalent elements at 1000°C. The anodic and cathodic limits are clearly visible.

The potential range that can be used for the measurements depends on the temperature and the nature of the glass. As an example, the potential limits for soda-lime-silica glass are given in figure 5.13.

#### 5.5.6.4 Overlapping peaks

If the glass melt contains more than one polyvalent element, more peaks may be present in the square wave voltammograms. The peaks can be separated from each other, even if they are positioned at about the same potential, by comparing the recorded voltammograms with theoretically derived voltammograms. These can be calculated by simply adding two theoretically derived voltammograms, as long as the reactions are independent.

Some polyvalent elements can undergo two or more reduction reactions with formal potentials in the workable potential range. If these peaks are overlapping, peak splitting is very difficult because the reactions are not independent: the concentration of the "oxidized" form for the second reaction depends on the progress of the first reaction. Theoretical voltammograms can then not be added simply. Usually the position of the peaks can be estimated from the recorded

voltammograms if the peaks are not too close, but other data on the reaction mechanism can not be obtained.

In some cases, the peak of the redox reaction of the polyvalent element in the glass melt is located closely to the potential limit. A blank voltammogram (recorded under the same conditions in a glass melt without the polyvalent element) must be subtracted from the recorded voltammogram in order to separate the peak of the reaction of interest from the peak due to the reduction of the glass matrix or the evolution of oxygen gas.

If no blank voltammogram is available, the current at the anodic or cathodic potential limit is regarded as the reaction current, originating from a reversible redox reaction. The peak from the reaction with the polyvalent element can then be separated from its background by comparing the recorded voltammogram with two added theoretical voltammograms. This is demonstrated in figures 5.14-5.17.

In figure 5.14, the square wave voltammogram recorded in a soda-lime-silica glass containing 0.4 weight-%  $\text{CrO}_3$  at  $1250^\circ\text{C}$  is given. A shoulder is visible at about  $-0.65\text{ V}$ . This shoulder is probably due to the reduction of  $\text{Cr}^{3+}$  to  $\text{Cr}^{2+}$  (see chapter 6.5). The half-wave potential of this reduction can not be determined accurately from this voltammogram.

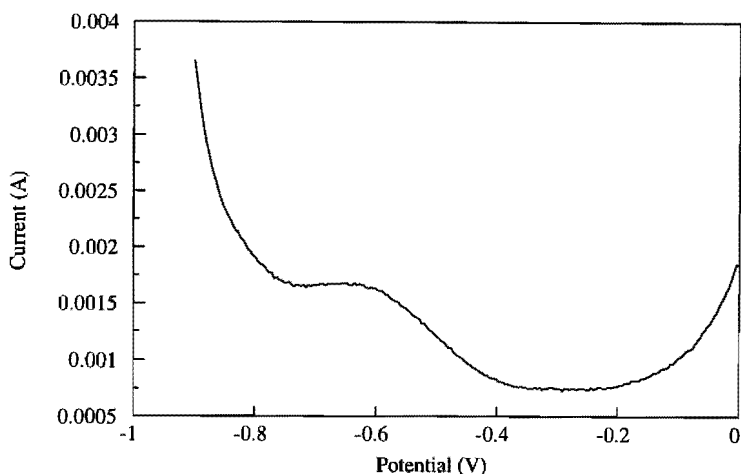


Figure 5.14

Square wave voltammogram recorded in a soda-lime-silica glass containing 0.4 weight-%  $\text{CrO}_3$  at  $1250^\circ\text{C}$

$$E_i = 0\text{ V}$$

$$\Delta E_b = 0.002\text{ V}$$

$$f = 100\text{ Hz}$$

$$R_u = 36.8\ \Omega$$

$$E_{\text{end}} = -0.9\text{ V}$$

$$\Delta E_p = 0.1\text{ V}$$

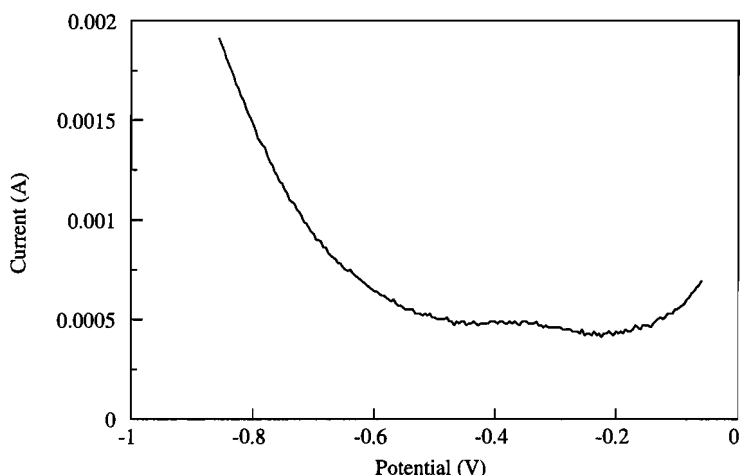


Figure 5.15  
Square wave voltammogram recorded in a soda-lime-silica glass without any polyvalent elements at 1250°C

$E_i = -0.05 \text{ V}$        $\Delta E_b = 0.002 \text{ V}$        $f = 100 \text{ Hz}$        $R_u = 0 \text{ V}$   
 $E_{\text{end}} = -0.85 \text{ V}$        $\Delta E_p = 0.1 \text{ V}$

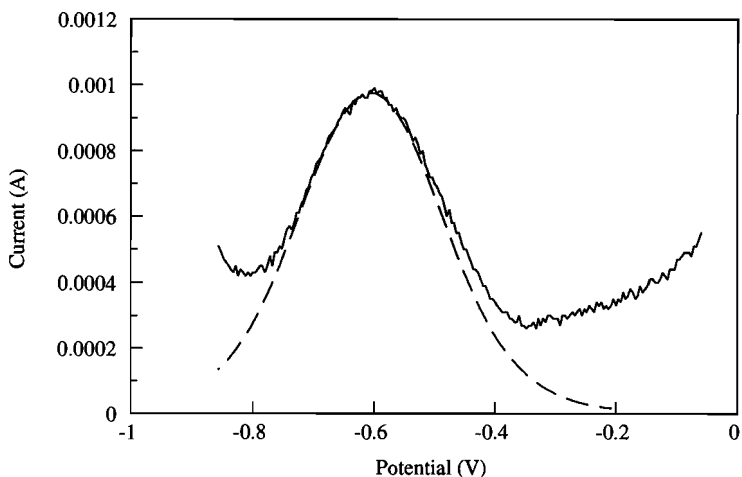


Figure 5.16  
Square wave voltammogram resulting from the subtraction of the blank from the voltammogram recorded in a soda-lime-silica glass containing 0.4 weight-%  $\text{CrO}_3$  at 1250°C. The theoretical curve for a redox reaction with a formal potential of -0.610 V is also reproduced

Measured curve	-----	Theoretically derived curve	- - - - -
$E_i = -0.05 \text{ V}$	$f = 100 \text{ Hz}$	$E_i = -0.2 \text{ V}$	$n = 2$
$E_{\text{end}} = -0.85 \text{ V}$	$R_u = 36.8 \Omega$	$E_{\text{end}} = -0.85 \text{ V}$	$E_{1/2} = -0.610 \text{ V}$
$\Delta E_b = 0.002 \text{ V}$		$\Delta E_b = 0.002 \text{ V}$	$nFAC_{\text{Ox}}\sqrt{D_{\text{Ox}}}/(\pi^{1/2}t_p) =$
$\Delta E_p = 0.1 \text{ V}$		$\Delta E_p = 0.1 \text{ V}$	0.00126



Figure 5.15 displays the square wave voltammogram of soda-lime-silica glass without polyvalent elements under the same conditions (blank). In figure 5.16, the blank is subtracted from the square wave voltammogram recorded in the glass melt containing chromium. This results in a voltammogram with a clearly visible peak at  $-0.610$  V. The theoretical curve calculated from equation 5.52 is also represented in figure 5.16. The electrode configuration during the measurements in the glass with and the glass without chromium have been slightly different. Therefore some residual background current still remains in the resulting voltammogram of figure 5.16; the "measured" voltammogram deviates from the theoretical curve.

If the blank had not been available, the position of the shoulder in figure 5.14 could have been determined by comparing the recorded voltammogram with the theoretical curves of two independent redox reactions (one for the reduction reaction of the glass matrix). This is done with the aid of the COOL program. The description of this program is beyond the scope of this thesis.

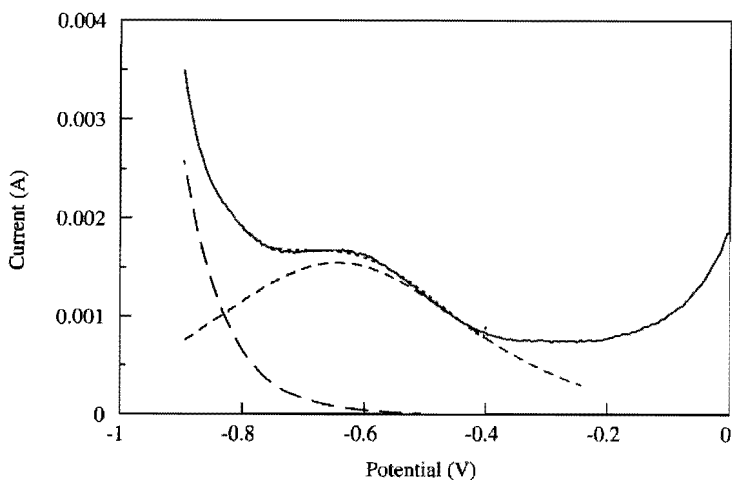


Figure 5.17

Square wave voltammogram recorded in a soda-lime-silica glass containing 0.4 weight-%  $\text{CrO}_3$  at  $1250^\circ\text{C}$ , compared with the curve obtained by adding two theoretical curves

Measured curve

$E_i = 0$  V  
 $E_{\text{end}} = -0.9$  V  
 $\Delta E_b = 0.002$  V  
 $\Delta E_p = 0.1$  V  
 $f = 100$  Hz  
 $R_u = 36.8$  V

Theoretically derived curves (added : - - - - -)

$E_i = -0.25$  V =  $-0.5$  V  
 $E_{\text{end}} = -0.9$  V =  $-0.9$  V  
 $\Delta E_b = 0.002$  V =  $0.002$  V  
 $\Delta E_p = 0.1$  V =  $0.1$  V  
 $n = 1$  =  $2$   
 $E_{1/2} = -0.620$  V =  $-1.114$  V  
 $n \cdot F \cdot A \cdot C_{\text{Ox}} \cdot \sqrt{D_{\text{Ox}}} / (\pi \cdot \frac{1}{2} t_p) = 0.0035$  =  $0.013$

The best fit was obtained when the half-wave potential of the chromium reduction was located at  $-0.620$  V, and the reduction of the glassmatrix at  $-1.144$  V (see figure 5.17).

### 5.5.7 Data derived from square wave voltammograms

#### 5.5.7.1 Diffusion coefficients of oxidized and reduced species

The height of the peak in the  $\delta$ -curve is proportional to the surface area of the working electrode, the concentration of the redox active species and the amount of electrons transferred, and to the square root of the diffusion coefficient (see equation 5.55). The value of one of these quantities can be calculated from the peak height if all others are known. However, as we have seen in section 5.3.5 the surface area of the working electrode is generally not known exactly.

Note: the diffusion coefficient mentioned is that of the oxidized polyvalent element, because the polyvalent element is assumed to be completely in the oxidized state at the initial potential  $E_i$ .

For a known surface area of the working electrode, the diffusion coefficient of the reduced form of the polyvalent element can be determined by scanning the potential range in the reverse direction. Before the beginning of the measurement the working electrode is held for some time (at least 15 s) at a potential at which the redox active species is stable in the reduced form. After this waiting time, the polyvalent element is almost entirely present in the reduced state at the working electrode and its environment. Then a square wave voltammogram is recorded while the potential varies from the very negative value to 0 V. Now, only diffusion of the reduced polyvalent element from the surroundings of the working electrode to its surface is of importance for the magnitude of the resulting current. The subscript Ox in equation 5.52 and 5.55 can be replaced by Red. The height of the peak in the voltammogram is proportional to the square root of the diffusion coefficient of the reduced species. By comparing the voltammograms recorded in both scan directions,  $D_{\text{Red}}/D_{\text{Ox}}$  can be calculated even if the concentrations of the reacting species and the surface area of the working electrode are unknown.

The diffusion coefficients of  $\text{Fe}^{3+}$  and  $\text{Fe}^{2+}$  in the investigated molten glasses are about the same, as will be seen in chapter 6.2. This seems also to be the case with the diffusion coefficients of  $\text{Sb}^{5+}$ ,  $\text{Sb}^{3+}$  and  $\text{Sb}^0$  (chapter 6.3), and of  $\text{Cr}^{6+}$  and  $\text{Cr}^{3+}$  (chapter 6.5).

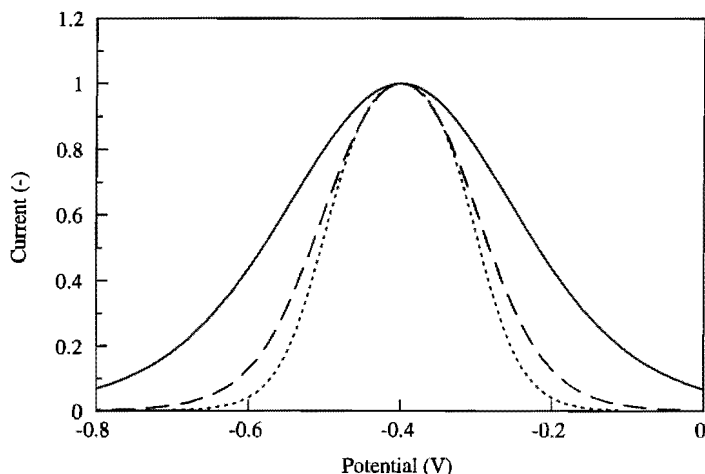


Figure 5.18

Theoretical square wave voltammograms for 1, 2 and 3-electron transfer reactions at a half-wave potential of -0.4 V, at 800°C

n = 1	n = 2	n = 3
$E_i = 0 \text{ V}$	$\Delta E_b = 0.002 \text{ V}$	$E_{1/2} = -0.4 \text{ V}$
$E_{\text{end}} = -0.8 \text{ V}$	$\Delta E_p = 0.1 \text{ V}$	$n \cdot F \cdot A \cdot C_{\text{Ox}} \cdot \sqrt{D_{\text{Ox}}} / (\pi \cdot \frac{1}{2} t_p) = 1$

### 5.5.7.2 The amount of electrons transferred

The shape of the curve depends on the amount of electrons transferred during the reduction of one molecule of reactant. If only one electron is transferred the peak is broad, more-electron reactions give rise to small peaks. Theoretical peaks for a 1, 2 and 3-electron transfer at 800°C are given in figure 5.18.

The width of the peak is also effected by the temperature. At higher temperatures, the  $\delta_i$  curves become broad. In figure 5.19, the theoretical voltammograms of a 2-electron transfer at 800 and at 1400°C are given.

The number of electrons that is transferred during the reduction of one mole of reactant can be derived by comparing the recorded square wave voltammogram with theoretical curves.

### 5.5.7.3 Reversibility of the redox reaction

The frequency of the applied potential (or the pulse time  $t_p$ ) should have no effect on the position of the peak for purely reversible reactions. However if the frequency is very high, the redox reactions appear to be quasi-reversible.

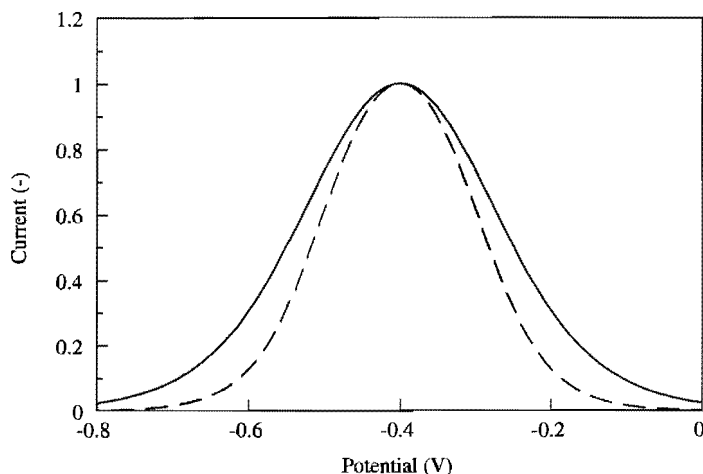


Figure 5.19

The theoretical voltammograms of a 2-electron transfer at 800 (---) and at 1400°C (—)

$$E_i = 0 \text{ V}$$

$$E_{\text{end}} = -0.8 \text{ V}$$

$$\Delta E_b = 0.002 \text{ V}$$

$$\Delta E_p = 0.1 \text{ V}$$

$$E_{1/2} = -0.4 \text{ V}$$

$$n \cdot F \cdot A \cdot C_{\text{Ox}} \cdot \sqrt{D_{\text{Ox}}} / (\pi \cdot \gamma \cdot t_p) = 1$$

Then the potential changes fast relative to the time needed to establish the equilibrium at the working electrode as given by equation 5.9. The base potential at which the concentration of the oxidized polyvalent element becomes almost zero depends on the frequency. The position of the peaks then do depend on the frequency: at high frequencies, the peaks shift towards the more negative potentials. Besides, the peaks are no longer symmetrical. In this case, the shape of the peak can give information on the reaction rates.

The frequency for the measurements mentioned in this thesis has been chosen as low as possible to make sure the occurring redox reactions are reversible. (The contribution of the charging current is then also smaller than at high frequencies) But the height of the peak also depends on the frequency: it is linear to the square root of the frequency (see equation 5.55). When the frequency is set to a very low value, the peak in the voltammogram may become too low to determine the exact position, especially if the concentration of the redox active species is low. Besides, the furnace has to be switched off during the measurement in order to avoid disturbance of the measuring signal by currents in the heating elements. If the frequency is low, the measurement lasts long and the temperature of the glass melt may drop considerably. Therefore the frequency is set to a value between 10

and 200 Hz. The voltammograms mentioned in this thesis are all checked on reversibility of the reactions by comparing the recorded voltammograms with theoretical voltammograms (derived from own calculations or the commercially available COOL program as mentioned in section 5.5.5).

According to Claes [25], the charging current has a large influence on the square wave voltammograms at frequencies more than 12.5 Hz, and this obstructs the accurate determination of the formal potential from voltammograms. This is in contradiction to the results obtained in the investigations of this thesis: the shape and position of the peaks did not vary much whether the blanks were subtracted from the recorded voltammograms in glasses containing polyvalent elements or not.

#### 5.5.7.4 The formal potential

The peaks are located at the half-wave potential of the redox reaction of the polyvalent element with regard to the potential of the reference electrode (if the redox reaction is reversible).

If the ratio  $D_{\text{Red}}/D_{\text{Ox}}$  is known the formal potential of the redox reaction can be calculated using equation 5.16.

#### 5.5.8 Calculation of the redox reaction equilibrium constant $K^{**}(\text{T})$

In equation 3.9, the redox reaction equilibrium constant  $K^{**}(\text{T})$  has been defined as:

$$K^{**}(\text{T}) = \frac{[\text{M}^{x+}] \cdot p_{\text{O}_2}^{n/4}(\text{melt})}{[\text{M}^{(x+n)+}]} \quad (5.56)$$

This equilibrium constant can be directly related to the formal potential  $E^0$  of the redox reaction.

From the square wave voltammograms the formal potential of the redox reaction at the working electrode with regard to the potential of the reference electrode can be found.

The potential of the reference electrode is given by:

$$E_{\text{reference}} = E_{\text{O}_2/\text{O}^{2-}}^0 + \frac{R_g \cdot T}{4 \cdot F} \ln \frac{p_{\text{O}_2}(\text{reference gas})}{(a_{\text{O}^{2-}})^2} \quad (5.57)$$

The activity of the free oxygen ion  $O^{2-}$  at the reference electrode is assumed to be at unity (just as its activity in the molten glass, see section 5.4.3). Then the potential of the reference electrode is:

$$E_{\text{reference}} = E_{O_2/O^{2-}}^0 + \frac{R_g \cdot T}{4 \cdot F} \ln p_{O_2}(\text{reference gas}) \quad (5.58)$$

In square wave voltammograms, a peak occurs at the half-wave potential of the reaction at the working electrode, relative to the potential of the reference electrode. The potential of this half-cell is given by:

$$E_{\text{working electrode}} = E_{M^{(x+n)^+}/M^{x+}}^0 + \frac{R_g \cdot T}{n \cdot F} \ln \frac{[M^{(x+n)^+}]}{[M^{x+}]} \quad (5.59)$$

For any potential  $E$ , the following equation is valid:

$$E = E_{\text{working electrode}} - E_{\text{reference}} \quad (5.60)$$

and thus:

$$E = E_{M^{(x+n)^+}/M^{x+}}^{0'} + \frac{R_g \cdot T}{n \cdot F} \ln \frac{[M^{(x+n)^+}]}{[M^{x+}]} - E_{O_2/O^{2-}}^{0'} - \frac{R_g \cdot T}{4 \cdot F} \ln p_{O_2}(\text{ref}) \quad (5.61)$$

or

$$E = E^{0'} + \frac{R_g \cdot T}{n \cdot F} \ln \frac{[M^{(x+n)^+}]}{[M^{x+}] \cdot p_{O_2}^{n/4}(\text{reference gas})} \quad (5.62)$$

with

$$E^{0'} = E_{M^{(x+n)^+}/M^{x+}}^{0'} - E_{O_2/O^{2-}}^{0'} = E_{M^{(x+n)^+}}^{0'} + \frac{n}{2} O^{2-}/M^{x+} + \frac{n}{4} O_2 \quad (5.63)$$

and  $E^{0'}$  is the position of the  $\delta$ -peak in the square wave voltammogram.

Before applying artificially a voltage difference, the potential difference  $\Delta E$  between working and reference electrode is governed by the oxygen equilibrium pressure in the melt  $p_{O_2}(\text{melt})$  close to the working electrode (see chapter 5.4):

$$\Delta E = \frac{R_g \cdot T}{4 \cdot F} \ln \frac{p_{O_2}(\text{melt})}{p_{O_2}(\text{reference gas})} \quad (5.64)$$

This potential difference  $\Delta E$  can be read from the measuring equipment before the beginning of the square wave voltammetry measurement.

Combination of equations 5.62 and 5.64 results in:

$$E^{0'} = \frac{R_g \cdot T}{n \cdot F} \ln \frac{[M^{x+}] \cdot p_{O_2}^{n/4}(\text{melt})}{[M^{(x+n)+}]} = \frac{R_g \cdot T}{n \cdot F} \ln K^{**}(T) \quad (5.65)$$

And so the redox reaction equilibrium constant  $K^{**}(T)$ , before the beginning of the square wave voltammetry measurement, can be derived from the peak position  $E^{0'}$  in the square wave voltammogram:

$$K^{**}(T) = \exp\left(\frac{n \cdot F \cdot E^{0'}}{R_g \cdot T}\right) \quad (5.66)$$

### 5.5.9 Calculation of the redox ratio

The oxygen pressure in the melt, close to the working electrode, is given by:

$$p_{O_2}(\text{melt}) = p_{O_2}(\text{reference gas}) \cdot \exp\left(\frac{4 \cdot F \cdot \Delta E}{R_g \cdot T}\right) \quad (5.67)$$

The potential difference between working and reference electrode,  $\Delta E$ , can be read from the measuring equipment before running a square wave voltammetry measurement.

The redox ratio  $[M^{x+}]/[M^{(x+n)+}]$  in the glass melt close to the working electrode is:

$$\frac{[M^{x+}]}{[M^{(x+n)+}]} = \frac{1}{p_{O_2}(\text{ref})} \cdot \exp\left\{\frac{n \cdot F \cdot \left(E^{0'} - \frac{4}{n} \Delta E\right)}{R_g \cdot T}\right\} \quad (5.68)$$

### 5.5.10 Calculation of the redox reaction enthalpy and entropy changes

The formal potential of the redox reaction  $E^{0'}$  can be measured using square wave voltammetry at a variety of temperatures. The redox reaction equilibrium constant  $K^{**}(T)$  as defined in equation 5.56 can be calculated for any temperature using equation 5.66. From the temperature dependency of  $K^{**}(T)$ , the redox reaction enthalpy and entropy changes,  $\Delta H^{**}$  and  $\Delta S^{**}$  can be calculated:

$$\Delta H^{**} = R_g \cdot \left(\frac{\delta \ln K^{**}(T)}{\delta T}\right) \quad (5.69)$$

$$\Delta S^{**} = R_g \cdot \left(\frac{1}{T} \cdot \frac{\delta \ln K^{**}(T)}{\delta T} + \ln K^{**}(T)\right) \quad (5.70)$$

### **5.5.11 Limitations of the application of square wave voltammetry in molten glass**

#### **5.5.11.1 Large uncompensated resistance**

If the uncompensated resistance in the molten glass is large (more than 100  $\Omega$ ), the voltammograms are erroneous even if the  $i\text{-}R_u$  compensation technique is used. The resistivity of a glass melt increases as the temperature decreases. Therefore square wave voltammetric measurements can not be performed in glass melts below a certain temperature limit. In the electrode configuration used for the measurements mentioned in this thesis, the temperature limit is about 700°C for soda-lime-silica and TV-screen glass melts, and about 1000°C for E-glass.

#### **5.5.11.2 Workable potential region**

If the half-wave potential of the redox reaction of a polyvalent element is outside the potential ranges as sketched in figure 5.13, it is not possible to investigate this reaction with square wave voltammetry as discussed in this chapter. However, if the anodic limit is due to the oxidation of the platinum working electrode, the potential range could perhaps be expanded in the anodic direction by applying another electrode material. Therefore platinum and some other materials have been tested as working electrodes.

#### **5.5.11.3 Attempts to find an electrode material, suitable for measurements in the positive potential region**

Various electric conductive materials have been tested by Miura and Takahashi [24]. The materials platinum, tungsten, iron, molybdenum, cobalt, nickel, chromium, graphite and stannic oxide were used as working electrodes in  $\text{Na}_2\text{O}\cdot 2\text{B}_2\text{O}_3$  and lead glass at 900°C. The potential of the working electrodes was increased in cathodic or in anodic direction with 0.001 to 5  $\text{V}\cdot\text{s}^{-1}$  to a value of -5 or 5 V (Linear Sweep Voltammetry). Platinum was found to have a wider cathodic scan range than any other material. A sodium platinum alloy was found when the potential of the working electrode had been less than -0.1 V. In the anodic direction, platinum also gave good results but a current arose due to the formation of a platinum oxide film. In the voltammogram a peak appeared at 1 V, followed by a long plateau.

Platinum was excelled in the positive potential region only by stannic oxide. However, some current was measured due to the evolution of oxygen gas in case stannic oxide was used as working electrode. In the molten glass many bubbles appeared.



Because of the results of Miura, stannic oxide was chosen as an alternative working electrode in soda-lime-silica glass at 1400°C. Furthermore the behaviour of Pt, TiB and ZrO<sub>2</sub> has been tested. The potential of the working electrode was increased linearly as a function of time with a sweep rate of 1 V·s<sup>-1</sup> from 0 to -0.5 V while the current was sampled. In figure 5.20 the voltammograms of these experiments are reproduced. Then the potential was hold at 1 V for 1 hour. Afterwards the electrodes were investigated using Scanning Electron Microscopy.

The TiB electrode was attacked by the melt and caused a blue colour.

In case platinum, SnO<sub>2</sub> or ZrO<sub>2</sub> had been used a large current was measured at positive potentials, with a peak in the voltammogram somewhere between +0.2 and +0.6 V, depending on the applied sweep rate. The visual and analytical examination of the electrodes showed no corrosion of the SnO<sub>2</sub> or ZrO<sub>2</sub> electrodes.

The structure of the outer layer of the platinum electrode was somewhat different from the structure within the electrode. This layer is probably built up of oxidized platinum.

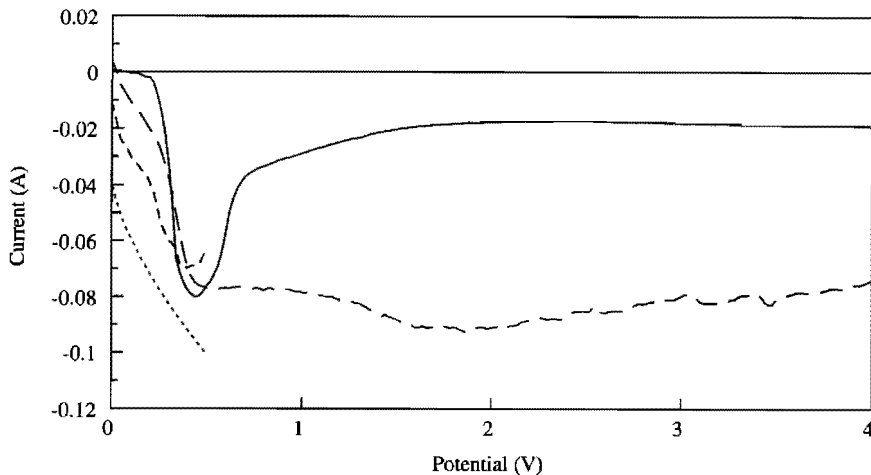


Figure 5.20

The linear sweep voltammograms of various working electrodes in soda-lime-silica glass without polyvalent elements at 1400°C

Pt	—————	ZrO <sub>2</sub>	-----
SnO <sub>2</sub>	- - - - -	TiB	.....
E <sub>i</sub>	= 0 V	scan rate	= 1 V·s <sup>-1</sup>
E <sub>end</sub>	= -0.5 or -4.0 V	scan increment	= 2 mV

The results indicate that the anodic limit is not solely due to the oxidation of platinum but at any rate partly to an irreversible reaction in the electrolyte, like the formation of gaseous oxygen. This means that the potential range that can be scanned with square wave voltammetry can not be expanded into the positive region.

#### 5.5.11.4 Consequences of the limited potential range for the investigations of the polyvalent elements

As we have seen in chapter 2, good fining agents give rise to the evolution of oxygen gas at a the melting temperature of the glass. The redox reaction equilibrium as defined in equation 5.36 then changes from a very low to a very high value at a relatively small increase of temperature.

At relatively low temperatures (800-1000°C) the polyvalent fining agent is predominantly present in the oxidized state. Then a peak is visible in the square wave voltammogram. At a small increase in temperature, the fining agent decomposes and oxygen gas is released. The polyvalent element is now mainly in its reduced state. The peaks in the square wave voltammograms have shifted into the positive potential region and can no longer be observed.

The redox reactions of some polyvalent elements can only be investigated with square wave voltammetry at relatively low temperatures. This is for instance the case with the  $\text{Sb}^{5+}/\text{Sb}^{3+}$  and the  $\text{Cr}^{6+}/\text{Cr}^{3+}$  reactions (see chapter 6.3 and 6.5). The behaviour of polyvalent elements that are already in the reduced form at temperatures above 700°C, like cerium, can not be investigated at all with this method (chapter 6.4). Only the elements that are predominantly in the oxidized state can give rise to a peak in square wave voltammograms. Good results have therefore been obtained for the  $\text{Fe}^{3+}/\text{Fe}^{2+}$  (chapter 6.2),  $\text{Sb}^{3+}/\text{Sb}^0$  (chapter 6.3) and  $\text{Cr}^{3+}/\text{Cr}^{2+}$  (chapter 6.5) reactions.

Literature

- [1] Bard, A.J.; Faulkner, L.R.  
Electrochemical methods: fundamentals and applications  
John Wiley & Sons New York Chichester Brisbane Toronto (1980)
- [2] Barendrecht, E.  
Elektrochemie  
Ditaaat Technische Universiteit Eindhoven (1986)
- [3] Moortgat-Hasthorpe; Vander Poorten, H.; Blave, A.  
Polarographie DC et AC en milieu silicate fondu  
*Silicates Industriels* **41** (1976) no.11 p.463-467
- [4] Simonis, F. (editor)  
"NCNG-Glascursus"  
TPD-TNO in samenwerking met de gezamenlijke Nederlandse Glasindustrieën (1990)
- [5] Rüssel, C.; Freude, E.  
Voltammetric studies of the redox behaviour of various multivalent ions in soda-lime-silica glass melts  
*Physics and Chemistry of Glasses* **30** (1989) no.2 p.62-68
- [6] Freude, E.  
Voltammetrische Untersuchung des Redoxverhaltens polyvalenter Ionen in Glasschmelzen, insbesondere von Technetium  
Thesis Erlangen (1989)
- [7] Baucke, F.G.K.  
Development of electrochemical cells employing oxide ceramics for measuring oxygen partial pressures in laboratory and technical glass melts  
*Glastechnische Berichte* **56K** (1983) p.307-312
- [8] Baucke, F.G.K.; Mücke, K.  
Measurements of standard Seebeck coefficients in non-isothermal glass melts by means of  $ZrO_2$  electrodes  
*Journal of Non-Crystalline Solids* **84** (1986) p.174-182
- [9] Tran, T.; Brungs, M.D.  
Application of oxygen electrodes in glass melts. Part I. Oxygen reference electrode  
*Physics and Chemistry of Glasses* **21** (1980) no.4 p.133-140
- [10] Frey, T.; Schaeffer, H.A.; Baucke, F.G.K.  
Entwicklung einer Sonde zur Messung des Sauerstoffpartialdrucks in Glasschmelzen  
*Glastechnische Berichte* **53** (1980) no.5 p.116-123
- [11] Müller-Simon, H.  
Die elektrochemische Sauerstoffaktivitätsmessung in industriellen Glasschmelzanlagen  
Thesis Berlin (1992)
- [12] Paul, A.; Douglas, R.W.  
Ferrous-ferric equilibrium in binary alkali-silicate glasses  
*Physics and Chemistry of Glasses* **6** (1965) no.6 p.207-211

- [13] Lenhart, A.; Schaeffer, H.A.  
Elektrochemische Messung der Sauerstoffaktivität in Glasschmelzen  
*Glastechnische Berichte* **58** (1985) no.6 p.139-147
- [14] Tran, T.; Brungs, M.D.  
Application of oxygen electrodes in glass melts. Part II. Oxygen probes for the measurement of oxygen potential in sodium disilicate glass  
*Physics and Chemistry of Glasses* **21** (1980) no.5 p.178-183
- [15] Sasabe, M.; Goto, K.S.  
Permeability, diffusivity and solubility of oxygen gas in liquid slag  
*Metallurgical Transactions* **5** (1974) p.2225-2233
- [16] Schreiber, H.D. et.al  
Solubility and diffusion of gases in a reference borosilicate melt  
*Diffusion and Defect Data* **53-54** (1987) p.345-350
- [17] Beerkens, R.G.C.  
Chemical equilibrium reactions as driving forces for growth of gas bubbles during refining  
*Glastechnische Berichte* **63K** (1990) p.222-242
- [18] Beerkens, R.G.C.; Kersbergen, M. van  
Properties of gases and redox reactions in glassmelts  
Final report NCNG-NOVEM Fining and redox of glass  
T.N.O.-T.P.D. report juli (1994)
- [19] Barker, G.C.  
Square wave polarography and some related techniques  
*Analytica Chimica Acta* **18** (1958) p.118-131
- [20] Christie, J.H.; Turner, J.A.; Osteryoung, R.A.  
Square wave voltammetry at the dropping mercury electrode: theory  
*Analytical Chemistry* **49** (1977) no. 13 p.1899-1903
- [21] O'Dea, J.J.; Wikiel, K.; Osteryoung, J.J.  
Square wave voltammetry for ECE mechanisms  
*Journal of Physics and Chemistry* **94** (1990) p.3628-3636
- [22] Osteryoung, J.G.; Osteryoung, R.A.  
Square wave voltammetry  
*Analytical Chemistry* **57** (1985) no.1 p.101A-110A
- [23] Claes, P.; Tilquin, J.Y.; Glibert, J.  
Electrochemical behaviour of the Ni(II) ion in soda-lime-silica melts  
*Bulletin des Societes Chimiques Belges* **97** (1988) no.11/12 p.1101-1112
- [24] Miura, Y.; Takahashi, K.  
Various electric conductive materials  
*Journal of Non-Crystalline Solids* **38-39** (1980) p.347-352
- [25] Claes, P.; Tilquin, J.-Y.; Duveiller, Ph.; Glibert, J.  
Electrochemical investigation of multivalent elements in molten silicates at 1273 K  
Proceedings of the XVI International Congress on Glass Madrid (1992) **6** p.247-252

## Chapter 6

### Results

#### 6.1 INTRODUCTION

The redox reaction equilibria of iron, antimony, cerium, chromium and sulphur in three commercially available glasses have been studied using oxygen equilibrium pressure measurements and square wave voltammetry measurements. From these measurements the redox reaction equilibrium constant  $K^{**}(T)$  has been calculated. This glass composition dependent constant is defined in chapter 4 as:

$$K^{**}(T) = \frac{[M^{x+}] \cdot p_{O_2}^{n/4}}{[M^{(x+n)+}]} \quad (6.1)$$

with  $p_{O_2}$  = the oxygen equilibrium pressure, this is the partial oxygen pressure in the atmosphere with which the glass melt would be in equilibrium, given in bar (see chapter 5.4.1).

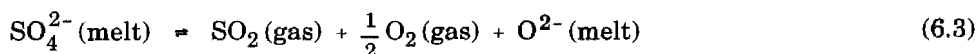
The results of the measurements at different temperatures will be expressed in the redox reaction enthalpy  $\Delta H^{**}$  and entropy  $\Delta S^{**}$  (see chapter 3.2.2):

$$\ln K^{**}(T) = \frac{-\Delta H^{**}}{R_g \cdot T} + \frac{\Delta S^{**}}{R_g} \quad (6.2)$$

Experimental results on the redox reaction equilibrium constants of the polyvalent elements have been obtained in three types of glasses: soda-lime-silica glass, TV-screen glass and E-glass.

Soda-lime-silica glass, as used in the experiments, has the molar composition 75 SiO<sub>2</sub>-15 Na<sub>2</sub>O- 10 CaO. The basicity number of this glass, as defined by Sun [1], is 33.3. The composition and basicity number of this soda-lime-silica glass strongly resemble those of the standard soda-lime-silica glass that has been used in a number of experimental studies [2,3,4,5,6], and some commercially available glasses like float glass, white container glass and table ware glass [7].

Soda-lime-silica glasses are usually fined with the aid of sulphate [7]. The redox reaction of sulphate under oxidizing conditions (as in the glasses mentioned) is generally described as:



Some attempts have been made to study the redox reaction equilibrium of this reaction with square wave voltammetry measurements (see chapter 6.6). Furthermore the behaviour of sulphate in this type of glass has been investigated with oxygen equilibrium pressure measurements in combination with the analysis of the sulphur content of the glass. The results are reported in section 6.6.

Green container glass has about the same bulk composition as white container glass [7]. The green colour is obtained by adding chromium ( $\text{Cr}_2\text{O}_3$ ) to the batch [7]. Chromium can be present in the melt as  $\text{Cr}^{6+}$ ,  $\text{Cr}^{3+}$  and  $\text{Cr}^{2+}$ . The redox reactions can be described as:



The behaviour of chromium in soda-lime-silica glass melts has been investigated using square wave voltammetry measurements (see section 6.5).

TV-screen glass compositions contain BaO and SrO, which are capable of absorbing X-ray radiation. In this thesis, two types of TV-screen glasses have been used for the determination of the redox reaction equilibrium constants: type A and type B. Type A contains a little more SrO and less BaO than type B. The basicity number of TV-screen glass type A, as defined by Sun, is 34, and that of type B is 36.

TV-screen glass is usually fined with antimony [7]. The antimony can be added in the pentavalent or in the trivalent form. In the second case an oxidizing agent like nitrate has to be added to the batch in order to oxidize the antimony during the heating of the batch. The fining action of antimony at elevated temperatures can be described as:



The equilibrium of this reaction has been investigated both by oxygen equilibrium pressure measurements and square wave voltammetry measurements. The results of both methods agree reasonably well as will be shown in section 6.3.

$\text{Sb}_2\text{O}_3$  is volatile and harmful. Fining with antimony may lead to environmental pollution. Therefore the possibility of (partly) replacing the fining agent antimony by some other polyvalent element has been investigated by some authors [3,8]. The most promising metal oxide was cerium oxide ( $\text{CeO}_2$ ). The fining reaction for this polyvalent element can be described by:



The equilibrium state of this reaction could not be studied with square wave voltammetry measurements (see section 6.4). Data on the reaction equilibrium constants have been derived from oxygen equilibrium pressure measurements in molten TV-screen glass in combination with wet-chemical analysis of the quenched glass samples at room temperature.

E-glass contains, besides  $\text{SiO}_2$ , mainly  $\text{CaO}$ ,  $\text{Al}_2\text{O}_3$  and  $\text{B}_2\text{O}_3$ . Hardly any alkali ions (like Na or K) are present [7]. The electrical conductivity of this type of glass is extremely low. E-glass is used for the production of textile fibres, as reinforcement fibres in polymers, and in printed circuitboards. The basicity number of this type of glass is about 37. For enhancement of the fining process, sulphate is added to the batch. Since the melting takes place under oxidizing conditions, the fining reaction can be described with equation 6.3. The equilibrium of this reaction has been studied using oxygen equilibrium pressure measurements (section 6.6).

E-glass also contains small amounts of chromium. In spite of the poor electrical conductivity of E-glass, square wave voltammetry could be used to study the equilibrium of reactions 6.4 in this glass. The results are reported in section 6.5.

The raw materials for the industrial glass making process always contain impurities, especially iron. Iron can be present in the glass as  $\text{Fe}^{3+}$  and as  $\text{Fe}^{2+}$ . The general equation of the redox reaction of iron is:



The divalent iron in the molten glass absorbs heat radiation and therefore influences the temperature distribution in the fossil fuel fired melting tank considerably [7]. Furthermore, divalent iron causes a (undesired) green colour in the final glass product. Besides, the iron redox reaction may interfere with

the redox reactions of the fining agents antimony and sulphate. Therefore the reaction equilibrium constant of reaction 6.7 has been investigated in soda-lime-silica, TV-screen and E-glass, using oxygen equilibrium pressure measurements and using square wave voltammetry (section 6.2). The agreement of the results, obtained by both methods, appears to be excellent for these glasses.

In the literature, some data on the redox ratios  $[\text{Fe}^{2+}]/[\text{Fe}^{3+}]$  [6,9,10,11],  $[\text{Sb}^{3+}]/[\text{Sb}^{5+}]$  [12,13,14],  $[\text{Ce}^{3+}]/[\text{Ce}^{4+}]$  [12,15],  $[\text{Cr}^{3+}]/[\text{Cr}^{6+}]$  [16] and  $p_{\text{SO}_2}/[\text{SO}_4^{2-}]$  [2,17,18,19], in various types of glasses have been published. Generally, the data have been derived by equilibrating a glass melt with a certain atmosphere (usually air), cooling quickly to room temperature and analysing the samples on the concentrations of reduced versus oxidized species. In this chapter, the data from the literature will be compared with the results presented in this thesis.

From the literature data [10,15] and the data, presented in this thesis, it is clear that the composition of the glass has a considerable effect on the redox reaction equilibrium constant. Some theories to account for this dependency have been discussed in chapter 3. The data, obtained in the present investigation, have been too few to support or reject the theories. Besides, the basicity numbers of soda-lime-silica, TV-screen and E-glass are relatively close. Yet, the difference in equilibrium constants of the iron reaction in these glasses indicate that the basicity number in itself gives insufficient information for the estimation of the equilibrium constant of the iron reaction on the basis of measurements in glasses with a different composition.

Furthermore, it will be shown that the total concentration of a polyvalent element can have a significant effect on the redox ratio. For example, the ratio  $[\text{Fe}^{2+}]/[\text{Fe}^{3+}]$  in soda-lime-silica glasses increases at decreasing total iron concentrations under otherwise equal conditions. This phenomenon has already been observed in alkali disilicate glasses [10]. However, the redox ratio  $[\text{Fe}^{2+}]/[\text{Fe}^{3+}]$  in TV-screen glasses decreases at decreasing total iron contents (see section 6.2.3.6). An explanation for this phenomenon might be found in the activity coefficients of the polyvalent elements, which may be dependent on the concentration and the glass composition.



## 6.2 IRON

### 6.2.1 Iron in glass

Generally iron is present as an impurity in some of the raw materials for the glass production, like sand (the main  $\text{SiO}_2$ -source). The concentrations of iron in the final glass products are usually low (in the range of 0.01 to 0.5 weight-% [7]). In the literature, many data on the iron redox reaction equilibrium have been published [6,9,10,11], but the iron concentrations in these investigations are generally in the order of some weight-%. From the paper of Paul [10], it is clear however that the total iron concentration has a significant effect on the ratio of divalent to trivalent iron (redox ratio) in binary alkali silicate glasses. The divalent form was favoured at low iron concentrations in these types of glass.

In this thesis, the redox reaction equilibria of iron in a wide range of concentrations in soda-lime-silica, TV-screen and E-glass have been measured and investigated. Most glasses were made from reagent grade oxides or carbonates ( $\text{SiO}_2$ ,  $\text{Na}_2\text{CO}_3$ ,  $\text{CaCO}_3$ ,  $\text{Al}_2\text{O}_3$  etc). To these glasses 0.1 to 2.5 weight-% reagent grade  $\text{Fe}_2\text{O}_3$  was added. In other glasses, industrial TV-screen batch materials were used. The total iron concentration in these glasses was about 0.04 weight-%.

### 6.2.2 Oxygen equilibrium pressure measurements

#### 6.2.2.1 Experimental procedure

The glasses containing iron were melted at  $1400^\circ\text{C}$  in platinum crucibles, until all grains were dissolved completely and the bubbles were nearly completely removed from the melt. Then the melt was quenched. The cullet was transferred to an  $\text{Al}_2\text{O}_3$ -crucible and placed in the furnace as sketched in figure 5.3. The glass was heated slowly to  $1400^\circ\text{C}$  again, and then the electrodes were dipped into the glass melt. The reference electrode was flushed with clean, dry air. The potential difference between the platinum plate and the reference electrode was measured continuously (electrodes 2 and 3 in figure 5.3).

As soon as the potential difference between the electrodes had reached a constant value, the temperature was lowered with a cooling rate of 3 to  $5^\circ\text{C}/\text{min}$  to  $1000^\circ\text{C}$ , while the potential difference was measured. Subsequently the temperature was increased again by 3 to  $5^\circ\text{C}/\text{min}$  to  $1400^\circ\text{C}$ . Generally, the potential difference between the electrodes followed the same course during

both scans, indicating that the redox reaction that accounts for the difference in potential is reversible, and indicating no losses of the reacting species.

### 6.2.2.2 Measured potential difference

An example of a measurement is given in figure 6.1. The potential difference between the platinum plate and the reference electrode is given as a function of increasing temperature for a TV-screen glass type A containing 0.4 weight-%  $\text{Fe}_2\text{O}_3$ . Notice that the curve follows roughly a straight line at temperatures below  $1200^\circ\text{C}$ . At higher temperatures, the curve becomes less steep and approaches a constant potential difference of about 55 mV, for reasons that will be explained later in this section.

The curves, measured in other glasses with about the same iron concentration, had about the same slope as the curve in figure 6.1, but the absolute voltage values could be very different.

### 6.2.2.3 Calculation of the oxygen equilibrium pressure

The oxygen equilibrium pressure in the melt,  $p_{\text{O}_2}(\text{melt})$ , can be calculated from the measured potential difference  $\Delta E$  by:

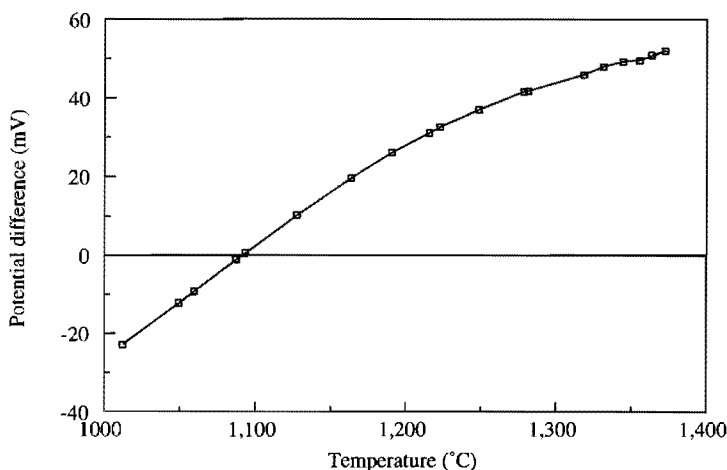


Figure 6.1

The measured potential difference between the platinum plate and the reference electrode in a TV-screen glass type A containing 0.4 weight-%  $\text{Fe}_2\text{O}_3$ , while the temperature was increased from 1000 up to  $1400^\circ\text{C}$  by  $3^\circ\text{C}/\text{min}$

$$p_{O_2}(\text{melt}) = 0.21 \cdot \exp\left(\frac{4 \cdot F \cdot \Delta E}{R_g \cdot T}\right) \quad (6.8)$$

with	$p_{O_2}(\text{melt})$	= oxygen equilibrium pressure in the melt	[bar]
	0.21	= partial oxygen pressure in air	[bar]
	4	= number of electrons transferred per molecule $O_2$ (see chapter 5.4)	
	F	= Faraday constant	96495 C·mole <sup>-1</sup>
	$\Delta E$	= potential difference between platinum plate and reference electrode	[V]
	$R_g$	= gas constant	8.314 J·mole <sup>-1</sup> ·K <sup>-1</sup>
	T	= absolute temperature	[K]

In figure 6.2, the oxygen equilibrium pressure in TV-screen glass containing 0.4 weight-%  $Fe_2O_3$  is presented as a function of temperature. The oxygen equilibrium pressure becomes close to 0.8 bar at 1300°C. If the oxygen equilibrium pressure in the melt is in the order of the atmospheric pressure (plus the hydrostatic pressure), heterogeneous bubble formation can occur (for example at the platinum plate), as has been explained in chapter 2.3.5. The bubbles will ascend to the surface of the melt, and an excess of oxygen is thus removed. Then, the oxygen equilibrium pressure remains at about the same value. For this reason, the potential difference between platinum plate and reference electrode does not increase further at increasing temperatures.

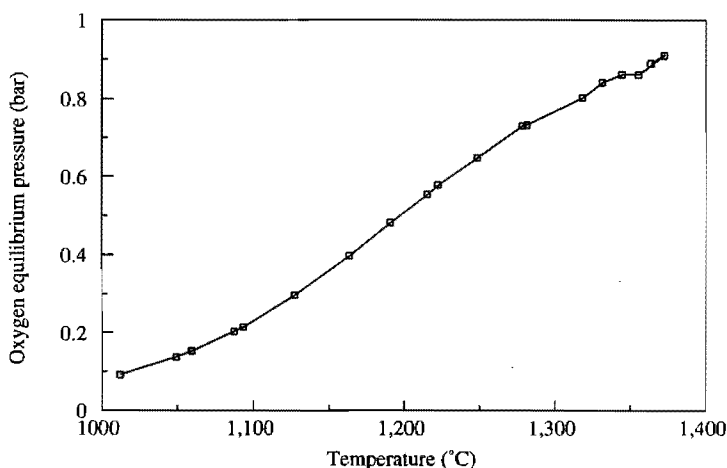


Figure 6.2

The oxygen equilibrium pressure in a TV-screen glass type A containing 0.4 weight-%  $Fe_2O_3$  while the temperature was increases from 1000 to 1400°C by 3 °C/min

In other experiments with the same glass composition, the absolute value of the oxygen equilibrium pressure could differ from the values in the example, but the shape of the  $p_{\text{O}_2}$ - $T$ -curve remained the same. The level of the oxygen pressure apparently depends on the amount of air, that is incorporated during the melting of the glass. Together with the equilibrium constant of the redox reaction



at the start of the measurement, this fixes the oxygen equilibrium pressure at the beginning of the experiment. The oxygen equilibrium pressure increases as the temperature increases, because then the equilibrium state of reaction 6.9 shifts to the right. This equilibrium is given by the redox reaction equilibrium constant  $K^{**}(T)$ , which of course is not affected by the initial oxygen equilibrium pressure.

#### 6.2.2.4 Calculation of $\Delta H^{**}$ , $\Delta S^{**}$ and $K^{**}(T)$

The redox reaction equilibrium constant  $K^{**}(T)$  is given by:

$$K^{**}(T) = \frac{[\text{Fe}^{2+}] \cdot (p_{\text{O}_2}(\text{melt}))^{1/4}}{[\text{Fe}^{3+}]} = \exp\left(\frac{-\Delta H^{**}}{R_g \cdot T} + \frac{\Delta S^{**}}{R_g}\right) \quad (6.10)$$

A change in the oxygen equilibrium pressure at a change in temperature from  $T_1$  to  $T_2$  for a closed system is given by (see chapter 5.4):

$$L_{\text{O}_2}(T_1) \cdot p_{\text{O}_2}(T_1) - L_{\text{O}_2}(T_2) \cdot p_{\text{O}_2}(T_2) = \frac{1}{4} \cdot C_{\text{Fe}} \left\{ \frac{K^{**}(T_1)}{K^{**}(T_1) + p_{\text{O}_2}^{1/4}(T_1)} - \frac{K^{**}(T_2)}{K^{**}(T_2) + p_{\text{O}_2}^{1/4}(T_2)} \right\} \quad (6.11)$$

with  $L_{\text{O}_2}(T)$  = physical solubility of oxygen  
in the glass melt at temperature  $T$  [mole·m<sup>-3</sup>·bar<sup>-1</sup>]  
 $p_{\text{O}_2}(T)$  = oxygen equilibrium pressure in  
the glass melt at temperature  $T$  [bar]  
 $C_{\text{Fe}}$  = total iron concentration in the glass melt [mole·m<sup>-3</sup>]

The physical solubility of oxygen is assumed to be about 1 mole·m<sup>-3</sup>·bar<sup>-1</sup> (see chapter 5.4 and 6.8). Equation 6.11 is valid as long as the iron concentration remains constant during the experiment, and no transport of oxygen between melt and atmosphere takes place. These requirements are assumed to be satisfied if the oxygen equilibrium pressure is less than 0.5 bar and the experiment is completed within some hours (see chapter 5.4).

With the aid of a computer fitting program (see chapter 5.4), the best values for  $\Delta H^{**}$  and  $\Delta S^{**}$ , and with those  $K^{**}(T)$ , for describing the measured oxygen equilibrium pressure as a function of temperature can be found. The oxygen equilibrium pressure at one temperature is imported in the computer program to account for the amount of air, included in the glass during the melting of the cullet before the start of the measurement.

In the presented experiment in TV-screen glass type A containing 0.4 weight-%  $\text{Fe}_2\text{O}_3$ , the total iron concentration  $C_{\text{Fe}}$  was  $115 \text{ mole}\cdot\text{m}^{-3}$ . At  $1092^\circ\text{C}$ , the oxygen equilibrium pressure was 0.21 bar. The fitting procedure resulted in the following values for the enthalpy and entropy changes:

$$\Delta H^{**} = 100 \text{ kJ}\cdot\text{mole}^{-1} \pm 5 \text{ kJ}\cdot\text{mole}^{-1}$$

$$\Delta S^{**} = 37 \text{ J}\cdot\text{mole}^{-1}\cdot\text{K}^{-1} \pm 2 \text{ J}\cdot\text{mole}^{-1}\cdot\text{K}^{-1}$$

In figures 6.3 and 6.4, the theoretical potential differences and oxygen equilibrium pressures are given as functions of temperature for these values of  $\Delta H^{**}$  and  $\Delta S^{**}$ , together with the measured data. In figure 6.3, the theoretical potential differences based on other values for  $\Delta H^{**}$  and  $\Delta S^{**}$  are included. The sensitivity of the calculation of the redox reaction enthalpy and entropy from oxygen equilibrium pressure measurements appears to be reasonably high.

It should be stressed, however, that the calculations are based on the assumption that the physical solubility of oxygen in the glass melt is about  $1 \text{ mole}\cdot\text{m}^{-3}\cdot\text{bar}^{-1}$ . In chapter 6.8 the sensitivity of the calculation of the enthalpy and entropy with regard to the chosen value of the physical solubility will be discussed in detail.

For other experiments with the same glass and with TV-screen glass type B containing 0.4 weight-%  $\text{Fe}_2\text{O}_3$ , about the same values for  $\Delta H^{**}$  and  $\Delta S^{**}$  are obtained (see section 6.2.2.5), although the absolute values of the oxygen equilibrium pressure differed. This indicates that the values for  $\Delta H^{**}$  and  $\Delta S^{**}$  are reproducible. The relative error is about 5%.

#### 6.2.2.5 Results

Oxygen equilibrium pressure measurements have been performed in different glasses. The results are summarized in table 6.1.

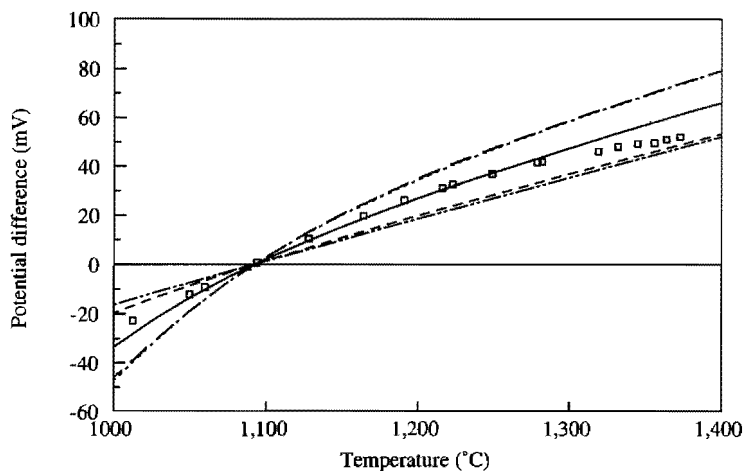


Figure 6.3

The temperature-dependent measured potential differences ( $\square$ ) for a TV-screen glass type A containing 0.4 weight-%  $\text{Fe}_2\text{O}_3$  and the theoretical potential differences, based on:

$$C_{\text{Fe}} = 115 \text{ mole}\cdot\text{m}^{-3}$$

$$p_{\text{O}_2}(1092^\circ\text{C}) = 0.21 \text{ bar}$$

Line	$\Delta H^{**}$	$\Delta S^{**}$
—	100	37
- - - -	100	32
· · · · ·	100	42
- · - · -	90	37
- - - -	110	37

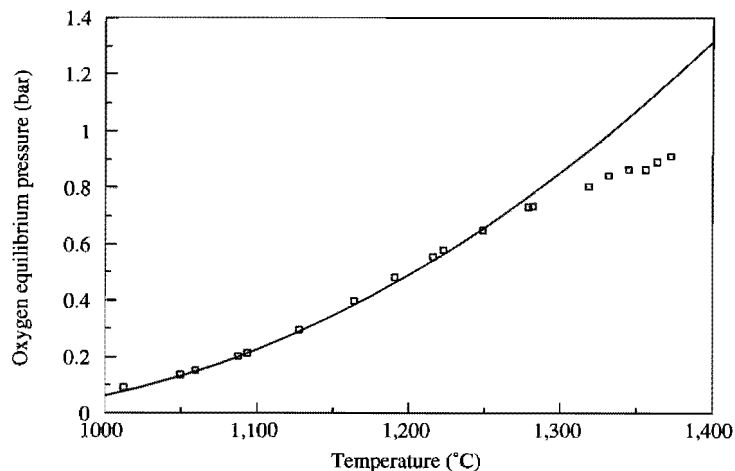


Figure 6.4

The oxygen equilibrium pressures ( $\square$ ) and the theoretical oxygen equilibrium pressures (—), based on

$$C_{\text{Fe}} = 115 \text{ mole}\cdot\text{m}^{-3}$$

$$p_{\text{O}_2}(1092^\circ\text{C}) = 0.21 \text{ bar}$$

$$\Delta H^{**} = 100 \text{ kJ}\cdot\text{mole}^{-1}$$

$$\Delta S^{**} = 37 \text{ J}\cdot\text{mole}^{-1}\cdot\text{K}^{-1}$$

as functions of temperature for a TV-screen glass type A containing 0.4 weight-%  $\text{Fe}_2\text{O}_3$

### 6.2.3 Square wave voltammetry measurements

#### 6.2.3.1 Experimental procedure

The glasses containing iron were melted in platinum crucibles at 1400°C until all grains were dissolved completely and the bubbles were nearly all removed from the melt. Then the melt was cooled down quickly. The cullet was transferred to an Al<sub>2</sub>O<sub>3</sub>-crucible and placed in the furnace as sketched in figure 5.3. In some experiments, the glass melts which first had been used for oxygen equilibrium pressure measurements were tested. Because square wave voltammetry measurements disturb the equilibrium state of the molten glass, the square wave voltammetry measurements have to be performed after the oxygen equilibrium pressure measurements. After the recording of a square wave voltammogram, the oxygen equilibrium pressure only reaches a stable, constant value after a waiting time of some minutes in soda-lime-silica and TV-screen glasses. In E-glass the waiting time will be a few decades of minutes because of the relatively low electrical conductivity.

Table 6.1

The results of oxygen equilibrium pressure measurements in some commercially available glasses containing iron (no other polyvalent ions), expressed in redox reaction enthalpy and entropy changes

Glass	Concentration (weight-%)	Concentration (mole Fe/m <sup>3</sup> )	$\Delta H^{**}$ (kJ·mole <sup>-1</sup> )	$\Delta S^{**}$ (J·mole <sup>-1</sup> ·K <sup>-1</sup> )
TV-screen (type A)	0.4	115	100 ± 5	37 ± 2
TV-screen (type B)	0.4	115	99 ± 5	42 ± 2
E-glass	0.5	144	105 ± 5	43 ± 2

The glass was heated slowly to 1450°C, and then the electrodes were dipped into the glass melt. The arrangement of the three electrodes is sketched in figure 5.3. The working electrode consists of a platinum wire, and the counter electrode is a platinum plate. The Pt/ZrO<sub>2</sub> reference electrode was flushed with clean, dry air.

The temperature of the furnace was held constant for 15 minutes. Then an  $iR_u$  measurement was performed (see chapter 5.3), followed by a square wave voltammetry measurement. During this measurement the furnace is temporarily switched off in order to avoid disturbance of the measured signal by the current in the heating elements. Generally the set-up of the measurement was:

Initial potential  $E_i$ : 0 V

Final potential  $E_{end}$ : -0.8 V

The frequency with which the base potential  $E_b$  is varied,  $f$ : 100 Hz

The height of the staircase increase of the base potential  $E_b$ ,  $\Delta E_b$ : -0.002 V

The height of the potential pulse, both in "forward" and in "reverse" direction, superimposed on the staircase base potential  $E_b$ ,  $\Delta E_p$ : 0.1 V

Usually an adequate square wave voltammogram is obtained with this set-up, giving one clear peak (due to the reaction  $Fe^{3+} \rightarrow Fe^{2+}$ ). In some experiments, other values for the parameters in the set-up are used to determine their effect on the position and shape of the peak. A waiting time of 15 minutes was used between two measurements at the same temperature, in order to allow the glass melt to retain its original state.

Then the temperature was decreased by 3°C/min to a lower level. Before running  $iR_u$  and square wave voltammetry measurements the temperature of the furnace was held constant at the new value for 15 minutes. In this way the temperature region of 1450 to 700°C was investigated with square wave voltammetry measurements in the case that soda-lime-silica or TV-screen glass was used. The uncompensated resistance in E-glass at temperatures below 1000°C became too high to obtain reliable square wave voltammograms, so for this type of glass the square wave voltammetry measurements were made at temperatures ranging from 1450 to 1000°C.

#### 6.2.3.2 The recorded square wave voltammograms

With the aid of an example the processing of the square wave voltammograms and the calculation of the redox reaction enthalpy and entropy will be explained.

The example glass is a TV-screen glass type A made of reagent grade ingredients containing 0.4 weight-%  $Fe_2O_3$ .



As has been explained in chapter 5.5, the currents that flow during the potential pulses in the "forward" direction (in the direction of the final potential) and during the pulses in the "reverse" direction are measured. In figure 6.5, the "forward" and "reverse" currents,  $i_f$  and  $i_r$ , measured in the example glass at 1440°C, are represented as functions of the base potential  $E_b$ . In both curves, a clear peak can be seen. This is a first indication of the reversibility of the redox reaction under study. If the reaction is irreversible, no peak occurs in the curve of the "reverse" current.

Then the "reverse" current is subtracted from the "forward" current (see chapter 5.5). The resulting current is indicated by the "differentiated" current  $\delta i$ . The almost symmetrical  $\delta i$ -curve shows a clear peak at the half-wave potential of the redox reaction of iron (measured relative to the potential of the reference electrode).

This  $\delta i$ -curve is used for further processing, because the exact shape of this peak is less effected by the geometry of the working electrode than the  $i_f$  and  $i_r$  curves (see chapter 5.5.4.1).

The position of the peak in the  $\delta i$ -curve can be determined with an accuracy of 1 mV and a reproducibility of 10 mV.

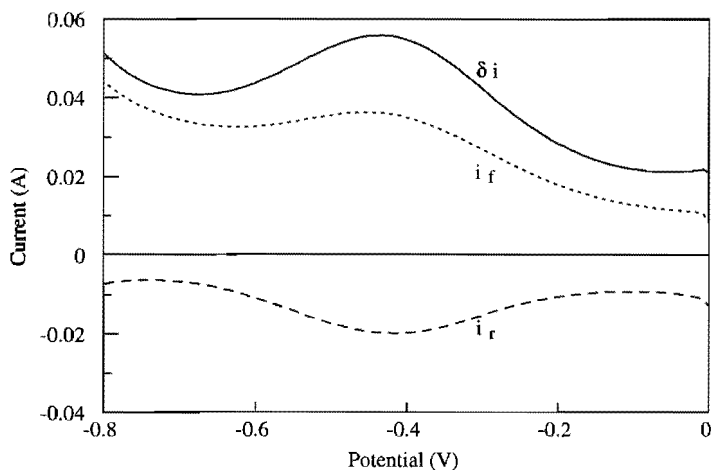


Figure 6.5

The complete square wave voltammogram measured in TV-screen glass type A containing 0.4 weight-%  $\text{Fe}_2\text{O}_3$  at 1440°C with the following set-up:

$$\Delta E_b = 0.002 \text{ V} \quad \Delta E_p = 0.1 \text{ V} \quad f = 100 \text{ Hz} \quad R_u = 0 \text{ } \Omega$$

### 6.2.3.3 Study of the effect of the values of $f$ , $\Delta E_b$ and $\Delta E_p$

#### The frequency $f$

The frequency  $f$  determines the time that the applied potential is held at a constant value before the current is measured. This waiting time is equal to  $1/2 \cdot f$  (see chapter 5.5). If the frequency is increased, the waiting time decreases. Consequently, the contribution of the charging current to the total measured curve increases (see chapter 5.2). The peak in the square wave voltammogram then becomes less distinct. This effect becomes significant for the example glass in the present experimental set-up for frequencies exceeding 250 Hz.

At lower frequencies the contribution of the charging current to the total measured current diminishes. But also the faradaic current decreases as the time between the change in potential and the measurement of the current increases (see chapter 5.2). This means that the total current decreases. The accuracy of the measurement becomes less, especially at frequencies less than 10 Hz. Besides, the total required measuring time increases fast at a lower frequency. Because the furnace is switched off during the measurement, the temperature of the glass melt would fall too much at frequencies less than 1 Hz.

After ample experiments it was decided to set the frequency to a value between 20 and 200 Hz. In this frequency range, the frequency was found to have no influence on the position of the peak in the square wave voltammograms. As an example, the square wave voltammograms recorded with three different frequencies in a TV-screen glass containing 0.4 weight-%  $\text{Fe}_2\text{O}_3$  at  $1370^\circ\text{C}$  are shown in figure 6.6. The peaks are located at a potential of  $-0.466 \text{ V}$  ( $\pm 0.002 \text{ V}$ ) with regard to the potential of the reference electrode.

Even at low temperatures, the frequency has no influence on the position of the peak. In figure 6.7, two square wave voltammograms recorded in a TV-screen glass containing 0.4 weight-%  $\text{Fe}_2\text{O}_3$  at  $900^\circ\text{C}$  with frequencies of 100 and 200 Hz are represented. After elimination of the background currents (which are influenced by the applied frequency) the peaks turn out to be located at the same potential:  $-0.453 \text{ V}$  ( $\pm 0.002 \text{ V}$ ).

The fact that the position of the peak is independent of the applied frequency at any temperature is a second indication that the reduction of iron is reversible (chapter 5.5).

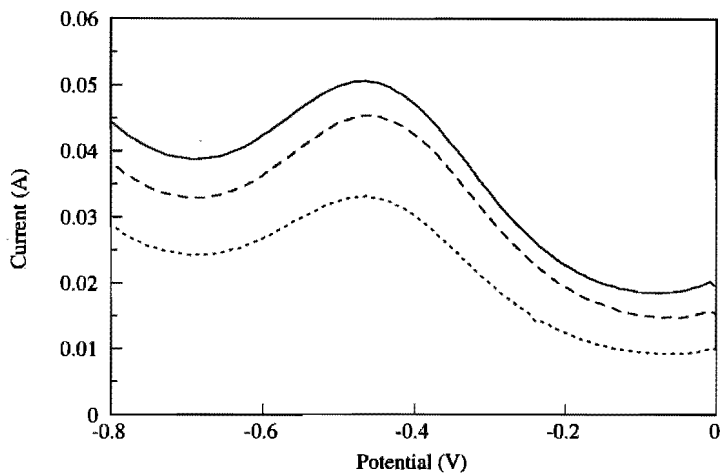


Figure 6.6

Square wave voltammograms recorded in TV-screen glass type A containing 0.4 weight-%  $\text{Fe}_2\text{O}_3$  at  $1370^\circ\text{C}$ , with the following set-ups:

-----	$f = 50 \text{ Hz}$	$\Delta E_b = 0.002 \text{ V}$	$\Delta E_p = 0.1 \text{ V}$	$R_u = 1.7 \Omega$
-----	$f = 100 \text{ Hz}$			
-----	$f = 150 \text{ Hz}$			

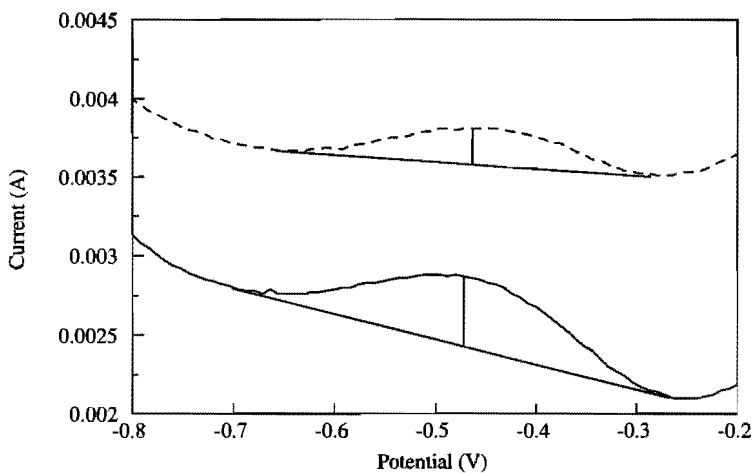


Figure 6.7

Square wave voltammograms recorded in TV-screen glass type A containing 0.4 weight-%  $\text{Fe}_2\text{O}_3$  at  $900^\circ\text{C}$ , with the following set-up:

-----	$f = 100 \text{ Hz}$	$\Delta E_b = 0.002 \text{ V}$	$\Delta E_p = 0.1 \text{ V}$
-----	$f = 200 \text{ Hz}$		

**The staircase increase of the base potential,  $\Delta E_b$** 

Each  $1/f$  second, the base potential  $E_b$  is increased by  $\Delta E_b$  (in the negative direction), until the final potential  $E_{\text{end}}$  has been reached. The time, needed to complete a scan of the potential range between the initial potential  $E_i$  and  $E_{\text{end}}$  is:

$$\text{scan time} = \frac{(|E_i - E_{\text{end}}| + \Delta E_b)}{\Delta E_b \cdot f} \quad (6.12)$$

The scan time should not exceed 1 minute, because the temperature in the furnace would then decrease too much. Therefore  $\Delta E_b$  should not be too small. But  $\Delta E_b$  also determines the number of measuring points. The measuring accuracy increases as  $\Delta E_b$  is set to a low value.

In all measurements  $\Delta E_b$  is set to a value of 0.002 V.

**The pulse height,  $\Delta E_p$** 

The height of the potential pulse  $\Delta E_p$  is usually 0.1 V. This means that the difference in the applied potential between two succeeding current measurements ( $i_f$  and  $i_r$ ) is 0.2 V. At a lower value of  $\Delta E_p$ , the resulting current becomes less. This diminishes the accuracy of the measurement. An increase in  $\Delta E_p$  provides for an increase in the faradaic current (see equation 5.11), but at the same time the charging current is promoted (see equation 5.7). Due to this last effect the  $i_f$  and  $i_r$  curves become more separated. However, the sensitiveness of the measurement is not increased. Besides, for the calculation of theoretical voltammograms the following condition should be satisfied:

$\Delta E_p < R_g \cdot T/n \cdot F$  (see chapter 5.5). For these reasons,  $\Delta E_p$  ranges between 0.02 and 0.2 V.

**6.2.3.4 Processing of the measured square wave voltammograms****Check of the reversibility of the redox reaction**

If the redox reaction is reversible (relative to the applied frequency of the measuring signal), peaks will be seen in the curves of the "forward" and "reverse" currents. Furthermore, the differentiated curve  $\delta i$  will show an almost symmetrical peak (at least if the contribution of the charging current to the total current is low). Besides, the position of the peak will be independent of the applied frequency. These statements are all valid for the reduction of iron in TV-screen and soda-lime-silica glass melts.

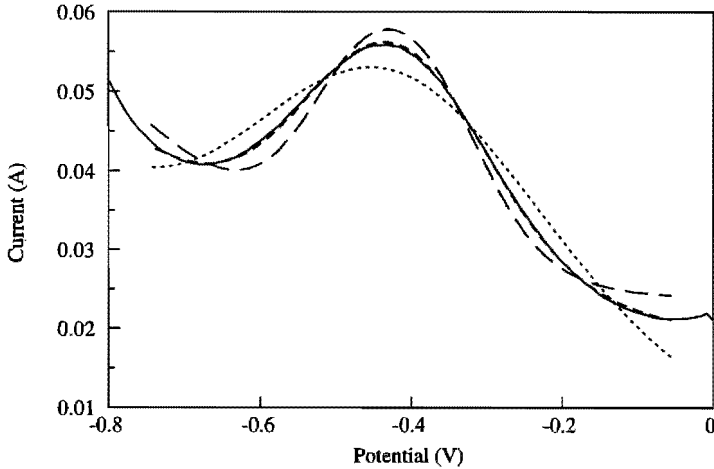


Figure 6.8

The square wave voltammogram (————) recorded in TV-screen glass type A containing 0.4 weight-%  $\text{Fe}_2\text{O}_3$  at  $1440^\circ\text{C}$  with the following set-up:

$\Delta E_p = 0.002 \text{ V}$        $\Delta E_p = 0.1 \text{ V}$        $f = 100 \text{ Hz}$        $R_u = 0 \Omega$

in comparison with theoretical square wave voltammograms for reversible redox reactions, with:

-----                      - - - - -                      - . - . - .  
 $n = 1$                                $n = 2$                                $n = 3$

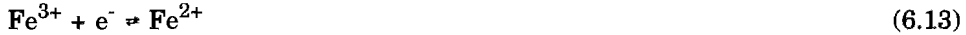
The reversibility of the reaction can be checked further by comparing the recorded voltammogram with theoretical voltammograms which can be derived for reversible and quasi-reversible reactions (see chapter 5.5). In all cases mentioned in this thesis, the recorded voltammograms agreed well with the theoretical voltammograms assuming reversible reactions.

In figure 6.8, the square wave voltammogram recorded for TV-screen glass type A containing 0.4 weight-%  $\text{Fe}_2\text{O}_3$  at  $1440^\circ\text{C}$  is compared with the different theoretical curves for reversible redox reactions at which one, two and three moles of electrons are transferred at the reduction of one mole reactant.

The measured curve closely resembles the theoretical curve for a reversible two-electron reaction. The increase of the current at  $-0.8 \text{ V}$  results from the reduction of other components of the glass melt, probably Si or Na (see chapter 5.5.6).

### The number of electrons transferred

The shape of the peak depends on the number of electrons that is transferred during reduction of the reactant. For an iron-containing glass, the peak in the square wave voltammogram is assumed to arise from the reaction



For a one-electron transfer process, the peak should be broad, particularly at high temperatures. However, the peak in the square wave voltammogram recorded in a TV-screen glass type A containing 0.4 weight-%  $\text{Fe}_2\text{O}_3$  at  $1440^\circ\text{C}$  agrees very well with a two-electron transfer process (see figure 6.8). At lower temperatures, the peak becomes less distinct and the shape corresponds reasonably well both with a one or a two-electron transfer.

This strange phenomenon seems to arise in all the glasses with relatively high iron levels that have been investigated in the present study. At temperatures above about  $1200^\circ\text{C}$ , the peaks resemble two-electron reactions, while at lower temperatures, the peaks can be reproduced both with a theoretical one and a two-electron transfer. The origin of this phenomenon is not clear yet. An explanation might be found in:

- an incomplete elimination of the background currents;
- an incorrect theoretical description of the curve, while the assumption that  $\Delta E_p \ll R_g \cdot T/n \cdot F$  is not fulfilled (see chapter 5.5.5);
- complex formation of two  $\text{Fe}^{3+}$ -ions and/or two  $\text{Fe}^{2+}$ -ions. This explanation, however, is in contradiction with the finding of Johnston [9]. According to Johnston, the ratio  $[\text{Fe}^{2+}]/[\text{Fe}^{3+}]$  at a given temperature is proportional to  $P_{\text{O}_2}^{1/4}$ .

At low iron concentrations (0.1 and 0.04 weight-%) the peaks in the square wave voltammogram are less distinct and can be ascribed both to a one and a two-electron transfer.

Until the question of the number of electrons transferred during the reduction is solved, the peak in the recorded voltammograms is attributed to the reaction  $\text{Fe}^{3+} + e^- \rightleftharpoons \text{Fe}^{2+}$ , and the processing of the results, and the calculation of the reaction enthalpy and entropy are based on a one-electron transfer process.

### The ratio of the diffusion coefficients of $\text{Fe}^{3+}$ and $\text{Fe}^{2+}$

From the height of the peak in the square wave voltammogram, the diffusion coefficient of the reacting species can be calculated if the concentration  $C$  and

the surface area of the working electrode,  $A$ , are known. Unfortunately, this last quantity is not known accurately enough in the present investigations (see chapter 5.3). Therefore only the order of magnitude of the diffusion coefficient can be calculated. At  $1400^{\circ}\text{C}$ , the diffusion coefficient of  $\text{Fe}^{2+}$  in TV-screen glass is about  $6 \cdot 10^{-10} \text{ m}^2 \cdot \text{s}^{-1}$ .

However, the ratio of the diffusion coefficients of oxidant and reductor can be estimated. Therefore two square wave voltammograms have to be recorded. In one square wave voltammetry experiment, the potential range is scanned in the negative direction. Figure 6.9 shows a square wave voltammogram, recorded from 0 V to  $-0.7$  V in a TV-screen glass containing 0.4 weight-% at  $1400^{\circ}\text{C}$ . At 0 V, the iron is assumed to be completely in the  $\text{Fe}^{3+}$  state. The height of the peak is then proportional to the surface area of the working electrode  $A$ , the concentration of  $\text{Fe}^{3+}$  which is now equal to the total iron concentration  $C_{\text{Fe}}$  and the square root of the diffusion coefficient of  $\text{Fe}^{3+}$  (see chapter 5.5):

$$\delta i \propto A \cdot [\text{Fe}^{3+}] \cdot \sqrt{D_{\text{Fe}^{3+}}} \approx A \cdot C_{\text{Fe}} \cdot \sqrt{D_{\text{Fe}^{3+}}} \quad (6.14)$$

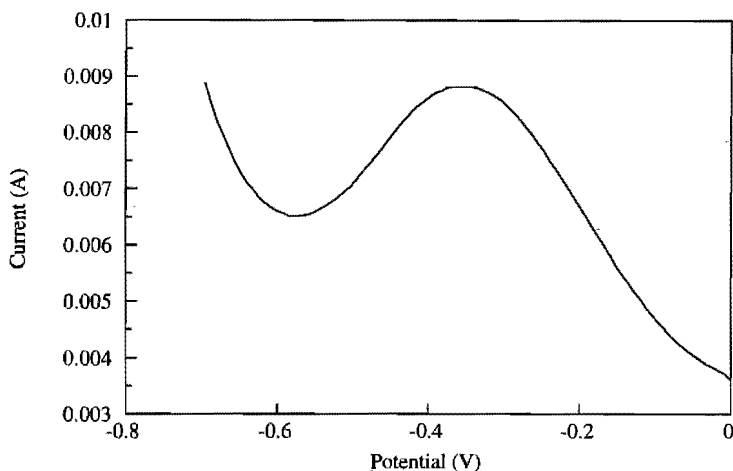


Figure 6.9

The square wave voltammogram recorded in TV-screen glass type B containing 0.4 weight-%  $\text{Fe}_2\text{O}_3$  at  $1400^{\circ}\text{C}$  with the following set-up:

$$\Delta E_b = 0.002 \text{ V}$$

$$f = 20 \text{ Hz}$$

$$\text{Initial potential } E_i = 0 \text{ V}$$

$$\Delta E_p = 0.1 \text{ V}$$

$$R_u = 6.2 \ \Omega$$

$$\text{Final potential } E_{\text{end}} = -0.7 \text{ V}$$

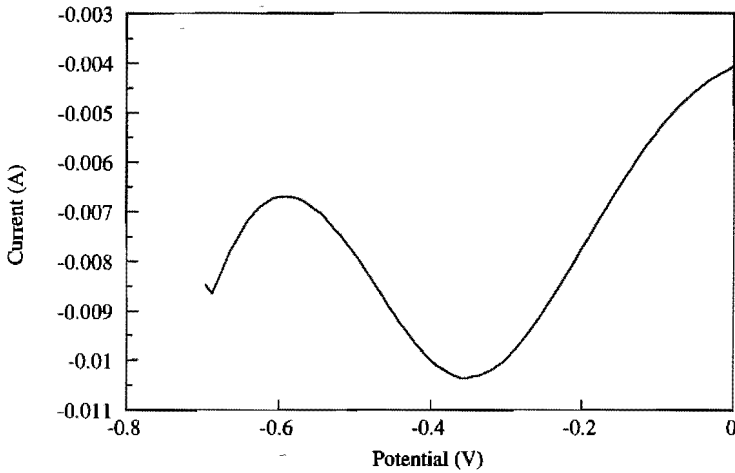


Figure 6.10  
The square wave voltammogram recorded in TV-screen glass type B containing 0.4 weight-%  $\text{Fe}_2\text{O}_3$  at  $1400^\circ\text{C}$  with the following set-up:

$\Delta E_b = 0.002 \text{ V}$	$f = 20 \text{ Hz}$	Initial potential $E_i = -0.7 \text{ V}$
$\Delta E_p = 0.1 \text{ V}$	$R_u = 6.2 \Omega$	Final potential $E_{\text{end}} = 0 \text{ V}$

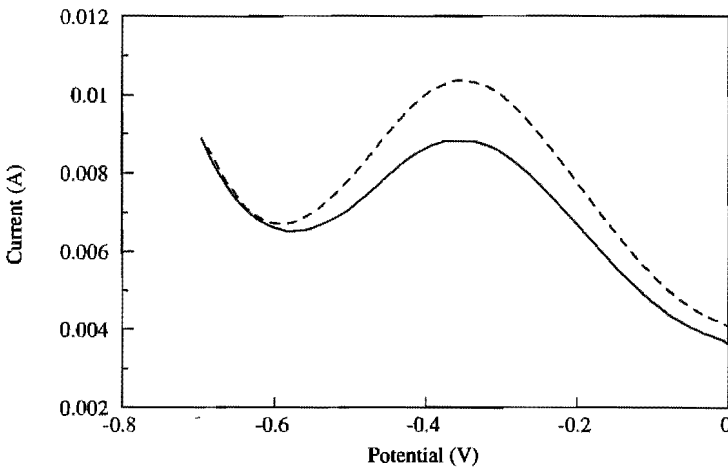


Figure 6.11  
The square wave voltammograms recorded in TV-screen glass type B containing 0.4 weight-%  $\text{Fe}_2\text{O}_3$  at  $1400^\circ\text{C}$  with the following set-up:

$\Delta E_b = 0.002 \text{ V}$	$E_i = 0 \text{ V}$	$\Delta E_b = 0.002 \text{ V}$	$E_i = -0.7 \text{ V}$
$\Delta E_p = 0.1 \text{ V}$	$E_{\text{end}} = -0.7 \text{ V}$	$\Delta E_p = 0.1 \text{ V}$	$E_{\text{end}} = 0 \text{ V}$
$f = 20 \text{ Hz}$		$f = 20 \text{ Hz}$	Current multiplied by -1
$R_u = 6.2 \Omega$		$R_u = 6.2 \Omega$	



During a second experiment, the same potential region is scanned, but now in the positive direction. Before the beginning of the experiment, the potential of the working electrode is held for 15 seconds at -0.7 V. At this potential, the  $\text{Fe}^{2+}$  state of iron is stable. At the surface of the working electrode and in its surroundings, all iron is assumed to be converted to the reduced state. Then a square wave voltammogram is recorded from -0.7 to 0 V, under otherwise equal conditions (see figure 6.10). During the experiment,  $\text{Fe}^{2+}$  is oxidized to  $\text{Fe}^{3+}$ , resulting in a negative differentiated current  $\delta i$ . The absolute height of the peak in the voltammogram is now proportional to:

$$\delta i \propto A \cdot [\text{Fe}^{2+}] \cdot \sqrt{D_{\text{Fe}^{2+}}} \approx A \cdot C_{\text{Fe}} \cdot \sqrt{D_{\text{Fe}^{2+}}} \quad (6.15)$$

In figure 6.11, both square wave voltammograms are displayed. The y-values of the voltammogram of figure 6.10 are multiplied by -1. Clearly, the peak of this voltammogram is somewhat higher. This indicates that at 1400°C the diffusion coefficient of  $\text{Fe}^{2+}$  is somewhat larger than the diffusion coefficient of  $\text{Fe}^{3+}$ :

$$\frac{\sqrt{D_{\text{Fe}^{2+}}}}{\sqrt{D_{\text{Fe}^{3+}}}} \propto \frac{10.36 \text{ Ampère}}{8.84 \text{ Ampère}} = 1.17 \quad \text{or} \quad \frac{D_{\text{Fe}^{2+}}}{D_{\text{Fe}^{3+}}} = 1.37 \quad (6.16)$$

Generally, the ratio of the diffusion coefficients of  $\text{Fe}^{2+}$  and  $\text{Fe}^{3+}$  in TV-screen and soda-lime-silica glass melts is approximately 1 for any temperature.

### The formal potential of the redox reaction

The peak in the square wave voltammograms is (for reversible reactions) located at the half-wave potential  $E_{1/2}$  of the reaction (see chapter 5.2). In the voltammograms of figures 6.9 and 6.10, this half-wave potential is -0.355 V. The formal potential  $E^{0'}$  of the reaction is given by:

$$E^{0'} = E_{1/2} - \frac{R_g \cdot T}{F} \ln \left( \frac{D_{\text{Fe}^{2+}}}{D_{\text{Fe}^{3+}}} \right)^{1/2} \quad (6.17)$$

(see equation 5.16). In the example glass, the formal potential of the redox reaction  $\text{Fe}^{3+} + e^- \rightleftharpoons \text{Fe}^{2+}$  is:

$$E^{0'}(1400^\circ\text{C}) = -0.355 - \frac{R_g \cdot 1673}{F} \ln 1.17 = -0.378 \text{ V} \quad (6.18)$$

### The redox reaction equilibrium constant

The formal potential is directly related to the redox reaction equilibrium constant  $K^{**}(T)$  (see equation 5.62 in chapter 5.5):

$$K^{**}(T) = \frac{[\text{Fe}^{2+}] \cdot p_{\text{O}_2}^{1/4}}{[\text{Fe}^{3+}]} = \exp \left\{ \frac{F \cdot E^0(T)}{R_g \cdot T} \right\} \quad (6.19)$$

In the example glass, the redox reaction equilibrium constant at 1400°C is:

$$K^{**}(1400^\circ\text{C}) = 0.0726 \quad (6.20)$$

### Determination of the enthalpy and entropy of the redox reaction

The outlined procedure is repeated at other temperatures. Every time the formal potential is determined. At lower temperatures, the peak in the square wave voltammogram shifts towards more negative potentials. For example the half-wave potential of the iron reduction at 1164°C is -0.476 V (see figure 6.12).

In the temperature range from 1400 down to about 1000°C, the formal potential decreases roughly linearly with temperature. This indicates that the redox reaction equilibrium decreases at decreasing temperatures, and then the

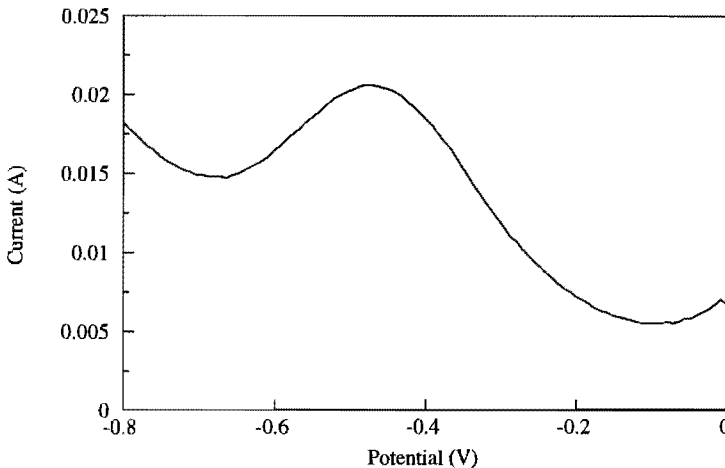


Figure 6.12

The square wave voltammogram measured in TV-screen glass type A containing 0.4 weight-%  $\text{Fe}_2\text{O}_3$  at 1164°C with the following set-up:

$$\Delta E_b = 0.002 \text{ V}$$

$$\Delta E_p = 0.1 \text{ V}$$

$$f = 100 \text{ Hz}$$

$$R_u = 2.91 \ \Omega$$

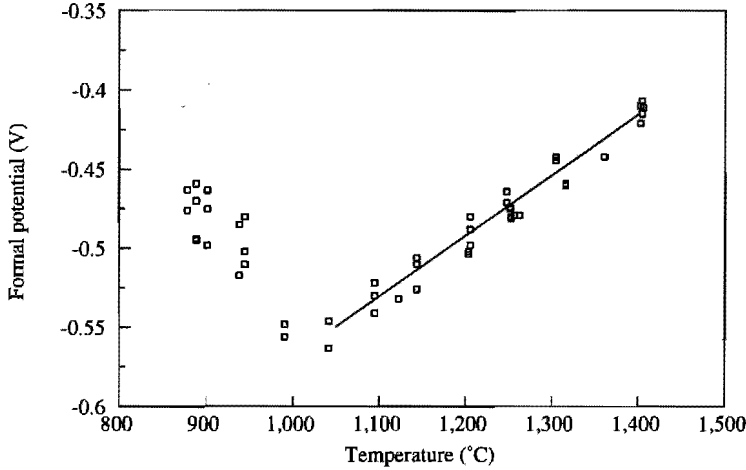


Figure 6.13  
The formal potential (□) of the iron reduction in TV-screen glass type A containing 0.4 weight-%  $\text{Fe}_2\text{O}_3$  as a function of temperature

equilibrium state of the reaction



shifts to the left side. In figure 6.13, the formal potentials of the iron reduction are plotted against the temperature.

The redox reaction enthalpy and entropy  $\Delta H^{**}$  and  $\Delta S^{**}$ , as defined in chapter 4, can be calculated from the formal potential  $E^{0'}$ :

$$\Delta H^{**} = F \left\{ T \cdot \left( \frac{\delta E^{0'}(T)}{\delta T} \right) - E^{0'}(T) \right\} \quad (6.22)$$

$$\Delta S^{**} = F \left( \frac{\delta E^{0'}(T)}{\delta T} \right)$$

For TV-screen glass containing 0.4 weight-%  $\text{Fe}_2\text{O}_3$ , the results are:

$$\Delta H^{**} = 102 \text{ kJ}\cdot\text{mole}^{-1} \pm 2 \text{ kJ}\cdot\text{mole}^{-1}$$

$$\Delta S^{**} = 37 \text{ J}\cdot\text{mole}^{-1}\cdot\text{K}^{-1} \pm 2 \text{ J}\cdot\text{mole}^{-1}\cdot\text{K}^{-1}$$

for temperatures above  $1000^\circ\text{C}$ . At lower temperatures the formal potentials deviate from the straight line. This will be discussed in chapter 6.2.3.6.

### 6.2.3.5 The effect of the total iron concentration

Square wave voltammetry experiments have been performed in soda-lime-silica and TV-screen glasses containing 0.04 to 2.6 weight-%  $\text{Fe}_2\text{O}_3$ . In all cases, one peak or shoulder was visible at any temperature between 1000 and 1400°C. As an example, the square wave voltammograms recorded in an industrial TV-screen glass type A containing about 0.04 weight-%  $\text{Fe}_2\text{O}_3$  at 1350 and 1000°C are given in figures 6.14 and 6.15.

The reduction of iron can be seen as a peak at -0.425 V at 1350°C and as a shoulder at -0.564 V at 1000°C. The shape of these peaks both matches a one- and a two electron transfer (see section 6.2.3.4).

This TV-screen-glass also contains  $\text{Sb}_2\text{O}_3$ . Reduction of the antimony results in a peak at about -0.23 V at 1350°C, and two shoulders at about -0.330 and -0.080 V at 1000°C (see chapter 6.3). The position of the peaks for the iron reduction is presumably not influenced by the presence of other polyvalent elements present, as will be seen in chapter 6.7. Because the reduction of antimony does not interfere with the reduction of iron, the peaks can be mathematically separated (see chapter 5.5).

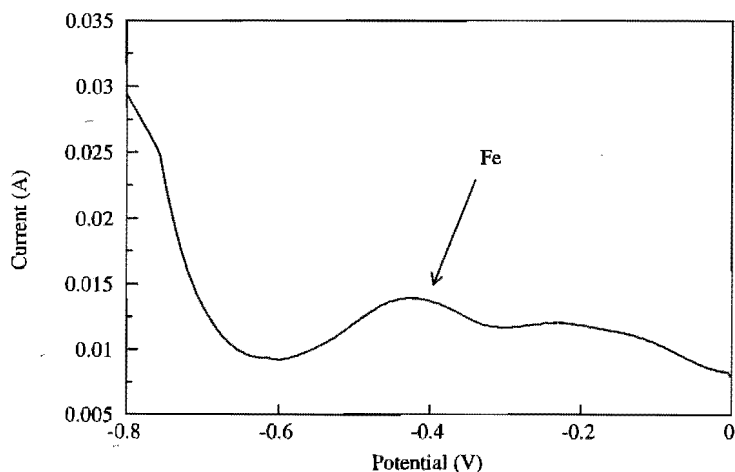


Figure 6.14

The square wave voltammogram measured in TV-screen-glass type A containing about 0.04 weight-%  $\text{Fe}_2\text{O}_3$  and about 0.4 weight-%  $\text{Sb}_2\text{O}_3$  at 1350°C with the following set-up:

$\Delta E_b = 0.002$  V       $\Delta E_p = 0.1$  V       $f = 100$  Hz       $R_u = 4.8$   $\Omega$

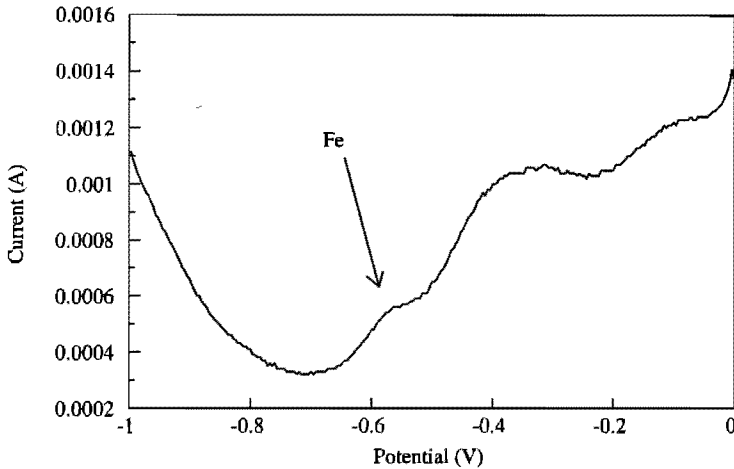


Figure 6.15

The square wave voltammogram measured in TV-screen-glass type A containing about 0.04 weight-%  $\text{Fe}_2\text{O}_3$  and about 0.4 weight-%  $\text{Sb}_2\text{O}_3$  at  $1000^\circ\text{C}$  with the following set-up:

$$\Delta E_p = 0.002 \text{ V} \quad \Delta E_p = 0.1 \text{ V} \quad f = 100 \text{ Hz} \quad R_u = 34.7 \Omega$$

The formal potentials of the iron reduction in TV-screen-glass type A with two different iron concentrations are plotted against the temperature in figure 6.16, and in TV-screen glass type B in figure 6.17. The calculated redox reaction enthalpies and entropies for these iron contents are given in table 6.2.

Table 6.2

The reaction enthalpy and entropy for the iron reduction in TV-screen glass with various iron contents

Glass	sym bol	Concen- tration $\text{Fe}_2\text{O}_3$ (weight-%)	Concen- tration (mole Fe/ $\text{m}^3$ glass)	$\Delta H^{**}$ ( $\text{kJ}\cdot\text{mole}^{-1}$ )	$\Delta S^{**}$ ( $\text{J}\cdot\text{mole}^{-1}\cdot\text{K}^{-1}$ )
type A	□	0.4	115	$102 \pm 1$	$37 \pm 2$
type A	▲	$\pm 0.04$	$\pm 12$	$132 \pm 4$	$56 \pm 1$
type B	■	0.4	115	$102 \pm 1$	$41 \pm 3$
type B	○	$\pm 0.04$	$\pm 12$	$136 \pm 1$	$56 \pm 1$

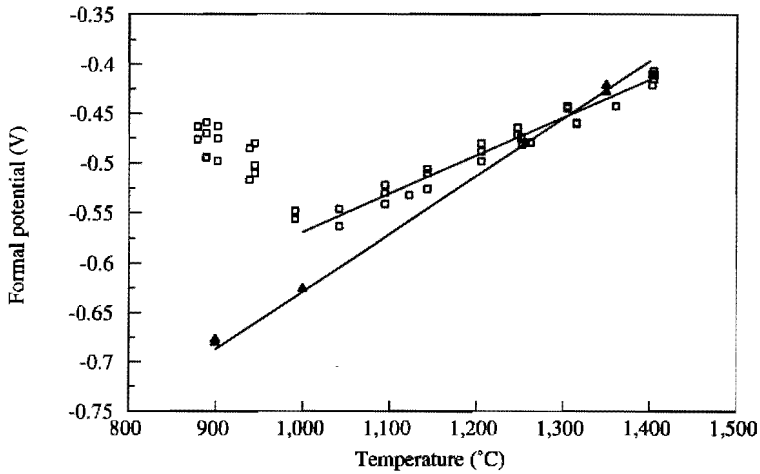


Figure 6.16

The formal potential of the iron reduction in TV-screen glass type A containing about 0.04 weight-% ( $\blacktriangle$ ) or 0.4 ( $\square$ )  $\text{Fe}_2\text{O}_3$  as a function of the temperature

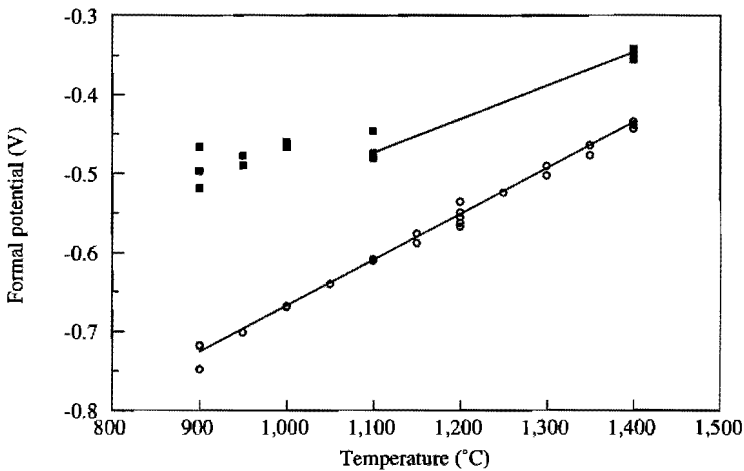


Figure 6.17

The formal potential of the iron reduction in TV-screen glass type B containing about 0.04 weight-% ( $\circ$ ) or 0.4 ( $\blacksquare$ )  $\text{Fe}_2\text{O}_3$  as a function of the temperature

The iron concentration obviously has an effect on the redox reaction enthalpy and entropy. The redox reaction equilibrium constant  $K^{**}(T)$  is directly proportional to the formal potential  $E^{0'}$  according to equation 6.19. Since  $E^{0'}$  is more negative for low iron contents than for higher iron concentrations, it follows that relatively more iron is present in the Fe<sup>3+</sup>-state at low iron contents under otherwise equal conditions. Probably the ratio of activity coefficients of Fe<sup>2+</sup> and Fe<sup>3+</sup> in TV-screen glass depend on the iron concentration. Then equation 6.10 can only be applied for a given iron concentration.

In figure 6.18, the formal potentials of the iron reduction in soda-lime-silica glass with four different iron contents are plotted as functions of the temperature. The calculated enthalpies and entropies are summarized in table 6.3

Table 6.3

The redox reaction enthalpy and entropy for the iron reduction in soda-lime-silica glass with four different iron contents

Concentration Fe <sub>2</sub> O <sub>3</sub> (weight-%)	symbol	Concentration (mole Fe/m <sup>3</sup> glass)	$\Delta H^{**}$ (kJ·mole <sup>-1</sup> )	$\Delta S^{**}$ (J·mole <sup>-1</sup> ·K <sup>-1</sup> )
0.1	■	29	114 ± 1	41 ± 4
0.50	*	144	80.5 ± 0.4	18 ± 1
0.53	▲	153	82.3 ± 0.2	18.3 ± 0.6
2.6	○	754	87.5 ± 0.5	20 ± 3

In soda-lime-silica glass, the total iron concentration has a significant effect on the calculated redox reaction enthalpy and entropy as well. But in this type of glass, the divalent form of iron, Fe<sup>2+</sup>, is favoured at low iron contents. This can be seen clearly from figure 6.18, because the formal potential  $E^{0'}$  (and therefore also the redox reaction equilibrium constant  $K^{**}(T)$ ) is higher for low iron concentrations than for high iron contents. Probably the ratio of activity coefficients of Fe<sup>2+</sup> and Fe<sup>3+</sup> in soda-lime-silica glass also depend on the concentrations, but suprisingly enough in the opposite way as in TV-screen glass.

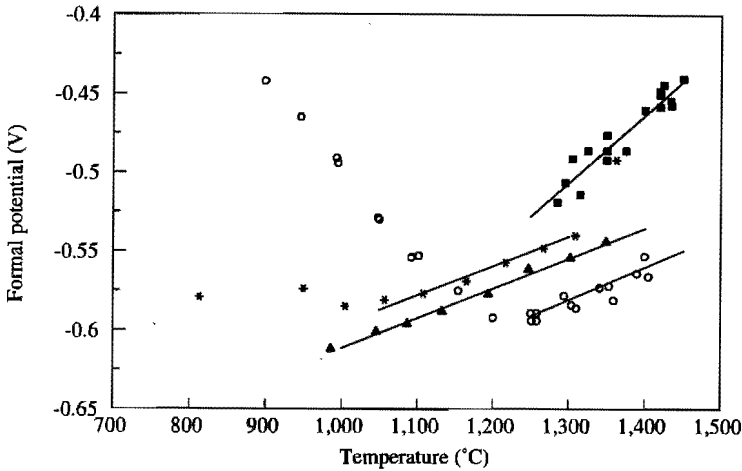


Figure 6.18

The formal potential of the iron reduction in soda-lime-silica glass containing 0.1 (■), 0.50 (\*), 0.53 (▲) or 2.6 (○) weight-%  $\text{Fe}_2\text{O}_3$  as a function of the temperature

The difference in the behaviour of iron at increasing iron contents in soda-lime-silica glass and TV-screen glass indicates that measurements, made in one type of glass, can not be used to predict the equilibrium state in glasses with different compositions. Even if the redox reaction equilibrium constants at a given iron concentration are equal in two glasses, they may be very different at other iron concentrations.

From the measurements it is clear that the equilibrium constant  $K^{**}(T)$ , as defined in equation 3.9 depends on the total iron concentration. This is probably due to the fact that the activities of  $\text{Fe}^{2+}$ ,  $\text{Fe}^{3+}$  and  $\text{O}^{2-}$  do depend on the iron concentration. Equation 3.4 should be used to describe the actual redox reaction equilibrium in the glass melt. However, the activities of  $\text{Fe}^{2+}$  and  $\text{Fe}^{3+}$  are generally unknown. The data presented in this thesis are too few to estimate the ratio of the activities of  $\text{Fe}^{2+}$  and  $\text{Fe}^{3+}$ .

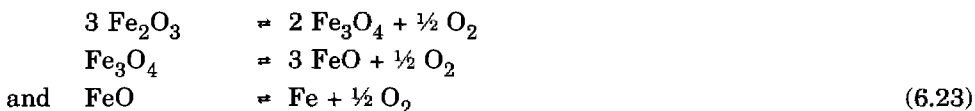
For practical application, the redox reaction equilibrium constant  $K^{**}(T)$  as defined in equation 3.9 is much more convenient than  $K(T)$ , as defined in equation 3.4. This brings on, that for iron the redox reaction equilibrium constant  $K^{**}(T)$  should be determined for any glass composition as a function of the iron concentration.



### 6.2.3.6 Deviating results at lower temperatures

At temperatures less than 1050°C, the formal potential of the iron reduction in TV-screen glass containing 0.4 weight-% Fe<sub>2</sub>O<sub>3</sub> seems to increase again (see figure 6.7 and figure 6.13). According to Freude [20] and Rüssel [11], the reduction of iron at low temperatures occurs in two steps. This theory is based on thermodynamical data on the reactions of iron in the pure Fe-O-system.

In pure solid Fe-O phases, iron can be present as Fe<sub>2</sub>O<sub>3</sub>, Fe<sub>3</sub>O<sub>4</sub>, FeO and Fe. The following reactions can occur:



Fe<sup>3+</sup> can also be reduced to Fe<sup>2+</sup> in one step:



With the aid of thermodynamic tables [21] the standard free energy  $\Delta G^0$  of these reactions in the pure solid phases can be calculated for any temperature T. Now the standard potential  $E^0$  of these reactions, relative to the Normal Hydrogen Electrode (see chapter 5.1) can be calculated by:

$$E^0(T) = - \frac{\Delta G^0(T)}{n \cdot F} \quad (6.25)$$

Rüssel [11] and Freude [20] assume, that the potential of the reference electrode used in this study would be equal to the potential of the Normal Hydrogen Electrode if the reference gas was pure O<sub>2</sub>. This means that the use of air as reference gas causes a shift in potential relative to the potential of the Normal Hydrogen Electrode of (see equation 5.33):

$$\frac{R_g \cdot T}{4 \cdot F} \ln \frac{p_{\text{O}_2}(\text{air})}{p_{\text{O}_2}(\text{pure O}_2)} = \frac{R_g \cdot T}{4 \cdot F} \ln 0.21 \quad (6.26)$$

The standard potentials of the reactions 6.23 and reaction 6.24 relative to the reference electrode flushed with air can now be obtained by adding the factor from equation 6.26 to the calculated standard potential  $E^0$ . In figure 6.19, the theoretical standard potentials of the different reduction steps of iron (in the pure solid phase) are plotted against the temperature.

According to Rüssel [11] and Freude [20], the reduction of iron in glass melts containing about 0.4 weight-% Fe<sub>2</sub>O<sub>3</sub> at relatively low temperatures occurs in two steps. The first reduction step, Fe<sub>2</sub>O<sub>3</sub> → Fe<sub>3</sub>O<sub>4</sub>, takes place at potentials,

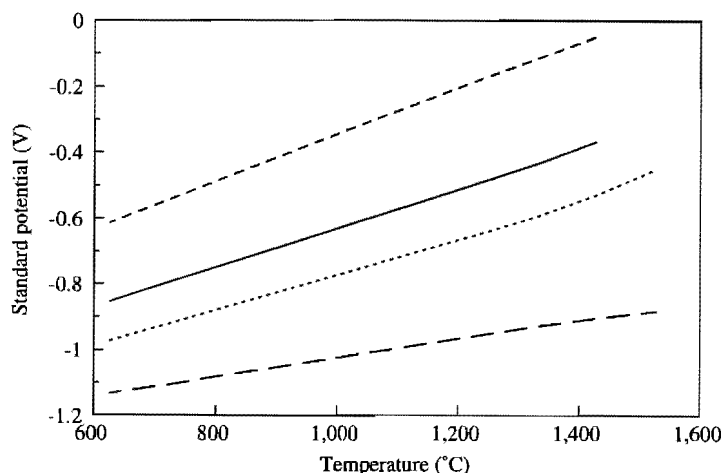
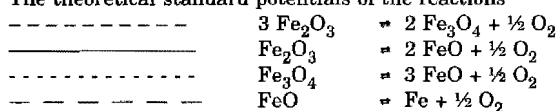


Figure 6.19

The theoretical standard potentials of the reactions



with regard to the potential of the reference electrode flushed with air as a function of temperature

higher than the formal potential of reaction 6.24. The second reduction step,  $\text{Fe}_3\text{O}_4 \rightarrow \text{FeO}$ , takes place at far lower potentials and can not be seen in the square wave voltammograms presented in this thesis. However, this second reduction step has been observed by Rüssel [11] and Freude [20].

At relatively high temperatures, the reduction occurs in one step:  $\text{Fe}^{3+} \rightarrow \text{Fe}^{2+}$  (reaction 6.24). At intermediate temperatures a transition area exists [11]. The position of this transition area depends on the total iron concentration and the composition of the glass melt [11]. In figure 6.20, the measured formal potentials of the iron reduction in TV-screen glass type A are compared to the theoretical potentials of the different reactions in the pure solid phases. Apparently the measurements at temperatures between 800 and 1050°C are located in the "transition area".

At higher iron concentrations, the transition area shifts towards higher temperatures. This means that at higher concentrations, the reduction of iron occurs in two steps, even at higher temperatures. This is also in accordance with the data measured in soda-lime-silica glass.

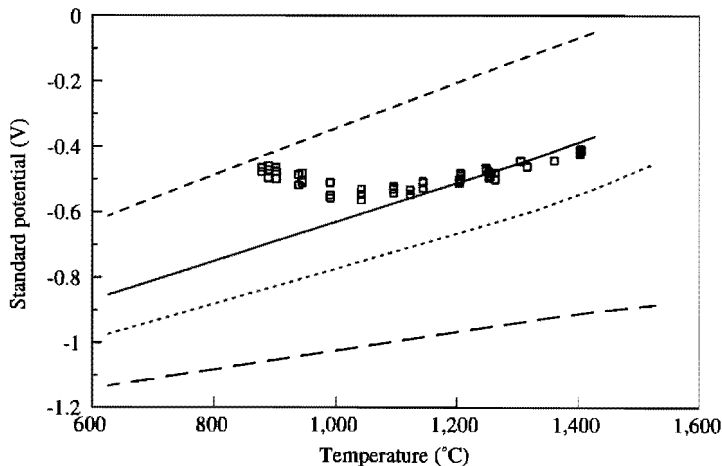


Figure 6.20

The measured formal potentials ( $\square$ ) of the iron reduction in TV-screen glass type A containing 0.4 weight-%  $\text{Fe}_2\text{O}_3$ , and the theoretical standard potentials of the different reduction steps of iron in the pure solid Fe-O system, as functions of the temperature

At a concentration of 0.5 weight-%  $\text{Fe}_2\text{O}_3$  the transition area is observed up to  $\pm 1050^\circ\text{C}$ , and at a concentration of 2.6 weight-%, the transition range exceeds up to  $1250^\circ\text{C}$  (see figure 6.18). At low iron concentrations, the reduction takes place in only one step at any temperature.

According to Rüssel [11], the reasonably fair agreement between the measured reaction potentials and the theoretical potentials for the pure solid Fe-O system (especially at high iron contents) indicate that in the molten glass with relatively high iron contents iron clustering occurs. The iron clusters have properties similar to those of crystalline species such as  $\text{Fe}_2\text{O}_3$ ,  $\text{Fe}_3\text{O}_4$  and FeO. This theory indeed offers an adequate explanation for the anomalies in the  $E^0(T)$  curve. The question on the number of electrons transferred during the reduction of iron at high temperatures still remains unsolved.

#### 6.2.3.7 Square wave voltammetry measurements in E-glass

The electrical conductivity in E-glass is poor (see chapter 5.3). The  $i\text{-}R_u$  measurements show that the uncompensated resistance in E-glass is indeed one order of magnitude higher than in soda-lime-silica and TV-screen glass. The capacity of the electrochemical double layer in E-glass does not differ much

from those in the other glasses. But in the square wave voltammetry experiments, the contribution of the charging current to the total current is relatively large because the charging current  $i_c$  depends both on the uncompensated resistance  $R_u$  and the capacity of the double layer  $C_D$ :

$$i_c = \frac{E}{R_u} \cdot \exp \left\{ \frac{-t}{R_u \cdot C_D} \right\} \quad (6.27)$$

The contribution of the charging current becomes less at a low frequency  $f$ . But then the faradaic current is also lower. This diminishes the sensitivity of the measurement. The frequency for the square wave voltammetry measurements should therefore not be lower than 10 Hz. Besides, the furnace is switched off during the measurement. If the frequency was set to a value of less than 10 Hz, the scan time would be about one minute (see equation 6.12). Then the temperature in the furnace and the glass melt would fall during the measurements.

The poor electrical conductivity in E-glass provides for a substantial charging current throughout the square wave voltammetry measurements. This can clearly be seen in figure 6.21. In this figure, the "forward", "reverse" and "differentiated" currents, recorded during a square wave voltammetry measurement in E-glass containing 0.5 weight-%  $\text{Fe}_2\text{O}_3$  at  $1400^\circ\text{C}$  are plotted against the base potential. Both  $i_f$  and  $i_r$  show a continuously increasing line, almost linearly with the base potential. Superimposed on an increasing line, the (positive) peak in  $i_f$  and the (negative) peak in  $i_r$  due to the redox reaction can be seen vaguely.

In the curve of the differentiated current  $\delta i$ , the peak resulting from the reduction of iron can be seen more clearly (see figure 6.22). The peak however is not symmetrical. Comparison of the recorded voltammogram with theoretical voltammograms shows that this asymmetrical shape does not arise due to a quasi-reversible or an irreversible reaction, but to a reversible one-electron reaction slightly deformed by the charging current.

The position of the peak can be obtained from the theoretical curve that best fit the recorded curve. The accuracy is  $\pm 5$  mV. The peak in figure 6.22 is located at  $-0.352$  V ( $\pm 0.005$  V).

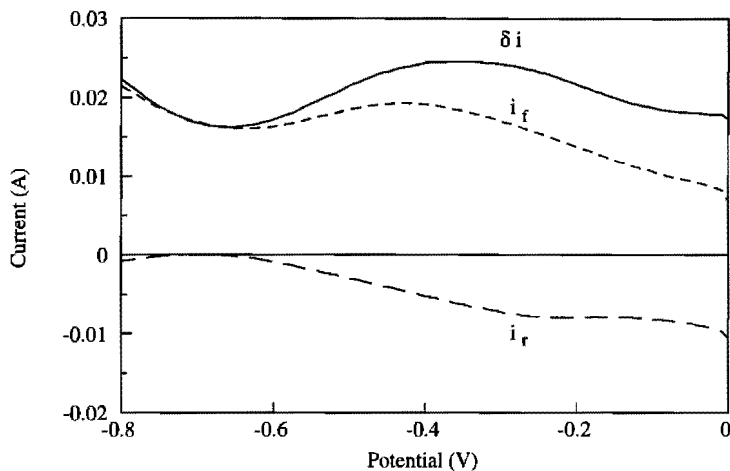


Figure 6.21

The square wave voltammogram with  $i_f$  and  $i_r$  recorded in E-glass containing 0.5 weight-%  $\text{Fe}_2\text{O}_3$  at  $1400^\circ\text{C}$  with the following set-up:

$$\Delta E_b = 0.002 \text{ V}$$

$$\Delta E_p = 0.1 \text{ V}$$

$$f = 50 \text{ Hz}$$

$$R_u = 5.82 \ \Omega$$

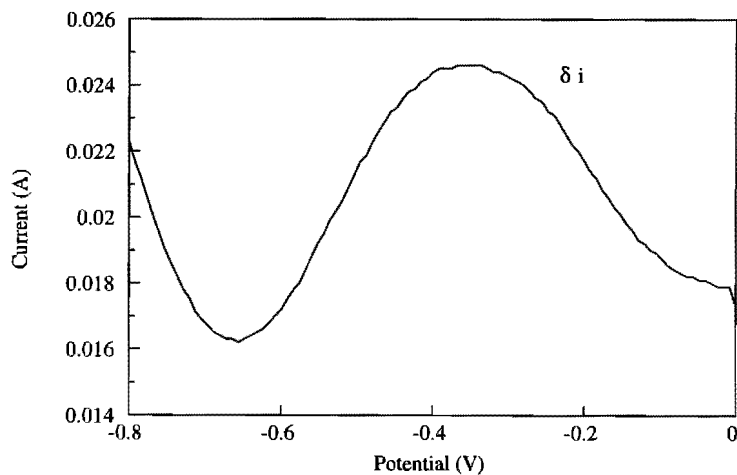


Figure 6.22

The resulting square wave voltammogram recorded in E-glass containing 0.5 weight-%  $\text{Fe}_2\text{O}_3$  at  $1400^\circ\text{C}$  with the following set-up:

$$\Delta E_b = 0.002 \text{ V}$$

$$\Delta E_p = 0.1 \text{ V}$$

$$f = 50 \text{ Hz}$$

$$R_u = 5.82 \ \Omega$$

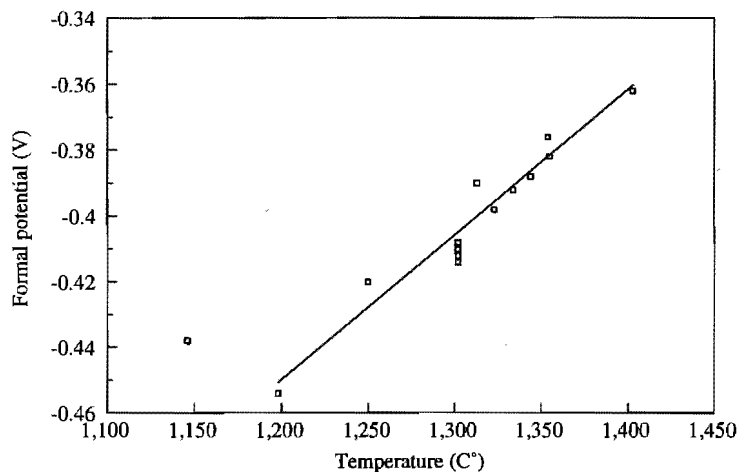


Figure 6.23

The formal potential of the iron reduction in E-glass (□) containing about 0.5 weight-%  $\text{Fe}_2\text{O}_3$  as a function of temperature

Square wave experiments have been performed in E-glass containing 0.5 weight-%  $\text{Fe}_2\text{O}_3$  at temperatures between 1000 and 1400°C. In figure 6.23, the obtained formal potentials are given as a function of temperature. The calculated redox reaction enthalpy and entropy are given in table 6.4.

Table 6.4

The redox reaction enthalpy and entropy for the iron reduction in E-glass containing 0.5 weight-%  $\text{Fe}_2\text{O}_3$

$\Delta H^{**} = 106 \text{ kJ}\cdot\text{mole}^{-1} \pm 0.6 \text{ kJ}\cdot\text{mole}^{-1}$ $\Delta S^{**} = 42.5 \text{ J}\cdot\text{mole}^{-1}\cdot\text{K}^{-1} \pm 3 \text{ J}\cdot\text{mole}^{-1}\cdot\text{K}^{-1}$
--

#### 6.2.4 Comparison of the results of oxygen equilibrium pressure measurements and square wave voltammetry measurements

In three glass melts, both oxygen equilibrium pressure measurements and square wave voltammetry measurements have been performed. The results are summarized together in table 6.5. As can be seen, the results obtained by both methods are in excellent agreement.

Table 6.5

The redox reaction enthalpy and entropy for the iron reduction in three glass melts, derived from oxygen equilibrium pressure measurements and square wave voltammetry measurements

Glass	Concentration $\text{Fe}_2\text{O}_3$ (weight-%)	Oxygen equilibrium pressure measurements		Square wave voltammetry measurements	
		$\Delta H^{**}$ (kJ·mole <sup>-1</sup> )	$\Delta S^{**}$ (J·mole <sup>-1</sup> ·K <sup>-1</sup> )	$\Delta H^{**}$ (kJ·mole <sup>-1</sup> )	$\Delta S^{**}$ (J·mole <sup>-1</sup> ·K <sup>-1</sup> )
TV type A	0.4	100	37	102	37
TV type B	0.4	99	42	102	41
E-glass	0.5	105	43	106	42.5

## 6.2.5 Comparison of the results with data from literature

### 6.2.5.1 Data from the literature

Johnston [12] equilibrated  $\text{Na}_2\text{O} \cdot 2\text{SiO}_2$  glass melts containing 2.5 weight-%  $\text{Fe}_2\text{O}_3$  with atmospheres with various partial oxygen pressures. After cooling down to room temperature, the glass samples were analysed for  $\text{Fe}^{2+}$  and total iron or  $\text{Fe}^{3+}$ . Johnston found that the redox ratio ( $[\text{Fe}^{2+}]/[\text{Fe}^{3+}]$ ) is proportional to the negative fourth root of the partial oxygen pressure at a given temperature, indicating that the redox reaction equilibrium constant as defined in equation 6.10 contains the correct ratio of  $\text{Fe}^{2+}$ ,  $\text{Fe}^{3+}$  and  $p_{\text{O}_2}$  for a given glass composition, temperature and iron content. The basicity number of  $\text{Na}_2\text{O} \cdot 2\text{SiO}_2$  as defined by Sun is 41.7.

Paul and Douglas [10] equilibrated various binary alkali silicate glasses containing 0.4 weight-%  $\text{Fe}_2\text{O}_3$  at 1400°C with air ( $p_{\text{O}_2}=0.21$  bar). The glasses were subsequently cooled to room temperature and  $\text{Fe}^{2+}$  and total iron concentration were determined. The composition of the glass had a significant influence on the final redox ratio. The basicity number of the samples varied between 26 and 51. At higher basicity numbers, the percentage of iron in the divalent state  $\text{Fe}^{2+}$  was smaller than at low basicity numbers.

At equal basicity numbers, the percentage  $\text{Fe}^{2+}$  in binary lithium, sodium and potassium silicate glasses were not equal. This indicates that the redox ratio of a glass with basicity number  $x$ , for a certain temperature and oxygen equilibrium pressure, can not be estimated from redox ratios measured in different glasses even with the same basicity number.

According to Paul [10] the total iron concentration has an effect on the percentage of iron present in the divalent state in the glass under otherwise equal conditions if the iron concentration is less than 1 weight-%. He found that the divalent state was favoured at low iron concentrations in alkali disilicate glasses. This is in agreement with the results presented in this thesis for soda-lime-silica glass. However, the measurements presented in this thesis indicate that in TV-screen glass relatively more iron is present in the trivalent state at low iron concentrations. An explanation for this phenomenon might be found in concentration and glass composition dependent activity coefficients for  $\text{Fe}^{2+}$  and  $\text{Fe}^{3+}$ .

Goldman [22] found, that the redox ratio  $[\text{Fe}^{2+}]/[\text{Fe}^{3+}]$  in a Ca-Al-borosilicate melt, in equilibrium with air, was 0.212 at 1260°C. The total iron content in this glass was 0.3 % Fe ( $\pm 1$  weight-%  $\text{Fe}_2\text{O}_3$ ). Goldman used the high-temperature spectral emission technique developed by Berg (see chapter 4.3.1).

Takahashi [23] measured the half wave potential  $E_{1/2}$  of the redox reaction of iron at 1250°C in  $\text{Na}_2\text{O}\cdot 2\text{SiO}_2$  and soda-lime-silica glass containing about 2.7 weight-%  $\text{Fe}_2\text{O}_3$  with Cyclic Voltammetry. Assuming that the diffusion coefficients of  $\text{Fe}^{2+}$  and  $\text{Fe}^{3+}$  are about the same, the redox reaction equilibrium  $K^{**}(T)$  can be derived from the half wave potential by applying equations 5.16 and 5.66. The equilibrium constant at 1250°C for the iron reaction appeared to be about 0.027. Cyclic Voltammetry is much less sensitive than Square Wave Voltammetry, because the peaks in the voltammograms are much broader. The establishment of the exact position of the peak is difficult.

Rüssel [6,11] measured the half wave potential of the iron reaction in different soda-lime-silica glasses at various temperatures using Square Wave Voltammetry. The basicity number of the glasses ranges from 29 to 44. At high iron concentrations (more than 1 weight-%) the reduction of iron appeared to take place in two steps. At lower concentrations (0.3 to 1 weight-%) the reduction occurs in one step. The equilibrium constant of this one-step reduction reaction can be calculated from the half wave potential with the aid of equations 5.16 and 5.66.



Oxygen equilibrium pressure measurements using an oxygen sensor were made by Tran [24] in  $\text{Na}_2\text{O}\cdot 2\text{SiO}_2$  containing about 5 weight-%  $\text{Fe}_2\text{O}_3$ . After the measurements the samples were cooled quickly to room temperature and the concentration of  $\text{Fe}^{2+}$  and the total iron concentration were determined.

### 6.2.5.2 Graphical presentations of the data from literature and own measurements

The data on the redox ratios from the literature have been converted to reaction equilibrium constants  $K^{**}(\text{T})$  as defined in equation 6.10. In figures 6.24a, b and c, the natural logarithm of the  $K^{**}(\text{T})$ 's have been plotted against the reciprocal temperature. Straight lines should be obtained with a slope equal to  $-\Delta H^{**}/R_g$ , and an intersect at  $\Delta S^{**}/R_g$  (assuming  $\Delta H^{**}$  and  $\Delta S^{**}$  to be independent of the temperature). In the plots, the results presented in this thesis are included.

The data can also be expressed as redox ratios in glass melts, that are equilibrated with air ( $p_{\text{O}_2}=0.21$  bar) at any given temperature. Then the data from the oxygen equilibrium pressure measurements and square wave voltammetry measurements must be converted to redox ratios:

$$\frac{[\text{Fe}^{2+}]}{[\text{Fe}^{3+}]} = \frac{K^{**}(\text{T})}{p_{\text{O}_2}^{1/4}} = \frac{K^{**}(\text{T})}{0.21^{1/4}} \quad (6.28)$$

It is more convenient to express the redox ratio as the percentage of iron in the divalent state:

$$\% \text{ Fe}^{2+} = 100\% * \frac{[\text{Fe}^{2+}]}{[\text{Fe}^{2+}] + [\text{Fe}^{3+}]} \quad (6.29)$$

or:

$$\% \text{ Fe}^{2+} = 100\% * \frac{K^{**}(\text{T})}{K^{**}(\text{T}) + p_{\text{O}_2}^{1/4}} = 100\% * \frac{K^{**}(\text{T})}{K^{**}(\text{T}) + 0.21^{1/4}} \quad (6.30)$$

The percentage of iron in the divalent state (with  $p_{\text{O}_2}=0.21$  bar) is plotted against the temperature in figures 6.25a, b and c. Now the relative shift of the redox reaction equilibrium (at constant oxygen pressure) can be seen more easily. Furthermore it is clear from these figures that in soda-lime-silica glass, the divalent form of iron,  $\text{Fe}^{2+}$ , is favoured at lower iron contents. In TV-screen glass, it is exactly the opposite.

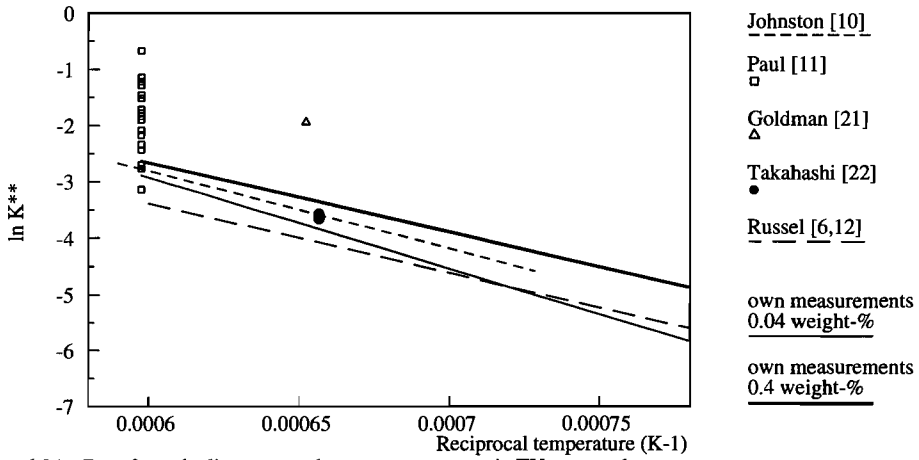


Figure 6.24a: Data from the literature and own measurements in TV-screen glass

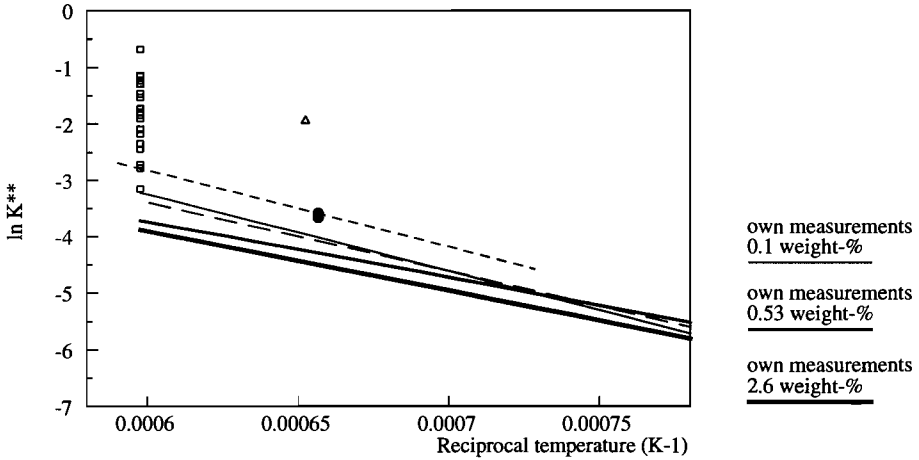


Figure 6.24b: Data from the literature and own measurements in soda-lime-silica glass

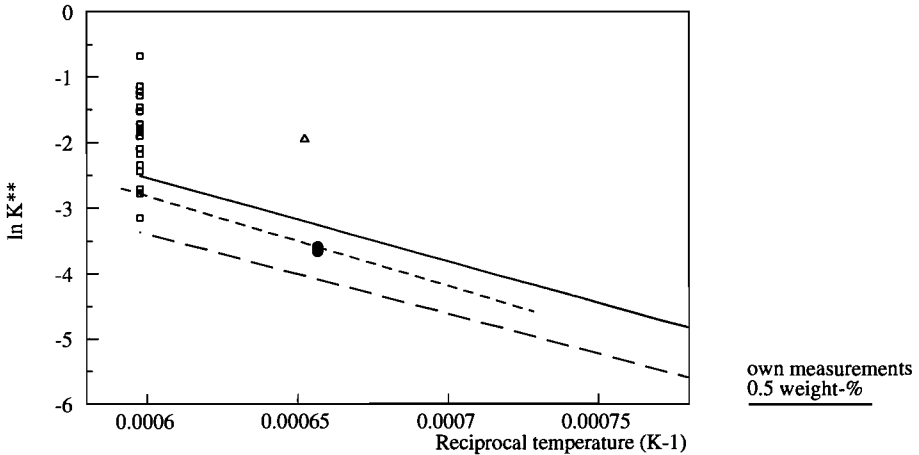


Figure 6.24c: Data from the literature and own measurements in E-glass presented as  $\ln K^{**}(T)$  as a function of the reciprocal temperature

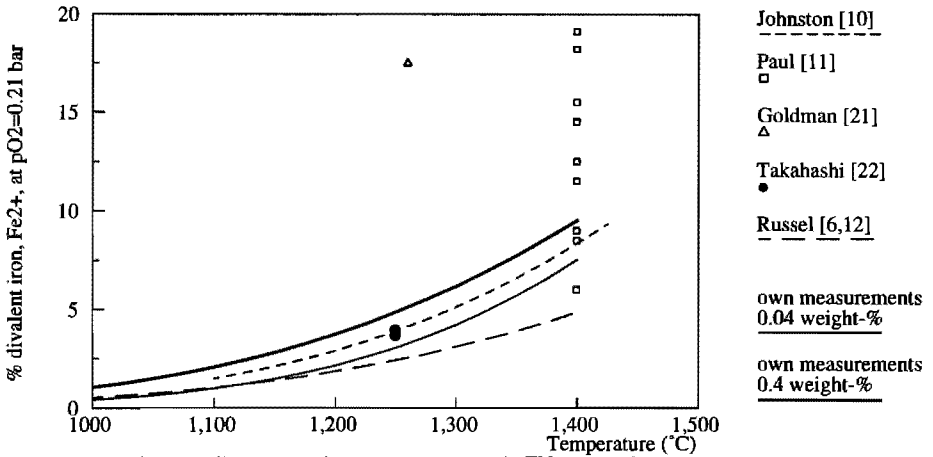


Figure 6.25a: Data from the literature and own measurements in TV-screen glass

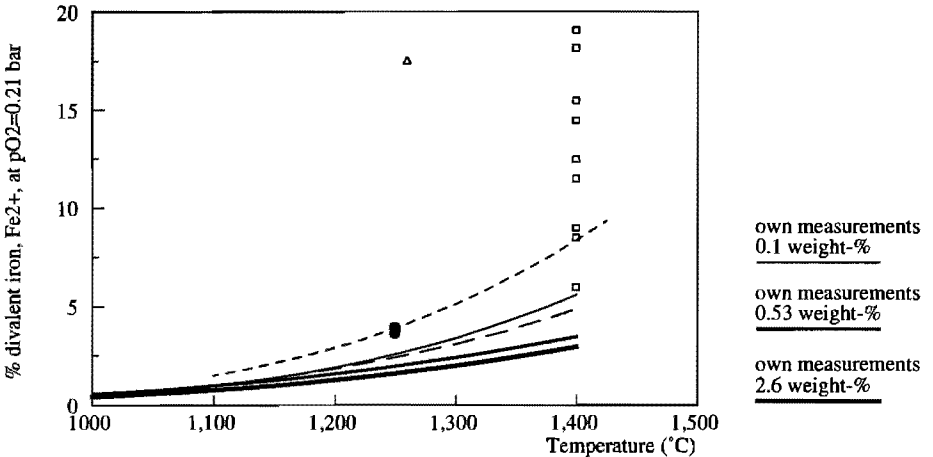


Figure 6.25b: Data from the literature and own measurements in soda-lime-silica glass

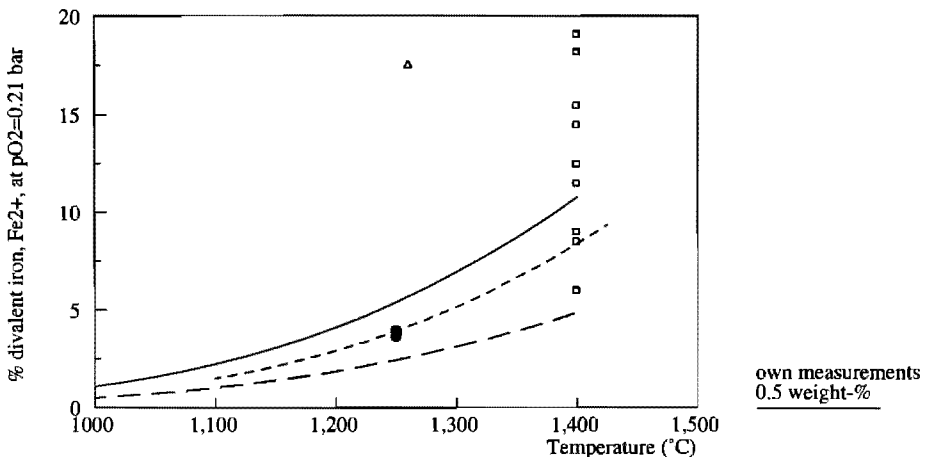


Figure 6.25c: Data from the literature and own measurements in E-glass presented as %Fe<sup>2+</sup> (at pO<sub>2</sub>=0.21 bar) as a function of the temperature

One must keep in mind however, that industrially molten glass is usually not in equilibrium with air. The percentage of divalent iron in industrial glass melts can therefore not be read from the plot directly. Furthermore, at a change in temperature the oxygen pressure changes. The plot can not be used to determine the amount of iron, that is reduced at an increase of temperature. The absolute shift of reaction 6.7 (or 6.21) is not represented in this plot.

The compositions of the glasses investigated in the literature and in this thesis are generally different, as well as the iron concentration in these glasses. Therefore a comparison is not possible. However, the calculated redox reaction equilibrium constants appear to be in the correct order of magnitude.

### 6.2.6 Conclusions

- Oxygen equilibrium pressure measurements can be used for the determination of the enthalpy and entropy of the iron reduction in soda-lime-silica, TV-screen and E-glass melts;
- square wave voltammetry measurements can be used for the determination of the enthalpy and entropy of the iron reduction in soda-lime-silica, TV-screen and E-glass melts;
- the results of oxygen equilibrium pressure measurements and square wave voltammetry measurements for molten glass with iron as the only polyvalent ion are in good agreement;
- the calculated redox reaction equilibrium constants are in the same order of magnitude as the equilibrium constants, derived from the literature, although the compositions of these glasses and the iron concentrations differ;
- the reaction equilibrium state for the iron reduction can be described with the redox reaction equilibrium constant  $K^{**}(T)$ . The value of  $K^{**}(T)$  can be calculated with the aid of equation 6.10 and the values of  $\Delta H^{**}$  and  $\Delta S^{**}$  as given in tables 6.1 to 6.5, but only for the given glass composition and iron concentration;
- an estimation of the redox reaction equilibrium constant can not be made on the basis of the redox reaction equilibrium constant for another glass composition or iron concentration. Only if the redox reaction equilibrium constant is known in two glasses with slightly different compositions and the same iron concentration, the redox reaction equilibrium constant in a third glass with an intermediate composition and the same iron concentration may be estimated with a reasonable accuracy;

- at low iron concentrations, the  $\text{Fe}^{3+}$  state is favoured in TV-screen glass and the  $\text{Fe}^{2+}$  state is favoured in soda-lime-silica glass with regard to the redox equilibrium in glasses with a higher iron content;
- the questions on the reaction mechanism and the different kinds of iron species in molten glasses with high Fe-concentration are still undissolved.

### 6.3 ANTIMONY

#### 6.3.1 Antimony in glass

Antimony is used as the fining agent in TV-screen glasses. The fining reaction is generally described by [12,14]:



and the redox reaction equilibrium constant  $K^{**}(\text{T})$  can be defined as:

$$K^{**}(\text{T}) = \frac{[\text{Sb}^{3+}] \cdot \sqrt{p_{\text{O}_2}}}{[\text{Sb}^{5+}]} = \exp \left\{ \frac{-\Delta H^{**}}{R_g \cdot T} + \frac{\Delta S^{**}}{R_g} \right\} \quad (6.32)$$

The antimony can be added to the batch in the pentavalent or trivalent form. In the second case, an oxidizing agent has to be added to convert the antimony to the pentavalent state before the melting temperature has been reached.

At the melting temperature, the pentavalent antimony will dissociate to the trivalent state according to equation 6.31, coupled with a release of  $\text{O}_2$  in the melt. The fining gas then diffuses to existing bubbles, causing them to grow. The enlarged bubbles easily ascend to the surface of the melt (see chapter 2.6). At a decrease of temperature, the equilibrium state of reaction 6.31 will shift to the left, and the trivalent antimony is able to take up the excess of  $\text{O}_2$  from the melt and the remaining small oxygen-containing bubbles (chapter 3.3.2).

The antimony concentration usually ranges between 0.4 and 0.6 weight-%  $\text{Sb}_2\text{O}_3$ . In the literature, some data on the redox reaction equilibrium constant of reaction 6.31 have been derived by wet-chemical analysis of the quenched glass sample [12] or by square wave voltammetry measurements [6], but the antimony concentrations in these experiments have been in the order of some weight-%  $\text{Sb}_2\text{O}_3$  in sodium disilicate [12] and soda-lime-silica glasses [6]. In this thesis, the redox reaction equilibrium constant of the antimony reduction in TV-screen glasses (types A and B) with concentrations of 0.4 to 2.4 weight-%

$\text{Sb}_2\text{O}_3$  is investigated by oxygen equilibrium pressure measurements and square wave voltammetry measurements.

### **6.3.2 Oxygen equilibrium pressure measurements**

#### **6.3.2.1 Experimental procedure**

The glasses were prepared by adding the desired amount of  $\text{Sb}_2\text{O}_5$  to reagent grade chemicals ( $\text{Si}_2\text{O}$ ,  $\text{Na}_2\text{CO}_3$ ,  $\text{BaCO}_3$  etc), or to technical raw batch materials containing impurities of iron (up to a concentration of about 0.04 weight-%  $\text{Fe}_2\text{O}_3$ ). The batches were melted at  $1400^\circ\text{C}$  in platinum crucibles until the glasses contained no grains and hardly any bubbles. Then the glasses were cooled down quickly and transferred to  $\text{Al}_2\text{O}_3$ -crucibles. These crucibles were heated slowly to  $1400^\circ\text{C}$  in the furnace as sketched in figure 5.3. At this temperature the electrodes were lowered until the reference electrode (electrode 2 in figure 5.3) just touched the melt.

#### **6.3.2.2 The measured potential difference**

The potential difference between the counter electrode (electrode 3 in figure 5.3) and the reference electrode was measured. The reference electrode was flushed with clean, dry air. As soon as the potential difference reached a stable value, the temperature of the furnace was decreased by  $3^\circ\text{C}/\text{min}$  down to  $800^\circ\text{C}$  while the potential difference was measured. Subsequently the temperature was increased again by  $3^\circ\text{C}/\text{min}$  to  $1400^\circ\text{C}$ .

Generally, the measured potential difference followed the same course during decrease and increase of the temperature. This indicates that the redox reaction that causes the potential difference at changes in temperature is reversible. Furthermore, it indicates that the total concentration of antimony remains constant during the experiment.

#### **6.3.2.3 Calculated oxygen equilibrium pressure**

The oxygen equilibrium pressure in the glass melt was calculated with the aid of equation 6.8. The oxygen equilibrium pressure as a function of temperature has been used to calculate the enthalpy and entropy of the redox reaction 6.31. The results are summarized in chapter 6.3.2.5.

#### **6.3.2.4 Calculated enthalpy and entropy**

The change in oxygen equilibrium pressure in the molten glass at a change in temperature from  $T_1$  to  $T_2$  can be described by:

$$L_{O_2}(T_1) \cdot p_{O_2}(T_1) - L_{O_2}(T_2) \cdot p_{O_2}(T_2) = \frac{1}{2} \cdot C_{Sb} \cdot \left\{ \frac{K^{**}(T_1)}{K^{**}(T_1) + p_{O_2}^{1/2}(T_1)} - \frac{K^{**}(T_2)}{K^{**}(T_2) + p_{O_2}^{1/2}(T_2)} \right\} \quad (6.33)$$

This equation is valid as long as the total antimony concentration remains constant, and no exchange of oxygen between melt and atmosphere takes place. We assume that these requirements are fulfilled if the oxygen equilibrium pressure remains below 0.5 bar.

With the aid of a computer program, the values of  $\Delta H^{**}$  and  $\Delta S^{**}$  (as defined in equation 6.32) that best describe the redox reaction of antimony as presented in equation 6.31 were calculated. The physical solubility of oxygen  $L_{O_2}$  is assumed to be  $1 \text{ mole} \cdot \text{m}^{-3} \cdot \text{bar}^{-1}$  (see chapter 6.8).

In figure 6.26, the potential difference between the counter and the reference electrode in a TV-screen glass type A containing 0.4 weight-%  $\text{Sb}_2\text{O}_3$  is given as a function of temperature. The measured potential difference can be described mathematically with equation 6.33, when the enthalpy  $\Delta H^{**}$  is set to a value of  $219 \text{ kJ} \cdot \text{mole}^{-1}$  and the entropy  $\Delta S^{**}$  is  $138 \text{ J} \cdot \text{mole}^{-1} \cdot \text{K}^{-1}$ .

In figure 6.27, the calculated oxygen equilibrium pressure is given as a function of temperature.

### 6.3.2.5 Results of the oxygen equilibrium pressure measurements

The procedure outlined in sections 6.3.2.1 to 6.3.2.4 was followed in TV-screen glass type A and B with different antimony concentrations. The results of the calculation of the redox reaction enthalpy and entropy are given in table 6.6.

For a better comparison of the results, the percentages of the antimony in the trivalent form  $\text{Sb}^{3+}$  have been calculated for three different temperatures with the assumption that the melts are equilibrated with air ( $p_{O_2}=0.21 \text{ bar}$ ):

$$\% \text{ Sb}^{3+}(T) = \frac{100\% \cdot K^{**}(T)}{K^{**}(T) + p_{O_2}^{1/2}} = \frac{100\% \cdot K^{**}(T)}{K^{**}(T) + 0.21^{1/2}} \quad (6.34)$$

As we can see from table 6.6, the reduced form of antimony,  $\text{Sb}^{3+}$ , seems to be favoured at the higher antimony content for TV-screen glass type A.

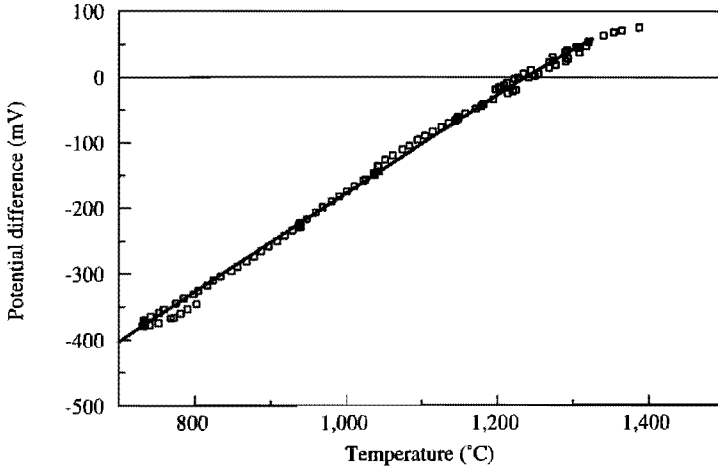


Figure 6.26

The measured ( $\square$ ) potential difference between the platinum plate and the reference electrode in a TV-screen glass type A containing 0.4 weight-%  $\text{Sb}_2\text{O}_3$  as a function of temperature. The theoretical curve (—) was calculated with:

$$C_{\text{Sb}} = 63 \text{ mole}\cdot\text{m}^{-3} \quad \Delta H^{**} = 219 \text{ kJ}\cdot\text{mole}^{-1}$$

$$p_{\text{O}_2}(1200^\circ\text{C}) = 0.089 \text{ bar} \quad \Delta S^{**} = 138 \text{ J}\cdot\text{mole}^{-1}\cdot\text{K}^{-1}$$

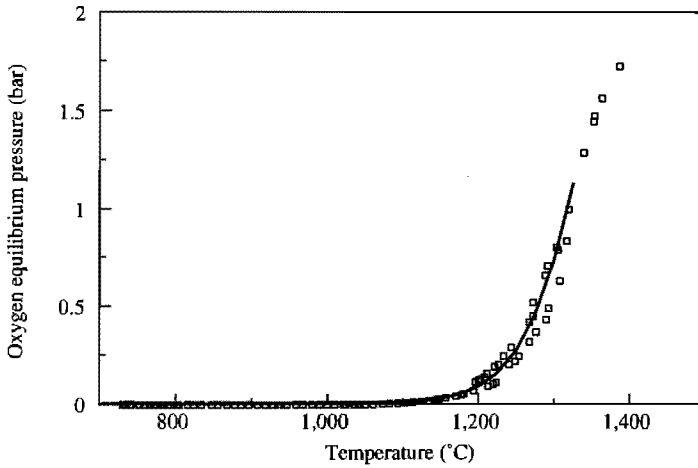


Figure 6.27

The oxygen equilibrium pressure ( $\square$ ) in a TV-screen glass type A containing 0.4 weight-%  $\text{Sb}_2\text{O}_3$  as a function of the temperature. The theoretical curve (—) was calculated with:

$$C_{\text{Sb}} = 63 \text{ mole}\cdot\text{m}^{-3} \quad \Delta H^{**} = 219 \text{ kJ}\cdot\text{mole}^{-1}$$

$$p_{\text{O}_2}(1200^\circ\text{C}) = 0.089 \text{ bar} \quad \Delta S^{**} = 138 \text{ J}\cdot\text{mole}^{-1}\cdot\text{K}^{-1}$$



Table 6.6

The results of oxygen equilibrium pressure measurements in two different TV-screen glasses containing antimony, expressed in redox reaction enthalpy and entropy changes

Glass	Concentration (weight-%)	$\Delta H^{**}$ (kJ·mole <sup>-1</sup> )	$\Delta S^{**}$ (J·mole <sup>-1</sup> ·K <sup>-1</sup> )	% Sb <sup>3+</sup> (p <sub>O2</sub> =0.21 bar)		
				1000°C	1200°C	1400°C
TV-screen type A	0.4	219 ± 11	138 ± 7	3.5	37.7	83.7
TV-screen type A	2.14	188 ± 9	134 ± 7	29.6	82.4	96.7
TV-screen type B	0.43	191 ± 10	121 ± 6	6.2	43.5	83.2
TV-screen type B	0.6	206 ± 10	121 ± 6	1.6	18.4	62.8

This is in accordance with the results from equilibrium measurements in TV-screen glass type A containing iron: at high iron concentrations, the reduced state Fe<sup>2+</sup> is favoured.

The antimony concentrations in both TV-screen glasses type B are in the same order of magnitude as in the first TV-screen glass type A. Therefore it can be expected that the redox ratios [Sb<sup>3+</sup>]/[Sb<sup>5+</sup>] in these glasses are about the same. For the TV-screen glass type B containing 0.43 weight-% Sb<sub>2</sub>O<sub>3</sub>, this assumption is correct; for the other glass, it is not. However, the glass containing 0.6 weight-% Sb<sub>2</sub>O<sub>3</sub> was made of technical raw batch materials and therefore contains also Fe<sub>2</sub>O<sub>3</sub>. This was not accounted for in the calculations of  $\Delta H^{**}$  and  $\Delta S^{**}$ . This means that a change in p<sub>O2</sub> is completely attributed to the antimony reaction. In practise, the oxygen equilibrium pressure is governed by the equilibrium states of the antimony and the iron reactions.

### 6.3.3 Square wave voltammetry measurements

#### 6.3.3.1 Experimental procedure

The glasses were prepared in the way described in section 6.3.2.1. The Al<sub>2</sub>O<sub>3</sub>-crucibles containing the glass was placed in the furnace sketched in figure 5.3. At 1400°C, the electrodes were lowered until the reference electrode just touched the melt. After a waiting time of 15 minutes, the uncompensated

resistance in the melt was measured (see section 5.3), and subsequently a square wave voltammogram was recorded. Generally the set-up for the measurements was:

Initial potential $E_i$ :	0 V
Final potential $E_{end}$ :	-0.8 V
Frequency $f$ :	100 Hz
Staircase increase of the base potential $\Delta E_b$ :	-0.002 V
Height of the potential pulse $\Delta E_p$ :	0.1 V

The currents were measured just before each change in potential.

### 6.3.3.2 Square wave voltammograms

#### The recorded voltammograms

The measurements were made at temperatures ranging from 1400°C to 800°C. Figure 6.28 shows the square wave voltammogram recorded in a TV-screen glass type A containing 2.14 weight-%  $Sb_2O_3$  at 1100°C. In this figure, the currents measured during the "forward" and "reverse" pulses are plotted against the base potential. Both curves display a clear peak, indicating that the redox reaction is reversible.

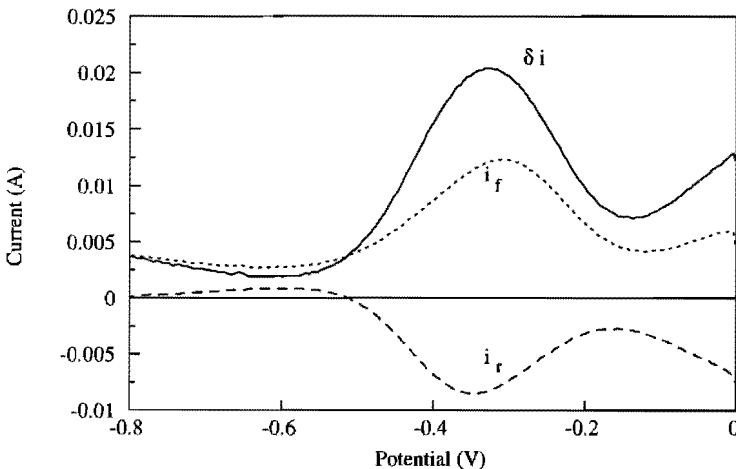


Figure 6.28

The complete square wave voltammogram recorded in TV-screen glass type A containing 2.14 weight-%  $Sb_2O_3$  at 1100°C with the following set-up:

$$\Delta E_b = 0.002 \text{ V} \quad \Delta E_p = 0.1 \text{ V} \quad f = 100 \text{ Hz} \quad R_u = 7.66 \Omega$$

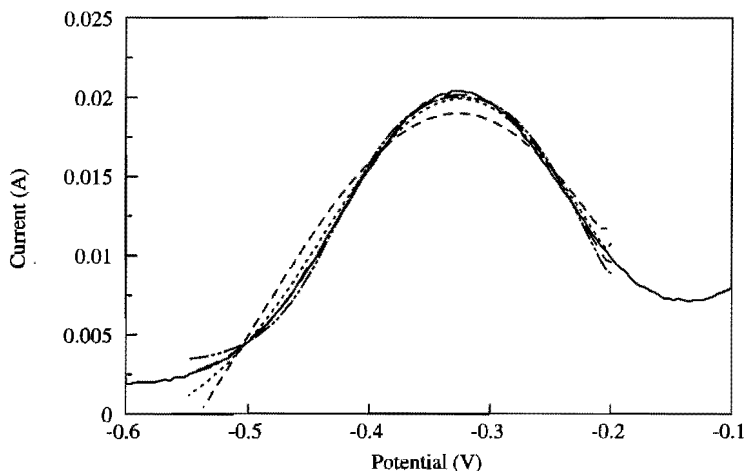


Figure 6.29

The square wave voltammogram (————) recorded in TV-screen glass type A containing 2.14 weight-%  $\text{Sb}_2\text{O}_3$  at  $1100^\circ\text{C}$  with the following set-up:

$$\Delta E_b = 0.002 \text{ V} \quad \Delta E_p = 0.1 \text{ V} \quad f = 100 \text{ Hz} \quad R_u = 7.66 \ \Omega$$

$$E_{1/2} = -0.325 \text{ V}$$

compared with theoretical square wave voltammograms for one (-----), two (.....), three (- . - . - .) and four (- - - - -) electron transfers

The current measured during the "reverse" pulse  $i_r$  is subtracted from the current measured during the preceding "forward" pulse  $i_f$ . The resulting current  $\delta i$  is plotted against the base potential in figure 6.29. This results in a clear, almost symmetrical peak at the half-wave potential (at  $-0.325 \text{ V} \pm 0.001 \text{ V}$ ) of the redox reaction. The curve is compared to theoretical curves for one, two, three and four electron transfers. The recorded curve agrees best with the theoretical curve describing a redox reaction during which three electrons are transferred. This indicates that the peak does not result from the reaction  $\text{Sb}^{5+} \rightarrow \text{Sb}^{3+}$ .

According to Rüssel [6] the peak can be attributed to the reduction of the trivalent form of antimony to metallic antimony. This reaction can be described by:



and the redox reaction equilibrium constant can be defined as:

$$K_{\text{Sb}^{3+}/\text{Sb}^0}^{**}(\text{T}) = \frac{[\text{Sb}^0] \cdot p_{\text{O}_2}^{3/4}}{[\text{Sb}^{3+}]} = \exp \left\{ \frac{-\Delta H_{\text{Sb}^{3+}/\text{Sb}^0}^{**}}{R_g \cdot T} + \frac{\Delta S_{\text{Sb}^{3+}/\text{Sb}^0}^{**}}{R_g} \right\} \quad (6.36)$$

It is not known if metallic antimony is really present in the bulk of the molten glass at high temperatures, or if a Pt/Sb-alloy could be formed.

The position of the peak in the  $\delta i$ -curve can be determined with an accuracy of 1 mV and a reproducibility of 10 mV. The reduction of the pentavalent to the trivalent form can not be seen in the square wave voltammogram between 0 and -0.8 V at these temperature levels.

### The effect of the temperature

At a decrease of the temperature, the peak resulting from the three-electron transfer shifts towards the negative direction, indicating that the equilibrium state of reaction 6.35 shifts towards the left (see figures 6.30 to 6.32). Furthermore, a second peak becomes visible at temperatures below 1000°C. This peak can be described theoretically with a two-electron transfer (see figure 6.30), and is therefore probably caused by the reduction of pentavalent to trivalent antimony.

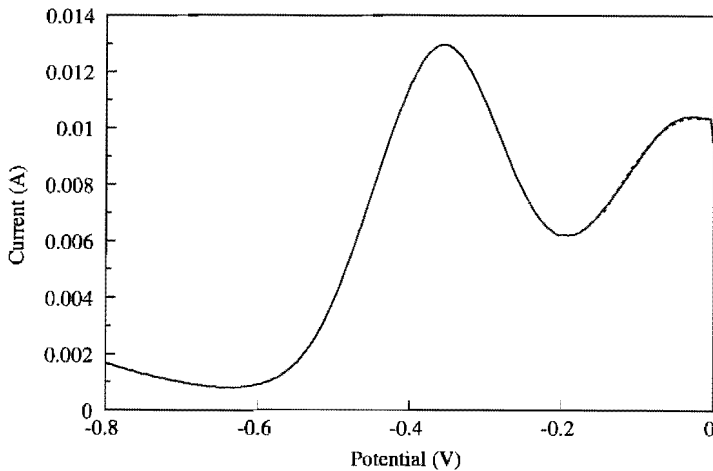


Figure 6.30

The square wave voltammogram recorded in TV-screen glass type A containing 2.14 weight-%  $\text{Sb}_2\text{O}_3$  at 1000°C with the following set-up:

$\Delta E_b = 0.002 \text{ V}$        $\Delta E_p = 0.1 \text{ V}$        $f = 100 \text{ Hz}$        $R_u = 13.7 \Omega$

$E_{1/2} = -0.356 \text{ and } -0.028 \text{ V}$

compared with the theoretical square wave voltammogram for a two electron transfer (-----)

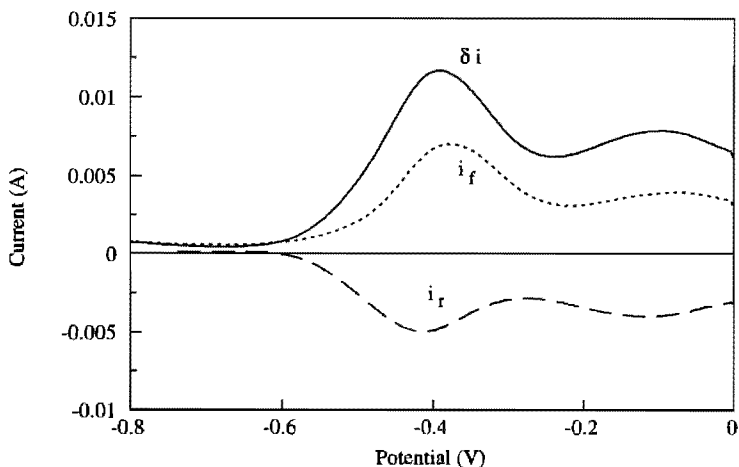


Figure 6.31

The complete square wave voltammogram recorded in TV-screen glass type A containing 2.14 weight-%  $\text{Sb}_2\text{O}_3$  at  $900^\circ\text{C}$  with the following set-up:

$$\Delta E_b = 0.002 \text{ V} \quad \Delta E_p = 0.1 \text{ V} \quad f = 100 \text{ Hz} \quad R_u = 29.6 \Omega$$

$$E_{1/2} = -0.391 \text{ and } -0.097 \text{ V}$$

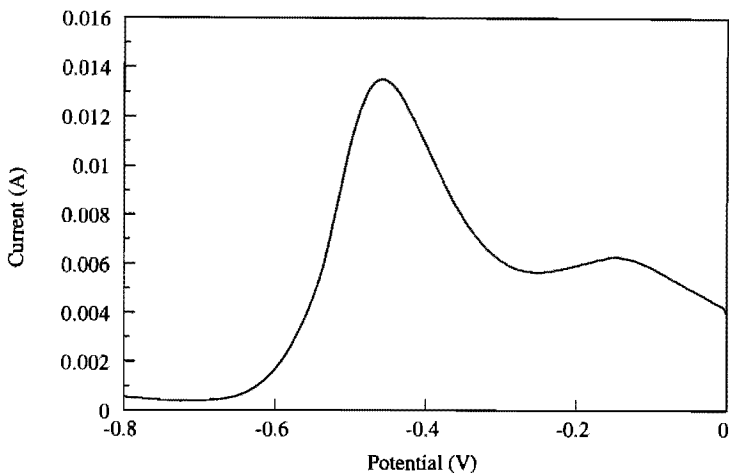


Figure 6.32

The square wave voltammogram recorded in TV-screen glass type A containing 2.14 weight-%  $\text{Sb}_2\text{O}_3$  at  $860^\circ\text{C}$  with the following set-up:

$$\Delta E_b = 0.002 \text{ V} \quad \Delta E_p = 0.1 \text{ V} \quad f = 100 \text{ Hz} \quad R_u = 43.8 \Omega$$

$$E_{1/2} = -0.459 \text{ and } -0.147 \text{ V}$$

### Check on the reversibility

In figure 6.31, the currents measured during the "forward" and "reverse" pulses are plotted against the base potential. Both curves display the two reduction peaks, indicating that both reduction steps are reversible.

A further check on the reversibility can be obtained by varying the frequency  $f$ . In figure 6.33, two voltammograms recorded in a TV-screen glass type A containing 2.35 weight-% at 1000°C with different frequencies are displayed. The positions of the peaks are not appreciably effected by the applied frequency. This again indicates that both reduction reactions are reversible under these conditions.

The ratio of the peak heights however does depend on the frequency. Since the height of the peak is in theory linearly proportional to the square of the number of electrons transferred (see equation 5.55), the ratio of the peaks should be about  $3^2:2^2$  or 9:4. At the relatively low frequencies of 50 and 100 Hz, this is indeed the case. But at higher frequencies, the peak of the reduction  $\text{Sb}^{5+} \rightarrow \text{Sb}^{3+}$  increases relative to the height of the peak of the  $\text{Sb}^{3+} \rightarrow \text{Sb}^0$

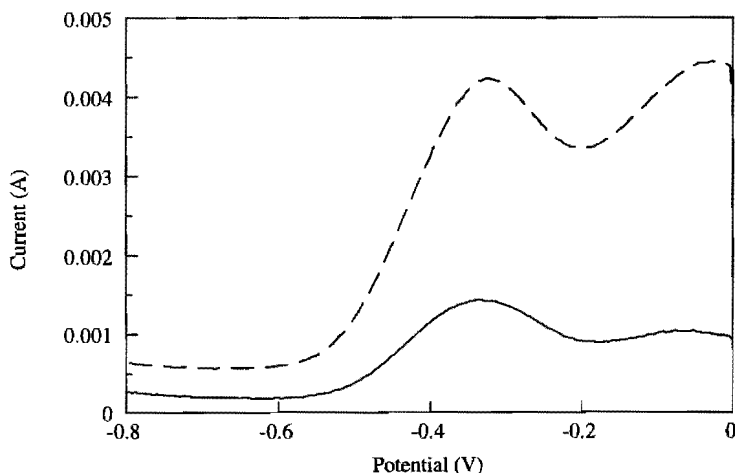


Figure 6.33

The square wave voltammograms recorded in TV-screen glass type A containing 2.35 weight-%  $\text{Sb}_2\text{O}_3$  at 1000°C with the following set-ups:

$f = 50 \text{ Hz}$   
 $R_u = 78.6 \ \Omega$

$\Delta E_b = 0.002 \text{ V}$   
 $\Delta E_p = 0.1 \text{ V}$

$f = 200 \text{ Hz}$   
 $R_u = 78.6 \ \Omega$

$\Delta E_b = 0.002 \text{ V}$   
 $\Delta E_p = 0.1 \text{ V}$

reduction reaction. The same phenomenon has been observed for the two reduction steps of arsenic [25]: at high frequencies, the height of the peak due to the reduction of the pentavalent to the trivalent form of arsenic is favoured.

An explanation for this phenomenon might be, that the reaction rate of the second reduction step is less than that of the first reduction step. At high frequencies, the height of the  $\text{Sb}^{5+}/\text{Sb}^{3+}$ -peak is then determined by the diffusion of  $\text{Sb}^{5+}$  to the surface of the working electrode, while the height of the  $\text{Sb}^{3+}/\text{Sb}^0$ -peak is governed by the reaction rate. In other words, the second reduction step is quasi-reversible at high frequencies.

During the first reduction step, the reactant for the second reduction step is formed. Since the two reduction steps are not independent, the peaks can not be separated mathematically. It is therefore not possible to compare the separate peaks with theoretical curves in order to obtain information on the exact reaction mechanism. However, it can be concluded from figures 6.31 and 6.33 that both reduction steps are reversible at frequencies of 100 Hz and less.

#### 6.3.3.3 Ratios of the diffusion coefficients

The ratio of the diffusion coefficients can be estimated by scanning the potential region in two directions (see chapter 5.5.7 and 6.2.3.4).

Figure 6.34 shows the voltammogram recorded in a TV-screen glass type A containing 0.63 weight-%  $\text{Sb}_2\text{O}_3$  at  $1300^\circ\text{C}$  while the base potential was decreased from 0 to  $-0.8$  V. A clear peak due to the reduction of  $\text{Sb}^{3+}$  to  $\text{Sb}^0$  is visible. The height of the peak is proportional to the square root of the diffusion coefficient of the reacting species  $\text{Sb}^{3+}$ .

In figure 6.35, the voltammogram recorded in the reverse direction, from  $-0.8$  to 0 V, is represented. In this voltammogram, a clear (negative) peak probably due to the oxidation of  $\text{Sb}^0$  to  $\text{Sb}^{3+}$  is visible. The absolute height of this peak is proportional to the square root of the diffusion coefficient of (probably)  $\text{Sb}^0$  in the glass melt.

The peak due to the reduction reaction is smaller than the peak due to the oxidation reaction as can be seen from figure 6.36.

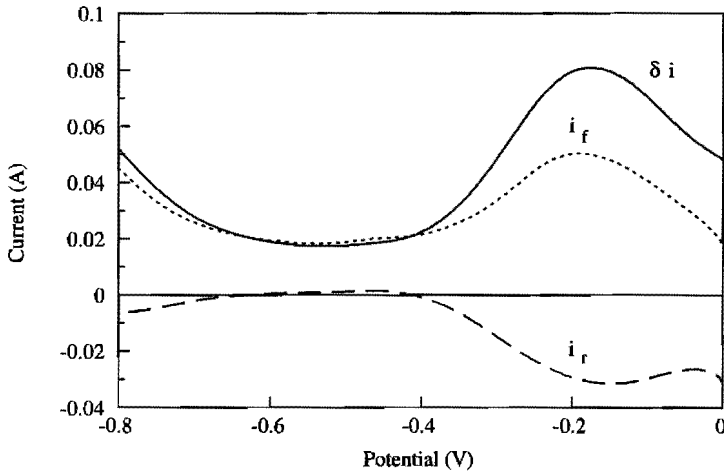


Figure 6.34

The square wave voltammogram recorded in TV-screen glass type A containing 0.63 weight-%  $\text{Sb}_2\text{O}_3$  at  $1300^\circ\text{C}$  with the following set-up:

$$\begin{array}{llll} \Delta E_b = 0.002 \text{ V} & f = 100 \text{ Hz} & E_i = 0 \text{ V} & E_{1/2} = -0.175 \text{ V} \\ \Delta E_p = 0.1 \text{ V} & R_u = 0 \Omega & E_{\text{end}} = -0.8 \text{ V} & \end{array}$$

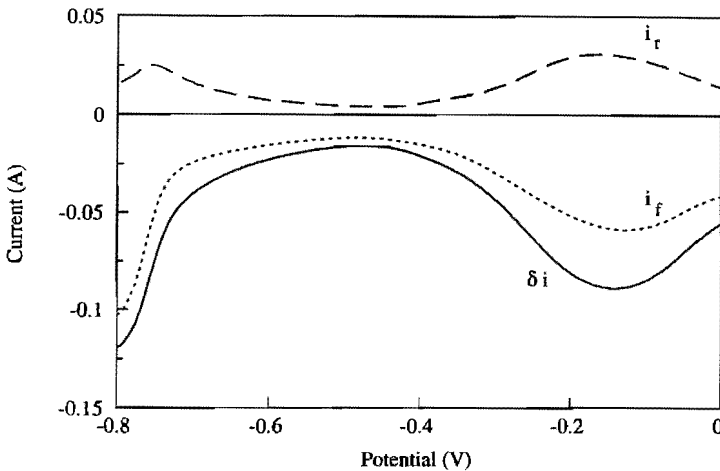


Figure 6.35

The square wave voltammogram recorded in TV-screen glass type A containing 0.63 weight-%  $\text{Sb}_2\text{O}_3$  at  $1300^\circ\text{C}$  with the following set-up:

$$\begin{array}{llll} \Delta E_b = 0.002 \text{ V} & f = 100 \text{ Hz} & E_i = -0.8 \text{ V} & E_{1/2} = -0.137 \text{ V} \\ \Delta E_p = 0.1 \text{ V} & R_u = 0 \Omega & E_{\text{end}} = 0 \text{ V} & \end{array}$$



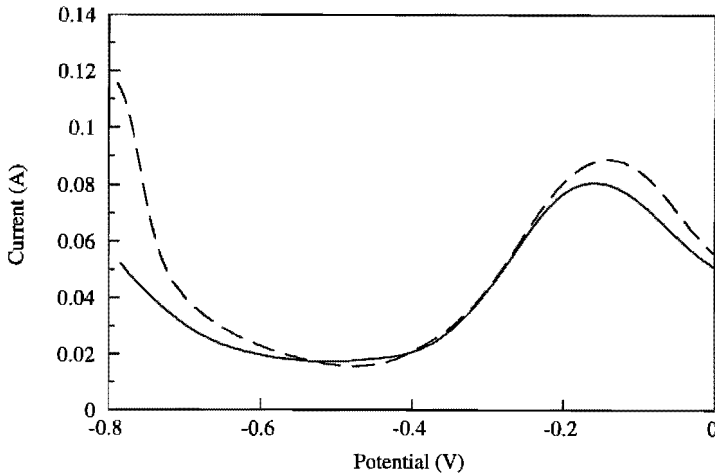


Figure 6.36

The square wave voltammograms recorded in TV-screen glass type A containing 0.63 weight-%  $\text{Sb}_2\text{O}_3$  at  $1300^\circ\text{C}$  with the following set-ups:

$$\begin{aligned} E_i &= 0 \text{ V} \\ E_{\text{end}} &= -0.8 \text{ V} \end{aligned}$$

$$\begin{aligned} \Delta E_b &= 0.002 \text{ V} \\ \Delta E_p &= 0.1 \text{ V} \\ f &= 100 \text{ Hz} \\ R_u &= 0 \ \Omega \end{aligned}$$

$$\begin{aligned} E_i &= -0.8 \text{ V} \\ E_{\text{end}} &= 0 \text{ V} \end{aligned}$$

Multiplied by: -1

$$\begin{aligned} \Delta E_b &= 0.002 \text{ V} \\ \Delta E_p &= 0.1 \text{ V} \\ f &= 100 \text{ Hz} \\ R_u &= 0 \ \Omega \end{aligned}$$

The ratio of the diffusion coefficients of  $\text{Sb}^0$  and  $\text{Sb}^{3+}$  in TV-screen glass type A at  $1300^\circ\text{C}$  is given by:

$$\sqrt{\frac{D_{\text{Sb}^0}}{D_{\text{Sb}^{3+}}}} = \frac{0.0884 \text{ Ampère}}{0.0810 \text{ Ampère}} = 1.09 \quad (6.37)$$

The ratio of the diffusion coefficients vary with varying temperature. The ratios of the diffusion coefficients of  $\text{Sb}^0/\text{Sb}^{3+}$  and  $\text{Sb}^{3+}/\text{Sb}^{5+}$  at  $800^\circ\text{C}$  can be calculated from the square wave voltammograms represented in figures 6.37 to 6.39. At  $800^\circ\text{C}$ , the ratio of the diffusion coefficients of  $\text{Sb}^0$  and  $\text{Sb}^{3+}$  is given by:

$$\sqrt{\frac{D_{\text{Sb}^0}}{D_{\text{Sb}^{3+}}}} = \frac{0.3600 \text{ Ampère}}{0.2311 \text{ Ampère}} = 1.56 \quad (6.38)$$

Besides the peaks due to the reaction  $\text{Sb}^{3+} = \text{Sb}^0$  the peaks due to the reaction  $\text{Sb}^{5+} = \text{Sb}^{3+}$  are visible. The ratio of the diffusion coefficients of  $\text{Sb}^{5+}$  and  $\text{Sb}^{3+}$  in TV-screen glass type A at  $800^\circ\text{C}$  is given by:

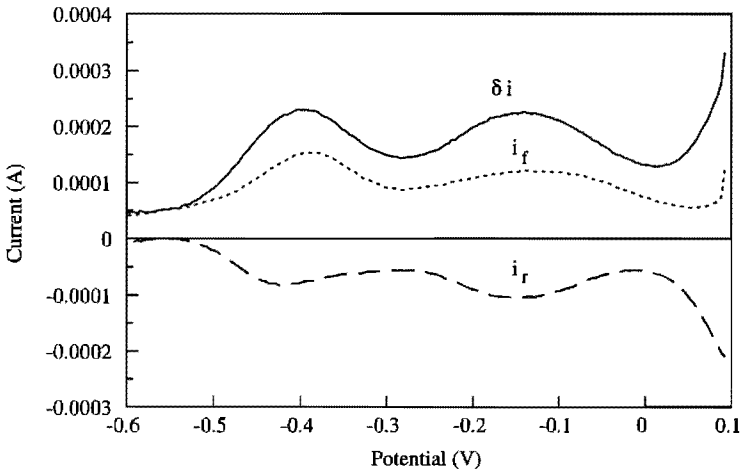


Figure 6.37  
 The square wave voltammogram recorded in TV-screen glass type A containing 0.63 weight-%  $\text{Sb}_2\text{O}_3$  at  $800^\circ\text{C}$  with the following set-up:  
 $\Delta E_b = 0.001 \text{ V}$        $f = 5 \text{ Hz}$        $E_i = 0 \text{ V}$        $E_{1/2}(3+/0) = -0.396 \text{ V}$   
 $\Delta E_p = 0.05 \text{ V}$        $R_u = 0 \Omega$        $E_{\text{end}} = -0.6 \text{ V}$        $E_{1/2}(5+/3+) = -0.141 \text{ V}$

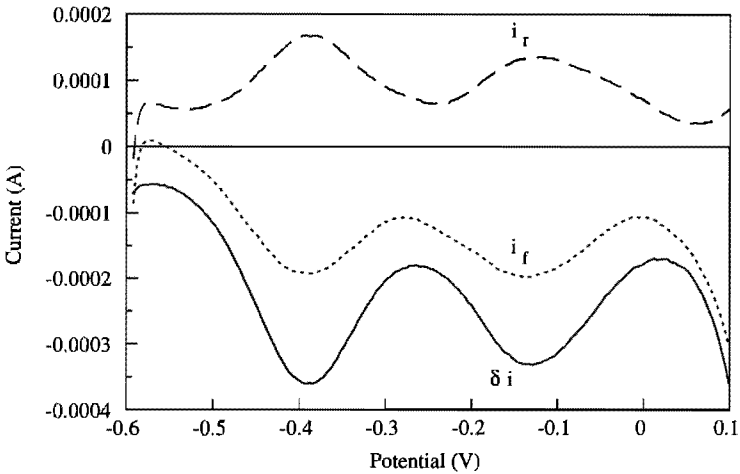


Figure 6.38  
 The square wave voltammogram recorded in TV-screen glass type A containing 0.63 weight-%  $\text{Sb}_2\text{O}_3$  at  $800^\circ\text{C}$  with the following set-up:  
 $\Delta E_b = 0.001 \text{ V}$        $f = 5 \text{ Hz}$        $E_i = -0.6 \text{ V}$        $E_{1/2}(3+/0) = -0.389 \text{ V}$   
 $\Delta E_p = 0.05 \text{ V}$        $R_u = 0 \Omega$        $E_{\text{end}} = 0.1 \text{ V}$        $E_{1/2}(5+/3+) = -0.130 \text{ V}$

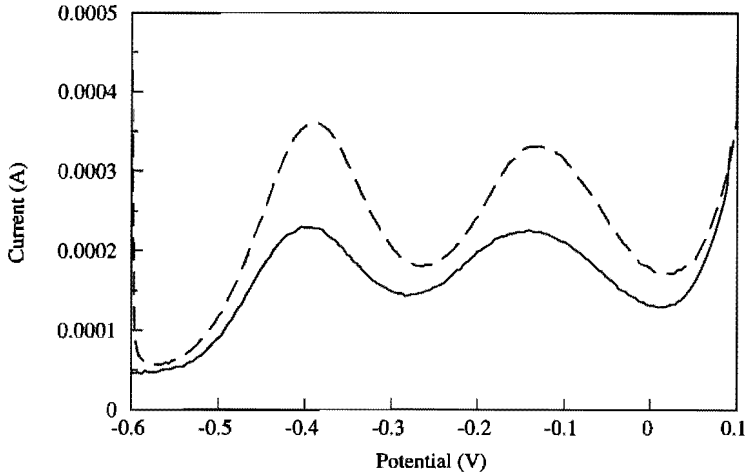


Figure 6.39

The square wave voltammograms recorded in TV-screen glass type A containing 0.63 weight-%  $\text{Sb}_2\text{O}_3$  at  $800^\circ\text{C}$  with the following set-ups:

$E_i = 0.1 \text{ V}$	$\Delta E_b = 0.001 \text{ V}$	$E_i = -0.6 \text{ V}$	$\Delta E_b = 0.001 \text{ V}$
$E_{\text{end}} = -0.6 \text{ V}$	$\Delta E_p = 0.05 \text{ V}$	$E_{\text{end}} = 0.1 \text{ V}$	$\Delta E_p = 0.05 \text{ V}$
	$f = 5 \text{ Hz}$		$f = 5 \text{ Hz}$
	$R_u = 0 \ \Omega$	Multiplied by: -1	$R_u = 0 \ \Omega$

$$\sqrt{\frac{D_{\text{Sb}^{3+}}}{D_{\text{Sb}^{5+}}}} = \frac{0.3313 \text{ Ampère}}{0.2254 \text{ Ampère}} = 1.47 \quad (6.39)$$

At any temperature, the ratios of the diffusion coefficients of antimony, measured in this way, are close to 1.

#### 6.3.3.4 The formal potential of the redox reactions

Now that the ratios of the diffusion coefficients are known, the formal potentials of the redox reactions can be derived from the half-wave potentials with the aid of equation 5.16. The formal potential of the reduction of pentavalent to trivalent antimony at  $800^\circ\text{C}$  is given by:

$$\begin{aligned} E_{\text{Sb}^{5+}/\text{Sb}^{3+}}^{0'} &= E_{1/2}(\text{Sb}^{5+}/\text{Sb}^{3+}) - \frac{R_g \cdot T}{2 \cdot F} \ln \sqrt{\frac{D_{\text{Sb}^{3+}}}{D_{\text{Sb}^{5+}}}} \\ -0.141 - 0.018 &= -0.159 \text{ V} \end{aligned} \quad (6.40)$$

The formal potential of the second reduction step, from trivalent to metallic antimony, at 800°C is:

$$E_{\text{Sb}^{3+}/\text{Sb}^0}^{0'} = E_{1/2}(\text{Sb}^{3+}/\text{Sb}^0) - \frac{R_g \cdot T}{3 \cdot F} \ln \sqrt{\frac{D_{\text{Sb}^0}}{D_{\text{Sb}^{3+}}}} \quad (6.41)$$

$$-0.396 - 0.014 = -0.410 \text{ V}$$

### 6.3.3.5 Calculation of the redox reaction enthalpy and entropy

The formal potential of the reaction  $\text{Sb}^{3+} \rightarrow \text{Sb}^0$  can be determined at any temperature between 800 and 1500°C. The formal potential of the reaction  $\text{Sb}^{5+} \rightarrow \text{Sb}^{3+}$  can only be determined at temperatures less than about 1100°C. The formal potentials appear to be linearly dependent on the temperature (see for example figures 6.45 and 6.46). With the aid of linear regression, straight lines are drawn through the measured potentials.

The values of  $\Delta H^{**}$  and  $\Delta S^{**}$  can be derived from the temperature dependency of the formal potential with the aid of equation 6.22. The results for the two reduction steps of antimony in TV-screen glass types A and B containing various concentrations of antimony are given in section 6.3.3.8. The indicated accuracy of  $\Delta H^{**}$  and  $\Delta S^{**}$  result from the linear regression of the measured formal potentials.

### 6.3.3.6 Frequency and concentration

At high antimony concentrations (over 2 weight-%  $\text{Sb}_2\text{O}_3$ ) the frequency of the applied signal has no influence on the position of the two peaks as can be seen in figure 6.33.

In the glass industry, the antimony concentration however ranges from 0.4 to 0.6 weight-%  $\text{Sb}_2\text{O}_3$ . In this range the frequency has a significant effect on the position of the peak due to the reduction of  $\text{Sb}^{5+}$  to  $\text{Sb}^{3+}$  as will be seen later in this section. The position of the other peak, due to the reduction of  $\text{Sb}^{3+}$  to  $\text{Sb}^0$ , is not effected by the applied frequency (as long as the frequency remains below 200 Hz, see section 6.2.3.2). This can be seen clearly in figure 6.40.

At low temperatures, the peak due to the reduction of the pentavalent to the trivalent antimony becomes visible. But the position of the peak depends on the applied frequency. When the applied frequency is set to a low value, the square wave voltammograms display two clearly separated peaks that can be

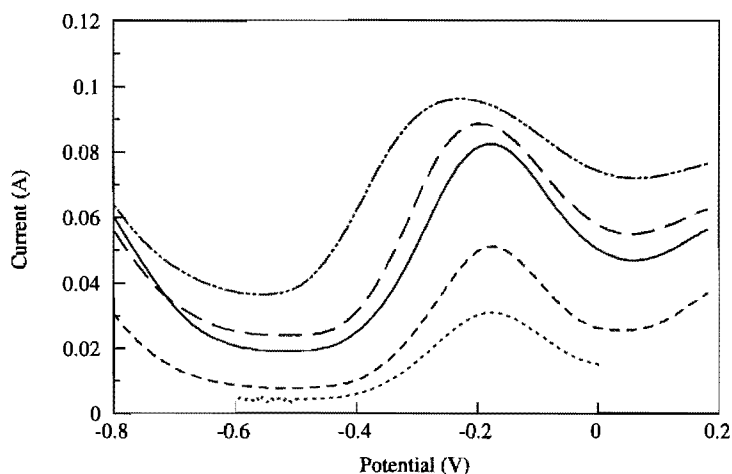


Figure 6.40

The square wave voltammograms recorded in a TV-screen glass type A containing 0.63 weight-%  $\text{Sb}_2\text{O}_3$  at  $1300^\circ\text{C}$ , with the following set-ups:

Line	-----	-----	-----	-----	-----
$f =$	5	20	100	200	500 Hz
$\Delta E_b =$	2	2	2	2	2 mV
$\Delta E_p =$	100	100	100	100	100 mV
$R_u =$	0	0	0	0	0 $\Omega$
$E_{1/2}(\text{Sb}^{3+}/\text{Sb}^0) =$	-0.176	-0.173	-0.177	-0.195	-0.227 V

attributed to the two reduction steps. The voltammograms closely resemble the voltammograms recorded in TV-screen glass with high antimony concentrations at any frequency between 5 and 200 Hz (see figure 6.41).

But if the frequency is set at 100 Hz, the peak due to the reduction of  $\text{Sb}^{5+}$  to  $\text{Sb}^{3+}$  at  $900^\circ\text{C}$  seems to shift towards the negative region, while the other peak remains at the same position. Now the peaks overlap and can only be seen as shoulders (see figure 6.42). Unfortunately the peaks cannot be separated mathematically because the two reduction steps are not independent. Therefore a thorough check of the reversibility of the reduction of the pentavalent to the trivalent antimony is not possible under these conditions.

But at low antimony concentrations, the reduction of  $\text{Sb}^{5+}$  to  $\text{Sb}^{3+}$  appears to be quasi-reversible. Only if the frequency is set to a value of 5 to 20 Hz, the peak seems to be reversible. However, for the correct determination of the formal potential of this reduction step, the reaction should be reversible.

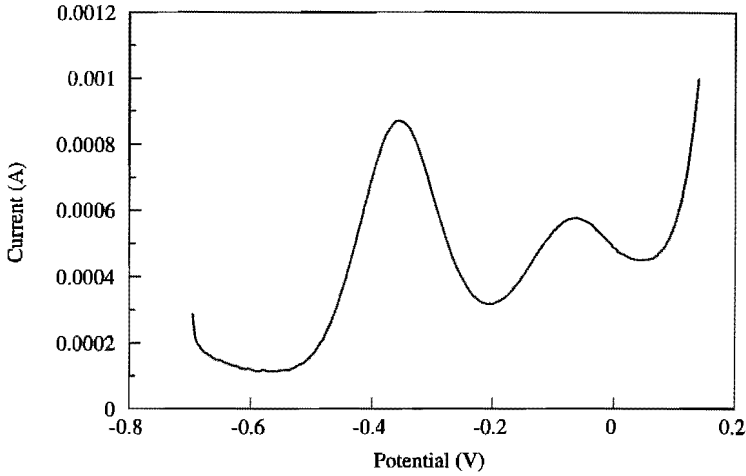


Figure 6.41

The square wave voltammogram recorded in TV-screen glass type A containing 0.63 weight-%  $\text{Sb}_2\text{O}_3$  at  $900^\circ\text{C}$  with the following set-up:

$$\Delta E_b = 0.001 \text{ V}$$

$$f = 5 \text{ Hz}$$

$$E_i = -0.7 \text{ V}$$

$$E_{1/2}(3+/0) = -0.354 \text{ V}$$

$$\Delta E_p = 0.05 \text{ V}$$

$$R_u = 0 \Omega$$

$$E_{\text{end}} = 0.3 \text{ V}$$

$$E_{1/2}(5+/3+) = -0.060 \text{ V}$$

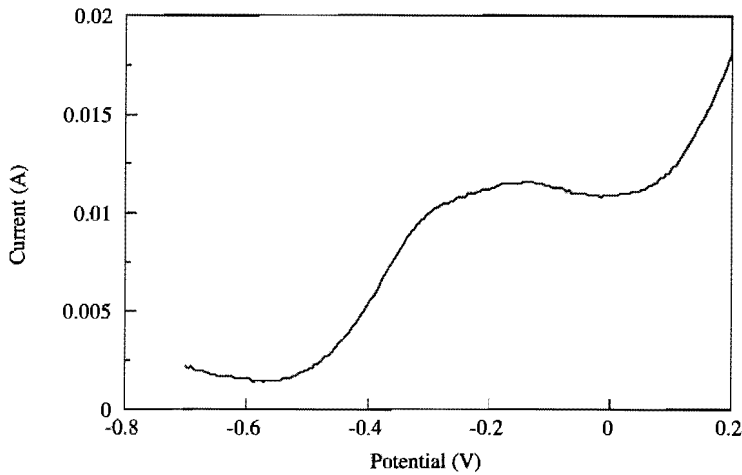


Figure 6.42

The square wave voltammogram measured in TV-screen glass type A containing 0.63 weight-%  $\text{Sb}_2\text{O}_3$  at  $900^\circ\text{C}$  with the following set-up:

$$\Delta E_b = 0.002 \text{ V}$$

$$f = 100 \text{ Hz}$$

$$E_i = -0.7 \text{ V}$$

$$E_{1/2}(3+/0) = ? \text{ V}$$

$$\Delta E_p = 0.100 \text{ V}$$

$$R_u = 0 \Omega$$

$$E_{\text{end}} = 0.3 \text{ V}$$

$$E_{1/2}(5+/3+) = ? \text{ V}$$

Therefore only the measurements with low frequencies can be used for the determination of the redox reaction enthalpy and entropy in TV-screen glasses containing relatively low amounts of antimony.

### 6.3.3.7 The influence of iron impurities

Some TV-screen glass melts were made from raw batch materials as used in the glass industry. The glass melts then contain, besides antimony, about 0.04 weight-%  $\text{Fe}_2\text{O}_3$ . Although the iron concentration is much lower than the antimony concentration, the peak due to the iron reduction is clearly visible in the square wave voltammograms displayed in figures 6.43 and 6.44.

The height of the peak is proportional to the concentration and to the square root of the diffusion coefficient of the reacting species. The diffusion coefficients of  $\text{Fe}^{3+}$  and  $\text{Sb}^{3+}$  in a soda-lime silica glass melt have been derived by Rüssel [26] from square wave voltammetry measurements. The results are:

$$D_{\text{Fe}^{3+}}(1100^\circ\text{C}) = 1.6 \cdot 10^{-11} \text{ m}^2 \cdot \text{s}^{-1}$$

$$D_{\text{Fe}^{3+}}(950^\circ\text{C}) = 2.0 \cdot 10^{-12} \text{ m}^2 \cdot \text{s}^{-1}$$

$$D_{\text{Sb}^{3+}}(1100^\circ\text{C}) = 2.0 \cdot 10^{-13} \text{ m}^2 \cdot \text{s}^{-1}$$

$$D_{\text{Sb}^{3+}}(950^\circ\text{C}) = 4.0 \cdot 10^{-14} \text{ m}^2 \cdot \text{s}^{-1}$$

The concentrations of iron and antimony in the TV-screen glass type B, expressed in mole·m<sup>-3</sup>, are: about 12 mole Fe·m<sup>-3</sup> and 95 mole Sb·m<sup>-3</sup> glass.

With the assumption that the ratio of the diffusion coefficients of  $\text{Fe}^{3+}$  and  $\text{Sb}^{3+}$  in TV-screen glass are in the same order of magnitude as in soda-lime-silica glass melts, the ratio of the peaks due to the reduction of  $\text{Fe}^{3+}$  and the reduction of  $\text{Sb}^{3+}$  at 1100°C is:

$$\frac{\delta i(\text{peak}_{\text{Fe}^{3+}/\text{Fe}^{2+}})}{\delta i(\text{peak}_{\text{Sb}^{3+}/\text{Sb}^0})} \propto \frac{C_{\text{Fe}} \cdot \sqrt{D_{\text{Fe}^{3+}}}}{C_{\text{Sb}} \cdot \sqrt{D_{\text{Sb}^{3+}}}} = 1.13 \quad (6.42)$$

and at 950°C, this ratio would be:

$$\frac{\delta i(\text{peak}_{\text{Fe}^{3+}/\text{Fe}^{2+}})}{\delta i(\text{peak}_{\text{Sb}^{3+}/\text{Sb}^0})} \propto \frac{C_{\text{Fe}} \cdot \sqrt{D_{\text{Fe}^{3+}}}}{C_{\text{Sb}} \cdot \sqrt{D_{\text{Sb}^{3+}}}} = 0.89 \quad (6.43)$$

This is in reasonable agreement with figures 6.43 and 6.44.

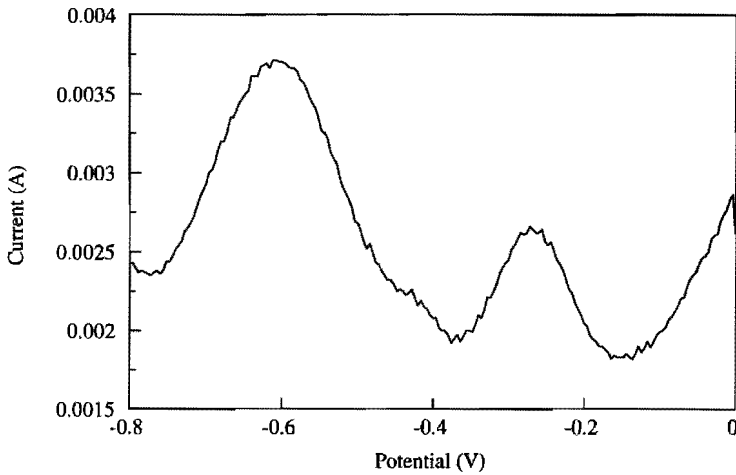


Figure 6.43

The square wave voltammogram measured in TV-screen glass type B containing 0.6 weight-%  $\text{Sb}_2\text{O}_3$  and 0.04 weight-%  $\text{Fe}_2\text{O}_3$  at  $1100^\circ\text{C}$  with the following set-up:

$$\begin{array}{lll} \Delta E_b = 0.002 \text{ V} & f = 100 \text{ Hz} & E_{1/2} = -0.608 \text{ V (Fe}^{3+}/\text{Fe}^{2+}) \text{ and } -0.269 \text{ V (Sb}^{3+}/\text{Sb}^0) \\ \Delta E_p = 0.020 \text{ V} & R_u = 4 \ \Omega & \end{array}$$

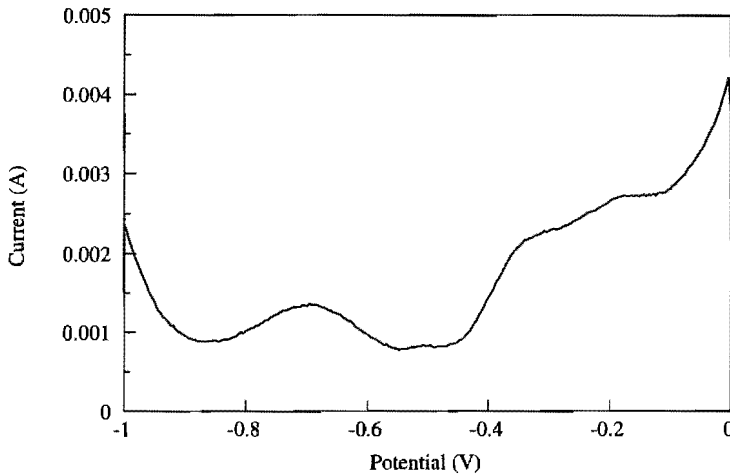


Figure 6.44

The square wave voltammogram measured in TV-screen glass type B containing 0.6 weight-%  $\text{Sb}_2\text{O}_3$  and 0.04 weight-%  $\text{Fe}_2\text{O}_3$  at  $950^\circ\text{C}$  with the following set-up:

$$\begin{array}{lll} \Delta E_b = 0.002 \text{ V} & f = 100 \text{ Hz} & E_{1/2} = -0.696 \text{ V (Fe}^{3+}/\text{Fe}^{2+}) \text{ and shoulders} \\ \Delta E_p = 0.020 \text{ V} & R_u = 9.5 \ \Omega & \text{at } -0.321 \text{ V (Sb}^{3+}/\text{Sb}^0) \text{ and } -0.175 \text{ V (Sb}^{5+}/\text{Sb}^{3+}) \end{array}$$



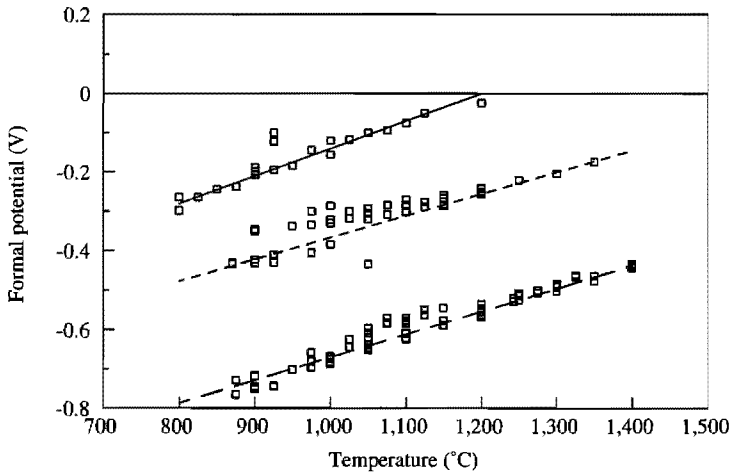


Figure 6.45

The position of the peaks due to the reduction of  $\text{Sb}^{5+}$ ,  $\text{Sb}^{3+}$  and  $\text{Fe}^{3+}$  in TV-screen glass type B as functions of the temperature

In figure 6.45, the position of the peaks due to the reduction of  $\text{Sb}^{5+}$ ,  $\text{Sb}^{3+}$  and  $\text{Fe}^{3+}$  in TV-screen glass type B are plotted as functions of the temperature. Now the redox reaction enthalpy and entropy can be calculated with the use of equation 6.21. The results for this type of glass are:

$\text{Sb}^{5+}/\text{Sb}^{3+}$	$\Delta H^{**} = 199 \text{ kJ}\cdot\text{mole}^{-1}$	$\Delta S^{**} = 135 \text{ J}\cdot\text{mole}^{-1}\cdot\text{K}^{-1}$
$\text{Sb}^{3+}/\text{Sb}^0$	$\Delta H^{**} = 310 \text{ kJ}\cdot\text{mole}^{-1}$	$\Delta S^{**} = 160 \text{ J}\cdot\text{mole}^{-1}\cdot\text{K}^{-1}$
$\text{Fe}^{3+}/\text{Fe}^{2+}$	$\Delta H^{**} = 136 \text{ kJ}\cdot\text{mole}^{-1}$	$\Delta S^{**} = 56 \text{ J}\cdot\text{mole}^{-1}\cdot\text{K}^{-1}$

Similar experiments have been performed in TV-screen glass type A, with and without iron. Glass I was made of reagent grade chemicals to which 0.70 weight-%  $\text{Sb}_2\text{O}_5$  was added ( $C_{\text{Sb}}=100 \text{ mole}\cdot\text{m}^{-3}$ ). Glass II was made of raw batch materials as used in the glass industry ( $C_{\text{Sb}}=80 \text{ mole}\cdot\text{m}^{-3}$ ,  $C_{\text{Fe}}=\pm 12 \text{ mole}\cdot\text{m}^{-3}$ ). The position of the peaks of the two antimony reduction steps turn out to be unaffected by the presence of iron. In figure 6.46, the position of the peaks due to the reduction of  $\text{Sb}^{5+}$ ,  $\text{Sb}^{3+}$  and  $\text{Fe}^{3+}$  in the two glass melts I and II are plotted as functions of the temperature. The enthalpy and entropy of the three redox reaction are:

$\text{Sb}^{5+}/\text{Sb}^{3+}$	$\Delta H^{**} = 192 \text{ kJ}\cdot\text{mole}^{-1}$	$\Delta S^{**} = 134 \text{ J}\cdot\text{mole}^{-1}\cdot\text{K}^{-1}$	} glass I
$\text{Sb}^{3+}/\text{Sb}^0$	$\Delta H^{**} = 261 \text{ kJ}\cdot\text{mole}^{-1}$	$\Delta S^{**} = 123 \text{ J}\cdot\text{mole}^{-1}\cdot\text{K}^{-1}$	
$\text{Fe}^{3+}/\text{Fe}^{2+}$	$\Delta H^{**} = 132 \text{ kJ}\cdot\text{mole}^{-1}$	$\Delta S^{**} = 56 \text{ J}\cdot\text{mole}^{-1}\cdot\text{K}^{-1}$	glass II

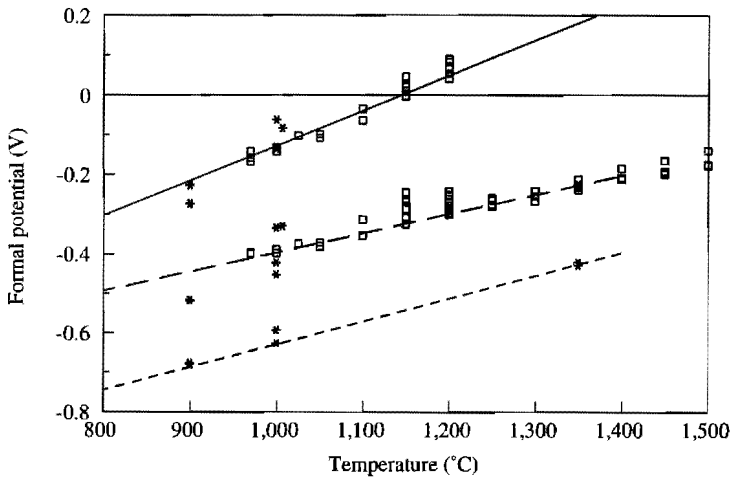


Figure 6.46

The position of the peaks due to the reduction of  $\text{Sb}^{5+}$ ,  $\text{Sb}^{3+}$  and  $\text{Fe}^{3+}$  in TV-screen glass type A with ( $\square$ , glass I) and without ( $*$ , glass II) iron as functions of the temperature

It should be noted, that  $\Delta H^{**}$  and  $\Delta S^{**}$  are used as parameter to describe the formal potential  $E^{0'}$  as a function of temperature. Two sets of  $\Delta H^{**}$  and  $\Delta S^{**}$ , that appear to be different, can result in comparable values of  $E^{0'}$  in a given temperature range. This is the case with the second antimony reduction step in glasses A and B.

### 6.3.3.8 Results of the square wave voltammetry measurements

In table 6.7, the calculated enthalpies and entropies of the two reduction steps of antimony in TV-screen glass are summarized.

The total antimony concentration has a significant effect on the equilibrium state of reaction 6.31. This can be seen most clearly from figure 6.47. In this figure, the natural logarithm of the redox reaction equilibrium constant  $\ln K^{**}(T)$  is plotted as a function of the reciprocal temperature for the various glass melts. Measured values for  $\ln K^{**}(T)$  are higher at high antimony concentrations. This means that in TV-screen glass with high antimony contents, the  $\text{Sb}^{3+}$  state is favoured relative to the equilibrium state in TV-screen melts with less antimony. And at low antimony concentrations, the (most) oxidized state of antimony is favoured. This resembles the behaviour of iron in TV-screen glasses: at low iron concentrations, the oxidized state  $\text{Fe}^{3+}$ , is favoured.

Table 6.7

The enthalpy and entropy of the reduction reactions  $\text{Sb}^{5+} \rightarrow \text{Sb}^{3+}$  and  $\text{Sb}^{3+} \rightarrow \text{Sb}^0$  in TV-screen glass with different antimony concentrations

Glass	Concentration (weight-% $\text{Sb}_2\text{O}_3$ )	$\text{Sb}^{5+} \rightarrow \text{Sb}^{3+}$		$\text{Sb}^{3+} \rightarrow \text{Sb}^0$	
		$\Delta H^{**}$ ( $\text{kJ}\cdot\text{mole}^{-1}$ )	$\Delta S^{**}$ ( $\text{J}\cdot\text{mole}^{-1}\cdot\text{K}^{-1}$ )	$\Delta H^{**}$ ( $\text{kJ}\cdot\text{mole}^{-1}$ )	$\Delta S^{**}$ ( $\text{J}\cdot\text{mole}^{-1}\cdot\text{K}^{-1}$ )
type A	0.4	$213 \pm 3$	$139 \pm 7$	$270 \pm 3$	$127 \pm 2$
type A	0.63	$192 \pm 5$	$134 \pm 4$	$261 \pm 4$	$123 \pm 4$
type A	2.14	$177 \pm 3$	$134 \pm 8$	$258 \pm 3$	$120 \pm 4$
type A	2.14	$210 \pm 6$	$160 \pm 18$	$260 \pm 4$	$121 \pm 4$
type B	0.43	$202 \pm 4$	$120 \pm 12$	$255 \pm 5$	$110 \pm 17$
type B	0.6	$199 \pm 2$	$135 \pm 6$	$310 \pm 9$	$160 \pm 29$

An explanation for this phenomenon may be, that the activity coefficients of  $\text{Sb}^{5+}$  and  $\text{Sb}^{3+}$  in TV-screen glass depend on the concentrations.

The extensiveness of the difference in behaviour of antimony in glasses with low and with high antimony contents can be seen in figure 6.48.

Here, the percentages of reduced antimony,  $\text{Sb}^{3+}$ , in glass melts which are in equilibrium with air, are given as a function of temperature. This percentage is calculated by:

$$\% \text{Sb}^{3+}(\text{T}) = \frac{100\% \cdot K^{**}(\text{T})}{K^{**}(\text{T}) + \sqrt{0.21}} \quad (6.44)$$

and the redox reaction equilibrium constants are calculated from the reaction enthalpies and entropies given in table 6.7. At  $1100^\circ\text{C}$ , the antimony in TV-screen glass melts with low antimony contents (0.4 weight-%  $\text{Sb}_2\text{O}_3$ ) is predominantly present in the pentavalent form, while the antimony in glasses with high antimony concentrations is almost entirely present as  $\text{Sb}^{3+}$ .

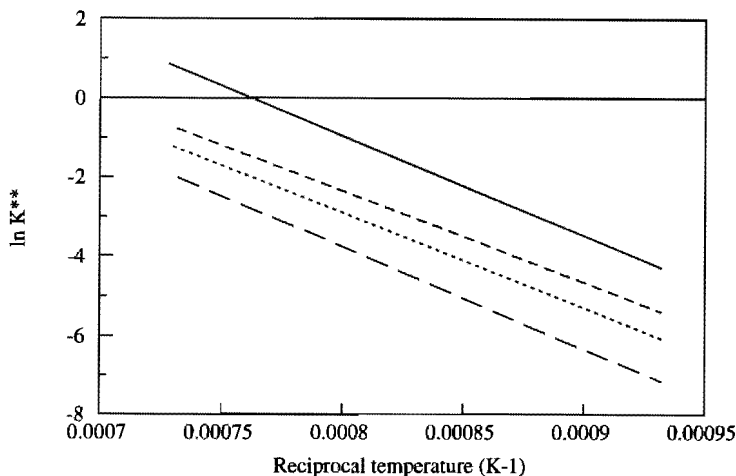


Figure 6.47

The natural logarithm of the redox reaction equilibrium constant  $K^{**}$  as a function of the reciprocal temperature for the data, presented in table 6.7

—————	2.14 weight-% $\text{Sb}_2\text{O}_3$ in TV-screen glass type A
-----	0.63 weight-% $\text{Sb}_2\text{O}_3$ in TV-screen glass type A
.....	0.6 weight-% $\text{Sb}_2\text{O}_3$ in TV-screen glass type B
- . - . - .	0.4 weight-% $\text{Sb}_2\text{O}_3$ in TV-screen glass type A

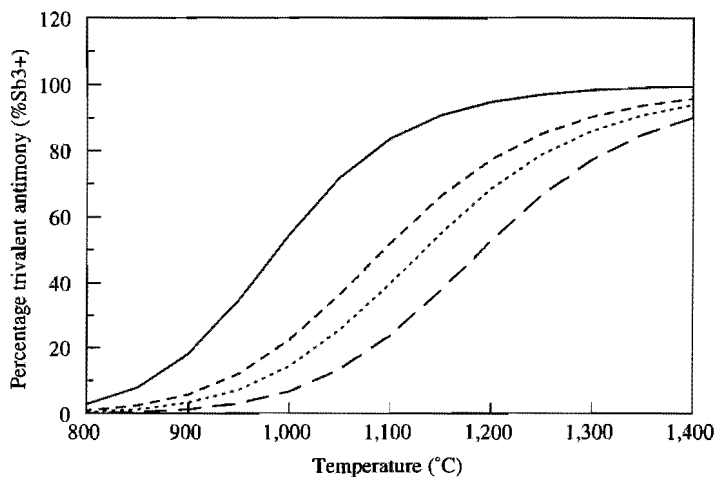


Figure 6.48

The percentage of antimony, present in the reduced state  $\text{Sb}^{3+}$ , as a function of the temperature for TV-screen glass melts in equilibrium with air ( $p_{\text{O}_2}=0.21$  bar)

—————	2.14 weight-% $\text{Sb}_2\text{O}_3$ in TV-screen glass type A
-----	0.63 weight-% $\text{Sb}_2\text{O}_3$ in TV-screen glass type A
.....	0.6 weight-% $\text{Sb}_2\text{O}_3$ in TV-screen glass type B
- . - . - .	0.4 weight-% $\text{Sb}_2\text{O}_3$ in TV-screen glass type A

Note, that figure 6.48 does not reflect the behaviour of antimony in industrial glass melting tanks, since the glass melt in these tanks is usually not in equilibrium with air. Furthermore, a change in the redox ratio  $[\text{Sb}^{3+}]/[\text{Sb}^{5+}]$  is coupled with a change in the oxygen equilibrium pressure in the melt. Therefore figure 6.48 can not be used to determine the effectiveness of antimony as a fining agent in industrial glass melts. A method to predict the effect of antimony additives to the fining of industrial glass melts will be described in chapter 7.

### 6.3.4 Comparison of the results from oxygen equilibrium pressure measurements and square wave voltammetry measurements

The results of oxygen equilibrium pressure measurements and square wave voltammetry measurements are in good agreement as can be seen from table 6.8. The square wave voltammetry measurements, however, could only be used to study the  $\text{Sb}^{5+}/\text{Sb}^{3+}$  equilibrium at temperatures below  $1100^\circ\text{C}$ . Even so, the calculated enthalpies and entropies agree very well with the data, derived from oxygen equilibrium pressure measurements at temperatures between  $800$  and  $1400^\circ\text{C}$ . Therefore it can be concluded that the data from the square wave voltammetry measurements at temperatures less than  $1100^\circ\text{C}$  can be used to predict the equilibrium constant of the  $\text{Sb}^{5+}/\text{Sb}^{3+}$  reaction at higher temperatures.

Table 6.8

The enthalpy and entropy of the redox reaction  $\text{Sb}^{5+} \rightarrow \text{Sb}^{3+}$  in TV-screen glass measured with oxygen equilibrium pressure measurements and square wave voltammetry measurements

Glass	Concentration (weight-% $\text{Sb}_2\text{O}_3$ )	Oxygen equilibrium pressure		Square wave voltammetry	
		$\Delta H^{**}$ ( $\text{kJ}\cdot\text{mole}^{-1}$ )	$\Delta S^{**}$ ( $\text{J}\cdot\text{mole}^{-1}\cdot\text{K}^{-1}$ )	$\Delta H^{**}$ ( $\text{kJ}\cdot\text{mole}^{-1}$ )	$\Delta S^{**}$ ( $\text{J}\cdot\text{mole}^{-1}\cdot\text{K}^{-1}$ )
type A	0.4	$219 \pm 11$	$138 \pm 7$	$213 \pm 3$	$139 \pm 7$
type A	2.14	$188 \pm 9$	$134 \pm 7$	$177 \pm 3$	$134 \pm 8$
type B	0.43	$191 \pm 10$	$121 \pm 6$	$202 \pm 4$	$120 \pm 12$
type B	0.6	contains iron impurities		$199 \pm 2$	$135 \pm 6$

### 6.3.5 Comparison of the results with data from the literature

#### 6.3.5.1 Investigations on the equilibrium of the $\text{Sb}^{5+}/\text{Sb}^{3+}$ reaction in literature

Johnston [12] exposed sodium disilicate glass containing about 2 weight-% Sb (250-380 mole  $\text{Sb}\cdot\text{m}^{-3}$  glass) at 1085°C during 1 to 3 days to air, pure  $\text{O}_2$  or an  $\text{Ar}/\text{O}_2$  mixture. After quenching of the melts, the samples were analysed on the concentration of  $\text{Sb}^{3+}$  and the total antimony content. The redox ratio  $[\text{Sb}^{3+}]/[\text{Sb}^{5+}]$  appeared to be proportional to the square root of the partial oxygen pressure in the atmosphere:

$$\frac{[\text{Sb}^{3+}]}{[\text{Sb}^{5+}]} \propto P_{\text{O}_2}^{1/2} \quad (6.45)$$

Furthermore sodium disilicate melts were equilibrated with air at 1200 and 1300°C. From the  $\text{Sb}^{3+}$  and total antimony concentrations, measured in the quenched samples, the temperature dependent redox reaction equilibrium constant  $K^{**}(\text{T})$  was calculated (see figure 6.49).

The equilibrium state of the  $\text{Sb}^{5+}/\text{Sb}^{3+}$  reaction in TV-screen glass was investigated by Krol [13]. TV-screen glasses containing 0.1 mole-%  $\text{Sb}_2\text{O}_5$  ( $\pm 77$  mole  $\text{Sb}\cdot\text{m}^{-3}$  glass) were exposed for 20 hours to air. Then the melts were quenched. The concentration of  $\text{Sb}^{3+}$  was determined with wet-chemical analysis and the total antimony content with inductively coupled plasma emission spectrometry. Further experiments, in which TV-screen glass melts were exposed to air at 1200°C for longer melting times (up to 200 hours), showed that the melts were not in equilibrium with air after 20 hours. The oxygen equilibrium pressure in the melt at 1200°C was estimated at 0.5 bar after 20 hours. Krol assumed that  $\text{NaNO}_3$ , present in the glass batch, was responsible for this high oxygen pressure. Since all glass melts contained the same amount of  $\text{NaNO}_3$ , the oxygen equilibrium pressure in the melts was in all cases assumed to be 0.5 bar. The redox reaction equilibrium constant can then be calculated from:

$$K^{**}(\text{T}) = \frac{[\text{Sb}^{3+}] \cdot 0.5^{1/2}}{C_{\text{Sb}} - [\text{Sb}^{3+}]} \quad (6.46)$$

The equilibrium constants thus calculated are represented in figure 6.49.

In the experiments of Stahlberg [14], glasses with the composition 70 mole-%  $\text{SiO}_2$ , 23 mole-% alkali and alkaline earth oxides and 0.2 mole-%  $\text{Sb}_2\text{O}_3$  ( $\pm 145$  mole  $\text{Sb}\cdot\text{m}^{-3}$  glass) were exposed to different atmospheres with various partial

oxygen pressures. After some time the oxygen equilibrium pressures in the melts were measured with an oxygen sensor. After quenching, the glass samples were analysed for the  $\text{Sb}^{5+}$  and  $\text{Sb}^{3+}$  concentrations using Mössbauer spectroscopy. The redox ratio  $[\text{Sb}^{3+}]/[\text{Sb}^{5+}]$  was found to be proportional to the square root of the oxygen equilibrium pressure in the melt. Furthermore the redox reaction equilibrium constants were calculated with the aid of equation 6.32. The equilibrium constants appeared not to be proportional to  $\exp(1/T)$ , indicating that the redox reaction enthalpy and entropy are not independent of the temperature. The equilibrium constants, derived from the redox reaction measurements presented in this thesis, however, can be adequately described with temperature independent reaction enthalpies and entropies.

Rüssel [6] used square wave voltammetry to measure the equilibrium state of the antimony reaction in soda-lime-silica glass melts containing 1 mole-%  $\text{Sb}_2\text{O}_3$  at various temperatures. The results are in agreement with the measurements in TV-screen glass with high antimony concentrations as presented in this thesis.

#### 6.3.5.2 Graphical presentation of the literature data and the data presented in this thesis

In order to compare the literature data with the data presented in this thesis, the redox reaction equilibrium constants  $K^{**}(T)$  were calculated. In figure 6.49, the natural logarithm of the equilibrium constants are plotted as a function of the reciprocal temperature. The percentage of  $\text{Sb}^{3+}$ , that would be present in the glass melt equilibrated with air, is calculated from equation 6.44. The results are represented in figure 6.50.

The data, derived from square wave voltammetry measurements in TV-screen glass melts containing relatively small amounts of antimony (0.4-0.6 weight-%  $\text{Sb}_2\text{O}_3$ , see table 6.7) are in excellent agreement with the literature data of Krol [13] and Stahlberg [14] for the same type of glasses and antimony concentrations, but measured with other techniques. This indicates that the data derived from square wave voltammetry measurements are as reliable as data, derived from much more laborious methods.

The redox reaction equilibrium constant containing large amounts of antimony in TV-screen glass is comparable to the equilibrium constant in soda-lime-silica glass (see table 6.7 and [6]), but differs substantially from  $K^{**}(T)$  in sodium

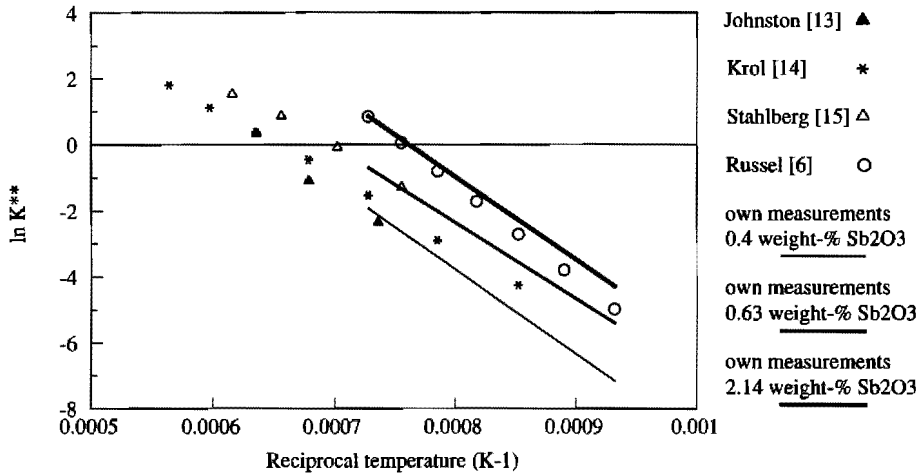


Figure 6.49

The natural logarithm of the redox reaction equilibrium constant  $K^{**}$  as a function of the reciprocal temperature for literature data and data, presented in this thesis

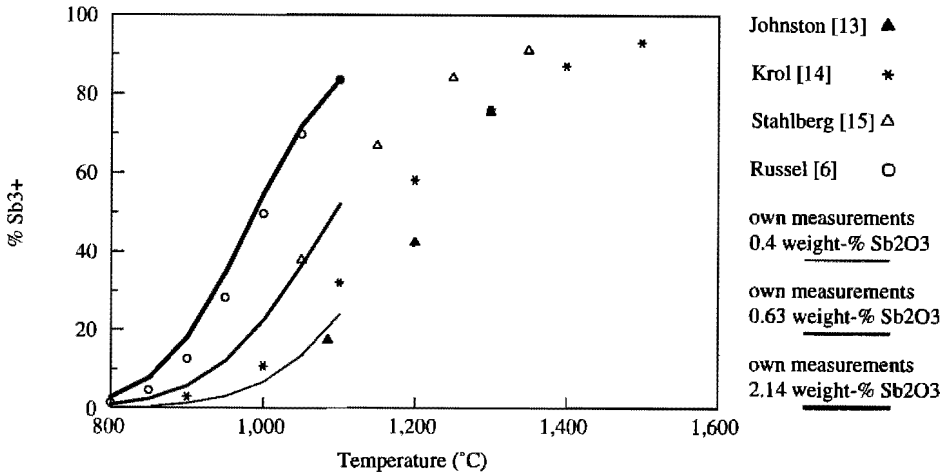


Figure 6.50

The percentage of antimony that would be present as  $\text{Sb}^{3+}$  in glass melts equilibrated with air ( $p_{\text{O}_2}=0.21$  bar) as functions of the temperature



disilicate glass [12]. Furthermore, the total antimony content has a significant effect on the equilibrium constant in TV-screen glass melts: at high antimony levels, the reduced state of the antimony is favoured. In the previous section, the same phenomenon was found in TV-screen glasses containing iron: at high iron levels, the reduced state of the iron was favoured. But in soda-lime-silica glass melts, the oxidized state of iron was favoured at high iron contents. So although the equilibrium constants of the antimony reaction in TV-screen glass and soda-lime-silica glass with high antimony concentrations are corresponding, this may not be the case at other antimony concentrations. This underlines the necessity to use the proper glass composition and antimony content in the measurements of the redox reaction equilibrium constants.

### 6.3.6 Conclusions

- Oxygen equilibrium pressure measurements at temperatures between 800 and 1400°C can be used for the determination of the redox reaction equilibrium constants of the  $\text{Sb}^{5+}/\text{Sb}^{3+}$  reaction in TV-screen glass melts;
- square wave voltammetry measurements can be used for the determination of the equilibrium constants of the  $\text{Sb}^{5+}/\text{Sb}^{3+}$  reaction at temperatures up to about 1100°C;
- the agreement between the results of both methods is good;
- the data on the redox reaction enthalpy and entropy, derived from square wave voltammetry measurements at temperatures less than 1100° can be used for the calculation of redox reaction equilibrium constants at temperatures up to 1400°C;
- the results of both oxygen equilibrium pressure measurements and square wave voltammetry measurements agree very well with the data on the reaction equilibrium of antimony in similar glass melts and concentrations, presented in the literature;
- the total concentration of antimony has a significant effect on the redox reaction equilibrium constant in TV-screen glasses (type A): at low antimony concentrations, the oxidized state is favoured, relative to the equilibrium state at higher antimony contents;
- the redox reaction equilibrium constant can be calculated from the redox reaction enthalpy and entropy as given in tables 6.6 and 6.7, for the given glass compositions and antimony concentrations;
- measurements in one type of glass can not be used to predict the equilibrium state of the antimony reaction in other glass compositions.

## 6.4 CERIUM

### 6.4.1 Cerium in glass

Due to the more strict environmental legislations, the use of the hazardous antimony should be reduced as much as possible. Therefore some investigators [3,8] have tried to find a less harmful metal oxide that could (partly) replace antimony oxide as a fining agent in the glass industry.

The most promising of the investigated metal oxides appeared to be cerium oxide. The fining action can be described by:



and the equilibrium state of this reaction can be given by the redox reaction equilibrium constant  $K^{**}(\text{T})$ :

$$K^{**}(\text{T}) = \frac{[\text{Ce}^{3+}] \cdot p_{\text{O}_2}^{1/4}}{[\text{Ce}^{4+}]} = \exp \left\{ \frac{-\Delta H^{**}}{R_g \cdot T} + \frac{\Delta S^{**}}{R_g} \right\} \quad (6.48)$$

In this thesis, the equilibrium state of cerium in TV-screen glass is studied with oxygen equilibrium pressure measurements and wet-chemical analysis of the quenched glass samples.

### 6.4.2 Oxygen equilibrium pressure measurements

#### 6.4.2.1 The experimental procedure

The TV-screen glass samples were made from reagent grade chemicals or raw batch materials to which  $\text{CeO}_2$  was added. The batch was molten at  $1400^\circ\text{C}$  in platinum crucibles until all grains were dissolved and the melt was almost bubble-free. Then the glass was quenched to room temperature and transferred to an  $\text{Al}_2\text{O}_3$ -crucible. This crucible was placed in the furnace as sketched in figure 5.3.

The temperature was increased slowly to  $1400^\circ\text{C}$  and then the electrodes were lowered until the reference electrode just touched the melt. After this procedure, the potential difference between the counter electrode (electrode 3 in figure 5.3) and the reference electrode which was flushed with clean, dry air, has been measured. As soon as the potential difference reached a stable value, the temperature was decreased by  $3^\circ\text{C}/\text{min}$  down to  $800^\circ\text{C}$  while the potential difference was measured on line. Subsequently the temperature was increased

again to 1400°C. Usually the potential difference between counter and reference electrode followed the same curve during cooling and heating. This indicates that the redox reaction that causes a change in the potential difference is reversible. Furthermore it can be concluded that the concentration of the redox active species cerium remains constant during the experiment.

#### 6.4.2.2 The measured potential difference

As an example, the potential difference between counter and reference electrode in TV-screen glass type A containing 0.2 weight-% CeO<sub>2</sub> is given as a function of temperature in figure 6.51.

#### 6.4.2.3 The calculation of the oxygen equilibrium pressure measurements

The oxygen equilibrium pressure can be calculated from the measured potential difference with the aid of equation 6.8.

In figure 6.52, the calculated oxygen equilibrium pressure in TV-screen glass type A containing 0.2 weight-% CeO<sub>2</sub> is given as a function of temperature.

#### 6.4.2.4 Calculation of $\Delta H^{**}$ , $\Delta S^{**}$ and $K^{**}(T)$

A change in the oxygen equilibrium pressure at a change in temperature from T<sub>1</sub> to T<sub>2</sub> is given by (see chapter 5.4):

$$L_{O_2}(T_1) \cdot p_{O_2}(T_1) - L_{O_2}(T_2) \cdot p_{O_2}(T_2) = \frac{1}{4} \cdot C_{Ce} \left\{ \frac{K^{**}(T_1)}{K^{**}(T_1) + p_{O_2}^{1/4}(T_1)} - \frac{K^{**}(T_2)}{K^{**}(T_2) + p_{O_2}^{1/4}(T_2)} \right\} \quad (6.49)$$

with  $L_{O_2}(T)$  = physical solubility of oxygen  
in the glass melt at temperature T [mole·m<sup>-3</sup>·bar<sup>-1</sup>]  
 $p_{O_2}(T)$  = oxygen equilibrium pressure in  
the glass melt at temperature T [bar]  
 $C_{Ce}$  = total cerium concentration in the glass melt [mole·m<sup>-3</sup>]

The physical solubility of oxygen is assumed to be 1 mole·m<sup>-3</sup>·bar<sup>-1</sup> (see chapter 6.8). Equation 6.49 is valid as long as the cerium concentration remains constant during the experiment, and hardly any transport of oxygen between melt and atmosphere takes place. These requirements are assumed to be satisfied if the oxygen equilibrium pressure is less than 0.5 bar and the experiment is completed within some hours (see chapter 5.4).

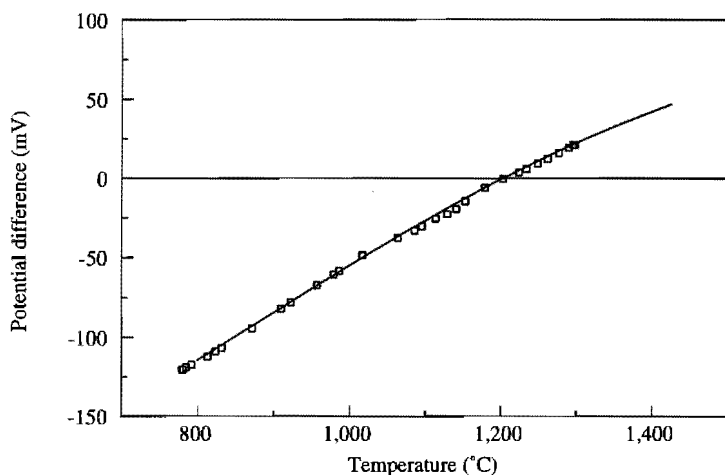


Figure 6.51

The measured potential difference ( $\square$ ) between counter and reference electrode in TV-screen glass type A containing 0.2 weight-%  $\text{CeO}_2$  as a function of temperature. The theoretical curve (—) is calculated with the following parameters (see section 6.4.2.4):

$$C_{\text{Ce}} = 27 \text{ mole}\cdot\text{m}^{-3} \quad p_{\text{O}_2}(1202^\circ\text{C}) = 0.21 \text{ bar} \quad \Delta H^{**} = 42 \text{ kJ}\cdot\text{mole}^{-3} \quad \Delta S^{**} = 30 \text{ J}\cdot\text{mole}^{-1}\cdot\text{K}^{-1}$$

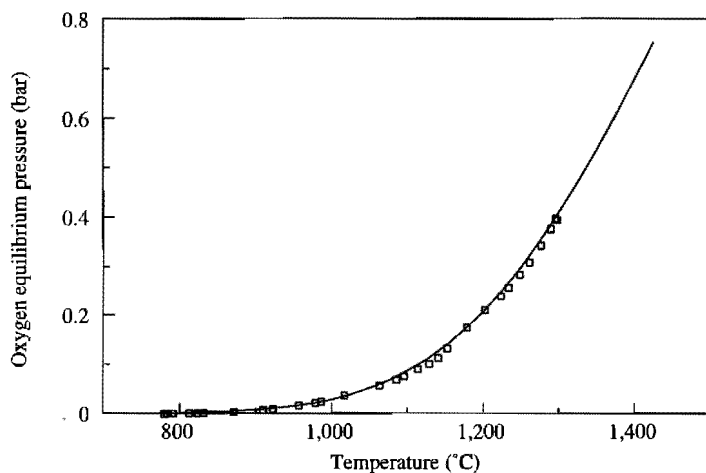


Figure 6.52

The oxygen equilibrium pressure ( $\square$ ) in TV-screen glass type A containing 0.2 weight-%  $\text{CeO}_2$  as a function of temperature. The theoretical curve (—) is calculated with the following parameters (see section 6.4.2.4):

$$C_{\text{Ce}} = 27 \text{ mole}\cdot\text{m}^{-3} \quad p_{\text{O}_2}(1202^\circ\text{C}) = 0.21 \text{ bar} \quad \Delta H^{**} = 42 \text{ kJ}\cdot\text{mole}^{-3} \quad \Delta S^{**} = 30 \text{ J}\cdot\text{mole}^{-1}\cdot\text{K}^{-1}$$

With the aid of a computer fitting program, the best values for  $\Delta H^{**}$  and  $\Delta S^{**}$ , and with those  $K^{**}(T)$ , for describing the measured oxygen equilibrium pressure as a function of temperature can be found. The oxygen equilibrium pressure at one temperature is imported in the computer program to account for the amount of air, included in the glass during the melting of the cullet.

In the presented experiment in TV-screen glass type A containing 0.2 weight-%  $\text{CeO}_2$ , the total cerium concentration  $C_{\text{Ce}}$  was  $27 \text{ mole}\cdot\text{m}^{-3}$ . At  $1202^\circ\text{C}$ , the melt was in equilibrium with the surrounding air. The potential difference between the electrodes was 0 V, and the oxygen equilibrium pressure was 0.21 bar. The fitting procedure resulted in the following values for the enthalpy and entropy:

$$\Delta H^{**} = 42 \text{ kJ}\cdot\text{mole}^{-1}$$

$$\Delta S^{**} = 30 \text{ J}\cdot\text{mole}^{-1}\cdot\text{K}^{-1}$$

In figures 6.51 and 6.52, the theoretical potential differences and oxygen equilibrium pressures are given as functions of temperature for these values of  $\Delta H^{**}$  and  $\Delta S^{**}$ , together with the measured data.

#### 6.4.2.5 Results of the oxygen equilibrium pressure measurements

The procedure described in section 6.4.2.1 to 6.4.2.4 has been followed in 2 types of TV-screen glass with different cerium concentrations. The results are summarized in table 6.9.

Table 6.9

The results of oxygen equilibrium pressure measurements in two TV-screen glasses containing cerium, expressed in redox enthalpy and entropy changes

Line Fig 6.53 and 6.54	Glass	Concen- tration (weight-% $\text{CeO}_2$ )	Concen- tration (mole Ce $\cdot\text{m}^{-3}$ glass)	$\Delta H^{**}$ ( $\text{kJ}\cdot\text{mole}^{-1}$ )	$\Delta S^{**}$ ( $\text{J}\cdot\text{mole}^{-1}\cdot\text{K}^{-1}$ )
—————	TV type A	0.2	27	42	30
-----	TV type A	0.6	80	40	40
-----	TV type B	0.5	67	33	32
	TV type B	0.6	80	41	35

The TV-screen glass type B containing 0.6 weight-%  $\text{CeO}_2$  was made of technical raw batch materials and contained therefore also a small amount of  $\text{Fe}_2\text{O}_3$ . When the temperature of a glass melt which contains two polyvalent elements is increased, the redox reaction equilibrium constants of both polyvalent elements will shift to a new value. The new oxygen equilibrium pressure is governed by both equilibrium constants. However, for the calculation of the enthalpy and entropy of the cerium reaction, the influence of the iron reaction has been neglected. Therefore the results for this type of glass may be erroneous.

### 6.4.3 Square wave voltammetry measurements

In TV-screen glasses containing 0.5 to 0.6 weight-%  $\text{CeO}_2$  some square wave voltammograms have been recorded. No peak was visible in the potential range from 0 to -0.8 V at any temperature. The half-wave potential of reaction 6.47 must therefore be located outside this potential range. Probably the redox reaction equilibrium constant of the cerium reaction in TV-screen glass is more than unity at temperatures above  $\pm 800^\circ\text{C}$ . Calculations of the redox reaction equilibrium constant with the values for the enthalpies and entropies, given in table 6.9, support this statement. This means that at melting temperatures, cerium is predominantly present in the reduced state  $\text{Ce}^{3+}$  in TV-screen glass with 0.5 to 0.6 weight-%  $\text{CeO}_2$  (see figure 6.54).

### 6.4.4 Wet-chemical analysis

#### 6.4.4.1 The analysis

In order to check the values of the redox reaction enthalpy and entropy, derived from oxygen equilibrium pressure measurements, some glass samples were analysed for  $\text{Ce}^{4+}$  and  $\text{Ce}^{3+}$ .

The samples were prepared as follows:

The glass melts containing cerium, but no other polyvalent elements, were held for half an hour at a certain melting temperature  $T$ . The oxygen equilibrium pressure  $p_{\text{O}_2}$  in the melt was measured with the aid of an oxygen sensor. Subsequently the melts were quenched to room temperature, and the concentrations of  $\text{Ce}^{4+}$  and the total cerium concentration  $C_{\text{Ce}}$  were determined following the procedure outlined by Johnston [12]. The redox reaction equilibrium constant  $K^{**}(T)$  at the melting temperature  $T$  can now be calculated by:

$$K^{**}(T) = \frac{(C_{Ce} - [Ce^{4+}]) \cdot p_{O_2}^{1/4}}{[Ce^{4+}]} \quad (6.50)$$

assuming that the equilibrium did not change during the cooling of the melt.

#### 6.4.4.2 The redox reaction equilibrium constant

The redox reaction equilibrium constant was determined for at least two temperatures for the different glass compositions and cerium concentrations. The results are summarized in table 6.10.

The total cerium content, determined with wet-chemical analysis, is always lower than the amount of cerium, added to the batch.

Table 6.10

The results of the wet-chemical analysis, expressed in reaction equilibrium constants  $K^{**}(T)$

Symbol	Glass	weight% CeO <sub>2</sub> (added)	weight% Ce (added)	T (°C)	p <sub>O<sub>2</sub></sub> (bar)	weight% Ce <sup>4+</sup> (found)	weight% C <sub>Ce</sub> (found)	K <sup>**</sup> (T)
•	type A	0.6	0.55	1000	0.029	0.059	0.449	2.730
•	type A	0.6	0.55	1300	0.194	0.0545	0.465	4.994
*	type B	0.2	0.16	1100	0.049	0.045	0.127	0.855
*	type B	0.2	0.16	1200	0.144	0.047	0.147	1.310
□	type B	0.35	0.28	1100	0.044	0.040	0.190	1.721
□	type B	0.35	0.28	1200	0.134	0.048	0.218	2.144
□	type B	0.35	0.28	1300	0.278	0.034	0.214	3.844
○	type B	0.6	0.55	1150	0.122	0.0765	0.4165	2.626
○	type B	0.6	0.55	1300	0.229	0.083	0.453	3.083
△	type B	0.7	0.57	1100	0.068	0.086	0.456	2.194
△	type B	0.7	0.57	1200	0.168	0.094	0.514	2.86
△	type B	0.7	0.57	1300	0.275	0.088	0.428	2.800

#### 6.4.4.3 Comparison of the results of the oxygen equilibrium pressure measurements and the wet-chemical analysis

For each type of glass and cerium concentration, only two or three redox reaction equilibrium constants have been determined. The data points are too few to calculate the reaction enthalpy and entropy with the aid of equation 5.68 and 5.69. The data points can be used, though, to check whether the values of the enthalpy and entropy of the cerium reaction, determined with the aid of oxygen equilibrium pressure measurements, are in the correct order of magnitude. Therefore the natural logarithm of the redox reaction equilibrium constants  $K^{**}(T)$ , presented in table 6.10, are plotted against the reciprocal temperature in figure 6.53. In the same figure, the equilibrium constants, calculated with the values from the enthalpies and entropies given in table 6.9, are reproduced.

The redox reaction equilibrium constants for the TV-screen glass containing 0.6 weight-%  $\text{CeO}_2$ , measured with oxygen equilibrium pressure measurements and those, derived from wet-chemical analysis, are in good agreement. This is also the case with TV-screen glasses type A and B, containing 0.2 weight-%  $\text{CeO}_2$ .

The data points from wet-chemical analyses in the TV-screen glasses type B containing 0.35, 0.6 or 0.7 weight-% are located in the same area. They are not positioned on a straight line. The scattering in the results is too large to be able to decide whether or not the enthalpy and entropy, given in table 6.9, adequately describe the redox reaction equilibrium constant in TV-screen glasses with about 0.5 weight-%  $\text{CeO}_2$ .

However, it is clear from figure 6.53, that the redox reaction equilibrium constant of the cerium reaction is lower at low cerium contents in TV-screen glass. This means that the oxidized form of cerium,  $\text{Ce}^{4+}$ , is favoured. This can be seen even more clearly from figure 6.54. Here, the percentage of cerium that is present in the reduced state  $\text{Ce}^{3+}$  is given as a function of temperature, for a TV-screen glass in equilibrium with air ( $p_{\text{O}_2}=0.21$  bar).

This resembles the behaviour of iron and antimony in TV-screen glasses: at low iron or antimony concentrations, the most oxidized state of the polyvalent element is favoured.



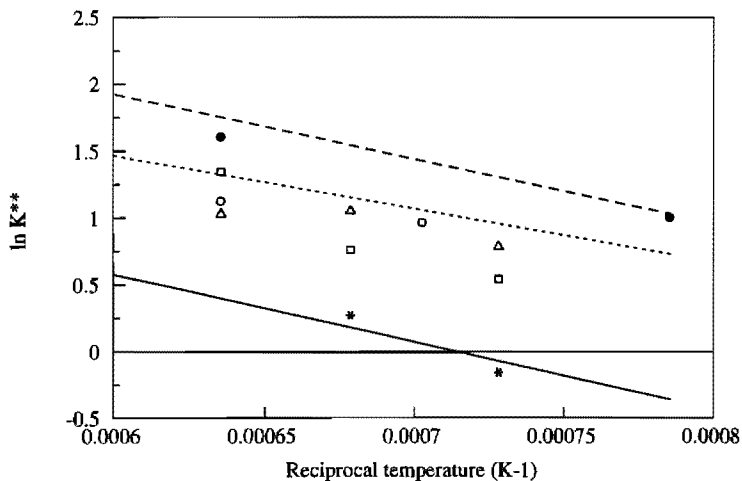


Figure 6.53

The natural logarithm of the redox reaction equilibrium constants of table 6.9 (oxygen measurements, lines) and 6.10 (wet-chemical analysis, symbols) as functions of the reciprocal temperature

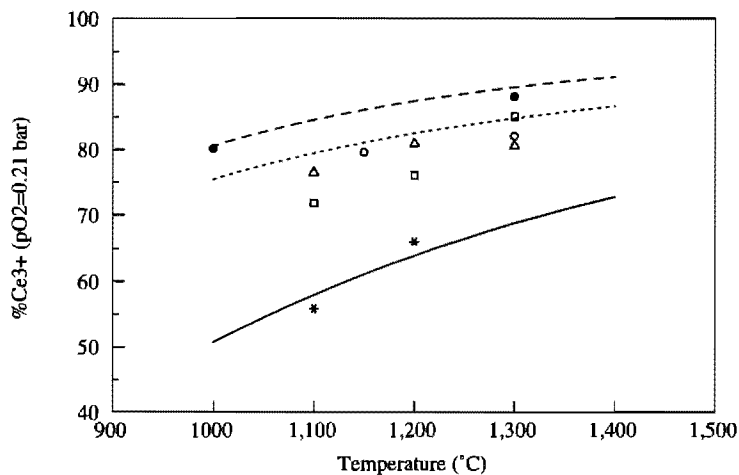


Figure 6.54

The percentage cerium in the reduced state  $\text{Ce}^{3+}$  as a function of temperature, for TV-screen glasses with varying cerium contents in equilibrium with air ( $p_{\text{O}_2}=0.21$  bar). Lines as in table 6.9, symbols as in table 6.10

### 6.4.5 Comparison of the results with data from the literature

#### 6.4.5.1 Literature on the equilibrium state of the cerium reaction in glass

Johnston [12] equilibrated 2.5 gram  $\text{Na}_2\text{O}\cdot 2\text{SiO}_2$  glass samples containing about 3 weight-% Ce (3.7 weight-%  $\text{CeO}_2$ ) in one to three days with different atmospheres ( $\text{O}_2$ , air, an  $\text{Ar}/\text{O}_2$  mixture or  $\text{CO}_2$ ). After quenching of the melts, the  $\text{Ce}^{4+}$  concentration and the total cerium content were determined using wet-chemical methods. Johnston found that the redox ratio  $[\text{Ce}^{3+}]/[\text{Ce}^{4+}]$  at  $1085^\circ\text{C}$  was proportional to the fourth root of the partial oxygen pressure in the atmosphere and concluded that the simple mass expression



is applicable for the cerium reaction in molten glass.

Furthermore, sodium disilicate glasses containing about 3 weight-% Ce were melted in air at 1000, 1200 and  $1300^\circ\text{C}$ . At increasing temperatures, the equilibrium state of reaction 6.51 shifted to the left. In all cases, cerium was predominantly present in the oxidized state  $\text{Ce}^{4+}$ .

Paul and Douglas [15] studied the cerous-ceric equilibrium in binary alkali borate and alkali silicate glasses. 10 gram samples of the glasses containing about 0.5 weight-% cerium (0.6 weight-%  $\text{CeO}_2$ ) were melted for several hours in an air atmosphere. Subsequently the melts were air quenched and analysed for total cerium and tetravalent cerium. The experiments showed, that equilibrium was reached after 10 hours for binary alkali borate glasses at  $1100^\circ\text{C}$ , and after 60 hours for silicate glasses at  $1400^\circ\text{C}$ . Cerium was added to the batch as  $\text{CeO}_2$  or as cerous oxalate. The valency state of the cerium in the batch had no effect on the final valency state after equilibrium had been established.

The composition of the glass, however, did have a significant influence on the equilibrium state. From equation 6.51, it would be expected that at increasing basicity of the melt, the reduced state  $\text{Ce}^{3+}$  would be favoured (see chapter 3). However, experiments have shown that the cerium equilibrium shifts towards the oxidized state when the alkali concentration in the glass is increased, or when molar equivalents of lithia are replaced by soda, and soda by potash [15]. In other words, the cerium equilibrium shifts towards the oxidized state at increasing basicity of the binary alkali borate and silicate glasses.

Paul and Douglas [15] also found, that the cerous-ceric equilibrium shifts towards the oxidized state with increasing cerium contents in the glass, up to

about 0.7 weight-% Ce (0.86 weight-%  $\text{CeO}_2$ ). In contrast with this, the experiments, presented in this thesis, show that in TV-screen glass, the reduced state of cerium is favoured at higher cerium contents.

Lenhart [5] equilibrated soda-lime-silica glass melts containing 0.4 mole-% Ce (1.1 weight-%  $\text{CeO}_2$ ) with air at different temperatures. The redox ratios were established in the quenched samples. The results agree well with the data given by Paul [15] for lithium silicate glasses with a comparable basicity number (see figure 6.55).

As mentioned in chapter 6.4.3, it was not possible to visualize the reduction of cerium in TV-screen glasses containing 0.6 weight-%  $\text{CeO}_2$  with the aid of square wave voltammetry measurements. However, Rüssel [6] found peaks in the positive region of square wave voltammograms recorded in soda-lime-silica glass melts containing 1 mole-%  $\text{CeO}_2$  (about 2.9 weight-%  $\text{CeO}_2$ ). This indicates that cerium is, under these circumstances, likewise predominantly present in the reduced state  $\text{Ce}^{3+}$ .

Takahashi and Miura [23] used another electrochemical method, Cyclic Voltammetry, to study the equilibrium state of several polyvalent elements in soda-lime-silica and sodium disilicate glass melts at 1250°C. In the cyclic voltammograms, recorded in the glass melts containing 1 mole-% Ce (2.9 weight-%  $\text{CeO}_2$ ), they found peaks in the negative region, which would indicate that under these conditions, cerium is mainly present as  $\text{Ce}^{4+}$ . However, the measurable potential range for cyclic voltammetry measurements in molten glass is small, while the peaks, resulting from a one-electron transfer reaction, are very broad. Therefore Cyclic Voltammetry is, in my opinion, not suitable for the determination of the formal potential of one-electron transfer reactions in glass melts at high temperatures.

#### 6.4.5.2 Graphical presentation of the literature data and results presented in this thesis

The literature data on the equilibrium state of the cerium reaction have been translated to the redox reaction equilibrium constants with the aid of equation 6.48 or equation 5.66. In equation 6.48,  $p_{\text{O}_2}$  was assumed to be equal to the partial oxygen pressure in the atmosphere. In figure 6.55, the redox reaction equilibrium constants, calculated from the literature data, are compared with the results of the oxygen equilibrium pressure measurements, presented in table 6.9.

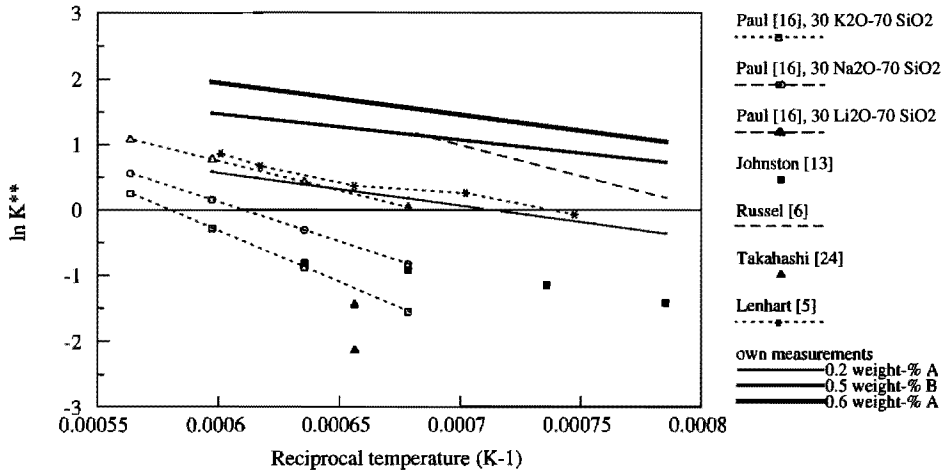


Figure 6.55

The natural logarithm of the redox reaction equilibrium constants of the cerium reaction, derived from literature data and from the data presented in this thesis in table 6.9

The basicity number as defined by Sun [1] of the glasses are:

30 K <sub>2</sub> O-70 SiO <sub>2</sub>	40.9	
30 Na <sub>2</sub> O-70 SiO <sub>2</sub>	38.8	
30 Li <sub>2</sub> O-70 SiO <sub>2</sub>	34.0	Paul [15]
33.3 Na <sub>2</sub> O-66.7 SiO <sub>2</sub>	41.6	Johnston [12], Takahashi [23]
soda-lime-silica glass	34.2	Rüssel [6], Lenhart [5]
soda-lime-silica glass	35.7	Takahashi [23]
TV-screen glass type A	34	
TV-screen glass type B	36	this thesis

The results of the cerium equilibrium measurements in soda-lime-silica glass, presented by Lenhart, agree very well with the data for lithium silicate glass, which has about the same basicity number. The equilibrium constant of the cerium reaction in TV-screen glass type A containing 0.2 weight-% CeO<sub>2</sub> lies in the same order of magnitude, too. However, the equilibrium constant in TV-screen glasses with higher cerium contents is apparently higher. This indicates that the basicity number in itself is unsuitable for the determination of the equilibrium state of cerium in molten glasses.

### 6.4.6 Conclusions

- Oxygen equilibrium pressure measurements can be used for the determination of the redox reaction enthalpy and entropy of cerium in TV-screen glasses;
- wet-chemical analyses confirm the results of the oxygen equilibrium pressure measurements in the TV-screen glass type A;
- The wet-chemical analyses in the TV-screen glass type B show some scattering. The results, however, do not contradict the results from the oxygen equilibrium pressure measurements in this type of glass;
- at low cerium contents in TV-screen glass, the oxidized form of cerium,  $\text{Ce}^{4+}$ , is favoured. The behaviour of cerium resembles that of iron and antimony in TV-screen glasses: at low concentrations of the polyvalent element, the oxidized state is favoured;
- the equilibrium constant of the cerium reaction in one type of glass can not be estimated on the basis of measurements in glasses with different compositions or concentrations.

## 6.5 CHROMIUM

### 6.5.1 Chromium in glass

In the container glass industry, chromium is added to the batch in order to obtain a green-coloured glass. The green colour originates from  $\text{Cr}^{3+}$ . Chromium can also be present as  $\text{Cr}^{6+}$  [7] and  $\text{Cr}^{2+}$ . The redox reactions can be briefly described by:



and



Chromium is also present in E-glass. It may influence the heat distribution in the glass melting tank, since  $\text{Cr}^{3+}$  partly absorbs infrared radiation.

The equilibrium state of reactions 6.52 and 6.53 can be described by the redox reaction equilibrium constants:

$$K_1^{**}(\text{T}) = \frac{[\text{Cr}^{3+}] \cdot p_{\text{O}_2}^{3/4}}{[\text{Cr}^{6+}]} = \exp \left\{ \frac{-\Delta H_1^{**}}{R_g \cdot \text{T}} + \frac{\Delta S_1^{**}}{R_g} \right\} \quad (6.54)$$

and

$$K_2^{**}(T) = \frac{[\text{Cr}^{2+}] \cdot p_{\text{O}_2}^{1/4}}{[\text{Cr}^{3+}]} = \exp \left\{ \frac{-\Delta H_2^{**}}{R_g \cdot T} + \frac{\Delta S_2^{**}}{R_g} \right\} \quad (6.55)$$

In this thesis, the equilibrium constants of chromium in soda-lime-silica glass and E-glass containing 0.4 weight-%  $\text{CrO}_3$  are investigated using square wave voltammetry measurements.

## 6.5.2 Square wave voltammetry measurements

### 6.5.2.1 The experimental procedure

The glasses containing chromium were melted in platinum crucibles at  $1400^\circ\text{C}$  until all grains were dissolved and the melt was bubble-free. Then the glass was quenched to room temperature and transferred to an  $\text{Al}_2\text{O}_3$ -crucible. This crucible was placed in the furnace, sketched in figure 5.3, and heated slowly to  $1400^\circ\text{C}$ . Then the electrodes were lowered until the reference electrode just touched the melt.

After a waiting time of 15 minutes to allow the glass melt to obtain a homogeneous temperature distribution, the uncompensated resistance of the melt was measured (see chapter 5). Subsequently a square wave voltammogram was recorded. Generally the experimental set-up was:

Initial potential: 0 V  
 Final potential: -0.8 V  
 $f$ : 100 Hz  
 $\Delta E_b$ : -0.002 V  
 $\Delta E_p$ : 0.1 V

but sometimes the parameters were set to other values in order to obtain a clear peak in the voltammograms.

### 6.5.2.2 The recorded square wave voltammograms

In figure 6.56 an example of a square wave voltammogram, recorded in a soda-lime-silica glass melt, is given. The currents measured during "forward" and "reverse" pulses are plotted against the base potential. The current that was measured during a "reverse" pulse,  $i_r$ , is subtracted from the current measured during the preceding "forward" pulse,  $i_f$ , resulting in the "differentiated" current  $\delta i$  (see chapter 5.5.3). In the curves of both  $i_f$  and  $i_r$ , a peak is vaguely visible at about -0.65 V. This indicates that the redox reaction that causes the peaks, is reversible.

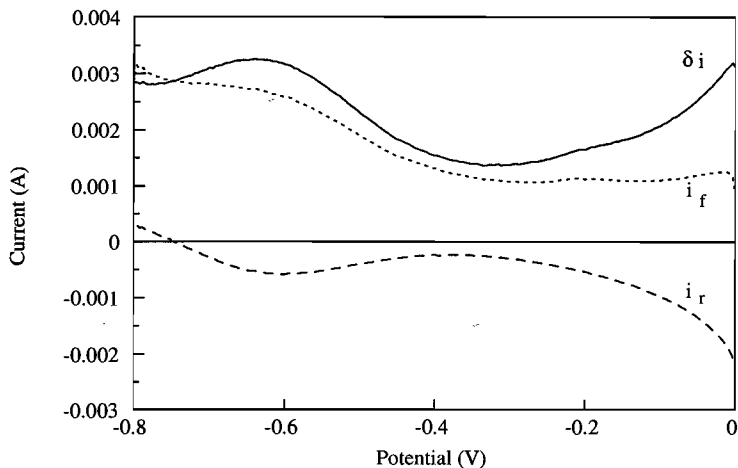


Figure 6.56

The complete square wave voltammogram recorded in soda-lime-silica glass containing 0.4 weight-%  $\text{CrO}_3$  at  $1300^\circ\text{C}$  with the following set-up:

$$\Delta E_b = 0.002 \text{ V}$$

$$\Delta E_p = 0.1 \text{ V}$$

$$f = 100 \text{ Hz}$$

$$R_u = 17.9 \ \Omega$$

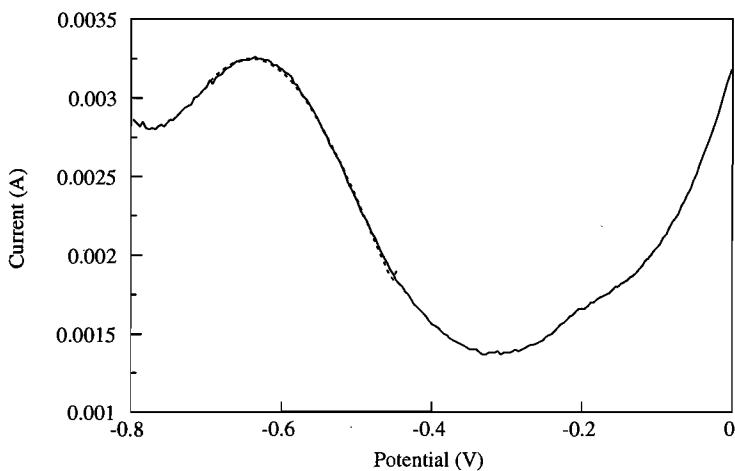


Figure 6.57

The square wave voltammogram recorded in soda-lime-silica glass containing 0.4 weight-%  $\text{CrO}_3$  at  $1300^\circ\text{C}$  with the following set-up:

$$\Delta E_b = 0.002 \text{ V}$$

$$\Delta E_p = 0.1 \text{ V}$$

$$f = 100 \text{ Hz}$$

$$R_u = 17.9 \ \Omega$$

compared to the theoretical curve of a one-electron transfer with the same set-up (-----)

In figure 6.57 only the "differentiated" current is displayed. Now the peak in  $\delta i$  can be seen more clearly. In the same figure, the theoretical curve for a reversible one-electron transfer with a peak at  $-0.642$  V is drawn. The agreement between the theoretical and experimental curve is very good. This is a further indication of the reversibility of the redox reaction. Since one electron is transferred, the redox reaction can not be the reduction of  $\text{Cr}^{6+}$  to  $\text{Cr}^{3+}$ . The peak is probably due to the reduction of  $\text{Cr}^{3+}$  to  $\text{Cr}^{2+}$ . This is in agreement with the supposition that chromium is predominantly present in the trivalent form at the melting temperatures.

The position of the peak can be established with a accuracy of  $\pm 1$  mV and a reproducibility of  $\pm 5$  mV.

The increase in current at 0 V is presumably resulting from the oxidation of platinum or the formation of oxygen gas, while the increase at  $-0.8$  V results from reduction of other glass components like Na or Si (see chapter 5.5).

#### 6.5.2.3 The influence of the frequency

The frequency of the applied signal has no effect on the position of the peak if the reaction is completely reversible. Experiments have shown that at  $1300^\circ\text{C}$ , the position of the  $\text{Cr}^{3+}/\text{Cr}^{2+}$  peak does not vary for frequencies up to 200 Hz. This is a third indication that the reduction of  $\text{Cr}^{3+}$  to  $\text{Cr}^{2+}$  is reversible.

#### 6.5.2.4 The influence of the temperature

At a decrease in temperature, the  $\text{Cr}^{3+}/\text{Cr}^{2+}$  peak shifts in the negative direction. This indicates that the equilibrium state of reaction 6.53 shifts to the left at decreasing temperatures. The  $\text{Cr}^{3+}$  state is favoured even more at lower temperatures (relative to  $\text{Cr}^{2+}$ ).

At still lower temperatures, the  $\text{Cr}^{3+}/\text{Cr}^{2+}$  peak approaches the negative potential limit of the square wave voltammetry measurements, which results from reduction reactions of other components of the glass melt (Na, Si) and charging of the electrochemical double layer (see chapter 5.5). At about  $1000^\circ\text{C}$ , the peak can not be distinguished from the background currents in square wave voltammograms recorded with the frequency set to 100 Hz.

However, the peak can be made visible by choosing another frequency. Both the faradaic and the charging current decrease if the frequency is set to a lower



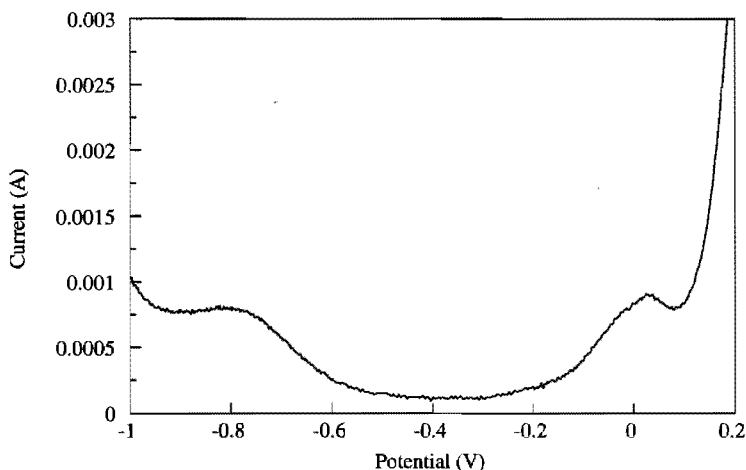


Figure 6.58

The square wave voltammogram recorded in soda-lime-silica glass containing 0.4 weight-%  $\text{CrO}_3$  at  $1000^\circ\text{C}$  with the following set-up:

$$\Delta E_b = 0.002 \text{ V}$$

$$\Delta E_p = 0.05 \text{ V}$$

$$f = 10 \text{ Hz}$$

$$R_u = 1.1 \Omega$$

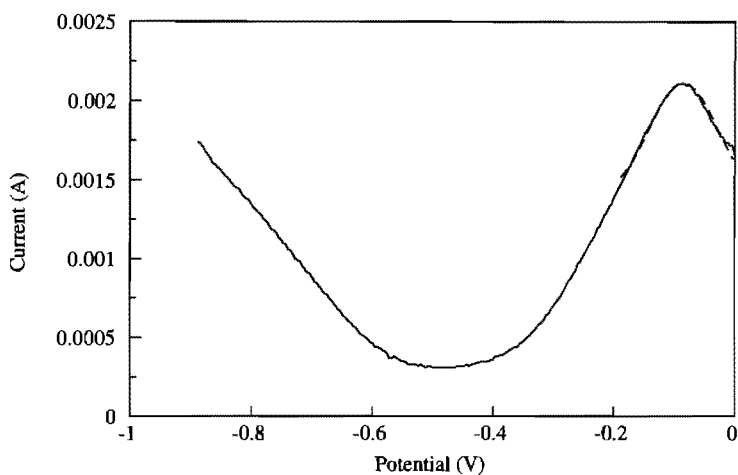


Figure 6.59

The square wave voltammogram (————) recorded in soda-lime-silica glass containing 0.4 weight-%  $\text{CrO}_3$  at  $780^\circ\text{C}$  with the following set-up:

$$\Delta E_b = 0.002 \text{ V}$$

$$\Delta E_p = 0.05 \text{ V}$$

$$f = 100 \text{ Hz}$$

compared to the theoretical voltammogram of a reversible three electron transfer with the same set-up (-----)

value, but the effect is more distinct in the charging current. This means that the contribution of the faradaic to the total current increases as the frequency is decreased (see chapter 5 and 6.2.3.3). In figure 6.58, the square wave voltammogram recorded in the soda-lime-silica glass containing 0.4 weight-%  $\text{CrO}_3$  at  $1000^\circ\text{C}$  with a frequency of 10 Hz is given. Now a clear peak due to a one electron transfer is visible at  $-0.803$  V. Besides, a peak becomes visible at about  $-0.030$  V.

If the temperature of the glass melt is decreased further, the peak due to the reduction of  $\text{Cr}^{3+}$  to  $\text{Cr}^{2+}$  can not be distinguished from the background current, independent of the applied frequency. The second peak shifts towards the negative potential region and can be seen more clearly in figures 6.58 and 6.59.

In figure 6.59, the recorded voltammogram is compared to a theoretical curve for a reversible three electron transfer. The agreement is good, and therefore it can be decided that the peak is due to the reduction of  $\text{Cr}^{6+}$  to  $\text{Cr}^{3+}$ . Furthermore it can be stated that the reduction reaction is reversible. The peak is located at  $-0.085$  V.

At temperatures below  $700^\circ\text{C}$ , the uncompensated resistance in the glass melt is too high to allow for a reliable determination of the position of the  $\text{Cr}^{6+}/\text{Cr}^{3+}$  peak. The position of this peak can therefore only be established at temperatures between  $\pm 700$  and  $1000^\circ\text{C}$ , while the  $\text{Cr}^{3+}/\text{Cr}^{2+}$  peak can be seen at temperatures between  $800$  and  $1500^\circ\text{C}$ .

#### 6.5.2.5 The ratio of the diffusion coefficients of $\text{Cr}^{6+}$ and $\text{Cr}^{3+}$

The height of the peak in the square wave voltammograms is proportional to the square root of the diffusion coefficient of the reacting species. For example, the height of the peak at  $-0.124$  V in figure 6.60 is proportional to the square root of the diffusion coefficient of  $\text{Cr}^{6+}$ , since the peak is due to the reduction of  $\text{Cr}^{6+}$ .

In figure 6.61, the square wave voltammogram that was recorded while the potential range was scanned from  $-1.0$  to  $0$  V is given. Before the voltammogram was recorded, the potential was held for 15 seconds at a value of  $-1.0$  V. In this time, the chromium in the vicinity of the working electrode is completely transferred to the  $\text{Cr}^{3+}$  state (or even the  $\text{Cr}^{2+}$  state).

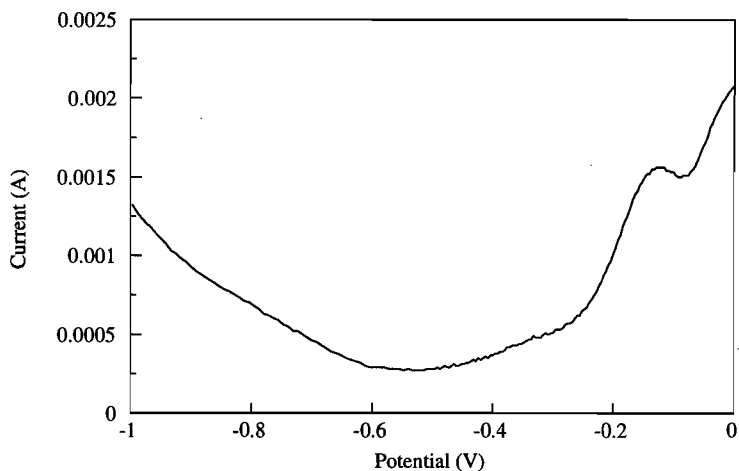


Figure 6.60

The square wave voltammogram recorded in soda-lime-silica glass containing 0.4 weight-%  $\text{CrO}_3$  at  $700^\circ\text{C}$  with the following set-up:

$$\begin{array}{lll} \Delta E_p = 0.002 \text{ V} & f = 100 \text{ Hz} & E_i = 0 \text{ V} \\ \Delta E_p = 0.05 \text{ V} & R_u = 41 \Omega & E_{\text{end}} = -1.0 \text{ V} \end{array}$$

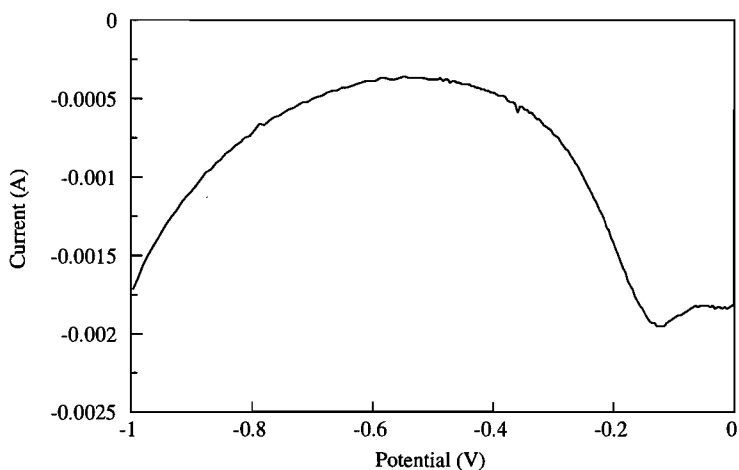


Figure 6.61

The square wave voltammogram recorded in soda-lime-silica glass containing 0.4 weight-%  $\text{CrO}_3$  at  $700^\circ\text{C}$  with the following set-up:

$$\begin{array}{lll} \Delta E_p = 0.002 \text{ V} & f = 100 \text{ Hz} & E_i = -1.0 \text{ V} \\ \Delta E_p = 0.05 \text{ V} & R_u = 41 \Omega & E_{\text{end}} = 0 \text{ V} \end{array}$$

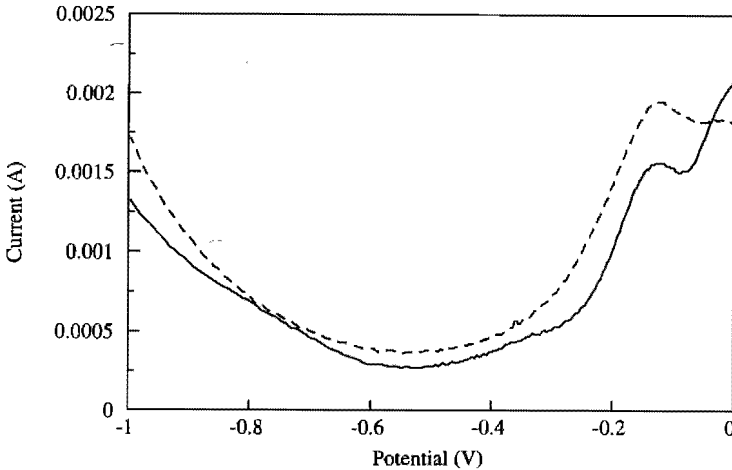


Figure 6.62

The square wave voltammograms recorded in soda-lime-silica glass containing 0.4 weight-%  $\text{CrO}_3$  at  $700^\circ\text{C}$  with the following set-ups:

$E_i = 0 \text{ V}$	$\Delta E_b = 0.002 \text{ V}$	-----	$E_i = -1.0 \text{ V}$	$\Delta E_b = 0.002 \text{ V}$
$E_{\text{end}} = -1.0 \text{ V}$	$\Delta E_p = 0.05 \text{ V}$		$E_{\text{end}} = 0 \text{ V}$	$\Delta E_p = 0.05 \text{ V}$
	$f = 100 \text{ Hz}$			$f = 100 \text{ Hz}$
	$R_u = 41 \Omega$		multiplied by -1	$R_u = 41 \Omega$

Now the negative peak at  $-0.122 \text{ V}$  in the voltammogram is due to the oxidation of  $\text{Cr}^{3+}$  to  $\text{Cr}^{6+}$ . The height of the peak is proportional to the square root of the diffusion coefficient of  $\text{Cr}^{3+}$ .

In figure 6.62, both voltammograms recorded at  $700^\circ\text{C}$  are displayed. The y-values of the voltammogram scanned from  $-1.0$  to  $0 \text{ V}$  are multiplied by  $-1$ .

The ratio of the diffusion coefficients of  $\text{Cr}^{3+}$  and  $\text{Cr}^{6+}$  in soda-lime-silica glass at  $700^\circ\text{C}$  can now be derived from the peak heights in figure 6.62:

$$\sqrt{\frac{D_{\text{Cr}^{3+}}}{D_{\text{Cr}^{6+}}}} = \frac{1.946 \text{ Ampère}}{1.572 \text{ Ampère}} = 1.24 \quad (6.56)$$

The ratio of the diffusion coefficients of  $\text{Cr}^{3+}$  and  $\text{Cr}^{6+}$  is close to 1 for temperatures ranging between  $700$  and  $1000^\circ\text{C}$ . The ratio of the diffusion coefficients of  $\text{Cr}^{2+}$  and  $\text{Cr}^{3+}$  has not been established and is assumed to be 1 in the following sections.

### 6.5.2.6 Calculation of the formal potentials $E^{0'}$ and the constants $K_1^{**}$ and $K_2^{**}$

Now that the ratio of the diffusion coefficients of  $\text{Cr}^{3+}$  and  $\text{Cr}^{6+}$  is known, the formal potential  $E^{0'}$  of reaction 6.52 can be derived from the position of the  $\text{Cr}^{6+}/\text{Cr}^{3+}$  peak in the square wave voltammogram ( $E_{1/2}$ ) with the aid of equation 5.16. The equilibrium constant of the  $\text{Cr}^{6+}/\text{Cr}^{3+}$  reaction  $K_1^{**}(T)$ , as defined in equation 6.54, can be calculated from the formal potential using equation 5.66.

The ratio of the diffusion coefficients of  $\text{Cr}^{3+}$  and  $\text{Cr}^{2+}$  is not known. However, it can be assumed to be at unity for any temperature. Then the  $\text{Cr}^{3+}/\text{Cr}^{2+}$  peak in the square wave voltammograms is located at the formal potential of reaction 6.53. The redox reaction equilibrium constant  $K_2^{**}(T)$ , defined in equation 6.55, can be calculated with the aid of equation 5.66.

### 6.5.2.7 The redox reaction enthalpies and entropies

The formal potentials of the  $\text{Cr}^{6+}/\text{Cr}^{3+}$  reaction have been determined for temperatures varying from 700 to 1000°C. From the temperature dependency, the enthalpy  $\Delta H_1^{**}$  and entropy  $\Delta S_1^{**}$  of reaction 6.52 can be calculated. The enthalpy  $\Delta H_2^{**}$  and entropy  $\Delta S_2^{**}$  of the  $\text{Cr}^{3+}/\text{Cr}^{2+}$  reaction was calculated from the temperature dependency of the position of the  $\text{Cr}^{3+}/\text{Cr}^{2+}$  peak between 800 and 1500°C (see figure 6.63). The results are summarized in table 6.11.

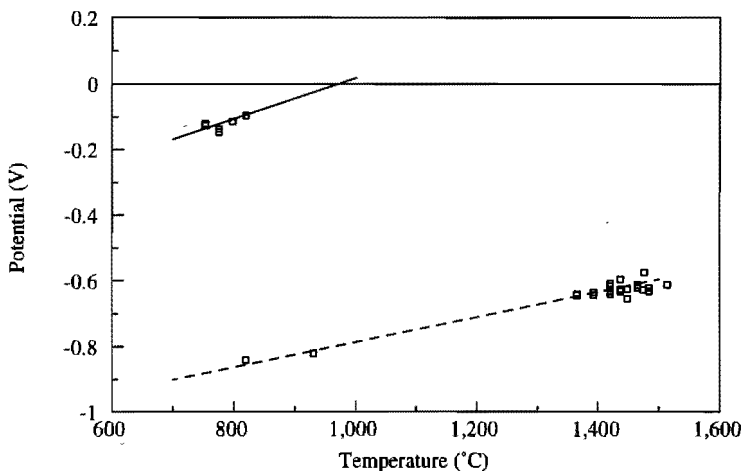


Figure 6.63

The formal potentials of the  $\text{Cr}^{6+}/\text{Cr}^{3+}$  (—) and the  $\text{Cr}^{3+}/\text{Cr}^{2+}$  (- - - -) reactions in a soda-lime-silica glass melt containing 0.4 weight-%  $\text{CrO}_3$

### 6.5.2.8 Chromium in E-glass

The capacity of the electrochemical double layer in E-glass lies in the same order of magnitude as those in soda-lime-silica and TV-screen glass melts (see chapter 5.3.6). On the other hand, the resistivity of E-glass is about ten times the resistivity of soda-lime-silica glass at the same temperature. The current, due to the charging of the electrochemical double layer after a change in the applied potential, is given by:

$$i_c = \frac{E}{R} \cdot e \frac{-t}{R \cdot C_d} \quad (6.57)$$

with $i_c$	= charging current	[A]
$E$	= (change in) applied potential	[V]
$R$	= resistance	[ $\Omega$ ]
$t$	= time elapsed since the change in potential	[s]
$C_d$	= double layer capacity	[F]

Therefore the contribution of the charging current to the total current is much more extensive for square wave voltammetry measurements in E-glass than in soda-lime-silica glass. This can be seen clearly from figure 6.64. Here, the complete square wave voltammogram recorded in E-glass containing 0.4 weight-%  $\text{CrO}_3$  at  $1000^\circ\text{C}$  is displayed. Both the "forward" and the "reverse" current show progressively rising curves, with only a tiny peak (positive for  $i_f$  and negative for  $i_r$ ) at about -0.7 V probably due to the reaction of  $\text{Cr}^{3+}$  to  $\text{Cr}^{2+}$ .

The exact position of this "peak" can be established by comparing the measured curve with the theoretical curve for a one-electron transfer, superimposed on a continuously increasing curve representing the capacitive current.

In figure 6.65, the positions of the  $\text{Cr}^{6+}/\text{Cr}^{3+}$  and  $\text{Cr}^{3+}/\text{Cr}^{2+}$  peaks in the square wave voltammograms, recorded at various temperatures in E-glass containing 0.4 weight-%  $\text{CrO}_3$  are displayed.

The enthalpy and entropy of reactions 6.52 and 6.53 in E-glass have been established following the procedure described in section 6.5.2.7. The results will be given in the next section.

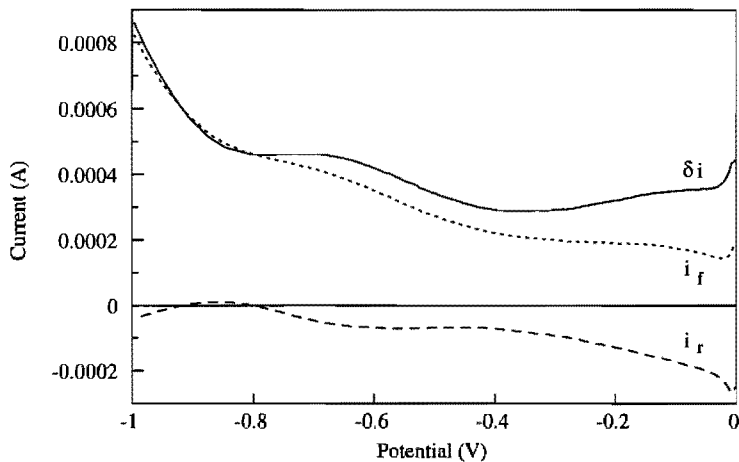


Figure 6.64

The square wave voltammogram recorded in E-glass containing 0.4 weight-%  $\text{CrO}_3$  at  $1000^\circ\text{C}$  with the following set-up:

$$\Delta E_p = 0.002 \text{ V}$$

$$\Delta E_p = 0.05 \text{ V}$$

$$f = 20 \text{ Hz}$$

$$R_u = 95.6 \ \Omega$$

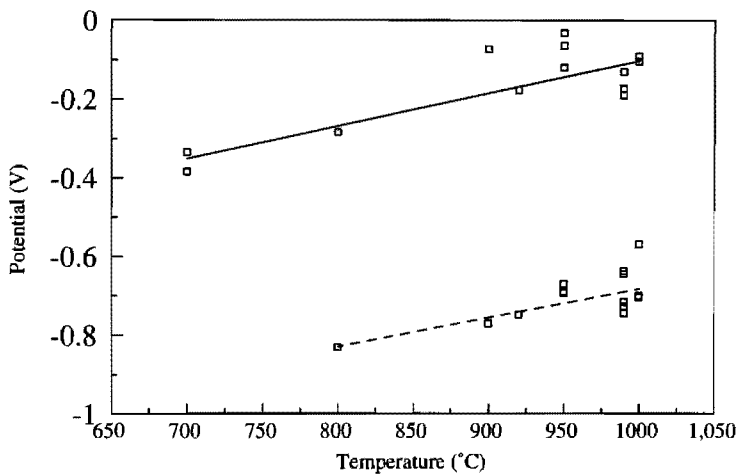


Figure 6.65

The positions of the  $\text{Cr}^{6+}/\text{Cr}^{3+}$  (————) and the  $\text{Cr}^{3+}/\text{Cr}^{2+}$  (- - - - -) peaks in E-glass containing 0.4 weight-%  $\text{CrO}_3$

### 6.5.2.9 Results of the square wave voltammetry measurements

With the aid of square wave voltammetry measurements, the enthalpies and entropies of both reduction reactions of chromium have been determined in soda-lime-silica and E-glass, containing 0.4 weight-%  $\text{CrO}_3$ .

Table 6.11

The enthalpies and entropies of the redox reactions of chromium in soda-lime-silica and E-glass

Glass	Concentration (weight-% $\text{CrO}_3$ )	$\text{Cr}^{6+}/\text{Cr}^{3+}$		$\text{Cr}^{3+}/\text{Cr}^{2+}$	
		$\Delta H_1^{**}$ (kJ·mole <sup>-1</sup> )	$\Delta S_1^{**}$ (J·mole <sup>-1</sup> ·K <sup>-1</sup> )	$\Delta H_2^{**}$ (kJ·mole <sup>-1</sup> )	$\Delta S_2^{**}$ (J·mole <sup>-1</sup> ·K <sup>-1</sup> )
soda-lime-silica	0.4	225 ± 4	181 ± 67	123 ± 2	37 ± 2
E-glass	0.4	335 ± 18	240 ± 48	155 ± 5	70 ± 23

### 6.5.3 Comparison of the results with data from literature

Rüssel [6] determined the formal potentials of the two chromium redox reactions in a  $16\text{Na}_2\text{O}-10\text{CaO}-74\text{SiO}_2$  glass melt containing 1 mole-% Cr (1.7 weight-%  $\text{CrO}_3$ ) at various temperatures using square wave voltammetry. The results are in agreement with the results, presented in this thesis, as can be seen from figure 6.66.

Takahashi and Miura [23] used Cyclic Voltammetry to study the equilibrium state of chromium in soda-lime-silica and sodium disilicate glass melts containing 1 mole-% Ce (1.7 weight-%  $\text{CrO}_3$ ) at 1250°C. They found peaks in the negative region, which they ascribed to the  $\text{Cr}^{6+}/\text{Cr}^{3+}$  reaction. This would indicate that under these conditions, chromium is mainly present as  $\text{Cr}^{6+}$ . The results of Rüssel [6], and the results presented in this thesis indicate, however, that chromium is predominantly present as  $\text{Cr}^{3+}$  in soda-lime-silica glasses at melting temperatures. Cyclic voltammetry is, especially at high temperatures, less accurate than square wave voltammetry. Therefore it is difficult to establish the peak position and the amount of electrons, transferred during the redox reaction. In my opinion, Cyclic Voltammetry is not suitable for the determination of the formal potentials of redox reactions in glass melts at high temperatures, especially if these formal potentials are located close to the limits of the measurable potential region.



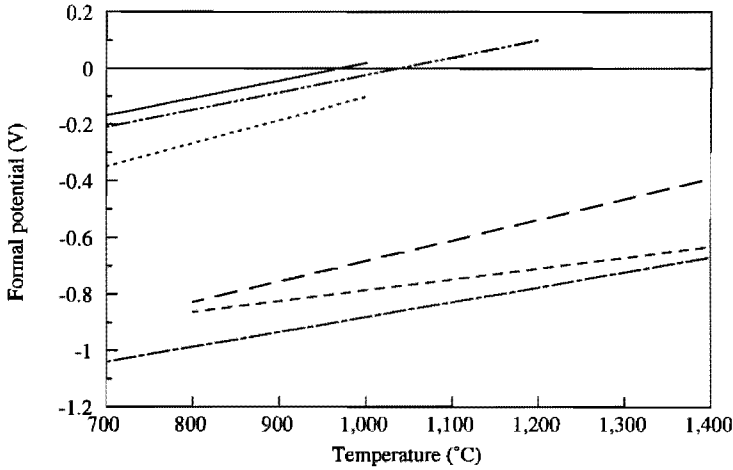


Figure 6.66  
The formal potentials of the  $\text{Cr}^{6+}/\text{Cr}^{3+}$  and the  $\text{Cr}^{3+}/\text{Cr}^{2+}$  reactions in 3 types of glass as functions of the temperature

	16Na <sub>2</sub> O-10CaO-74SiO <sub>2</sub> [6]	15Na <sub>2</sub> O-10CaO-75SiO <sub>2</sub>	E-glass (this thesis)
$\text{Cr}^{6+}/\text{Cr}^{3+}$	-----	-----	-----
$\text{Cr}^{3+}/\text{Cr}^{2+}$	-----	-----	-----

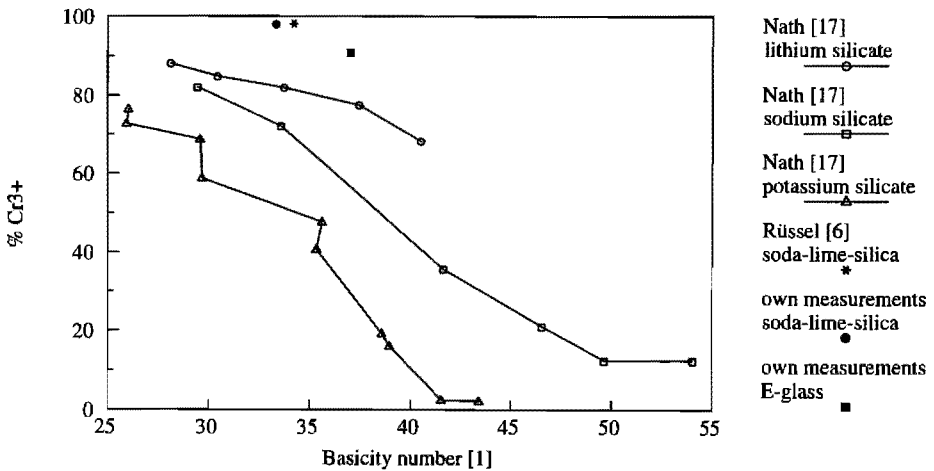


Figure 6.67  
The percentage of chromium in the trivalent state  $\text{Cr}^{3+}$  in glass melts in equilibrium with air ( $P_{\text{O}_2}=0.21$  bar) as a function of the basicity number

Nath and Douglas [16] equilibrated various binary alkali silicate glass melts containing about 0.1 %  $\text{Cr}_2\text{O}_3$  (0.07 weight-%  $\text{CrO}_3$ ) at  $1400^\circ\text{C}$  with air. After quenching, the  $\text{Cr}^{6+}$  and total chromium contents were determined chemically, and the concentration  $\text{Cr}^{3+}$  was calculated from the optical absorption. The redox ratio  $[\text{Cr}^{3+}]/[\text{Cr}^{6+}]$  was found to decrease with increasing alkali content and, at the same molar alkali content, to decrease in the order Li, Na, K (see figure 6.67). This indicates that equation 6.52 does not describe the reduction of  $\text{Cr}^{6+}$  in the melt correctly.

In figure 6.67, the percentage chromium present in the trivalent state  $\text{Cr}^{3+}$  for glass melts equilibrated with air at  $1400^\circ\text{C}$  is given as a function of the basicity number of the glass as defined by Sun [1]. Clearly, the basicity number is not a good parameter to estimate the redox equilibrium state of chromium in molten glasses.

The results of the wet-chemical analyses [16] differ considerably from those, derived by square wave voltammetry [6, this thesis]. This may be caused by the difference in compositions or concentrations. Further investigations might provide an explanation.

#### 6.5.4 Conclusions

- Square wave voltammetry measurements can be used to establish the equilibrium state of chromium in soda-lime-silica and E-glass: the equilibrium state of the  $\text{Cr}^{6+}/\text{Cr}^{3+}$  reaction between  $700$  and  $1000^\circ\text{C}$  and the equilibrium state of the  $\text{Cr}^{3+}/\text{Cr}^{2+}$  reaction between  $800$  and  $1500^\circ\text{C}$ ;
- for the calculation of the redox reaction equilibrium constants of chromium in soda-lime-silica or E-glass containing 0.4 weight-%  $\text{CrO}_3$  the values of the enthalpies and entropies, given in table 6.11, can be used;
- at melting temperatures ( $1100$ - $1500^\circ\text{C}$ ) chromium is predominantly present in the  $\text{Cr}^{3+}$  state;
- more investigations are needed to decide whether the differences in the results from square wave voltammetry measurements and wet-chemical analyses result from differences in glass compositions, chromium concentrations or other causes.

## 6.6 SULPHUR

### 6.6.1 Sulphur in glass

Sulphur is added to the batch for different reasons:

- to obtain an amber colour (in combination with iron);
- to enhance the melting process;
- to aid the fining of the molten glass.

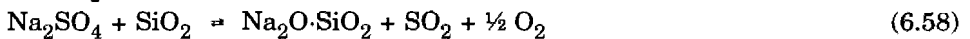
The effectiveness of the sulphur as colouring or fining agent or melting accelerator depends on its valency state. Sulphur appears in the valency states  $S^{6+}$ ,  $S^{4+}$ ,  $S^0$  and  $S^{2-}$ . Under oxidizing conditions, sulphur in glass melts is present mainly as sulphate, while under reducing atmospheres the sulphide form predominates [2].

#### 6.6.1.1 The amber colour

The amber colour of glass is caused by the  $Fe^{3+}/S^{2-}$ -complex [27]. Therefore amber glass is melted under reducing atmospheres.

#### 6.6.1.2 The enhancement of the melting process

In general, sulphur is added to the batch as  $Na_2SO_4$ . Other forms of sulphate, for instance  $CaSO_4$  or  $K_2SO_4$ , are less stable [2,28], and will therefore be partly converted to  $Na_2SO_4$  in the initial stage of the melting process [29].  $Na_2SO_4$  forms a liquid phase with a low surface tension at  $884^\circ C$ . It "moisturizes" the  $SiO_2$ -grains which would by themselves only melt at elevated temperatures. The  $SiO_2$ -grains dissolve in the liquid phase:

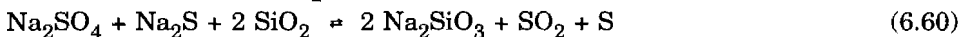


This dissolution reaction occurs at temperatures above  $1050^\circ C$ , but is really important at temperatures exceeding  $1288^\circ C$  [28,30]. Because gases evolve during this reaction, the fining of the melt is enhanced at the same time.

When a reducing agent like carbon is added to the batch, a part of the sulphate is converted into sulphide:



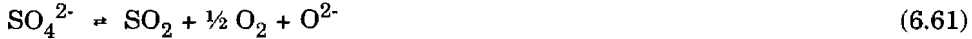
at  $740$  to  $800^\circ C$ . The combination sulphate and sulphide provides for an eutectic melt in which  $SiO_2$ -grains dissolve:



This reaction occurs at temperatures exceeding  $860^\circ C$  [28].

### 6.6.1.3 Sulphur as a fining agent

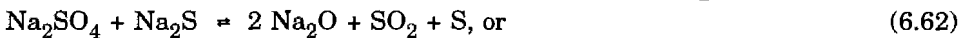
At elevated temperatures ( $\pm 1450^\circ\text{C}$  [17,18,19,30]) the (remaining) sulphate, dissolved in the molten glass, dissociates:



The fining gases  $\text{SO}_2$  and  $\text{O}_2$  diffuse to existing bubbles, causing them to grow (see chapter 2.6). In contrast with reaction 6.58, reaction 6.61 should take place at temperatures at which gas bubbles can easily ascend to the surface of the low-viscous glass melt.

Under reducing conditions, sulphate and sulphide react at low temperatures according to reaction 6.60 and thus  $\text{SO}_2$  is released. This  $\text{SO}_2$  may diffuse to existing bubbles, but the melt viscosity is yet too high to allow for a rapid removal of the bubbles.

Sulphate and sulphide can also form  $\text{SO}_2$  gas when no  $\text{SiO}_2$  is available:



so the glass melt becomes supersaturated with  $\text{SO}_2$  [29]. At an increase of temperature, the dissociation of the remaining sulphate will be prohibited by this excess of  $\text{SO}_2$ , and only at very high temperatures, at which the viscosity of the glass melt is low and bubbles can easily ascend to the surface of the melt, the sulphate dissociation occurs [29]. The residual sulphate is therefore a very effective fining agent.

According to other authors [2,19,31], sulphur is predominantly present as sulphide in reduced melts. It is not known whether sulphide can act as a fining agent. The incorporation of sulphur in the reduced melt is assumed to take place as [19,31]:



followed by:

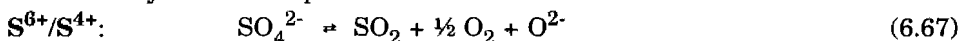


or without the intermediate  $\text{S}_2$ :



### 6.6.1.4 General reaction equations

The subjoined reaction equations are generally used to describe the conversion of one valency state of sulphur into another.



with the redox reaction equilibrium constant  $K_1^{**}(\text{T})$ :

$$K_1^{**} (T) = \frac{P_{SO_2} \cdot \sqrt{P_{O_2}}}{[SO_4^{2-}]} = \exp \left( \frac{-\Delta H_1^{**}}{R_g \cdot T} + \frac{\Delta S_1^{**}}{R_g} \right) \quad (6.68)$$

$$S^{4+}/S^0: \quad 2 SO_2 \rightleftharpoons S_2 + 2 O_2 \quad (6.69)$$

with the redox reaction equilibrium constant  $K_2^{**} (T)$ :

$$K_2^{**} (T) = \frac{P_{S_2} \cdot P_{O_2}^2}{P_{SO_2}^2} = \exp \left( \frac{-\Delta H_2^{**}}{R_g \cdot T} + \frac{\Delta S_2^{**}}{R_g} \right) \quad (6.70)$$

$$S^0/S^{2-}: \quad S_2 + 2 O^{2-} \rightleftharpoons 2 S^{2-} + O_2 \quad (6.71)$$

with the redox reaction equilibrium constant  $K_3^{**} (T)$ :

$$K_3^{**} (T) = \frac{[S^{2-}]^2 \cdot P_{O_2}}{P_{S_2} \cdot [O^{2-}]^2} = \exp \left( \frac{-\Delta H_3^{**}}{R_g \cdot T} + \frac{\Delta S_3^{**}}{R_g} \right) \quad (6.72)$$

$$S^{4+}/S^{2-}: \quad SO_2 + O^{2-} \rightleftharpoons S^{2-} + 1/2 O_2 \quad (6.73)$$

with the redox reaction equilibrium constant  $K_4^{**} (T)$ :

$$K_4^{**} (T) = \frac{[S^{2-}] \cdot P_{O_2}^{1/2}}{P_{SO_2} \cdot [O^{2-}]} = \exp \left( \frac{-\Delta H_4^{**}}{R_g \cdot T} + \frac{\Delta S_4^{**}}{R_g} \right) \quad (6.74)$$

### 6.6.1.5 Objective of this section

In this section the suitability of oxygen equilibrium pressure measurements for the determination of the redox reaction enthalpy and entropy of reaction 6.67,  $\Delta H_1^{**}$  and  $\Delta S_1^{**}$ , will be investigated.

Furthermore square wave voltammetry measurements will be used to investigate the redox reaction enthalpies and entropies of reactions 6.67, 6.69 and 6.71.

## 6.6.2 Oxygen equilibrium pressure measurements

### 6.6.2.1 The theoretical oxygen equilibrium pressure

In an oxidizing glass melt containing  $C_S$  mole sulphur per cubic meter, the concentration of  $SO_4^{2-}$  and the  $SO_2$  and  $O_2$ -pressures will satisfy the following equation at any temperature  $T$ :

$$\frac{p_{\text{SO}_2} \cdot \sqrt{p_{\text{O}_2}}}{[\text{SO}_4^{2-}]} = K_1^{**}(\text{T}) = \exp \left( \frac{-\Delta H_1^{**}}{R_g \cdot \text{T}} + \frac{\Delta S_1^{**}}{R_g} \right) \quad (6.75)$$

At an increase of temperature from an arbitrary initial temperature  $T_i$  to an arbitrary final temperature  $T_f$ , some sulphate will be dissociated. For each mole of sulphate that disappears, one mole of  $\text{SO}_2$  and half a mole of  $\text{O}_2$  are liberated. If no  $\text{SO}_2$  or  $\text{O}_2$  leaves or enters the glass melt (closed system), the following equation holds:

$$[\text{O}_2]_{T_f} - [\text{O}_2]_{T_i} = \frac{1}{2} \{ [\text{SO}_2]_{T_f} - [\text{SO}_2]_{T_i} \} \quad (6.76)$$

The concentration of dissolved  $\text{SO}_2$  at any temperature  $T$ ,  $[\text{SO}_2]_T$ , is given by the  $\text{SO}_2$ -pressure and the solubility of  $\text{SO}_2$  at this temperature, according to Henry's Law:

$$[\text{SO}_2]_T = L_{\text{SO}_2}(\text{T}) \cdot p_{\text{SO}_2}(\text{T}) \quad (6.77)$$

and the  $\text{SO}_2$ -pressure at this temperature  $T$  is determined by the redox reaction equilibrium constant  $K_1^{**}(\text{T})$ :

$$p_{\text{SO}_2}(\text{T}) = \frac{K_1^{**}(\text{T}) \cdot [\text{SO}_4^{2-}]_T}{\sqrt{p_{\text{O}_2}(\text{T})}} \quad (6.78)$$

As long as the total sulphur content in the glass melt remains at the constant value  $C_S$ , the following equation holds:

$$[\text{SO}_4^{2-}]_T = C_S - L_{\text{SO}_2}(\text{T}) \cdot p_{\text{SO}_2}(\text{T}) \quad (6.79)$$

Equation 6.78 can now be written as:

$$p_{\text{SO}_2}(\text{T}) = \frac{C_S \cdot K_1^{**}(\text{T})}{K_1^{**}(\text{T}) \cdot L_{\text{SO}_2}(\text{T}) + \sqrt{p_{\text{O}_2}(\text{T})}} \quad (6.80)$$

and the concentration of dissolved  $\text{SO}_2$  is:

$$[\text{SO}_2]_T = \frac{C_S \cdot K_1^{**}(\text{T}) \cdot L_{\text{SO}_2}(\text{T})}{K_1^{**}(\text{T}) \cdot L_{\text{SO}_2}(\text{T}) + \sqrt{p_{\text{O}_2}(\text{T})}} \quad (6.81)$$

The concentration of physically dissolved oxygen,  $[O_2]$ , is also given by Henry's Law:

$$[O_2]_T = L_{O_2}(T) \cdot p_{O_2}(T) \quad (6.82)$$

The combination of equations 6.81 and 6.82 results in: (6.83)

$$L_{O_2}(T_f) \cdot p_{O_2}(T_f) - L_{O_2}(T_i) \cdot p_{O_2}(T_i) = \frac{1}{2} \cdot C_S \left( \frac{K_1^{**}(T_f)}{K_1^{**}(T_f) \cdot L_{SO_2}(T_f) + \sqrt{p_{O_2}(T_f)}} - \frac{K_1^{**}(T_i)}{K_1^{**}(T_i) \cdot L_{SO_2}(T_i) + \sqrt{p_{O_2}(T_i)}} \right)$$

### 6.6.2.2 The conditions for the application of oxygen equilibrium pressure measurements in sulphate-containing glass melts

The oxygen equilibrium pressure in the melt can be measured as a function of the temperature with the aid of an oxygen sensor (see chapter 5.4). Now the redox reaction enthalpy  $\Delta H_1^{**}$  and entropy  $\Delta S_1^{**}$  of the sulphate dissociation can be estimated from the measurements using equations 6.68 and 6.83, but only if the following conditions are all satisfied:

- only reaction 6.67 takes place. Reactions 6.69, 6.71 and 6.73 are of no importance;
- the total concentrations of sulphur and oxygen remain constant (closed system);
- the physical solubility of oxygen and the  $SO_2$ -solubility are known.

Ad a.

The melt is assumed to be oxidizing as long as the oxygen equilibrium pressure remains above 0.0001 bar [31]. The oxygen equilibrium pressure in the melt is determined by measuring the potential difference  $\Delta E$  between a measuring electrode (electrode 3 in figure 5.3) and a reference electrode (electrode 2 in figure 5.3). The reference electrode is flushed with air ( $p_{O_2}=0.21$  bar). The oxygen equilibrium pressure in the melt,  $p_{O_2}$ , is then given by:

$$p_{O_2}(\text{melt}) = 0.21 \cdot \exp \left( \frac{4 \cdot F \cdot \Delta E}{R_g \cdot T} \right) \quad (6.84)$$

The oxygen equilibrium pressure exceeds 0.0001 bar as long as the potential difference  $\Delta E$  fulfils:

$$\Delta E > \frac{R_g \cdot T}{4 \cdot F} \ln \frac{0.0001}{0.21} = -0.0001648 \cdot T \text{ Volt} \quad (6.85)$$

Under this condition, sulphur is assumed to be present as sulphate and  $\text{SO}_2$ , and not as  $\text{S}^0$  or  $\text{S}^{2-}$ .

Ad b.

Sulphate is dissociated at high temperatures into  $\text{SO}_2$  and  $\text{O}_2$ . These gases can diffuse to existing bubbles or form new bubbles, and so leave the melt. Formation of new bubbles will occur if the total gas pressure in the melt exceeds 1 bar. Then  $\text{SO}_2$  and  $\text{O}_2$  are removed rapidly from the glass melt.  $\text{SO}_2$  and  $\text{O}_2$  are released by dissociation of sulphate in the ratio 2:1. The partial pressures of  $\text{SO}_2$  and  $\text{O}_2$  are given by equations 6.77 and 6.82. The total gas pressure will presumably exceed 1 bar when the oxygen equilibrium pressure fulfils equation 6.86:

$$p_{\text{O}_2} \geq \frac{L_{\text{SO}_2}}{L_{\text{SO}_2} + 2 \cdot L_{\text{O}_2}} \quad (6.86)$$

In case the physical solubility of oxygen is roughly equal to the  $\text{SO}_2$ -solubility, the total gas pressure exceeds 1 bar when the partial oxygen pressure is 0.33 bar or more. But even if the total gas pressure is less than 1 bar,  $\text{SO}_2$  may well diffuse from the melt to the atmosphere, thus lowering the total sulphur content.

In figure 6.68, the oxygen equilibrium pressure measured in soda-lime-silica glass containing 1 weight-%  $\text{Na}_2\text{SO}_4$  (162 mole  $\text{SO}_4^{2-}/\text{m}^3$  glass) is represented. The glass was heated to  $1250^\circ\text{C}$ . Then the electrodes were dipped in the melt. The potential difference between the platinum plate and the reference electrode was measured continuously while the temperature was lowered by  $3^\circ\text{C}\cdot\text{min}^{-1}$  to  $800^\circ\text{C}$ . Subsequently, the temperature was increased by  $3^\circ\cdot\text{min}^{-1}$  to  $1320^\circ\text{C}$ . The potential difference does not follow the same course during temperature decrease and increase. This indicates that  $\text{SO}_2$  escapes from the melt during the measurements, or that oxygen from the atmosphere is taken up by the melt. Since the total concentrations of sulphur and oxygen in the melt at every temperature is not known, these measurements can not be used for the determination of the redox reaction enthalpy and entropy.



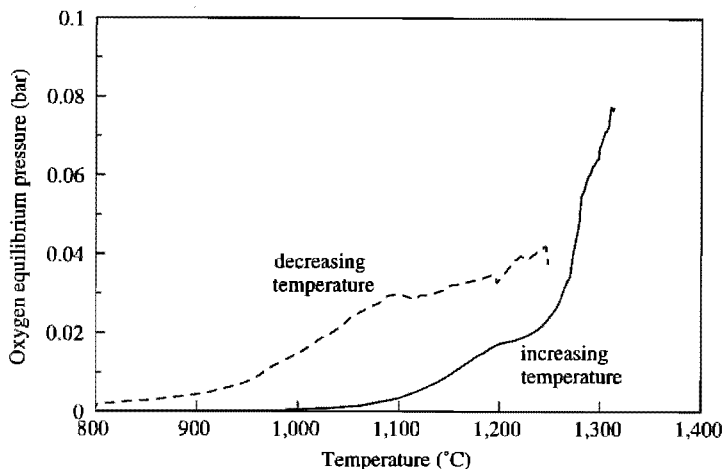


Figure 6.68

The measured oxygen equilibrium pressure in soda-lime-silica glass initially containing 1 weight-%  $\text{Na}_2\text{SO}_4$  as a function of temperature during temperature decrease and subsequent increase

Some precautions must be taken in order to be able to use the oxygen equilibrium pressure measurements for the determination of the redox reaction enthalpy  $\Delta H_1^{**}$  and entropy  $\Delta S_1^{**}$ . Firstly the glass melt containing sulphate is heated to  $1450^\circ\text{C}$ . The equilibrium state of reaction 6.67 shifts to the right, and  $\text{SO}_2$  and  $\text{O}_2$  are formed. A large number of bubbles appears. The bubbles ascend to the surface of the melt and thus transport  $\text{SO}_2$  and  $\text{O}_2$  to the atmosphere.

Then the melt is held for half an hour at  $1450^\circ\text{C}$ , while the oxygen equilibrium pressure is measured. After this time, the glass melt is presumably bubble-free and saturated with  $\text{SO}_2$  and  $\text{O}_2$ .

Subsequently, the temperature of the glass melt is lowered by  $3^\circ\text{C}\cdot\text{min}^{-1}$  while the oxygen equilibrium pressure is measured. Now  $\text{SO}_2$  will react with  $\text{O}_2$  to form  $\text{SO}_4^{2-}$ . Transfer of large amounts of  $\text{SO}_2$  to the atmosphere is unlikely. The sulphur content in the melt is now assumed to be constant.

Finally the electrodes are removed from the melt. The glass melt is quenched and the remaining sulphur content is measured using X-ray fluorescence. This sulphur concentration can then be used in equation 6.83 to estimate the redox

reaction enthalpy  $\Delta H_1^{**}$  and entropy  $\Delta S_1^{**}$ . Only the data points at which the oxygen equilibrium pressure is less than 0.2 bar are used in the calculation, because then the total gas pressure in the melt is assumed to be well under 1 bar.

Ad c.

The physical solubilities of  $O_2$  and  $SO_2$  in soda-lime-silica and E-glass are not known exactly. On account of literature data (see chapter 5.4.8) and own measurements (see chapter 6.8), the physical solubility of oxygen,  $L_{O_2}$ , in soda-lime-silica and TV-screen glass melts is estimated at  $1 \text{ mole}\cdot\text{m}^{-3}\cdot\text{bar}^{-1}$  at melting temperatures. For the time being, the oxygen solubility in E-glass melts is assumed to be about  $1 \text{ mole}\cdot\text{m}^{-3}\cdot\text{bar}^{-1}$  as well.

In the literature, hardly any data on the solubility of  $SO_2$  have been published at all. Beerkens [32] assumed the physical solubility of  $SO_2$  in soda-lime-silica glass melts to be  $0.1 \text{ mole}\cdot\text{m}^{-3}\cdot\text{bar}^{-1}$ . Recent experiments using the helium-extraction technique indicate, however, that the  $SO_2$ -solubility is about 4 to 10  $\text{mole}\cdot\text{m}^{-3}\cdot\text{bar}^{-1}$  in soda-lime-silica glass [33].

### 6.6.2.3 Experimental procedure

E-glass batch materials containing no polyvalent elements were heated at  $1400^\circ\text{C}$  in a platinum crucible until all grains were dissolved. Then the glass melt was quenched and transferred to an  $Al_2O_3$ -crucible.  $Na_2SO_4$  was added to the cullet to a total of 1 weight-%  $Na_2SO_4$  ( $162 \text{ mole } SO_4^{2-}/\text{m}^3$  glass). The  $Al_2O_3$ -crucible was placed in the furnace sketched in figure 5.3. The glass was heated slowly to  $1150^\circ\text{C}$ , and then the electrodes were lowered until the reference electrode (electrode 2 in figure 5.3) just touched the melt. The potential difference between the platinum plate and the reference electrode was measured while the temperature was increased to  $1450^\circ\text{C}$ . In figure 6.69, the oxygen equilibrium pressure in the E-glass melt is given as a function of temperature. As we can see the oxygen equilibrium pressure initially increases as the temperature increases, until at  $1350^\circ\text{C}$  the maximum oxygen equilibrium pressure of 0.34 bar has been reached. Then the oxygen equilibrium pressure decreases, even though the temperature still increases, to 0.29 bar. Presumably oxygen is transferred from the melt to the atmosphere in order to establish an equilibrium between melt and atmosphere.

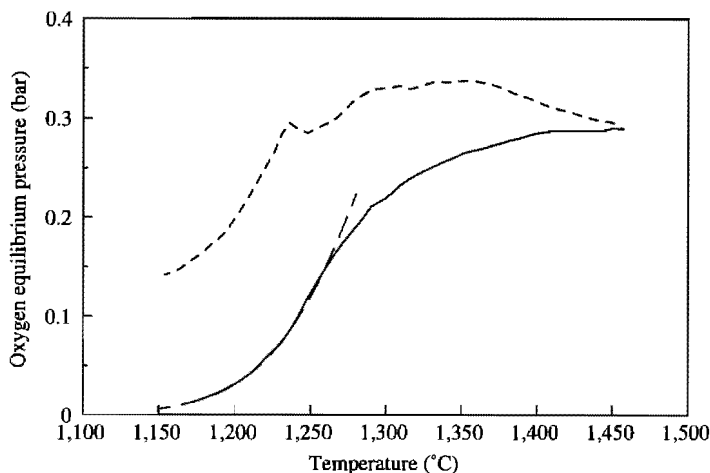


Figure 6.69

The measured oxygen equilibrium pressure in E-glass initially containing 1 weight-%  $\text{Na}_2\text{SO}_4$  as a function of temperature during increase (-----) and subsequent decrease (————) of temperature. The theoretical curve for the oxygen equilibrium pressure in the melt during temperature decrease (— · — ·) was calculated with:

$$C_S = 10 \text{ mole}\cdot\text{m}^{-3}$$

$$L_{\text{O}_2} = 1 \text{ mole}\cdot\text{m}^{-3}\cdot\text{bar}^{-1}$$

$$\Delta H_{1^{**}} = 292 \text{ kJ}\cdot\text{mole}^{-1}$$

$$p_{\text{O}_2}(1200^\circ\text{C}) = 0.034 \text{ bar}$$

$$L_{\text{SO}_2} = 10 \text{ mole}\cdot\text{m}^{-3}\cdot\text{bar}^{-1}$$

$$\Delta S_{1^{**}} = 187 \text{ J}\cdot\text{mole}^{-1}\cdot\text{K}^{-1}$$

Then the temperature was held at  $1450^\circ\text{C}$  for half an hour. The oxygen equilibrium pressure remained at 0.29 bar. Subsequently the temperature was decreased by  $3^\circ\cdot\text{min}^{-1}$  while the potential difference was measured. From  $1275^\circ\text{C}$  downward, the oxygen equilibrium pressure clearly decreases. Presumably the equilibrium state of reaction 6.67 shifts to the left, and so oxygen is combined with  $\text{SO}_2$  to form  $\text{SO}_4^{2-}$ .

At temperatures less than  $1150^\circ\text{C}$ , the E-glass melt becomes too viscous to lift the electrodes from the melt. Therefore, the electrodes were removed from the melt as soon as a temperature of  $1150^\circ\text{C}$  had been reached. After that, the melt was quenched. The sulphur content in the glass sample was measured by means of X-ray fluorescence, and was found to be 0.036 weight-%  $\text{SO}_3$  (10 mole  $\text{SO}_4^{2-}/\text{m}^3$ ). This means that 94% of the initial sulphur content of the E-glass has vanished to the atmosphere.

#### 6.6.2.4 Calculation of $\Delta H_1^{**}$ and $\Delta S_1^{**}$

The oxygen equilibrium pressures in the E-glass melt containing sulphate at temperatures between 1275 and 1150°C fulfil the conditions mentioned in section 6.6.2.2. These data points will be used to calculate the enthalpy  $\Delta H_1^{**}$  and entropy  $\Delta S_1^{**}$  of reaction 6.67. In the fitting procedure, which is based on equation 6.83, the oxygen equilibrium pressure at one temperature must be fixed. From the measured oxygen equilibrium pressure, the point ( $T=1200^\circ\text{C}$ ,  $p_{\text{O}_2}=0.034$  bar) has arbitrarily been chosen as starting point for the fitting procedure. The concentration of sulphur,  $C_S$ , in equation 6.83 is of course 10 mole  $\text{SO}_4^{2-}/\text{m}^3$ .

Unfortunately the physical solubilities of  $\text{SO}_2$  and  $\text{O}_2$  in E-glass are unknown. For the time being, the solubilities are assumed to be equal to those in soda-lime-silica glass: the solubility of  $\text{SO}_2$  is set to 10, and the physical solubility of  $\text{O}_2$  to 1 mole·m<sup>-3</sup>·bar<sup>-1</sup>. The fitting procedure resulted, under these conditions, in the following values for the enthalpy and entropy:

$$\Delta H_1^{**} = 292 \text{ kJ}\cdot\text{mole}^{-1}$$

$$\Delta S_1^{**} = 187 \text{ J}\cdot\text{mole}^{-1}\cdot\text{K}^{-1}$$

The calculated value for the enthalpy  $\Delta H_1^{**}$  does not depend significantly on the chosen values for the  $\text{SO}_2$  and  $\text{O}_2$ -solubilities, but the entropy  $\Delta S_1^{**}$  changes by 10% when the  $\text{SO}_2$  or  $\text{O}_2$ -solubility varies one order of magnitude. Therefore it is essential to find out the exact  $\text{SO}_2$  and  $\text{O}_2$ -solubilities in E-glass and use these in future calculations.

In order to check the obtained values for the enthalpy and entropy, the  $\text{SO}_2$ -pressures in the glass melt were calculated using equation 6.79.  $p_{\text{SO}_2}$  appeared to be about 1 bar at 1275°C under the conditions mentioned above. The  $\text{SO}_2$ -pressure depends strongly on the value for the  $\text{SO}_2$ -solubility. Probably the  $\text{SO}_2$ -solubility in E-glass deviates from the chosen value of 10 mole·m<sup>-3</sup>·bar<sup>-1</sup>. Another explanation for the calculated high  $\text{SO}_2$ -pressure might be found in a decreasing total sulphur content  $C_S$  during the measurements. Even though the total gas pressure remains well below 1 bar,  $\text{SO}_2$  may leave the melt by diffusion, since the  $\text{SO}_2$  pressure in the atmosphere is negligibly small. This can easily be checked in future measurements, by increasing the temperature once again from 1150 to 1450°C instead of quenching the glass melt. The oxygen equilibrium pressure will follow the same course during increase of temperature if no sulphur is lost.

### 6.6.2.5 Conclusions

The oxygen equilibrium pressure measurements might be used for the determination of the enthalpy and entropy of reaction 6.67. Theoretical equations and a set of conditions have been drawn up, but the following questions remain to be answered:

- does the total sulphur content in the molten glass indeed remains constant under the conditions mentioned in section 6.6.2.2 ?
- what are the values for the physical solubilities of  $\text{SO}_2$  and  $\text{O}_2$  in the glass melt ?

## **6.6.3 Square wave voltammetry measurements**

### 6.6.3.1 Experimental procedure

Soda-lime-silica glass containing 1 weight-%  $\text{Na}_2\text{SO}_4$  (162 mole  $\text{SO}_4^{2-}\cdot\text{m}^{-3}$  glass) was melted at  $1400^\circ\text{C}$  in a platinum crucible until all grains were dissolved completely and hardly any bubbles remained. Then the melt was quenched. The cullet was transferred to an  $\text{Al}_2\text{O}_3$ -crucible and placed in the furnace as sketched in figure 5.3. The glass was heated slowly to  $1400^\circ\text{C}$ , and the electrodes were dipped in the glass melt.

The temperature was held constant for 15 minutes. Then an  $i\cdot R_u$  measurement was performed (see chapter 5.3), followed by a square wave voltammetry measurement. During this measurement the furnace is temporarily switched off in order to avoid disturbance of the measured signal by the current in the heating elements. Generally the set-up of the square wave voltammetry measurements was:

$$f = 100 \text{ Hz}$$

$$\Delta E_b = -0.002 \text{ V}$$

$$\Delta E_p = 0.100 \text{ V}$$

After the measurements, the temperature was decreased by  $3^\circ\text{C}\cdot\text{min}^{-1}$  to a lower level. Before running  $i\cdot R_u$ -measurements and square wave voltammetry measurements, the temperature was held constant at the new value for 15 minutes. In this way the temperature region from  $1400$  down to  $1000^\circ\text{C}$  was investigated.

### 6.6.3.2 The recorded square wave voltammogram

During the square wave voltammetry measurements, the currents that flow at "forward" and "reverse" potential pulses are measured. These currents are plotted against the base potential (see chapter 5.5) in the square wave voltam-

mograms. Subsequently, the current that flows during a reverse potential pulse,  $i_r$ , is subtracted from the current that flew during the preceding forward pulse,  $i_f$ . The resulting current is indicated by  $\delta i$ . Usually only  $\delta i$  is used to determine the formal potentials of the redox reactions and other interesting parameters (for instance the diffusion coefficient of the reacting species or the number of electrons transferred).

In figure 6.70, the forward and reverse currents that were measured in soda-lime-silica glass containing 1 weight-%  $\text{Na}_2\text{SO}_4$  at  $1000^\circ\text{C}$  are plotted against the base potential. In the same figure,  $\delta i$  is represented. In the  $\delta i$ -curve, two overlapping peaks can be seen, at about  $-0.39$  and  $-0.515$  V, probably resulting from two reduction steps of sulphur. However, in the  $i_r$ -curve, only one peak is visible, at  $-0.526$  V. This indicates that the reduction step at  $-0.39$  V is irreversible or quasi-reversible at the given frequency of 100 Hz.

Theoretically the overlapping peaks can not be separated into two independent peaks, because the reaction product of the first reduction step is the reactant of the second reduction step. Therefore the number of electrons, transferred during each reduction step, can not be estimated from the shape of the peaks. This obstructs the identification of the peaks.

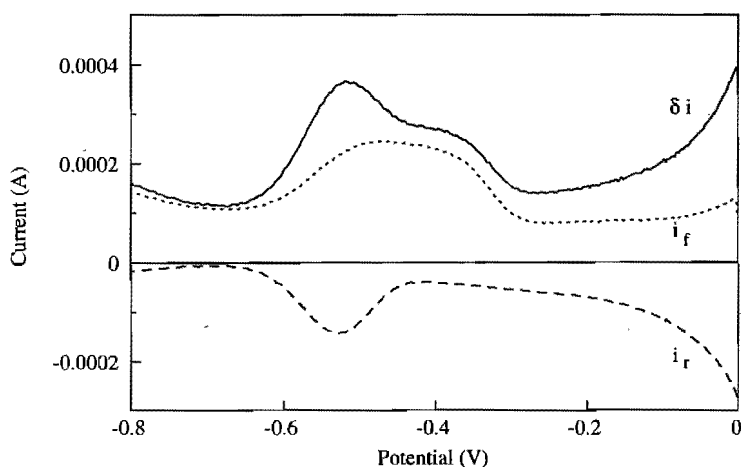


Figure 6.70

The square wave voltammogram recorded in soda-lime-silica glass containing 1.0 weight-%  $\text{Na}_2\text{SO}_4$  at  $1000^\circ\text{C}$ , using the following set-up:

$$\Delta E_p = 0.002 \text{ V}$$

$$\Delta E_p = 0.100 \text{ V}$$

$$f = 100 \text{ Hz}$$

$$R_u = 59.0 \ \Omega$$

According to Kordon [34], in square wave voltammograms recorded in sulphate-containing glasses at temperatures between 1100°C and 1400°C two peaks can be seen, due to the reductions  $S^{4+}/S^0$  and  $S^0/S^{2-}$ . He bases this statement on the idea, that since the fining process takes place at 1400°C, already a large amount of the  $SO_4^{2-}$  should have been converted to  $SO_2$  and  $O_2$ . This means that the standard potential of this reduction step (the reduction step  $S^{6+}/S^{4+}$ ) is located at a positive potential. Since the two reduction peaks in the square wave voltammograms are visible at all temperatures in the temperature region mentioned, the peaks can not result from the  $S^{6+}/S^{4+}$  reaction.

However, at low temperatures (800-1200°C), sulphur is present as sulphate in the oxidizing glass melt [2]. By applying a sufficiently negative potential to the melt, the sulphate will be reduced to  $SO_2$ . Then at these low temperatures, the reaction of  $S^{6+}$  to  $S^{4+}$  must surely be visible in the square wave voltammograms. Therefore it seems more likely that the reduction peak at about -0.39 V in the square wave voltammograms recorded at 1000°C in soda-lime-silica glass is caused by the reduction of  $SO_4^{2-}$  to  $SO_2$  (and in that case the reduction step at -0.515 V is caused by either  $SO_2/S^0$  or  $SO_2/S^{2-}$ ).

Besides, if the solubility of  $SO_2$  is indeed in the order of  $10 \text{ mole}\cdot\text{m}^{-3}\cdot\text{bar}^{-1}$ , only a small amount of  $SO_4^{2-}$  needs to be dissociated to obtain a large  $SO_2$  equilibrium pressure in the melt. The equilibrium constant  $K_1^{**}(T)$  of reaction 6.67 may well be less than unity, even at 1400°C, and then the formal potential of this reaction is negative. Because  $SO_2$  disappears to the atmosphere, the dissociation of  $SO_4^{2-}$  will continue until nearly all  $SO_4^{2-}$  has been converted into  $SO_2$  and  $O_2$ .

The hypothesis that the peak at about -0.39 V in the square wave voltammogram is caused by the reduction of  $SO_4^{2-}$ , is supported by the indication that the first reduction step is irreversible or quasi-reversible at a frequency of 100 Hz. The  $SO_2$  gas that is formed by the reduction of  $SO_4^{2-}$  may diffuse to existing bubbles or form new bubbles. This gaseous  $SO_2$  is not immediately available for the oxidation to  $SO_4^{2-}$  during potential pulses in the positive direction. However, during potential pulses in the negative direction, the reaction  $SO_4^{2-} \rightarrow SO_2$  is followed directly by the reaction  $SO_2 \rightarrow S^0$ , and  $SO_2$  does not get a chance to diffuse to bubbles. Therefore the oxidation of  $SO_2$  to  $SO_4^{2-}$  does not seem to occur, while the reduction of  $SO_2$  to  $S^0$  does. The reduction of  $SO_4^{2-}$  to  $SO_2$  then appears to be irreversible at high measuring frequencies.

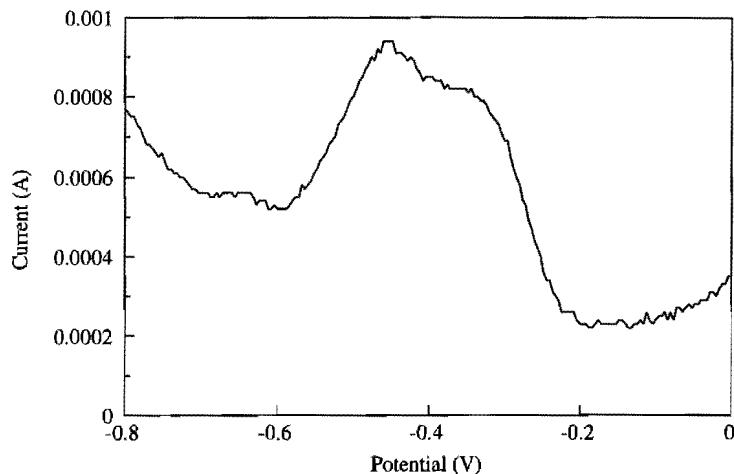


Figure 6.71

The square wave voltammogram recorded in soda-lime-silica glass containing 1.0 weight-%  $\text{Na}_2\text{SO}_4$  at  $1150^\circ\text{C}$ , using the following set-up:

$$\Delta E_b = 0.002 \text{ V}$$

$$\Delta E_p = 0.100 \text{ V}$$

$$f = 100 \text{ Hz}$$

$$R_u = 19.9 \Omega$$

### 6.6.3.3 The influence of the temperature

At increasing temperatures, both reduction peaks shift towards the positive potential region with about the same velocity. Therefore the two peaks show an overlap in the  $\delta$ -curve at any temperature. In the reverse current,  $i_r$ , only the second reduction step is visible in all cases examined using a frequency of 100 Hz.

At  $1150^\circ\text{C}$ , the reduction peaks are located at about  $-0.340$  and  $-0.453$  V, as can be seen in figure 6.71. However, at this temperature, a third peak seems to appear at about  $-0.655$  V. At lower temperatures, this peak was probably hidden under the increasing background current due to the reduction of Si or Na. This peak might be due to the third reduction step of sulphur:  $\text{S}^0/\text{S}^{2-}$ . Then the second peak in the square wave voltammograms must result from the reaction  $\text{S}^{4+}/\text{S}^0$ , and the first peak from  $\text{S}^{6+}/\text{S}^{4+}$ .

### 6.6.3.4 The influence of the frequency

The frequency with which the base potential varies,  $f$ , has a great influence on the height of the peaks in the square wave voltammogram. At high frequencies (between 100 and 500 Hz), the first reduction peak becomes smaller relative to the second reduction peak, or perhaps it shifts towards more negative poten-



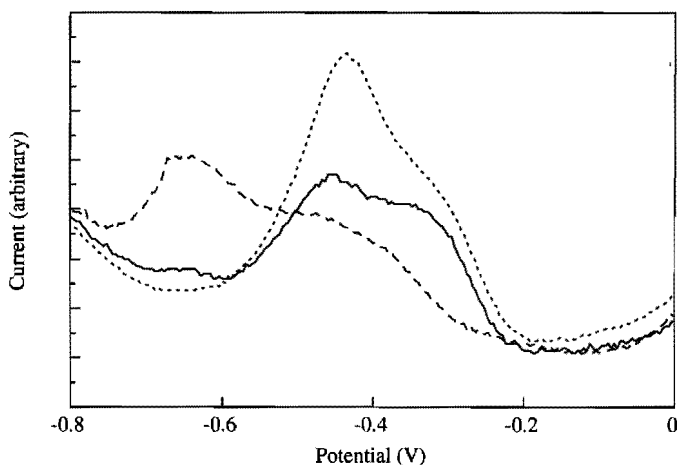


Figure 6.72

The square wave voltammogram recorded in soda-lime-silica glass containing 1.0 weight-%  $\text{Na}_2\text{SO}_4$  at  $1150^\circ\text{C}$ , using the following set-ups:

-----	$f = 10 \text{ Hz}$	$\Delta E_b = 0.002 \text{ V}$
—————	$f = 100 \text{ Hz}$	$\Delta E_p = 0.100 \text{ V}$
.....	$f = 200 \text{ Hz}$	$R_u = 19.9 \Omega$

tials and coincides with the second peak. This again indicates that the first reduction step is quasi-reversible. The exact location of the second reduction step can easily be determined at high frequencies. The peak is very small, indicating that a "large" number of electrons is transferred during this reduction step. This is in agreement with the assumption that the second peak results from the reduction of  $\text{SO}_2$  to  $\text{S}^0$  or  $\text{S}^{2-}$ . Due to the overlap with the first peak, no definite answer can be given.

As an example, the square wave voltammograms recorded in soda-lime-silica melt containing 1.0 weight-%  $\text{Na}_2\text{SO}_4$  at  $1150^\circ\text{C}$  using different frequencies are displayed in figure 6.72. At a low frequency of 10 Hz, the first reduction step is reversible. In the "reverse" current  $i_r$ , a very broad peak is visible between -0.3 and -0.5 V. Because now the first and the second reduction step give overlapping peaks in both the "forward" and the "reverse" current, the second reduction step can not be seen as a second peak in the  $\delta i$ -curve. The third reduction step, however, is clearly visible as a peak at low frequencies. This facilitates the determination of the exact peak position.

### 6.6.3.5 The calculation of the enthalpies and entropies of the three reduction steps

Square wave voltammograms have been recorded in soda-lime-silica glass containing 1.0 weight-%  $\text{Na}_2\text{SO}_4$  at various temperatures. The potentials, at which a peak could be seen, are plotted as a function of the temperature in figure 6.73.

With the aid of linear regression, straight lines have been drawn through the data points which have been attributed to the  $\text{SO}_4^{2-}/\text{SO}_2$  and  $\text{SO}_2/\text{S}^0$  reactions. For the further processing of the results, it is assumed, that the peaks indeed arise due to the  $\text{S}^{6+}/\text{S}^{4+}$  and the  $\text{S}^{4+}/\text{S}^0$  conversions, at which respectively 2 and 4 electrons are transferred. Furthermore the diffusion coefficients of  $\text{SO}_4^{2-}$ ,  $\text{SO}_2$ ,  $\text{S}^0$  and  $\text{S}^{2-}$  are assumed to be in the same order of magnitude. Then the peaks in the square wave voltammograms are located at the formal potentials of the three reduction reactions (see chapter 5.2.8). Now the enthalpies and entropies of the reduction steps can be calculated from the temperature dependency of the formal potentials using equation 6.22. The results are listed in table 6.12.

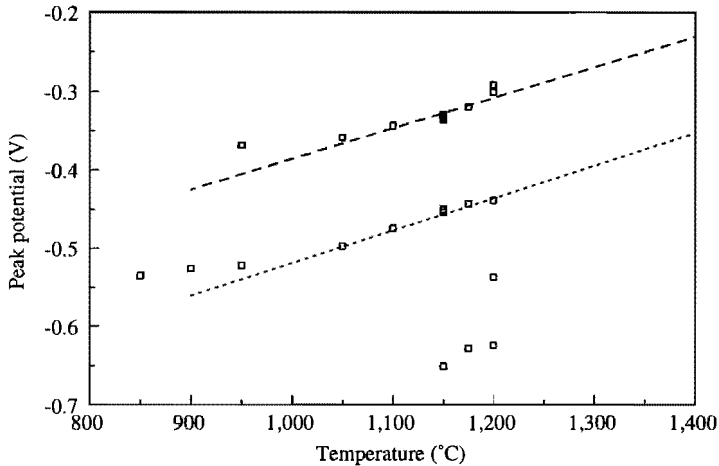


Figure 6.73

The potentials, at which a peak could be seen, in the square wave voltammograms recorded in soda-lime-silica glass containing 1.0 weight-%  $\text{Na}_2\text{SO}_4$ , as a function of the temperature

Table 6.12

The enthalpies and entropies of two reduction steps of in soda-lime-silica glass containing 1 weight-%  $\text{Na}_2\text{SO}_4$

Reaction number	Proposed reaction scheme	Simplified reaction	Number of electrons transferred	$\Delta H^{**}$ (kJ·mole <sup>-1</sup> )	$\Delta S^{**}$ (J·mole <sup>-1</sup> ·K <sup>-1</sup> )
(6.67)	$\text{SO}_4^{2-} \rightleftharpoons \text{SO}_2 + \frac{1}{2} \text{O}_2 + \text{O}^{2-}$	$\text{S}^{6+} \rightleftharpoons \text{S}^{4+}$	2	170	75
(6.69)	$\text{SO}_2 \rightleftharpoons \frac{1}{2} \text{S}_2 + \text{O}_2$	$\text{S}^{4+} \rightleftharpoons \text{S}^0$	4	404	160

In future square wave voltammetry measurements, the experimental set-up (frequency, pulse height, initial and final potentials) should be varied in order to obtain clear peaks. This will enable the identification of the peaks and the check on the reversibility of the redox reactions. From the position of the peaks, the half-wave potentials of the reactions can be derived. Furthermore, the diffusion coefficients of the reacting species should be established in order to calculate the formal potentials. The formal potentials might deviate significantly from the half-wave potentials, and then the enthalpies and entropies of the reduction steps may differ well from those given in table 6.12.

The calculated enthalpy and entropy of the reduction step  $\text{S}^{6+}/\text{S}^{4+}$  should be checked with the enthalpy and entropy resulting from the oxygen equilibrium pressure measurements performed in identical glass melts. Also some other techniques should be applied, for example equilibrating the glass melt with known  $\text{SO}_2$  and  $\text{O}_2$  pressures by bubbling, and estimating the  $\text{SO}_4^{2-}$  concentration in the melt by determining the remaining sulphur content in the quenched glass.

### 6.6.3.6 Conclusions

In square wave voltammograms recorded in a soda-lime-silica melt containing 1 weight-%  $\text{Na}_2\text{SO}_4$  and no other multivalent elements, three peaks can be made visible at temperatures between 1000 and 1400°C. These peaks have been attributed to the three different reduction steps of sulphate:  $\text{SO}_4^{2-} \rightarrow \text{SO}_2$ ,  $\text{SO}_2 \rightarrow \text{S}^0$  and  $\text{S}^0 \rightarrow \text{S}^{2-}$ . Arguments in support of this hypothesis are:

- the first reduction peak shows quasi-reversible behaviour;
- at high frequencies, the second reduction peak is very small, indicating that

more than two electrons are involved in this reduction step;

- only a small amount of  $\text{SO}_2$  in the glass melt causes a large  $\text{SO}_2$  equilibrium pressure (under the assumption that the physical solubility is indeed in the order of  $10 \text{ mole}\cdot\text{m}^{-3}\cdot\text{bar}^{-1}$ ). This indicates that the equilibrium constant  $K_1^{**}(\text{T})$ , as defined in equation 6.68, may be far less than unity at melting temperatures. The formal potential of the dissociation reaction of sulphate is then negative. The dissociation of sulphate is promoted because the reaction products  $\text{SO}_2$  and  $\text{O}_2$  are removed from the melt during the fining process.

Under the assumptions that:

- the peaks indeed result from the proposed reactions;
- the peaks are located at the half-wave potentials of the reactions (as is the case for reversible reactions);
- the diffusion coefficients of  $\text{SO}_4^{2-}$ ,  $\text{SO}_2$  and  $\text{S}^0$  are about equal (in other words: the half-wave potential is about equal to the formal potential);

the enthalpy and entropy of the reactions  $\text{SO}_4^{2-} \rightarrow \text{SO}_2$  and  $\text{SO}_2 \rightarrow \text{S}^0$  have been calculated from the temperature dependency of the peaks in the square wave voltammograms. The obtained values are given in table 6.12.

More investigations using square wave voltammetry and other techniques (oxygen equilibrium pressure measurements, X-ray fluorescence, etc.) in glass melts containing various amounts of sulphur are needed to check if the assumptions are justified.

#### 6.6.4 Comparison of the results with data from the literature

Papadopoulos [2] equilibrated various soda-lime-silica melts without polyvalent elements with mixtures of  $\text{SO}_2$  and  $\text{O}_2$  and determined the amount of sulphur (as  $\text{SO}_3$ ) in the quenched glass samples using X-ray fluorescence. He found that the  $\text{SO}_3$ -solubility is proportional to the parameter  $[\text{Na}^+]^2[\text{O}^-]^2/[\text{O}^0]$  (see chapter 3.5.4).

Furthermore, one soda-lime-silica glass, with the molar composition 66  $\text{SiO}_2$ -20  $\text{CaO}$ -14  $\text{Na}_2\text{O}$ , was selected for a study of the effect of temperature on the  $\text{SO}_3$  solubility. This glass was equilibrated with a stoichiometric mixture  $\text{SO}_2 + \frac{1}{2}\text{O}_2$  at 5 different temperatures ranging from 1373 to 1483°C. By assuming that the measured  $\text{SO}_3$ -content in the quenched glass sample is equal to the concentration of  $\text{SO}_4^{2-}$  in the molten glass, and taking  $p_{\text{SO}_2}$  to be 0.67 and  $p_{\text{O}_2}$  to be 0.33 bar, the redox reaction equilibrium constant  $K_1^{**}(\text{T})$ , as defined in equation

6.68, can be calculated. From the dependency of  $K_1^{**}$  of the temperature, the reaction enthalpy  $\Delta H_1^{**}$  and entropy  $\Delta S_1^{**}$  can be calculated using equations 5.68 and 5.69. The results are:

$$\Delta H_1^{**} = 363 \text{ kJ}\cdot\text{mole}^{-1}$$

$$\Delta S_1^{**} = 161 \text{ J}\cdot\text{mole}^{-1}\cdot\text{K}^{-1}$$

These values are, suprisingly enough, roughly twice the values, given in table 6.12. Those values were determined for a soda-lime-silica glass with molar composition 75 SiO<sub>2</sub>-10 CaO-15 Na<sub>2</sub>O using square wave voltammetry. The difference between the results from literature and the results obtained by square wave voltammetry measurements, presented in this thesis, seems to indicate that the assumptions made in section 6.6.3.5 are not all satisfied.

## 6.7 COMBINATIONS OF TWO POLYVALENT ELEMENTS

### 6.7.1 Purpose of this section

Up to now, the redox reaction equilibrium constants of iron, antimony, cerium, chromium and sulphur have been determined in glass melts containing only one polyvalent element. It was found that the equilibrium constant strongly depends on the composition of the glass and on the total concentration of the polyvalent element. Therefore it is necessary to perform the measurements in the glass melts with the composition and concentration of the redox active element in which one is interested.

However, industrial glass melts usually contain more than one polyvalent element. In this section, the effect of one polyvalent element on the redox reaction equilibrium constant of another polyvalent element will be investigated.

### 6.7.2 Effect of iron impurities on the redox reaction equilibrium constant of antimony

As mentioned in section 6.3.3.7, the redox reaction equilibrium constants of the two antimony reduction steps in TV-screen glass type A containing about 0.6 weight-% Sb<sub>2</sub>O<sub>3</sub> have been determined using square wave voltammetry. Two different glass melts were investigated: one of them was prepared from reagent grade chemicals, the other from raw batch materials. Therefore the latter contained, besides 0.6 weight-% Sb<sub>2</sub>O<sub>3</sub>, about 0.04 weight-% Fe<sub>2</sub>O<sub>3</sub>. It was found that the position and the shape of the two reduction peaks of antimony were unaffected by the presence of iron. In the square wave voltammograms,

recorded in the latter TV-screen glass, a third peak occurred apart from the two antimony peaks. This peak was due to the iron impurity. Because no square wave voltammograms have been recorded in TV-screen glass containing only 0.04 weight-%  $\text{Fe}_2\text{O}_3$ , and no other polyvalent elements, it is not possible to conclude with certainty that the position and shape of this peak were not influenced by the presence of antimony.

### 6.7.3 Interaction of iron and cerium

#### 6.7.3.1 Introduction

In chapter 6.2, the enthalpy  $\Delta H^{**}$  and entropy  $\Delta S^{**}$  of the reaction



in TV-screen glass containing 0.4 weight-%  $\text{Fe}_2\text{O}_3$  have been determined using oxygen equilibrium pressure measurements and square wave voltammetry measurements. The results were:

$$\Delta H_{\text{Fe}}^{**} = 102 \text{ kJ}\cdot\text{mole}^{-1}$$

$$\Delta S_{\text{Fe}}^{**} = 37 \text{ J}\cdot\text{mole}^{-1}\cdot\text{K}^{-1}$$

The equilibrium constant  $K_{\text{Fe}}^{**}(\text{T})$  of reaction 6.87 has been defined as:

$$K_{\text{Fe}}^{**}(\text{T}) = \frac{[\text{Fe}^{2+}] \cdot p_{\text{O}_2}^{1/4}}{[\text{Fe}^{3+}]} = \exp \left( \frac{-\Delta H_{\text{Fe}}^{**}}{R_g \cdot \text{T}} + \frac{\Delta S_{\text{Fe}}^{**}}{R_g} \right) \quad (6.88)$$

The enthalpy and entropy of the reduction of cerium in TV-screen glass containing 0.6 weight-%  $\text{CeO}_2$  have been determined in chapter 6.4 using oxygen equilibrium pressure measurements. The reduction reaction is given by:



with the redox reaction equilibrium constant  $K_{\text{Ce}}^{**}(\text{T})$ :

$$K_{\text{Ce}}^{**}(\text{T}) = \frac{[\text{Ce}^{3+}] \cdot p_{\text{O}_2}^{1/4}}{[\text{Ce}^{4+}]} = \exp \left( \frac{-\Delta H_{\text{Ce}}^{**}}{R_g \cdot \text{T}} + \frac{\Delta S_{\text{Ce}}^{**}}{R_g} \right) \quad (6.90)$$

and the calculated values for the enthalpy and entropy are:

$$\Delta H_{\text{Ce}}^{**} = 40 \text{ kJ}\cdot\text{mole}^{-1}$$

$$\Delta S_{\text{Ce}}^{**} = 40 \text{ J}\cdot\text{mole}^{-1}\cdot\text{K}^{-1}$$

In this section, the mutual effect of iron and cerium in a TV-screen glass containing 0.4 weight-%  $\text{Fe}_2\text{O}_3$  and 0.6 weight-%  $\text{CeO}_2$  will be investigated.

### 6.7.3.2 Preparation of the glass

TV-screen glass type A containing 0.4 weight-%  $\text{Fe}_2\text{O}_3$  and 0.6 weight-%  $\text{CeO}_2$  was melted in a platinum crucible at  $1400^\circ\text{C}$  until all grains were dissolved and all bubbles were removed from the melt. Then the melt was quenched and transferred to an  $\text{Al}_2\text{O}_3$ -crucible. This crucible was placed in the furnace sketched in figure 5.3. Then the glass was slowly heated to  $1400^\circ\text{C}$ .

### 6.7.3.3 Square wave voltammetry measurements

At  $1400^\circ\text{C}$ , the electrodes were lowered until the reference electrode just touched the melt (see figure 5.3). The reference electrode was flushed with clean, dry air. The temperature was held constant for 15 minutes. Then an  $i\text{-}R_u$  measurement was performed (see chapter 5.3), followed by a square wave voltammetry measurement. The general set-up of the square wave voltammetry measurements was the same as the set-up used for the measurements in the TV-screen glass type A containing only 0.4 weight-%  $\text{Fe}_2\text{O}_3$ :

$$f = 100 \text{ Hz}$$

$$\Delta E_b = 0.002 \text{ V}$$

$$\Delta E_p = 0.1 \text{ V}$$

In this way,  $i\text{-}R_u$  and square wave voltammetry measurements were performed at various temperatures ranging from  $1400$  down to  $900^\circ\text{C}$ .

In figure 6.74, the square voltammogram recorded at  $1400^\circ\text{C}$  is displayed, showing one clear peak at  $-0.465 \text{ V}$ . Just as in square wave voltammograms recorded in TV-screen glass containing only iron, the peak in the voltammogram recorded in the glass containing both iron and cerium agrees best with a theoretical curve for a two electron transfer reaction. This phenomenon has already been discussed in chapter 6.2.

At lower temperatures, the recorded voltammograms still show only one peak that can be attributed to the  $\text{Fe}^{3+}/\text{Fe}^{2+}$  reaction. The peak shifts in the negative direction as the temperature decreases. The peak position is similar to the peak position in square wave voltammograms recorded in TV-screen glass containing only 0.4 weight-%  $\text{Fe}_2\text{O}_3$  (see figure 6.16). The  $\text{Ce}^{4+}/\text{Ce}^{3+}$  reaction can not be seen, just as in the square wave voltammograms which have been recorded in TV-screen glass containing only 0.6 weight-%  $\text{CeO}_2$ .

Apparently the equilibrium constant of the iron reduction reaction in TV-screen glass is not effected by the presence of cerium.

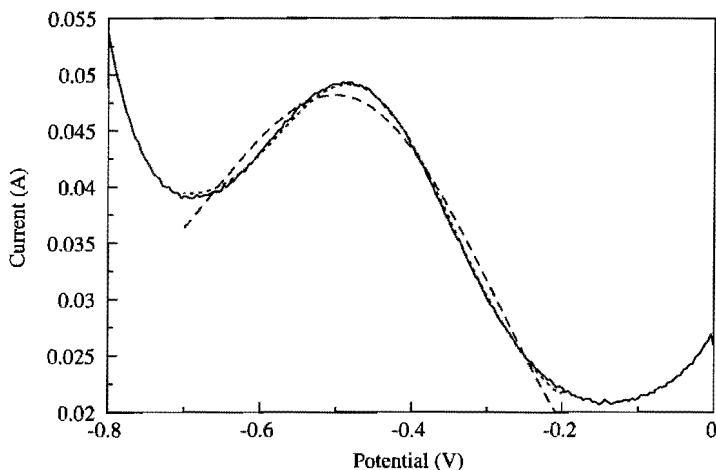


Figure 6.74

The square wave voltammogram (—) recorded in TV-screen glass type A containing 0.4 weight-%  $\text{Fe}_2\text{O}_3$  and 0.6 weight-%  $\text{CeO}_2$  at  $1400^\circ\text{C}$  with the following set-up;

$$\Delta E_p = 0.002 \text{ V} \quad f = 100 \text{ Hz} \quad R_u = 1.55 \Omega \quad E^{\circ'} = -0.465 \text{ V}$$

$$\Delta E_p = 0.1 \text{ V}$$

compared with the theoretical curves for reversible reactions at which one (---) or two (- · - · - · -) electrons are transferred

#### 6.7.3.4 Oxygen equilibrium pressure measurements

Following the square wave voltammetry measurements, the temperature in the furnace is held at  $900^\circ\text{C}$  for half an hour while the potential difference between the platinum plate and the reference electrode is measured. After some minutes, the potential difference  $\Delta E$  reaches a value of  $-0.116 \text{ V}$  and remains at that value. The oxygen equilibrium pressure  $p_{\text{O}_2}$  can be calculated from this potential difference using equation 5.34 (or 6.8). The reference electrode is flushed with clean, dry air. At  $900^\circ\text{C}$ , the oxygen equilibrium pressure is determined on 0.002 bar in this glass.

Then the temperature is increased by  $3^\circ\text{C}/\text{min}$  to  $1000^\circ\text{C}$  while the potential difference is measured. In figure 6.75, the potential difference calculated by equation 6.8 is given as a function of temperature.

From the square wave voltammetry measurements, the enthalpies and entropies of reactions 6.87 and 6.89 appear to be unaffected by the presence of the other polyvalent element.



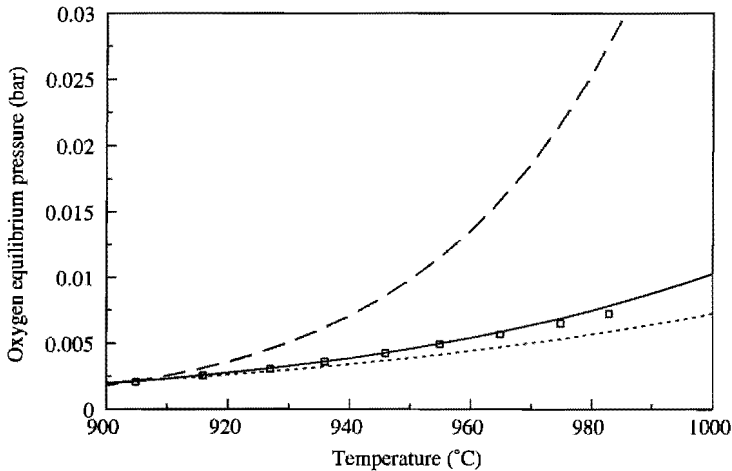


Figure 6.75

The oxygen equilibrium pressure calculated from the potential difference (□) as a function of temperature in TV-screen glass type A containing 0.4 weight-%  $\text{Fe}_2\text{O}_3$  and 0.6 weight-%  $\text{CeO}_2$ . The theoretical curves were calculated using the following parameter:

$$\begin{aligned} C_{\text{Fe}} &= 114 \text{ mole}\cdot\text{m}^{-3} \\ C_{\text{Ce}} &= 80 \text{ mole}\cdot\text{m}^{-3} \end{aligned}$$

$$\begin{aligned} C_{\text{Fe}^0} &= 114 \text{ mole}\cdot\text{m}^{-3} \\ C_{\text{Ce}^0} &= 0 \text{ mole}\cdot\text{m}^{-3} \end{aligned}$$

$$\begin{aligned} C_{\text{Fe}^{3+}} &= 0 \text{ mole}\cdot\text{m}^{-3} \\ C_{\text{Ce}^{4+}} &= 80 \text{ mole}\cdot\text{m}^{-3} \end{aligned}$$

The enthalpies and entropies of the redox reactions are:

$$\Delta H_{\text{Fe}} = 102 \text{ kJ}\cdot\text{mole}^{-1}$$

$$\Delta H_{\text{Ce}} = 40 \text{ kJ}\cdot\text{mole}^{-1}$$

$$\Delta S_{\text{Fe}} = 37 \text{ J}\cdot\text{mole}^{-1}\cdot\text{K}^{-1}$$

$$\Delta S_{\text{Ce}} = 40 \text{ J}\cdot\text{mole}^{-1}\cdot\text{K}^{-1}$$

and the initial oxygen equilibrium pressure is fixed at

$$p_{\text{O}_2} = 0.002 \text{ bar at } 900^\circ\text{C}$$

The enthalpies and entropies mentioned in section 6.7.3.1 can still be applied to describe the equilibrium state of the iron and cerium reactions in TV-screen glass containing 0.4 weight-%  $\text{Fe}_2\text{O}_3$  and 0.6 weight-%  $\text{CeO}_2$ . The increase of the oxygen equilibrium pressure in the glass melt at an increase of the temperature is due to the shift in the equilibrium state of both reactions.

At the initial temperature  $T_i$  of  $900^\circ\text{C}$ , the oxygen equilibrium pressure was 0.002 bar. At an increase of temperature from  $T_i$  to  $T_f$ , the equilibrium states of both reaction 6.87 and 6.89 shift to the right. Iron and cerium are transferred into the reduced state, resulting in the release of  $\text{O}_2$ . Each mole of  $\text{Fe}^{3+}$  that is being reduced to  $\text{Fe}^{2+}$  yields  $1/4$  mole  $\text{O}_2$ , and at the reduction of one mole of  $\text{Ce}^{4+}$  into  $\text{Ce}^{3+}$ ,  $1/4$  mole  $\text{O}_2$  is formed. Assuming that no transport of oxygen takes place between melt and atmosphere (closed system), the following equation holds:

$$[\text{O}_2]_{\text{T}_f} - [\text{O}_2]_{\text{T}_i} = \frac{1}{4} \cdot \left\{ [\text{Fe}^{2+}]_{\text{T}_f} - [\text{Fe}^{2+}]_{\text{T}_i} \right\} + \frac{1}{4} \cdot \left\{ [\text{Ce}^{3+}]_{\text{T}_f} - [\text{Ce}^{3+}]_{\text{T}_i} \right\} \quad (6.91)$$

Iron and cerium are hardly volatile. Therefore the iron and cerium concentration,  $C_{\text{Fe}}$  and  $C_{\text{Ce}}$ , are assumed to be constant during the experiment. The total iron content is 0.4 weight-%  $\text{Fe}_2\text{O}_3$ , which is equal to 114 mole  $\text{Fe} \cdot \text{m}^{-3}$  glass, the total cerium content is 0.6 weight-%  $\text{CeO}_2$ , which is equal to 80 mole  $\text{Ce} \cdot \text{m}^{-3}$  glass. The concentration of the reduced form of iron,  $[\text{Fe}^{2+}]$ , can be written as a function of the total iron concentration  $C_{\text{Fe}}$ , the redox reaction equilibrium constant of the iron reduction,  $K_{\text{Fe}}^{**}$ , and the oxygen equilibrium pressure  $p_{\text{O}_2}$ :

$$[\text{Fe}^{2+}]_{\text{T}} = \frac{C_{\text{Fe}} \cdot K_{\text{Fe}}^{**}(\text{T})}{K_{\text{Fe}}^{**}(\text{T}) + p_{\text{O}_2}^{1/4}(\text{T})} \quad (6.92)$$

Likewise, the reduced form of cerium,  $[\text{Ce}^{3+}]$ , can be written as a function of the total cerium concentration  $C_{\text{Ce}}$  and the redox reaction equilibrium constant of the cerium reduction,  $K_{\text{Ce}}^{**}$ :

$$[\text{Ce}^{3+}]_{\text{T}} = \frac{C_{\text{Ce}} \cdot K_{\text{Ce}}^{**}(\text{T})}{K_{\text{Ce}}^{**}(\text{T}) + p_{\text{O}_2}^{1/4}(\text{T})} \quad (6.93)$$

The relation between the oxygen equilibrium pressure in the melt,  $p_{\text{O}_2}$ , and the concentration of the physically dissolved oxygen,  $[\text{O}_2]$ , is given by:

$$p_{\text{O}_2}(\text{T}) = \frac{[\text{O}_2]_{\text{T}}}{L_{\text{O}_2}(\text{T})} \quad (6.94)$$

and  $L_{\text{O}_2}$  is the physical solubility of  $\text{O}_2$  in the glass melt.

Combining equations 6.91, 6.92, 6.93 and 6.94 results in:

$$L_{\text{O}_2}(\text{T}_f) \cdot p_{\text{O}_2}(\text{T}_f) - L_{\text{O}_2}(\text{T}_i) \cdot p_{\text{O}_2}(\text{T}_i) = \frac{1}{4} \cdot C_{\text{Fe}} \cdot \left\{ \frac{K_{\text{Fe}}^{**}(\text{T}_f)}{K_{\text{Fe}}^{**}(\text{T}_f) + p_{\text{O}_2}^{1/4}(\text{T}_f)} - \frac{K_{\text{Fe}}^{**}(\text{T}_i)}{K_{\text{Fe}}^{**}(\text{T}_i) + p_{\text{O}_2}^{1/4}(\text{T}_i)} \right\} + \frac{1}{4} \cdot C_{\text{Ce}} \cdot \left\{ \frac{K_{\text{Ce}}^{**}(\text{T}_f)}{K_{\text{Ce}}^{**}(\text{T}_f) + p_{\text{O}_2}^{1/4}(\text{T}_f)} - \frac{K_{\text{Ce}}^{**}(\text{T}_i)}{K_{\text{Ce}}^{**}(\text{T}_i) + p_{\text{O}_2}^{1/4}(\text{T}_i)} \right\} \quad (6.95)$$

Now the theoretical oxygen equilibrium pressure in the TV-screen glass containing 0.4 weight-%  $\text{Fe}_2\text{O}_3$  and 0.6 weight-%  $\text{CeO}_2$  can be calculated using equations 6.88, 6.90 and 6.95, with the enthalpies and entropies given in section 6.7.3.1. The physical solubility of oxygen is assumed to be about  $1 \text{ mole}\cdot\text{m}^{-3}\cdot\text{bar}^{-1}$  (see chapter 6.8). The resulting oxygen equilibrium pressures are given in figure 6.75 as the continuous curve. The agreement between the measured and the theoretical oxygen equilibrium pressures is very good. In figure 6.75, the theoretical oxygen equilibrium pressures in TV-screen glasses containing only 0.4 weight-%  $\text{Fe}_2\text{O}_3$  (dashed curve) or only 0.6 weight-%  $\text{CeO}_2$  (dotted curve), starting with the same oxygen equilibrium pressure at  $900^\circ\text{C}$ , are given as well. It is clear that the oxygen equilibrium pressure in the glass melt is governed by the equilibrium states of both redox reactions.

#### 6.7.3.5 Redox ratios in the glass melt containing iron and cerium

Even though the redox reaction equilibrium constant of iron is not effected by the presence of cerium, the redox ratio  $[\text{Fe}^{2+}]/[\text{Fe}^{3+}]$  is influenced. The oxygen equilibrium pressure  $p_{\text{O}_2}$  is governed by the equilibrium constants of both iron and cerium reduction reactions. Therefore the oxygen equilibrium pressure in TV-screen glasses containing 0.4 weight-%  $\text{Fe}_2\text{O}_3$  and 0.6 weight-%  $\text{CeO}_2$  differs from the oxygen equilibrium pressure in TV-screen glasses containing only 0.4 weight-%  $\text{Fe}_2\text{O}_3$ . For instance, in the glass melt containing both ions, the oxygen equilibrium pressure at  $1000^\circ\text{C}$  is 0.0087 bar. The redox ratio  $[\text{Fe}^{2+}]/[\text{Fe}^{3+}]$  at this temperature and pressure is given by:

$$\frac{[\text{Fe}^{2+}]_{1000^\circ\text{C}}}{[\text{Fe}^{3+}]_{1000^\circ\text{C}}} = \frac{K_{\text{Fe}}(1000^\circ\text{C})}{p_{\text{O}_2}^{1/4}(1000^\circ\text{C})} = 0.018 \quad (6.96)$$

In the case the melt had contained only iron, the oxygen equilibrium pressure at  $1000^\circ\text{C}$  would have been 0.046 bar (starting from an oxygen pressure of 0.002 bar at  $900^\circ\text{C}$ ). Then the redox ratio  $[\text{Fe}^{2+}]/[\text{Fe}^{3+}]$  would have been 0.012.

#### 6.7.3.6 Redox ratios in the glass containing both iron and cerium during cooling

The glass melt contains  $114 \text{ mole}\cdot\text{m}^{-3}$  and  $80 \text{ mole}\cdot\text{m}^{-3}$ . According to equation 6.96, the ratio  $[\text{Fe}^{2+}]/[\text{Fe}^{3+}]$  is 0.018 at  $1000^\circ\text{C}$ . This means that the concentration of divalent iron,  $[\text{Fe}^{2+}]$ , is  $2 \text{ mole}\cdot\text{m}^{-3}$ . The concentration of reduced cerium,  $[\text{Ce}^{3+}]$ , can be calculated in the same way. It is  $72 \text{ mole}\cdot\text{m}^{-3}$ .

In chapter 3.2.5, the possibility that the redox ratios of polyvalent elements

shift during cooling has already come up for discussion. The experiments described below have been carried out in order to check whether such a change in redox ratios actually occurs in the TV-screen glass under investigation, containing both iron and cerium.

After the oxygen equilibrium pressure measurements, the electrodes were removed from the melt at 1000°C and subsequently the melt was quenched. The cooled-down glass was found to be soft yellow. According to Bamford [27], reduced form of iron,  $\text{Fe}^{2+}$ , provides for a strong green colour, even at low concentrations. The oxidized form  $\text{Fe}^{3+}$  causes the soft, yellow colour. This means that the major part of the iron in the glass sample was present in the oxidized form after cooling of the melt. Unfortunately, the exact amount of trivalent iron in the glass could not be estimated by redox titration, because the presence of cerium in the glass would interfere with the measurement. Therefore the amount of divalent iron in the glass sample was estimated on the basis of the yellow colour.

Firstly it was investigated whether cerium (as  $\text{Ce}^{3+}$  or  $\text{Ce}^{4+}$ ) could be responsible for the soft yellow colour of the glass sample. Therefore a TV-screen glass containing only 0.6 weight-%  $\text{CeO}_2$  and no iron was melted for some time at 1000°C, until the melt was free of grains and bubbles. Then the oxygen equilibrium pressure in the melt was measured with the aid of an oxygen sensor. It was found to be 0.029 bar. With this oxygen equilibrium pressure, the concentration of trivalent cerium in the melt was calculated to be 70 mole  $\text{Ce}^{3+} \cdot \text{m}^{-3}$ , and the concentration of tetravalent cerium,  $\text{Ce}^{4+}$ , was 10 mole  $\cdot \text{m}^{-3}$  at 1000°C. Subsequently the melt was quenched.

The physical solubility of oxygen in the glass melt is assumed to be about 1 mole  $\cdot \text{m}^{-3} \cdot \text{bar}^{-1}$  at melting temperatures. This implies that the concentration of physically dissolved oxygen is about 0.03 mole  $\cdot \text{m}^{-3}$  in the glass melt at 1000°C. Although the equilibrium state of reaction 6.89 shifts to the right during cooling, hardly any oxygen is available for the oxidation of the trivalent cerium. Therefore the valency state of the cerium ions is assumed to be constant during cooling. This assumption was checked by determining the concentration of trivalent cerium,  $\text{Ce}^{3+}$ , and the total cerium content  $C_{\text{Ce}}$  by wet-chemical analysis in the cooled-down glass sample. The  $\text{Ce}^{3+}$ -concentration was found to be 64 mole  $\cdot \text{m}^{-3}$ , and the total cerium content was 74 mole  $\cdot \text{m}^{-3}$ , and so the equilibrium state of reaction 6.89 had indeed hardly changed during cooling.

The glass sample containing  $\text{Ce}^{3+}$  and  $\text{Ce}^{4+}$  was colourless, indicating that the soft yellow colour in the glass sample containing both iron and cerium was indeed caused by the trivalent iron.

Secondly the concentration of divalent iron in the glass sample containing both iron and cerium had to be estimated on the basis of the colour of a glass sample containing only iron. The concentration  $\text{Fe}^{2+}$  could not be derived from the absorption spectrum of the glass sample, since the sample contained cords.

For the comparison a TV-screen glass containing only 0.4 weight-%  $\text{Fe}_2\text{O}_3$  (and no other polyvalent elements) was molted at  $1000^\circ\text{C}$  until it was free from grains and bubbles. Then the oxygen equilibrium pressure was measured. It was found to be 0.084 bar. According to equation 6.88, the concentration of divalent iron,  $\text{Fe}^{2+}$ , in this melt is only  $1.2 \text{ mole}\cdot\text{m}^{-3}$ , while the concentration of trivalent iron,  $\text{Fe}^{3+}$ , is  $112.8 \text{ mole}\cdot\text{m}^{-3}$ . The melt was quenched to room temperature. The concentration of physically dissolved oxygen was assumed to be too low to oxidize  $\text{Fe}^{2+}$  to a noticeable extent during cooling. Therefore the concentration  $\text{Fe}^{2+}$  in the cooled-down glass was assumed to be  $1.2 \text{ mole}\cdot\text{m}^{-3}$ .

The colour of the glass sample containing only iron was clearly green. So even at the low concentration of  $1.2 \text{ mole}\cdot\text{m}^{-3}$  glass, divalent iron causes a green colour. This indicates that the concentration of divalent iron in the TV-screen glass containing both iron and cerium is less than  $1.2 \text{ mole}\cdot\text{m}^{-3}$  at room temperature. During the cooling of the glass melt, some divalent iron must have been oxidized. Since the concentration of physically dissolved oxygen in the glass melt was about  $0.009 \text{ mole}\cdot\text{m}^{-3}$  (assuming a physical solubility of oxygen of about  $1 \text{ mole}\cdot\text{m}^{-3}\cdot\text{bar}^{-1}$ ),  $\text{Fe}^{2+}$  must have been oxidized by  $\text{Ce}^{4+}$ .

From this experiment, it can be concluded that the redox ratios of polyvalent ions indeed shift during cooling when other polyvalent elements are present in the glass melt.

#### 6.7.4 Conclusions

- The redox reaction equilibrium constants of the reduction of iron and cerium in a TV-screen glass melt at melting temperatures are not influenced by the presence of the other polyvalent element;
- the oxygen equilibrium pressure in TV-screen glass melts containing both iron and cerium can be adequately described by equation 6.95, which is based

on the redox reaction equilibrium constants of the redox reactions of iron and cerium in TV-screen melts;

- the equilibrium states of the iron and cerium reactions shift as the melt is quenched.

## 6.8 PHYSICAL SOLUBILITY OF O<sub>2</sub>

### 6.8.1 Measurements of the physical solubility of O<sub>2</sub>

The oxygen equilibrium pressure measurements can be used for the determination of the redox reaction enthalpy and entropy if the physical solubility of oxygen is known (see chapter 5.4.7). Unfortunately, hardly any literature data on the physical solubility of O<sub>2</sub> in soda-lime-silica, TV-screen and E-glass exists (chapter 5.4.8). According to Sasabe [35], the physical solubility of oxygen in various PbO-SiO<sub>2</sub>-melts ranges from 20 to 200 mole·m<sup>-3</sup>·bar<sup>-1</sup>. On the basis of the physical solubility of N<sub>2</sub> in soda-lime-silica glasses given by Mulfinger [36], Beerkens [32] estimated the solubility of O<sub>2</sub> at about 0.1 mole·m<sup>-3</sup>·bar<sup>-1</sup>. Recent experiments [33] using the helium extraction technique indicate, that the physical solubility of oxygen in soda-lime-silica and TV-screen glass melts at temperatures ranging from 1200 to 1450°C is about 0.1 to 1 mole·m<sup>-3</sup>·bar<sup>-1</sup>.

However, if the redox reaction enthalpy and entropy are already known, for example from square wave voltammetry measurements, the physical solubility of O<sub>2</sub> can be estimated from the oxygen equilibrium pressure measurements.

For a glass melt containing only one polyvalent element with a concentration C<sub>M</sub> mole·m<sup>-3</sup>, the following equation (see equation 5.43) is valid under the conditions that no exchange of oxygen and the polyvalent element takes place between glass melt and atmosphere (closed system):

$$L_{O_2}(T_1) \cdot p_{O_2}(T_1) - L_{O_2}(T_2) \cdot p_{O_2}(T_2) = \frac{n}{4} \cdot C_M \cdot \left\{ \frac{K^{**}(T_1)}{K^{**}(T_1) + p_{O_2}^{n/4}(T_1)} - \frac{K^{**}(T_2)}{K^{**}(T_2) + p_{O_2}^{n/4}(T_2)} \right\} \quad (6.97)$$

The physical solubility of oxygen may depend on temperature, but if the difference between the two temperatures T<sub>1</sub> and T<sub>2</sub> is small, the solubility will remain roughly constant:

$$L_{O_2}(T_1) \approx L_{O_2}(T_2) \quad (6.98)$$

and equation 6.97 can be simplified to:

$$L_{O_2} \left( \text{at } \frac{T_1 + T_2}{2} \right) \approx \frac{n \cdot C_M}{4 \cdot (p_{O_2}(T_1) - p_{O_2}(T_2))} \cdot \left\{ \frac{K^{**}(T_1)}{K^{**}(T_1) + p_{O_2}^{n/4}(T_1)} - \frac{K^{**}(T_2)}{K^{**}(T_2) + p_{O_2}^{n/4}(T_2)} \right\} \quad (6.99)$$

The redox reaction equilibrium constant  $K^{**}(T)$  is given by:

$$K^{**}(T) = \exp \left( \frac{-\Delta H^{**}}{R_g \cdot T} + \frac{\Delta S^{**}}{R_g} \right) \quad (6.100)$$

In some glass melts containing different amounts of iron or antimony, both oxygen equilibrium pressure measurements and square wave voltammetry measurements have been performed (see tables 6.5 and 6.8). By replacing  $\Delta H^{**}$  and  $\Delta S^{**}$  in equation 6.100 with the values for the reaction enthalpy and entropy, derived by square wave voltammetry measurements, the physical solubility of  $O_2$  in these glass melts can be estimated using equation 6.99.

For example, the redox reaction enthalpy and entropy for the iron reduction in TV-screen glass type A containing 0.4 weight-%  $Fe_2O_3$  were determined using square wave voltammetry. The results were:

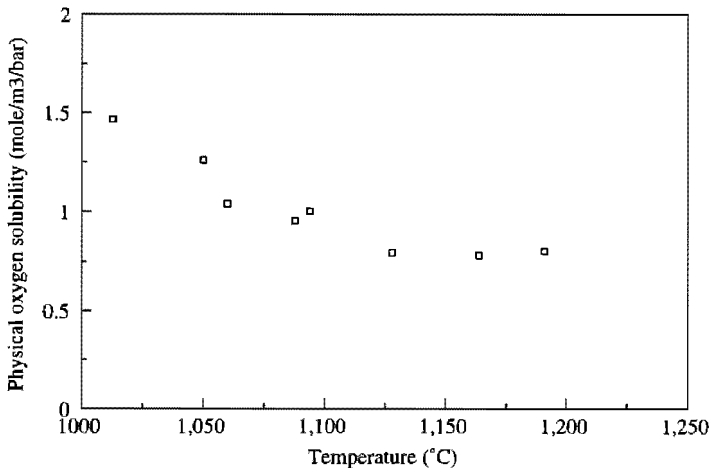


Figure 6.76

The physical solubility of  $O_2$  in TV-screen glass type A, calculated by applying equation 6.99 to oxygen equilibrium pressure measurements in the TV-screen glass type A containing 0.4 weight-%  $Fe_2O_3$

$$\Delta H^{**} = 102 \text{ kJ}\cdot\text{mole}^{-1}$$

$$\Delta S^{**} = 37 \text{ J}\cdot\text{mole}^{-1}\cdot\text{K}^{-1}$$

In this glass melt, oxygen equilibrium pressure measurements were performed as well. The physical solubility of  $\text{O}_2$  in this melt at temperatures between 1000 and 1200°C was found to be about  $1 \text{ mole}\cdot\text{m}^{-3}\cdot\text{bar}^{-1}$  (see figure 6.76). Roughly the same results were obtained from square wave voltammetry and oxygen equilibrium pressure measurements in the TV-screen glass type B containing 0.4 weight-%  $\text{Fe}_2\text{O}_3$  at temperatures ranging from 900 to 1400°C.

In E-glass containing 0.5 weight-%  $\text{Fe}_2\text{O}_3$ , TV-screen glass type A containing 0.4 weight-%  $\text{Sb}_2\text{O}_3$ , TV-screen glass type A containing 2.14 weight-%  $\text{Sb}_2\text{O}_3$  and TV-screen glass type B containing 0.43 weight-%  $\text{Sb}_2\text{O}_3$ , both square wave voltammetry and oxygen equilibrium pressure measurements have been performed likewise. However, applying equations 6.99 and 6.100 to the results obtained in these glasses, results in improbable values for the physical solubility of  $\text{O}_2$ : the solubility fluctuates between positive and negative values (ranging from -500 to + 500  $\text{mole}\cdot\text{m}^{-3}\cdot\text{bar}^{-1}$ ). This is probably due to small deviations in the oxygen equilibrium pressure measurements or in temperature.

### 6.8.2 Effect of the value chosen for the physical solubility of oxygen on the calculated enthalpy and entropy

For the processing of the oxygen equilibrium pressure measurements, the physical solubility of  $\text{O}_2$  was assumed to be  $1 \text{ mole}\cdot\text{m}^{-3}\cdot\text{bar}^{-1}$  at any temperature between 800 and 1400°C. Calculations of the redox reaction enthalpy and entropy, based on other values for the physical solubility of oxygen, have shown that the exact value of the solubility has hardly any influence on the resulting enthalpy. However, the calculated entropy depends on the value of the solubility. As an example, the enthalpy and entropy for the reduction of iron respectively antimony in TV-screen glass type A are given in tables 6.13 and 6.14 for different values of the physical solubility of  $\text{O}_2$ .

The results of oxygen equilibrium pressure measurements agree very well with the results obtained by square wave voltammetry measurements if the oxygen solubility is set to a value of  $1.0 \text{ mole}\cdot\text{m}^{-3}\cdot\text{bar}^{-1}$ . For this reason, it is assumed that, for the time being, a value of  $1.0 \text{ mole}\cdot\text{m}^{-3}\cdot\text{bar}^{-1}$  is the best estimate for the physical solubility of oxygen in TV-screen glasses at temperatures between 1000 and 1400°C.



Table 6.13

The enthalpy  $\Delta H^{**}$  and entropy  $\Delta S^{**}$  calculated from oxygen equilibrium pressure measurements in TV-screen glass type A containing 0.4 weight-%  $\text{Fe}_2\text{O}_3$ , for different values of the physical solubility of oxygen,  $L_{\text{O}_2}$

$L_{\text{O}_2}$ (mole·m <sup>-3</sup> ·bar <sup>-1</sup> )	$\Delta H^{**}$ (kJ·mole <sup>-1</sup> )	$\Delta S^{**}$ (J·mole <sup>-1</sup> ·K <sup>-1</sup> )
0.1	100	15
0.5	100	30
1.0	100	37
2.0	100	44
10.0	100	60
Square wave voltammetry measurements	102	37

Table 6.14

The enthalpy  $\Delta H^{**}$  and entropy  $\Delta S^{**}$  of the reaction  $\text{Sb}^{5+}/\text{Sb}^{3+}$  calculated from oxygen equilibrium pressure measurements in TV-screen glass type A containing 0.4 weight-%  $\text{Sb}_2\text{O}_3$ , for different values of the physical solubility of oxygen,  $L_{\text{O}_2}$

$L_{\text{O}_2}$ (mole·m <sup>-3</sup> ·bar <sup>-1</sup> )	$\Delta H^{**}$ (kJ·mole <sup>-1</sup> )	$\Delta S^{**}$ (J·mole <sup>-1</sup> ·K <sup>-1</sup> )
0.1	219	154
0.5	219	143
1.0	219	138
2.0	219	133
10.0	221	115
Square wave voltammetry measurements	213	139

### 6.8.3 Conclusions

- Oxygen equilibrium pressure measurements might be used for the estimation of the physical solubility of oxygen in glass melts. However, this method is over-sensitive for small deviations in the measurements. Therefore, more accurate oxygen equilibrium pressure measurements have to be performed before the oxygen solubility can be established with certainty;
- at this moment, the best estimate for the physical solubility of oxygen in TV-screen glass melts is probably 1.0 mole·m<sup>-3</sup>·bar<sup>-1</sup>.

Literature

- [1] Sun, K.H.  
A scale of acidity and basicity in glass  
*The Glass Industry* **29** (1948) p. 73-74
- [2] Papadopoulos, K.  
The solubility of  $\text{SO}_3$  in soda-lime-silica melts  
*Physics and Chemistry of Glasses* **14** (1973) no.3 p.60-65
- [3] Apak, C.; Cable, M.  
Effect of transition metal oxides on the refining behaviour of soda-lime-silica glasses  
Proceedings of the XI International Congress on Glass Prague (1977) **4** p.167-176
- [4] Kohl, R.; Schaeffer, H.A.  
Oxidation states of glass melts  
*Diffusion and Defect Data* **53-54** (1987) p.325-334
- [5] Lenhart, A.; Schaeffer, H.A.  
Redox behaviour of glass melts  
*Diffusion and Defect Data* **53-54** (1987) p.335-344
- [6] Rüssel, C.; Freude, E.  
Voltammetric studies of the redox behaviour of various multivalent ions in soda-lime-silica glass melts  
*Physics and Chemistry of Glasses* **30** (1989) no.2 p.62-68
- [7] Simonis, F. (editor)  
"NCNG-Glascursus"  
TPD-TNO in samenwerking met de gezamenlijke Nederlandse Glasindustrieën (1990)
- [8] Langer, A.; Scholze, H.  
Untersuchungen zum Ersatz von  $\text{As}_2\text{O}_3$  als Läutermittel für Kristallgläser  
*Glastechnische Berichte* **54** (1981) no.7 p.223-230
- [9] Johnston, W.D.  
Oxidation-reduction equilibria in iron-containing glass  
*Journal of the American Ceramic Society* **47** (1964) no.4 p.198-201
- [10] Paul, A.; Douglas, R.W.  
Ferrous-ferric equilibrium in binary alkali silicate glasses  
*Physics and Chemistry of Glasses* **6** (1965) no.6 p.207-211
- [11] Rüssel, C.; Kohl, R.; Schaeffer, H.A.  
Interaction between oxygen activity of  $\text{Fe}_2\text{O}_3$  doped soda-lime-silica glass melts and physically dissolved oxygen  
*Glastechnische Berichte* **61** (1988) no.8 p.209-213
- [12] Johnston, W.D.  
Oxidation-reduction equilibria in molten  $\text{Na}_2\text{O}\cdot 2\text{SiO}_2$  glass  
*Journal of the American Ceramic Society* **48** (1965) no.4 p.184-191

- [13] Krol, D.M.; Rommers, P.J.  
Oxidation-reduction behaviour of antimony in silicate glasses prepared from raw materials and cullet  
*Glass Technology* **25** (1984) no.2 p.115-118
- [14] Stahlberg, B. et.al.  
Combined electrochemical and Mössbauer studies of the  $Sb^{3+}/Sb^{5+}$  equilibrium in a silicate glassforming melt  
*Glastechnische Berichte* **61** (1988) p.335-340
- [15] Paul, A.; Douglas, R.W.  
Cerous-ceric equilibrium in binary alkali borate and alkali silicate glasses  
*Physics and Chemistry of Glasses* **6** (1965) no.6 p.212-215
- [16] Nath, P.; Douglas, R.W.  
 $Cr^{3+}-Cr^{6+}$  equilibrium in binary alkali silicate glasses  
*Physics and Chemistry of Glasses* **6** (1965) no.6 p.197-206
- [17] Chopinet, M.H.; Massol, J.J.; Barton, J.L.  
Factors determining the residual sulfate content of glass  
*Glastechnische Berichte* **56K** (1983) no.1 p.596-601
- [18] Chopinet, M.H.; Barton, J.L.  
The effect of melting temperatures on the residual sulfate content of glass  
Proceedings of the XIV International Congress on Glass New Delhi **3** (1986) p.9-15
- [19] Schreiber, H.D. et.al.  
Sulfur chemistry in a borosilicate melt  
Part I. Redox equilibria and solubility  
*Glastechnische Berichte* **60** (1987) no.12 p.389-398
- [20] Freude, E.  
Voltammetrische Untersuchungen des Redoxverhaltens polyvalenter Ionen in Glasschmelzen, insbesondere von Technetium  
Thesis Universität Erlangen (1989)
- [21] Barin, I.  
"Thermochemical data of pure substances"  
ISBN 3-527-27812-5 VCH (1989)
- [22] Goldman, D.S.  
Oxidation equilibria of iron in borosilicate glass  
*Journal of the American Ceramic Society* **66** (1983) p.205-210
- [23] Takahashi, K.; Miura, Y.  
Electrochemical studies on diffusion and redox behaviour of various metal ions in some molten glasses  
*Journal of Non-Crystalline Solids* **38-39** (1980) p.527-532
- [24] Tran, T.; Brungs, M.D.  
Application of oxygen electrodes in glass melts. Part II. Oxygen probes for the measurement of oxygen potential in sodium disilicate glass  
*Physics and Chemistry of Glasses* **21** (1980) no.5 p.178-183

- [25] Rüssel, C.; Freude, E.  
Voltammetric studies in a soda-lime-silica glass melt containing two different polyvalent ions  
*Glastechnische Berichte* **63** (1990) no.6 p.149-153
- [26] Rüssel, C.  
Polyvalent ions in glass melts  
*Glastechnische Berichte* **63K** (1990) p.197
- [27] Bamford, C.R.  
"Colour generation and control in glass (Glass science and technology 2)"  
Elsevier Scientific Publishing Company Amsterdam-Oxford-New York (1977)
- [28] Ngyen Viet Duc  
Untersuchungen zur Sulfatläuterung von Glasschmelzen mit ZrO<sub>2</sub>-Festelektrolytsonden  
Thesis Bergakademie Freiberg (1989)
- [29] Jebesen-Marwedel, H.; Brückner, R.  
"Glastechnische Fabrikationsfehler"  
Springer-Verlag Berlin Heidelberg (1980)
- [30] Conroy, A.R.; Manring, W.H.; Bauer, W.C.  
Role of sulfate in the melting and fining of glass batch  
Part I  
*The Glass Industry* **47** (1966) no.2 p.84-89,110  
Part II  
*The Glass Industry* **47** (1966) no.3 p.133-141
- [31] Goldman, D.S.  
Redox and sulphur solubility in glass melts  
"Gas bubbles in glass"  
The International Commission on Glass (1985) p.74-91
- [32] Beerkens, R.G.C.  
Chemical equilibrium reactions as driving forces for growth of gas bubbles during refining  
*Glastechnische Berichte* **63K** (1990) p.222-242
- [33] Beerkens, R.G.C.; Kersbergen, M. van  
Properties of gases and redox reactions in glassmelts  
Final report NCNG-NOVEM Fining and redox of glass  
Report T.N.O.-T.P.D. juli (1994)
- [34] Kordon, T.; Rüssel, C.; Freude, E.  
Voltammetric investigations in Na<sub>2</sub>SO<sub>4</sub> refined soda-lime-silica glass melts  
*Glastechnische Berichte* **63** (1990) no.8 p.213-218
- [35] Sasabe, M.; Goto, K.S.  
Permeability, diffusivity and solubility of oxygen gas in liquid slag  
*Metallurgical Transactions* **5** (1974) p.2225-2233
- [36] Mulfinger, H.O.  
Physical and chemical solubility of nitrogen in glass melts  
*Journal of the American Ceramic Society* **49** (1966) no.9 p.462-467

## Chapter 7

### The application of the measured data in computer models

#### 7.1 INTRODUCTION

In chapter 6, the values for the enthalpy and entropy of the redox reactions concerning iron, antimony, cerium and chromium in various concentrations in soda-lime-silica, TV-screen and E-glass have been given. These values can be used to calculate the redox reaction equilibrium constants, the ratios of reduced to oxidized species and/or the oxygen equilibrium pressure in glass melts as a function of temperature. And these quantities influence the temperature distribution (by heat radiation into the melt) and the fining process in industrial glass melting tanks, and therefore the quality of the final glass product.

This chapter describes in which way computer models, based on the redox reaction equilibrium constants, can be used to predict the influence of multivalent elements on the quality of the final glass product. As an example, the effect of the antimony concentration on the fining progress is demonstrated in section 7.5.

#### 7.2 MATHEMATICAL MODELS

In the past, the efficiency of chemical fining agents has mainly been investigated in laboratory experiments, since experiments in industrial glass melting tanks would have been much too expensive and risky. Therefore small amounts of glass batch were melted in crucibles [1,2,3,4,5] at a fixed temperature during a fixed period. After cooling down, the number of bubbles and their size distribution and/or composition were determined. On the basis of these data, investigators have tried to decide which fining agent at which concentration should be used for the fining process in industrial glass melting tanks.

However, it is very difficult to translate the results from the laboratory experiments to efficiency data for industrial tanks. For example, the (initial) number, size and composition of bubbles in the laboratory experiments may differ significantly from those in the industrial tanks. Furthermore, the flow patterns and temperature distribution in the industrial tanks can not be simulated in crucibles. And just the residence time and temperature course of the glass melt containing the bubbles will determine whether a bubble can ascend to the surface or dissolve completely, or remain in the melt.

Therefore two computer models which simulate (some aspects of) the fining process have been developed at the TNO Institute of Applied Physics (the Netherlands). One of these models, the "3-D glass tank model", is used to calculate the temperature distribution, flow pattern and gas concentration profiles in industrial glass melting tanks [6,7]. Another model, the "bubble behaviour model", describes the behaviour of single bubbles in the glass melt containing multivalent elements [8,9].

By combining the two computer models, it is possible to predict whether an existing industrial glass melting tank may, under certain processing conditions, be able to produce bubble-free glass [10]. But also the source of bubbles, detected in the final glass product, may be found by back-tracing procedures, based on the composition, size and position of the bubble [9,11]. Furthermore, computer calculation may become an important tool for the optimization of the furnace design and operation [7].

An important parameter in the computer models is the "redox" of the glass melt. As we have seen in chapter 3.4.3, no unambiguous definition for the "redox" of the glass melt is available. Here, the "redox" refers to the valency state of the multivalent elements present.

The valency states of iron and chromium determine the heat penetration in the glass melt.  $\text{Fe}^{2+}$  en  $\text{Cr}^{3+}$  absorb far more infrared radiation than  $\text{Fe}^{3+}$ ,  $\text{Cr}^{6+}$  and  $\text{Cr}^{2+}$ . Since the glass melt in the industrial glass melting tanks is generally heated from above by gas or oil fired flames, the temperature of the melt at the bottom of the furnace depends on the concentrations of  $\text{Fe}^{2+}$  and  $\text{Cr}^{3+}$  present in the melt.

Furthermore, the multivalent elements determine the oxygen pressure in the melt (and the  $\text{SO}_2$  pressure in case the melt contains sulphate). Small bubbles in the glass melt can grow or shrink by diffusion of gases (see chapter 2.6), and therefore the equilibrium states of the redox reactions control the fining process.

Both computer models contain equations concerning the equilibrium state of the redox reactions of all multivalent elements present. The equilibrium constants can be calculated from the redox reaction enthalpies and entropies given in chapter 6.

### 7.3 THE "BUBBLE BEHAVIOUR MODEL"

During the melting of the batch in industrial glass melting tanks, bubbles are formed due to reactions of the batch materials, air inclusions or interaction of the melt with refractory materials. Under the influence of the gravitation, these bubbles ascend to the surface of the melt (buoyancy driven bubble removal). The rising velocity strongly depends on the bubble radius (see chapter 2.3.1).

During its residence time in the glass melt, a single bubble may grow or shrink due to exchange of gases between bubble and melt. The growth or shrinkage rate depends on:

- the surface area of the bubble;
- the partial pressures of the different gases in the bubble;
- the gas concentrations in the melt;
- the solubilities of the gases in the melt;
- the diffusivity of the gases;
- the renewal of the melt near the surface of the bubble (and therefore on the rising velocity of the bubble).

The chemical fining agents aid the removal of the gas bubbles by changing the concentration of gas(es) in the melt. At an increase in temperature, large amounts of fining gases are produced. This can lead to a super-saturation of the melt with the fining gas. The surplus of gas is removed by diffusion of the gas to existing bubbles (or by heterogeneous formation of new bubbles). The bubbles grow, and as a consequence the rising velocity of the bubble is increased, the partial pressures of the other gases in the bubble are reduced and the surface area increases. This enhances the transport of the other gases from the bubble to the melt as well. In this way, effective degassing of the melt takes place at high temperatures (primary fining).

At a decrease of temperatures, the fining agents react with the fining gas(es). In the melt, the concentration of these gases will be very low after the primary fining stage due to the effective degassing process at high temperatures. Fining gas will be resorbed at lower temperatures, the partial pressures of the other gases in the bubbles increase, and as a result the transport of these gases from the bubbles into the melt is enhanced.

Beerkens [8,9] developed a computer model which describes the composition and size of a single bubble in a glass melt (the "bubble behaviour model") for a

given temperature course. It may be clear that both for bubble growth and for bubble shrinkage, the concentration of the fining gas (physically dissolved) in the glass melt is of major importance. This concentration is calculated for any temperature with the aid of the enthalpy and entropy of the redox reaction of the fining agent. The values of the enthalpy and entropy of various multivalent elements in different concentrations can be found in chapter 6. The bubble behaviour model can be used to compare the fining action of various fining agents, or to estimate the temperature at which the fining of the glass melt should preferably take place.

#### **7.4 THE "3-D GLASS TANK MODEL"**

The residence time of the glass melt in an industrial tank may show a distribution. Therefore not all bubbles that arise during the melting of the batch materials may have sufficient time to grow and ascend to the surface or dissolve completely before the melt enters the furnace. In order to be able to predict whether a bubble-free melt can be obtained, it is important to know the flow pattern, the temperature distribution and the gas profiles in the tank.

At the TNO Institute of Applied Physics (the Netherlands), a computer model has been developed which calculates flow pattern, temperature distribution and gas profiles in industrial glass melting tanks [6,7]. This "3-D glass tank model" is based on finite difference numerical calculation methods. For that purpose, the industrial tank, with a given construction and dimensions, is divided in the mathematical model into a given number of cells. Batch blanket, combustion chamber, local heat sources (i.e. electrical boosting) and local cooling sources (i.e. glass line cooling) are included.

Now the continuity, energy conservation and Navier-Stokes equations are solved numerically for each cell, using realistic boundary conditions. The concentrations of the different valency states of the multivalent elements and the oxygen concentration are calculated by equilibrium equations based on the redox reaction enthalpies and entropies, which are tabled for various multivalent elements in different concentrations in chapter 6. As a result, the temperature, flow direction, and concentration of all components of the glass melt can be calculated for any cell.

Bubbles will grow if the oxygen equilibrium pressure in the melt exceeds 1 bar,



because then the melt becomes super-saturated with oxygen. When bubbles spend sufficient time in an area in the glass melting tank where the gas pressure is high, the bubbles will become large enough to averse the distance to the surface of the melt in short time. If on the other hand bubbles are directly transported by the flow in the melt to the working end and feeders, the low temperature in that area will prohibit ascension of the bubble. In that case, the bubbles may turn up in the final glass products.

By thorough examination of the calculated flow patterns and gas concentration profiles for various processing conditions (for example the concentration of the fining agent, the redox of the batch or the batch load), the fining process in an industrial glass melting tank can be optimized.

### **7.5 EXAMPLES OF CALCULATIONS WITH THE "3-D GLASS TANK MODEL"**

In this section, the application of the "3-D glass tank model" for the optimization of the fining process in an industrial glass melting tank will be illustrated with an example. The example glass tank is 28 meter long and 5.8 meter wide. The height of the glass melt in this tank is 1 meter. At 0 meter, the batch is added to the tank (see figure 7.1); the size of the batch blanket is about 5 meter. The melting area of the tank is 18 meter long and includes bubblers at 6 meter and a flow barrier at 14 meter. The molten glass passes the throat, which has a length of 2.5 meter, to enter the working end. From there, the glass is transported to the section where the forming of the final product takes place.

In this example tank, 110 ton glass is produced each day. The final glass product contains 40 moles of Sb and 13 moles of Fe per cubic meter (about 0.25 weight-%  $\text{Sb}_2\text{O}_3$  and 0.045 weight-%  $\text{Fe}_2\text{O}_3$ ). No other polyvalent elements are present.

For the calculation of the temperature distribution, flow pattern and concentration profiles in the tank, the tank is divided mathematically into 85 cells lengthwise, 23 cells breadthways and 18 cells in the vertical direction.

The roof temperatures are fixed at certain values (the temperatures can also be calculated using a combustion model which is based on actual fuel supplies).

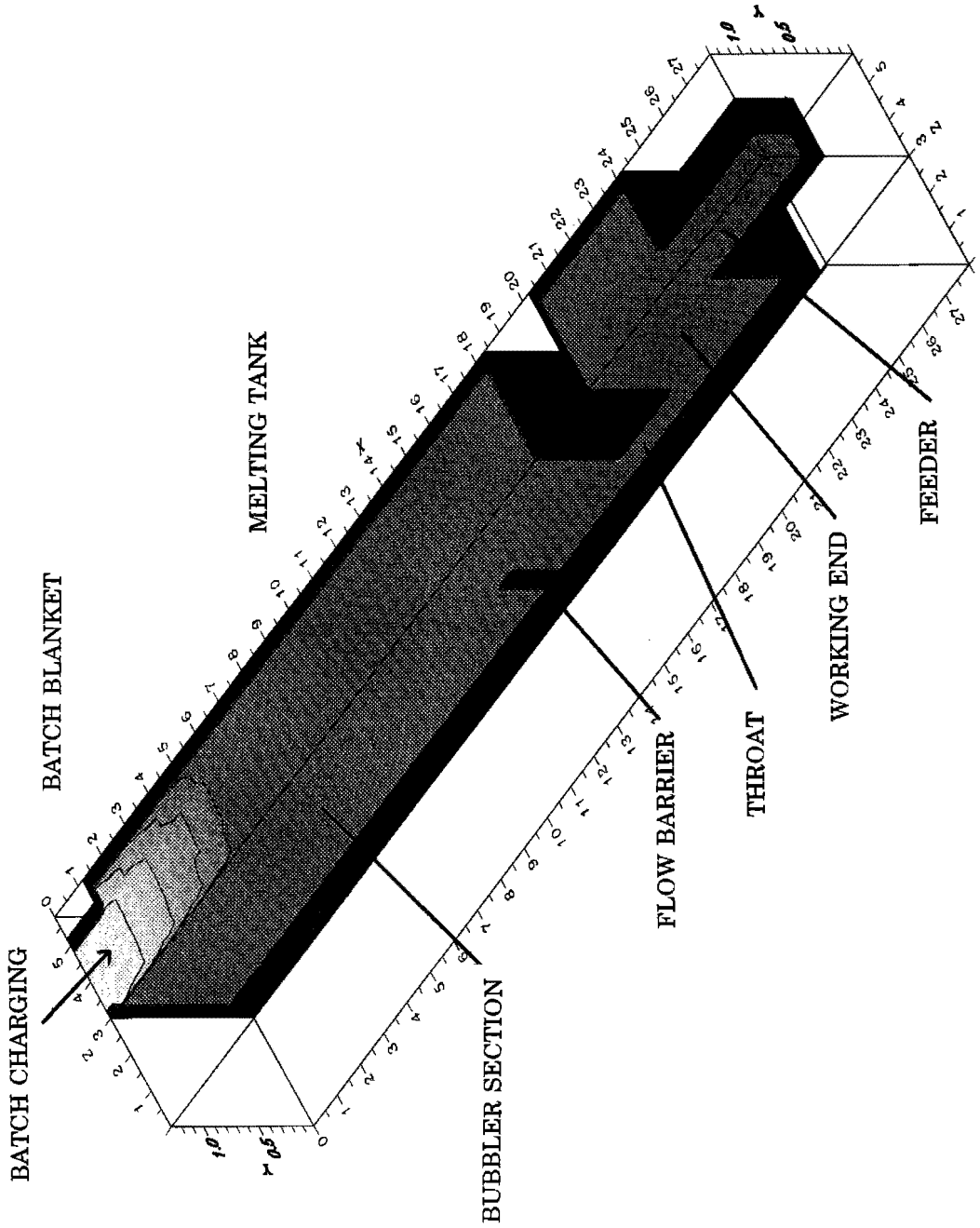


Figure 7.1

An overview (top-view/side-view of the lengthwise section) of the example glass melting tank. In the figure, the walls of the tank are black, the molten glass is grey and the batch blanket is white

This determines the heat flux to the glass melt. The temperatures in the melt depend on the heat conductivity of the melt, which in turn depends on the concentration of divalent iron in the melt. But the  $\text{Fe}^{2+}$  content is determined by the equilibrium constant of the iron reaction and the oxygen content of the glass melt, and therefore also by the equilibrium constant of the antimony reaction. And both equilibrium constants depend on the temperature!

For the first approximation of the  $\text{Fe}^{2+}$ -concentration in the tank, the glass melt is assumed to be very oxidizing. Then only a small part of the iron is present in the reduced state, and the influence of  $\text{Fe}^{2+}$  on the heat conductivity of the melt is approximated with a small, constant value.

Now the temperature and velocity vectors in each cell can be calculated by solving the continuity, energy conservation and Navier-Stokes equations numerically for each cell. The heat loss through the walls is calculated using empirical relations. In figure 7.2, the calculated temperature distribution of the lengthwise-section in the tank is given. It can be seen clearly from figure 7.2 that the glass is locally cooled due to forced bubbling at about 6 meter. However, since the roof temperatures are the highest at about 6 meter (in industrial glass melting tanks due to the position of the burners), the temperature of the glass melt obtains the highest values at the surface at this point (hot spot). The temperature exceeds  $1300^{\circ}\text{C}$  almost everywhere in the melting area. The temperature drops fast to values below  $1200^{\circ}\text{C}$  as soon as the glass enters the working end.

The calculated flow pattern is given in figure 7.3. The influence of the bubblers on the velocity profiles is clearly visible at 6 meter. Right below the batch blanket a strong backward flow enhances the dissolution of the batch particles. At the bottom of the tank, between the bubblers and the flow barrier, the velocity of the glass melt is low. The temperature in this part of the tank is rather low, an unfavourable condition for the dissolution and melting of remaining batch particles or for the (primary) fining of the melt. However, the flow barrier prevents the bottom glass to enter directly the working end of the tank. Only the surface glass, with relatively high temperatures, passes over the flow barrier.

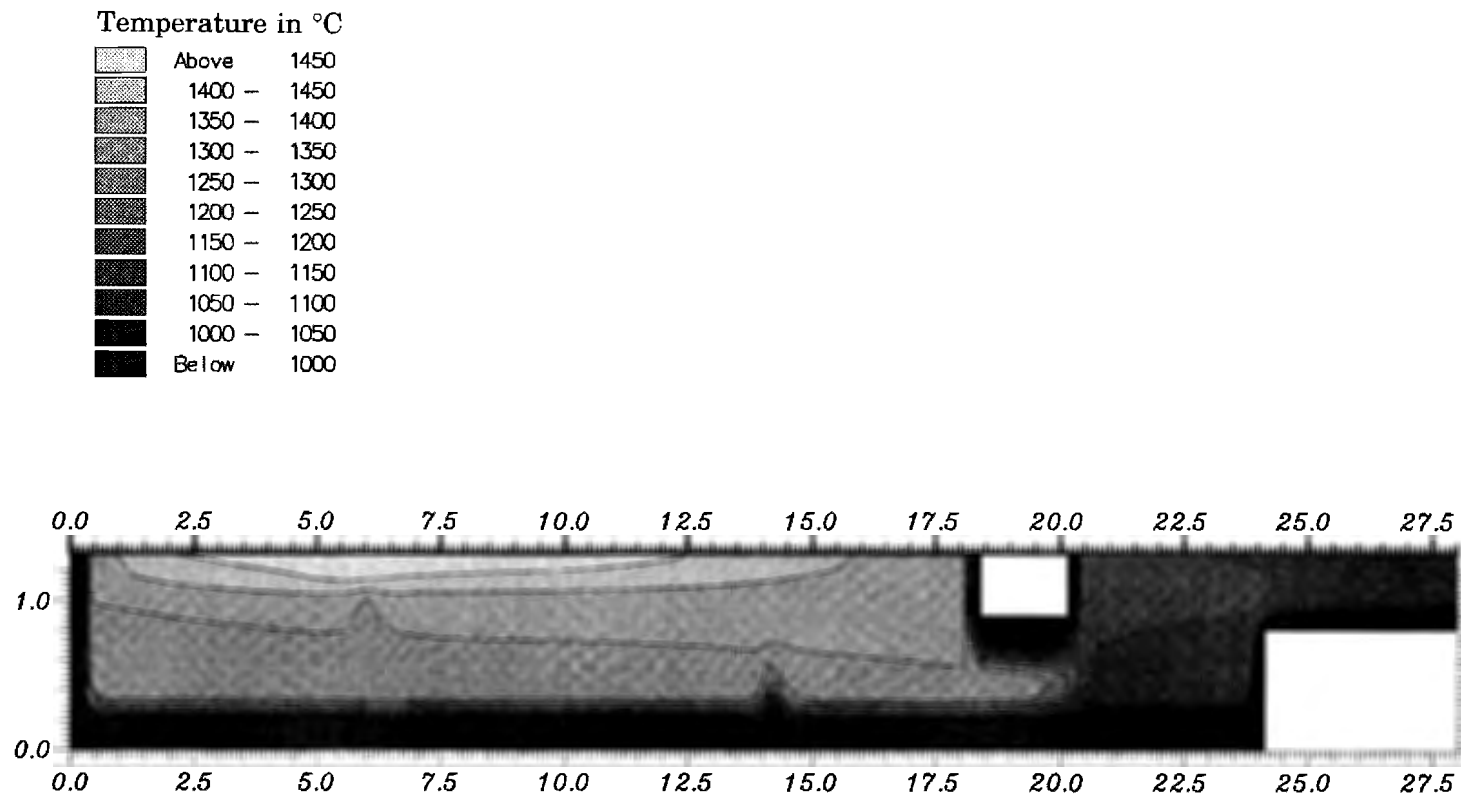


Figure 7.2  
The temperature distribution along the lengthwise section of the glass melting tank

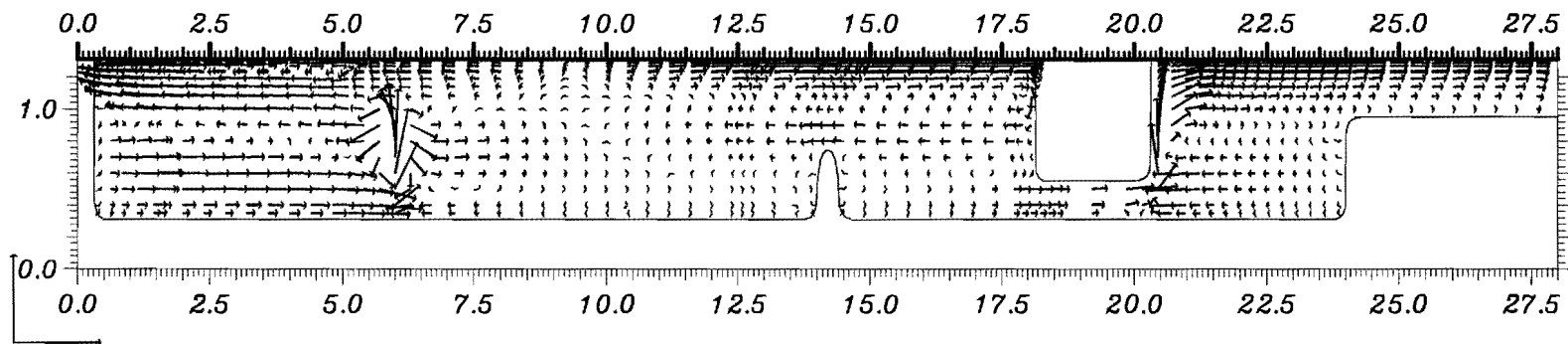


Figure 7.3  
The velocity vectors along the lengthwise section of the glass melting tank

Starting from the calculated temperature distribution, the redox reaction equilibria concerning iron, antimony and oxygen are subsequently calculated. The data for the equilibrium constants have been taken from chapter 6 and are reproduced in table 7.1.

Table 7.1

The parameters with which the redox sub-program calculates the concentrations of  $\text{Sb}^{5+}$ ,  $\text{Sb}^{3+}$ ,  $\text{Fe}^{3+}$ ,  $\text{Fe}^{2+}$  and  $\text{O}_2$

$C_{\text{Sb}} = 40 \text{ mole}\cdot\text{m}^{-3}$	$\Delta H_{\text{Sb}} = 213 \text{ kJ}\cdot\text{mole}^{-1}$	$\Delta S_{\text{Sb}} = 139 \text{ J}\cdot\text{mole}^{-3}\cdot\text{K}^{-1}$
$C_{\text{Fe}} = 13 \text{ mole}\cdot\text{m}^{-3}$	$\Delta H_{\text{Fe}} = 144 \text{ kJ}\cdot\text{mole}^{-1}$	$\Delta S_{\text{Fe}} = 37 \text{ J}\cdot\text{mole}^{-3}\cdot\text{K}^{-1}$

Figure 7.4 represents the percentage of antimony, present as  $\text{Sb}^{3+}$ , in the glass melt. 10% of the antimony is assumed to be present in the batch as trivalent antimony,  $\text{Sb}^{3+}$ . The batch blanket is therefore visible as a dark region between 0 and 5 meter in the upper left corner of figure 7.4. At the high temperatures of the glass melt, the (pentavalent) antimony is rapidly converted to trivalent antimony, until about 75% of the antimony is present in the reduced form (see figure 7.4).

During the reduction of antimony, gaseous oxygen is formed. The excess of oxygen is transported to existing bubbles, or new bubbles are formed. In the computer model, the oxygen is assumed to leave the melt when the oxygen equilibrium pressure exceeds 1 bar. At this moment, it is not certain whether this assumption is valid in the entire glass melting tank. Especially oxygen that is formed just below the batch blanket, might well be prevented by the batch blanket to leave the melt. If this is the case, more antimony will be present in the pentavalent state in this area than predicted by the computer calculations.

The removed oxygen is of course no longer available for the oxidation of the trivalent antimony at a decrease of temperature. For this reason, the concentration of trivalent antimony in the working end is almost as high as in the last part of the melting area, although the temperature in the working end is below  $1200^\circ\text{C}$ .

In figure 7.5, the oxygen equilibrium pressure in the glass melt is given. At the

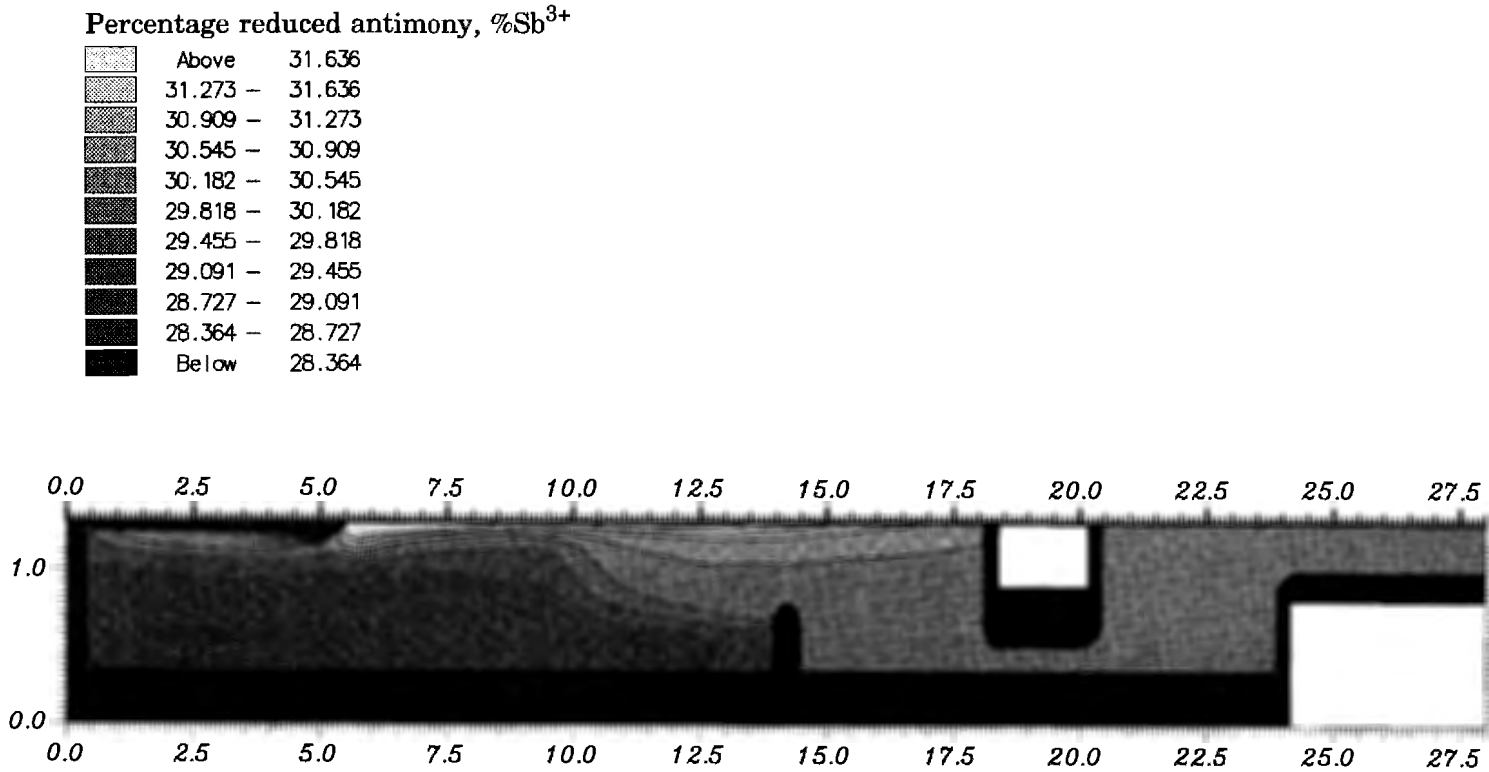


Figure 7.4

The percentage of antimony, present as Sb<sup>3+</sup>, as a function of position in the lengthwise-section of the glass melting tank

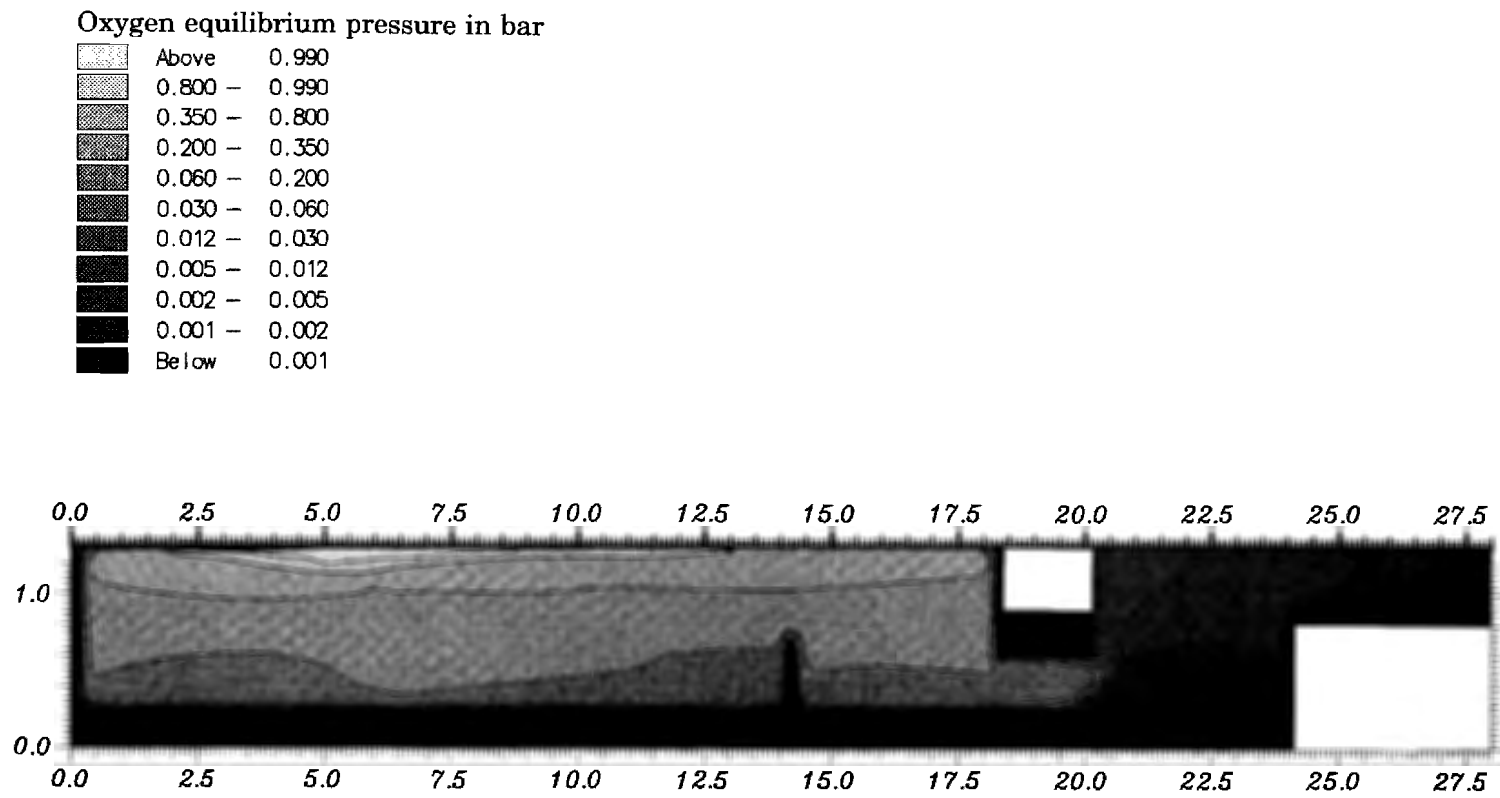


Figure 7.5  
The oxygen pressure (in bar) as a function of position in the lengthwise-section of the example glass melting tank



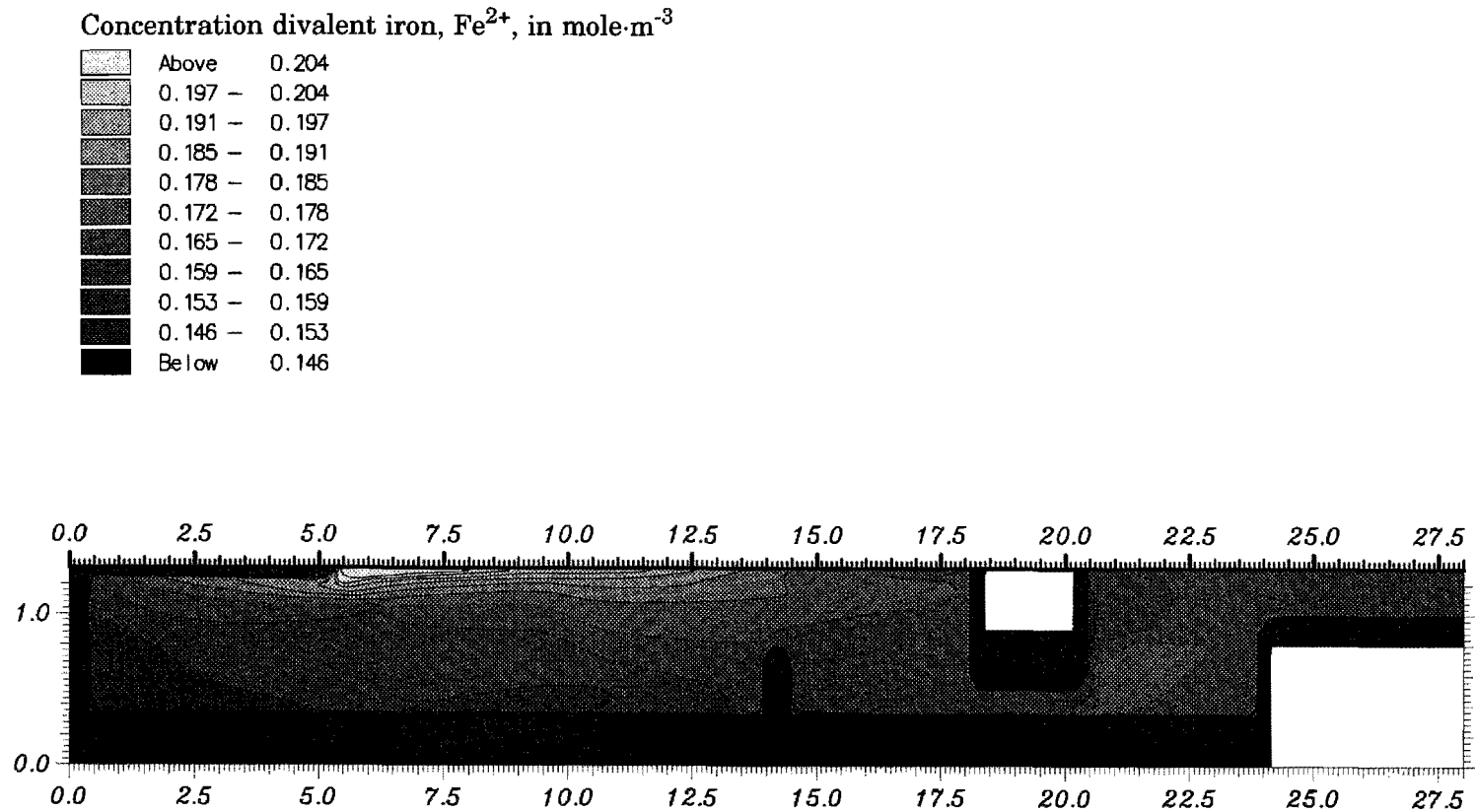


Figure 7.6

The concentration of  $\text{Fe}^{2+}$  (in  $\text{mole}\cdot\text{m}^{-3}$ ) as a function of position in the lengthwise-section of the example glass melting tank

surface of the glass melt, and especially around the hot-spot, the oxygen pressure is high (about 1 bar). In this area, existing small bubbles resulting from the melting process grow fast due to the in-diffusing oxygen gas. The produced large bubbles ascend fast to the (near-by) surface of the melt, also because the temperature in this part of the tank is high and therefore the viscosity of the melt is low. This indicates that the primary fining process particularly takes place in this region.

A large part of the produced oxygen is removed from the melt in the form of bubbles. The oxygen pressure in the melt is less than 0.2 bar when the melt passes the throat. The remaining oxygen in the melt is taken up very fast by the trivalent antimony in the melt during cooling in the working end, as can be seen by the drastic fall in the oxygen pressure in figure 7.5. If the glass melt would still contain any bubbles in the working end, the oxygen from these bubbles would also be taken up by the trivalent antimony. The partial pressures of the other gases in the bubble would increase, which would enhance the diffusion of these gases into the melt as well. The bubbles would shrink and might even dissolve completely. This indicates that the secondary fining process, or refining, takes place at the working end under these circumstances.

In order to check the assumption concerning the concentration of divalent iron in the melt, the calculated  $\text{Fe}^{2+}$  concentration profile is given in figure 7.6. The  $\text{Fe}^{2+}$  content appears to be between 0.15 en 0.20 mole·m<sup>-3</sup> throughout the glass melting tank. This indicates that the contribution of  $\text{Fe}^{2+}$  to the heat conductivity of the melt will indeed be small, and can presumably be approximated by a constant value.

#### Concluding:

From the velocity distribution it appears that most of the glass melt flows at or close to the surface in order to pass the flow barrier. At this point, the temperature of the melt is high, its viscosity is low and the oxygen pressure is in the order of 1 bar. The conditions for an optimal progress of the primary fining of the glass melt are all fulfilled. This lowers the possibility that the glass melt contains bubbles (resulting from the melting process) as it enters the working end. There, remaining bubbles will shrink or disappear completely due to the secondary fining, and the chance that the final glass product contains bubbles is lowered even more.

One should always keep in mind, however, that some bubbles (for instance resulting from interaction with refractory material) might be found in the final glass product.

Due to the more strict environmental legislation, the use of (large amounts of) antimony as a fining agent has been brought up for discussion. Supposing that the antimony concentration is halved, the performance of the example glass-melting tank can be calculated with the 3-D glass tank model, and compared to the performance of the same tank when the batch contains the original amount of antimony.

The antimony concentration is  $20 \text{ mole}\cdot\text{m}^{-3}$  (0.125 weight-%  $\text{Sb}_2\text{O}_3$ ). All other processing conditions, particularly the iron content, remain the same. Therefore both the temperature distribution and the velocity profiles will be similar to the ones presented in figures 7.2 and 7.3.

Under the new conditions, 10% of the antimony is assumed to be in the trivalent state in the batch blanket as well. At the high temperatures of the molten glass, antimony is reduced until about 75% is present as  $\text{Sb}^{3+}$  (see figure 7.7). But now, less oxygen is released. The oxygen pressure in the melt does not reach the high level of 1 bar (see figure 7.8). This means that the primary fining process does not take place under optimal circumstances, and the chance of finding bubbles in the final product is now much larger than in case the antimony concentration is  $40 \text{ mole}\cdot\text{m}^{-3}$ .

For the example glass melting tank, the decrease of the antimony content by 50% is unfavourable on the basis of the calculations presented above.

In practise, about 0.4 to 0.6 weight-%  $\text{Sb}_2\text{O}_3$  is added to TV-screen glass for an optimal progress of the fining process. From the practise in various industrial glass melting tanks evidence has arisen that lowering the antimony concentration by 50% would lead to serious problems in the fining process, presumably resulting in an unacceptable amount of bubbles in the final glass product.

Percentage reduced antimony, %Sb<sup>3+</sup>

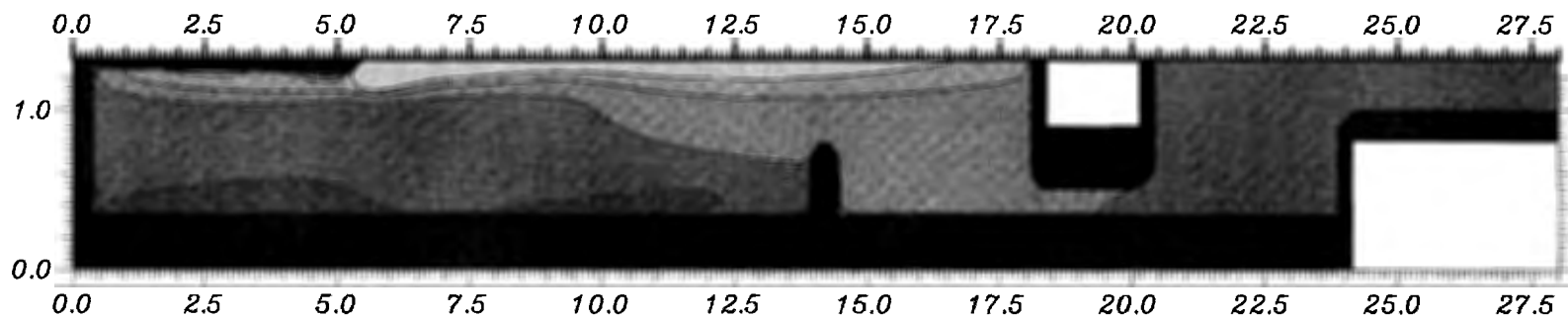
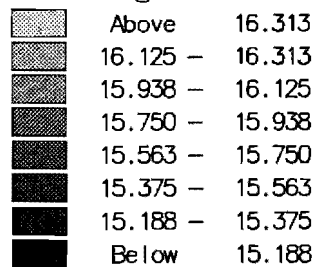


Figure 7.7

The percentage of antimony, present as Sb<sup>3+</sup>, as a function of position in the lengthwise-section of the glass melting tank. Total antimony concentration is 0.125 weight-% Sb<sub>2</sub>O<sub>3</sub>

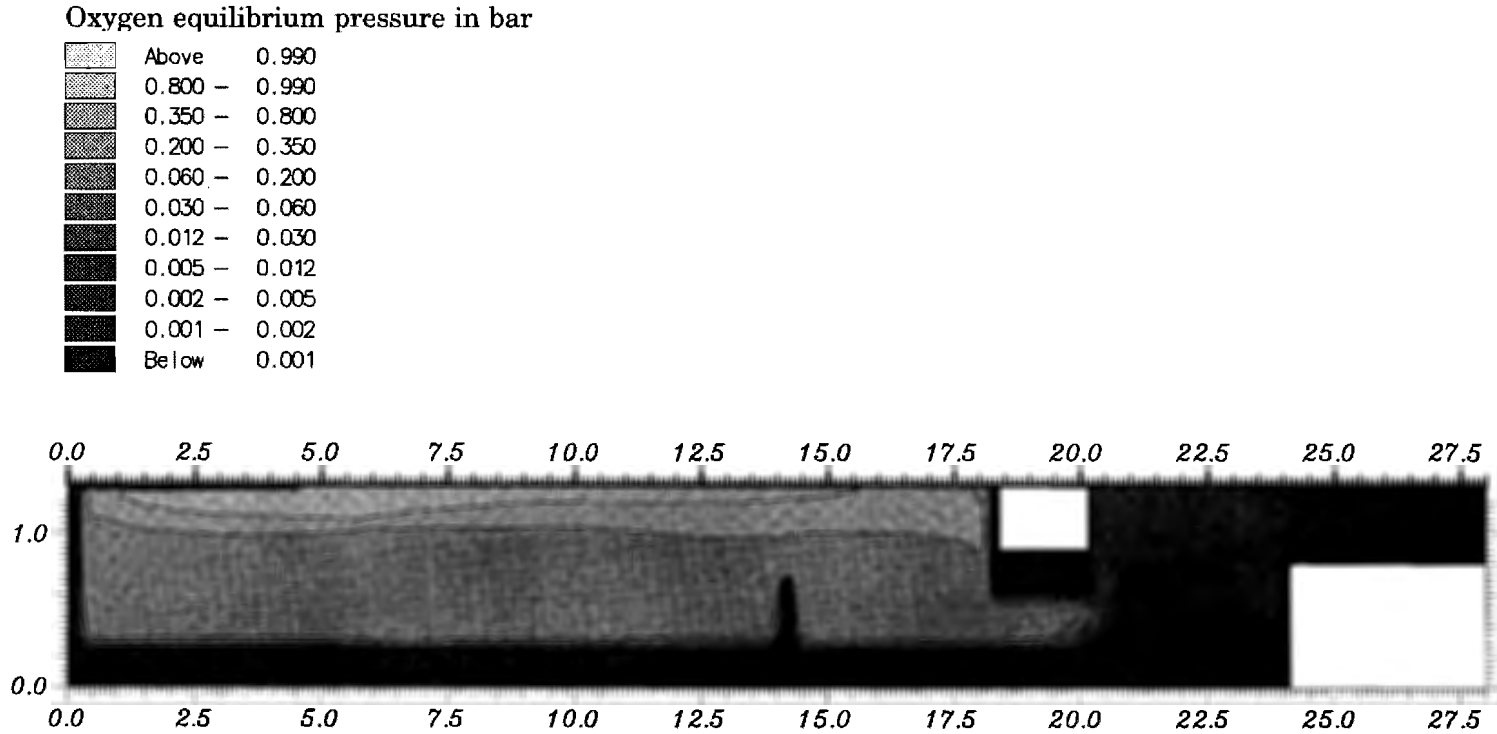


Figure 7.8

The oxygen pressure (in bar) as a function of position in the lengthwise-section of the example glass melting tank. Total antimony concentration is 0.125 weight-%  $\text{Sb}_2\text{O}_3$

Literature

- [1] Gehlhoff, G.; Kalsing, H.; Thomas, M.  
Ueber die Läuterung des Glases  
*Glastechnische Berichte* **8** (1930) no.1 p.1-24
- [2] Mulfinger, H.O.  
Gasanalytische Verfolgung des Läutervorganges im Tiegel und in der Schmelzwanne  
*Glastechnische Berichte* **49** (1976) no.10 p.232-245
- [3] Erk, K. van; Papanikolau, E.; Pelt, W. van  
The effect of fluorides on antimony refining  
Proceedings of the 11<sup>th</sup> International Congress on Glass Prague (1977) **4** p.137-146
- [4] Apak, C.; Cable, M.  
Effect of transition metal-oxides on the refining behaviour of soda-lime-silica glasses  
Proceedings of the 11<sup>th</sup> International Congress on Glass Prague (1977) **4** p.167-176
- [5] Langer, A.; Scholze, H.  
Untersuchungen zum Ersatz von  $As_2O_3$  als Läutermittel für Kristallgläser  
*Glastechnische Berichte* **54** (1981) no.7 p.223-230
- [6] Simonis, F.  
Estimation of the local redox distribution in the melt by numerical flow modeling  
*Glastechnische Berichte* **63K** (1990) p.29-38
- [7] Beerkens, R.G.C.; Van der Heijden, T.; Muysenberg, H.  
Possibilities of glass tank modeling for the prediction of the quality of melting processes  
*Ceramic Engineering and Science Proceedings* **14** (1993) p.139-160
- [8] Beerkens, R.G.C.  
Chemical equilibrium reactions as driving forces for growth of gas bubbles during refining  
*Glastechnische Berichte* **63K** (1990) p.222-242
- [9] Beerkens, R.; Van der Heijden, T.; Muysenberg, H.  
A model study on degassing of sulphate refined glass melts  
Proceedings of the XVI International Congress on Glass Madrid **6** (1992) p.15-21
- [10] Wondergem-de Best, A.; Beerkens, R.G.C.; De Waal, H.  
A comparative model study of antimony and cerium oxide refining  
Proceedings of the first Conference of the European Society of Glass Science and Technology Sheffield (1991) p.195-199
- [11] Simonis, F.  
Modeling of glass processing  
Colloquium Maastricht 6 november 1991  
*Klei Glas Keramiek* **13** (1992) no.5 p.148

## Appendix I

### APPENDIX I

Composition of glasses in wt%

Product	SiO <sub>2</sub>	Na <sub>2</sub> O	K <sub>2</sub> O	CaO	MgO	Al <sub>2</sub> O <sub>3</sub>	Fe <sub>2</sub> O <sub>3</sub>	Other
Container glass								
- white	72.6	13.7	0.5	11.0	0.1	1.6	0.05	0.2 SO <sub>3</sub> ; 0.1 TiO <sub>2</sub>
- green	72.0	15.1	-	8.4	2.1	1.1	0.4	0.15 Cr <sub>2</sub> O <sub>3</sub>
- amber	72.7	13.8	1.0	10.0	-	1.9	0.2	0.03 SO <sub>3</sub>
Float glass	72.8	12.8	0.8	8.2	3.8	1.4	0.1	0.3 SO <sub>3</sub>
TV screen	63.2	9.9	7.5	1.8	1.1	3.3	-	12.7 BaO
Lamp bulbs	72.4	17.4	-	5.3	3.7	0.8	-	
Table ware	75.6	13.5	4.1	3.7	2.6	0.4	0.02	
E glass fibre	55.2	0.3	0.2	17.7	4.3	14.8	0.3	7.3 B <sub>2</sub> O <sub>3</sub>
A glass fibre	72.0	12.5	1.5	9.0	0.9	2.5	0.5	0.5 B <sub>2</sub> O <sub>3</sub>
Borosilicate	80.2	4.5	0.3	0.1	-	2.6	0.07	12.3 B <sub>2</sub> O <sub>3</sub>
Lead glass	54.9	0.2	12.3	-	-	-	0.02	32.0 PbO

## **DANKWOORD**

Het in dit proefschrift beschreven onderzoek is financieel mogelijk gemaakt door het Nationaal Committee van de Nederlandse Glasindustrie (N.C.N.G.). De begeleidingcommissie van de N.C.N.G. heeft het onderzoek nauwlettend gevolgd en waar nodig geadviseerd over de te volgen richting. De wetenschappelijke discussies met onder andere dhr. Tromp, Rob Bonn, Jan Peelen en Jan Hermans waren daarbij van onschatbare waarde.

Veel dank ben ik verschuldigd aan Ruud Beerkens, die als copromotor het schrijven van dit proefschrift intensief heeft begeleid. Verder wil ik alle collega's van de afdeling Glastechnologie van TNO/TPD bedanken voor de prettige samenwerking gedurende de afgelopen jaren. In het bijzonder bedank ik Tom van der Heijden, die altijd direct bereid was de helpende hand te bieden bij de ontelbare praktische problemen.

De mensen van de werkplaats en glasblazerij wil ik bedanken voor de snelle levering van bestellingen.

Tot slot bedank ik Harry voor de vele discussies en de opbouwende kritiek.



## **CURRICULUM VITAE**

De auteur werd op 1 september 1965 als Annemieke de Best geboren in Berchem (België). In 1983 behaalde ze het diploma VWOb aan het Newman College te Breda. Aansluitend studeerde ze Scheikundige Technologie aan de Technische Universiteit te Eindhoven.

Gedurende een aantal jaren was de schrijfster als vrijwilligerster werkzaam bij de Chemiewinkel Eindhoven. Van maart 1987 tot maart 1988 was ze voorzitter van deze studentenvereniging.

Het afstudeerwerk op het gebied van beschermende coatings op glas resulteerde in oktober 1988 tot het behalen van het ingenieursdiploma.

In 1989 trouwde Annemieke met Harry Wondergem. In datzelfde jaar begon ze het promotieonderzoek dat tot dit proefschrift leidde bij TNO-Glastechnologie onder leiding van prof. H. de Waal en dr.ir. R.G.C. Beerkens.

**Stellingen behorende bij het proefschrift van  
A.W.M. Wondergem-de Best**

1. De aanname van Krämer, dat de stijgsnelheid van gasbellen in gesmolten natronkalkglas met lage viscositeit de wet van Stokes volgt, is gebaseerd op onbetrouwbare metingen van Němec (in een smelt met veel bellen) en een ongeoorloofde vertaling van onverklaarde metingen in visceuze olie van Gailhbaud en Zortea. Tot het tegendeel bewezen is, moet worden aangenomen dat de stijgsnelheid van bellen in natronkalkglas bij alle temperaturen de wet van Hadamard volgt.  
Krämer, F.W.: in "Glastechnische Fabrikationsfehler" (1980), hoofdstuk 4.4.1  
Němec, L.: *Proc. XI International Congress on Glass Prague* (1977) p.155-165  
Gailhbaud, J.; Zortea, M.: *Rev. Gen. Therm.* **8** (1969) p.433-453  
Dit proefschrift, hoofdstuk 2.3.1
2. De basiciteit van glas is geen betrouwbare parameter voor de schatting van verschuivingen van de evenwichtsliggingen van redoxreacties in het gesmolten glas bij veranderingen in de glassamenstelling.  
Douglas, R.W.; Nath, P.; Paul, A.: *Phys. Chem. Glasses* **6** (1965) p.216-223  
Dit proefschrift, hoofdstuk 3.5 en 3.6
3. De meeste van de in de literatuur gegeven verklaringen voor afwijkingen tussen gemeten redoxreactie-evenwichtsliggingen en voorspellingen hiervan op basis van de glassamenstelling zijn zinloos omdat ze resulteren in de definitie van nieuwe onbekende grootheden.  
Dit proefschrift, hoofdstuk 3.6
4. De evenwichtsliggingen van de redoxreacties van zwavel in gesmolten glas kunnen niet worden bepaald met behulp van square wave voltammetry metingen zolang geen goede piekidentificatie heeft plaatsgevonden.  
Dit proefschrift, hoofdstuk 6.7
5. De evenwichtsliggingen van redoxreacties in gesmolten glas met meerdere polyvalente ionen kunnen niet worden bepaald aan de hand van metingen van de valentietoestand van die ionen in afgekoelde monsters, omdat de evenwichtsliggingen tijdens het afkoelen onderling verschuiven.  
Dit proefschrift, hoofdstuk 6.8
6. Onderzocht moet worden, of een geringe hoeveelheid CO in de ovenatmosfeer daadwerkelijk zo'n grote invloed heeft op de glaskwaliteit en de aantasting van vuurvast materiaal als in het algemeen wordt aangenomen. Is dit niet het geval, dan is enigszins reducerend stoken een betere manier om de NO<sub>x</sub>-uitstoot van industriële glasovens te verminderen dan de gebruikelijke dure end-of-pipe zuivering.
7. De effectiviteit van seleen als ontkleuringsmiddel zou sterk verhoogd, en de milieubelasting door verdamping van seleencomponenten zou sterk omlaag gebracht worden, als het seleen in de juiste valentietoestand en sterk gebonden in het mengsel zou worden toegevoegd.

8. Bij het bepalen van glaseigenschappen zoals viscositeit en warmtegeleiding aan de hand van de glassamenstelling zou ook het watergehalte in beschouwing moeten worden genomen, omdat juist de aanwezige -OH groepen een grote invloed op deze eigenschappen hebben.
9. Er is in Nederland geen gebrek aan werk, er schijnt alleen geen geld te zijn om dit werk te betalen.
10. Hoewel stamboomonderzoek zeer geschikt is om iemands culturele achtergrond te bepalen, moet sterk worden getwijfeld aan het genetische waarheidsgehalte van de stamboom, omdat bij de burgerlijke stand niet altijd de juiste vader (of zelfs moeder) werd en wordt opgegeven.
11. In verband met de voorstellen om a.i.o.-ers in de toekomst de student-status te geven zou het beter zijn als promovendi geen stellingen meer opnemen in hun proefschrift. Doen ze dat wel, dan zullen de ministers ervan uitgaan dat a.i.o.-ers naast hun "studie" nog tijd over hebben om zich bezig te houden met andere zaken, en dat in de "studietijd" dus nog flink gesnoeid kan worden.